Squaramide-Based Rotaxane Host Structures for Anion and Ion-Pair Recognition



Arya Arun

Lady Margaret Hall

A thesis submitted for the degree of Doctor of Philosophy

in Inorganic Chemistry

Trinity 2023

I would like to dedicate this thesis to my late grandmother, Mom and Dad.

What's next?

-President Bartlet, The West Wing

Squaramide-Based Rotaxane Host Structures for Anion and Ion-Pair Recognition

Abstract

***Arya Arun**, Lady Margaret Hall, University of Oxford*

Abstract of thesis submitted for the degree of D.Phil., Trinity Term 2023

This thesis describes the synthesis and characterisation of squaramide containing [2]rotaxanes exploiting hydrogen bonding (HB) and halogen bonding (XB) interactions for the purposes of host-guest anion and ion-pair recognition and salt extraction in polar organic and aqueous solvent mixtures.

Chapter 1 introduces the general concepts of supramolecular host-guest chemistry highlighting the areas pertinent to the topics explored in this DPhil thesis. A particular emphasis is placed on the themes of ion-pair recognition and the preparation of mechanically interlocked host frameworks and their applications.

Chapter 2 details the synthesis and characterisation of a series of heteroditopic squaramide-based [2]rotaxane frameworks possessing HB and XB donor groups, followed by extensive ^{1}H NMR studies to explore their lithium halide ion-pair binding properties. Integration of a coumarin chromophore enables qualitative absorption and fluorescence-based sensing studies to explore the impact of ion-pair recognition on the optical properties of the receptors. Additionally, the chapter also discusses preliminary lithium halide ion-pair salt solid-liquid extraction experiments using these receptors in polar organic solvents.

Chapter 3 presents the synthesis of a series of squaramide functionalised interlocked rotaxane hosts using an unprecedented sodium cation-template directed approach involving the Lewis basic squaramide carbonyls. Wherein investigation of the sodium halide ion-pair recognition capabilities of the [2]rotaxanes in polar organic solvent media are presented. Moreover, the chapter delves into preliminary experiments conducted to investigate the potential use of these receptors as agents for extracting sodium halide ion-pair salts into organic solvents.

Chapter 4 details the preparation and characterisation of bis-squaramide axle containing [2]rotaxane structures linked *via* rigid aryl and flexible alkyl spacers and explores their anion recognition properties in aqueous-organic solvent mixtures.

Chapter 5 outlines the major conclusions and future work of this thesis.

Chapter 6 describes the experimental procedures utilised in this work, including synthetic protocols and characterisation data for novel compounds.

Acknowledgements

I would like to start by thanking first my supervisor, Prof. Paul Beer for giving me the opportunity to study at the University of Oxford and for his support, guidance and patience throughout my DPhil. He has been an encouraging mentor and I have always valued the warm and welcoming work environment he created for us.

My time in the Beer group has been incredibly enriching and I would like to thank both current and former group members who have contributed to making my time here memorable. First and foremost, I would like to extend an indebted thanks to Dr. Jessica Pancholi who mentored and took care of me when I started. I am also grateful for the guidance extended by Dr. Andrew Docker whose suggestions benefited my work greatly. A special thanks to Dr. Vihanga Munasinghe and Dr. Edward Mitchell for lending me valuable synthons. Furthermore, a big thank you to the people who very kindly read and helped out with my thesis chapters, Jamie Wilmore, Hui Min Tay and Andrew Taylor. Without their inputs and comments, this thesis would not have been possible. I would especially like to mention Hui Min Tay, who made my time in the Beer group so much more enjoyable from singing and discussing different musicals to sharing woes of many failed experiments.

I would be remiss if I did not also thank Dr. Dalip Kumar, for supervising me during my Master's thesis project and for introducing me to the world of chemistry research. I am forever grateful for his counsel and advise.

Outside the lab, I have been extremely lucky to have made wonderful and dependable friends (Shivani, Gayatri, Navoneel and Ashwin) who have supported me through various

ups and downs in the last four years. I will always cherish the memories we made cooking, playing Court-piece and travelling.

Lastly, I would have never made it this far without Mumma, Dad, Didi, Jiju and Shivi, my most adored support system and cheerleaders. A special shoutout to Jhunna Maamaji, Archana Maamiji and Rahul for taking such good care of me and giving me a home away from home in a new country.

Previously published work

Squaramide-Based Heteroditopic [2]Rotaxanes for Sodium Halide Ion-Pair Recognition
A. Arun, A. Docker, H. Min Tay and P. D. Beer, *Chemistry – A European Journal*, 2023, **29**, e202301446.

Abbreviations

δ	*chemical shift*
β_x	*binding constant*
λ	*wavelength*
µ	*micro*
Δ	*change in (a physical quantity)*
ν	*frequency*
°	*degree*
°C	*degrees Celsius*
Å	*Ångstrom*
A^-	*anion*
abs	*absorption*
a.u.	*arbitrary units*
aq.	*aqueous*
Ar	*aromatic*
Arg	*arginine*
Asp	*aspartate*

AMT	*active metal template*
br.	*broad*
Br^-	*bromide ion*
BODIPY	*boron-dipyrromethene (4,4-difluoro-4-bora-3a,4a-diaza-s-indacene)*
Bar^F_4	*tetrakis[3,5-bis(trifluoromethyl)phenyl]borate*
bipy	*2,2'-bipyridine*
Boc	*di-tert-butyl dicarbonate*
br	*broad*
Bu	*butyl*
cat.	*catalytic*
Ch	*chalcogen*
ChB	*chalcogen bonding*
Cl^-	*chloride ion*
conc.	*concentrated*
COSY	*homonuclear correlation spectroscopy*
CuAAC	*copper(I)-catalysed azide-alkyne cycloaddition*

D	*donor*
d	*doublet*
d	*deuterated*
DBU	*1,8-diazabicyclo[5.4.0]undec-7-ene*
DCM	*dichloromethane*
dd	*doublet of doublets*
DFT	*density functional theory*
DIPEA	*N,N-di-iso-propylethylamine*
DMAP	*4-dimethylaminopyridine*
DMF	*N,N-dimethylformamide*
DMSO	*dimethyl sulfoxide*
DNA	*deoxyribonucleic acid*
e.g.	*exempli gratia*
e	*electron*
EDTA	*ethylenediaminetetraacetate*
eq., equiv.	*equivalents*
ESI	*electrospray ionisation (mass spectrometry)*

Et	*ethyl*
et al.	*et alia*
EtOAc	*ethyl acetate*
E.T.	*energy transfer*
EWG	*electron withdrawing groups*
g	*gram*
G	*Gibbs free energy*
Grubbs' I/ II	*Grubbs' first/ second generation catalyst*
H	*enthalpy*
HB	*hydrogen bonding*
HRMS	*high resolution mass spectrometry*
$H_2PO_4^-$	*dihydrogen phosphate ion*
HSO_4^-	*hydrogen sulfate ion*
Hz	*Hertz*
ICT	*Isothermal titration calorimetry*
i.e.	*id est*
I^-	*iodide ion*

ITC	*Isothermal titration calorimetry*
J	*coupling constant*
K	*Kelvin (Temperature SI Unit)*
Ka	*association constant*
Kd	*dissociation constant*
L	*litre*
M	*molar (moles per litre)*
m/z	*mass to charge ratio*
Me	*methyl*
MIM	*mechanically-interlocked molecule*
MS	*mass spectrometry*
Ms	*mesyl*
NDI	*naphthalenediimide*
NMR	*nuclear magnetic resonance*
NO_3^-	*nitrate ion*
NO_2^-	*nitrite ion*
o	*ortho*

o/n	*overnight*
OAc^-	*acetate ion*
OBz^-	*benzoate ion*
PEG	*polyethylene glycol*
PET	*photo-induced electronic transfer*
ppm	*parts per million*
PTLC	*preparative thin layer chromatography*
pH	$-log_{10}[H^+]$
Ph	*phenyl*
Phe	*phenylalanine*
pKa	$-log_{10}K_a$
q	*quartet*
quant.	*quantitative*
quin.	*quintet*
R	*chemical substituent*
rt / RT	*room temperature*
RCM	*ring-closing metathesis*

Rf	*retention factor*
ROESY	*Rotating-frame Nuclear Overhauser Enhancement Spectroscopy*
S	*entropy*
TBA	*tetrabutylammonium*
TBTA	*tris[(1-benzyl-1,2,3-triazol-4-yl)methyl]amine*
TEG	*triethylene glycol*
TFA	*trifluoroacetic acid*
THF	*tetrahydrofuran*
TLC	*thin layer chromatography*
TMS	*trimethylsilyl (protecting group)*
Ts	*tosyl*
UV	*ultra-violet*
v/v	*volume/ volume percent*
vis.	*visible*
XB	*halogen bond*
XRD	*X-ray diffraction*

Table of Contents

Abstract ..... **iv**

Acknowledgements ..... **vi**

Previously published work ..... **viii**

Abbreviations ..... **ix**

Chapter 1: Introduction **1**

1.1 Supramolecular chemistry **2**

1.2 Non-covalent interactions **4**

1.2.1 Electrostatic interactions 4

1.2.2 Hydrogen bonding 5

1.2.3 Halogen bonding 6

1.2.4 Hydrophobic Interactions 7

1.2.5 Ion-π interactions 7

1.3 Anion recognition **8**

1.3.1 The importance of anion recogntion 8

1.3.2 The challenges of anion recognition 10

1.3.3 Receptors for anion recognition: Biotic/Natural Receptors 12

1.3.4 Receptors for anion recognition: Synthetic Receptors 14

1.3.5 Anion sensing 26

1.4 Ion-pair recognition 30

1.4.1 Heteroditopic receptors for ion-pair recognition 31

1.4.2 Applications of heteroditopic receptors 36

1.5 Mechanically interlocked molecules 39

1.5.1 Synthesis of mechanically interlocked molecules 41

1.5.2 Applications of mechanically interlocked molecules 49

1.6 Project aims and objectives 57

Chapter 2: Squaramide-based Heteroditopic [2]Rotaxanes for Lithium Halide Ion-pair Recognition and Extraction 59

2.1 Introduction 60

2.1.1 MIMs for heteroditopic ion pair recognition 60

2.1.2 Squaramide containing MIMs 65

2.2 Chapter objectives 66

2.3 Synthesis and characterisation 68

2.3.1 Synthesis of squaramide axle precursor synthons 69

2.3.2 Synthesis of HB/XB macrocycles for AMT-directed [2]rotaxane preparation ... 72

2.3.3 Synthesis of squaramide-functionalised HB [2]rotaxane 72

2.3.4 Synthesis of squaramide-functionalised XB [2]rotaxane 76

2.4 Host-guest recognition studies 79

2.4.1 Preliminary anion binding studies 79

2.4.2 Quantitative ^{1}H NMR halide binding titration studies 82

2.4.3 Quantitative ^{1}H NMR alkali metal cation binding titration studies 85

2.4.4 Quantitative ^{1}H NMR ion-pair binding titration studies 88

2.4.5 Solid-liquid extraction studies 91

2.4.6 Conclusions 93

2.5 Coumarin containing [2]rotaxane analogues 93

2.5.1 Synthesis of coumarin functionalised squaramide axle precursor 95

2.5.2 Synthesis of coumarin-squaramide HB [2]rotaxane 97

2.5.3 Synthesis of coumarin-squaramide XB [2]rotaxane 100

2.6 Host-guest recognition studies 102

2.6.1 Quantitative ^{1}H NMR halide binding titration studies 102

2.6.2 Quantitative ^{1}H NMR alkali metal cation binding titration studies 106

2.6.3 Quantitative ^{1}H NMR ion-pair binding titration studies 109

2.6.4 Preliminary optical studies 113

2.6.5 Solid-liquid extraction studies 117

2.7 Conclusions and Future work 120

Chapter 3: Squaramide-based Heteroditopic [2]Rotaxanes for Sodium Halide Ion-pair Recognition and Extraction 123

3.1 Introduction 124

3.2 Chapter objectives 127

3.3 Synthesis and characterisation 128

3.3.1 Pseudo-rotaxane studies 128

3.3.2 Synthesis of acyclic squaramide-based bis-azide precursor 132

3.3.3 Synthesis of the target [2]rotaxanes 133

3.4 Host-guest recognition studies 139

3.4.1 Quantitative ^{1}H NMR halide binding titration studies 139

3.4.2 Quantitative ^{1}H NMR sodium cation binding titration studies 143

3.4.3 Quantitative ^{1}H NMR ion-pair binding titration studies 148

3.4.4 Preliminary solid-liquid extraction studies 154

3.5 Conclusions and Future work 156

Chapter 4: Bis-squaramide-based [2]Rotaxanes for Anion Recognition in Aqueous-organic Solvent Mixtures 159

4.1 Introduction 160

4.2 Chapter objectives 161

4.3 Synthesis and characterisation 162

4.3.1 Synthesis of bis-azide functionalised bis-squaramide axle precursors 162

4.3.2 Synthesis of bis-squaramide [2]rotaxanes 164

4.4 Host-guest recognition studies 172

4.4.1 Quantitative ^{1}H NMR anion binding titration studies with [2]rotaxane **3.14** .172

4.4.2 Quantitative ^{1}H NMR anion binding titration studies with bis-squaramide [2]rotaxane **4.4** 176

4.4.3 Quantitative ^{1}H NMR anion binding titration studies with [2]rotaxane **4.5** ...185

4.5 Conclusions and Future work 189

Chapter 5: Conclusions and Future Work 193

Chapter 6: Experimental 199

6.1 General procedures 200

6.1.1 Materials and methods foy synthesis and characterisation....200

6.1.2 Instrumentation 200

6.1.3 Solution-based studies....201

6.2 Synthesis from Chapter 2 204

6.3 Experimental from Chapter 3 218

6.4 Experimental from Chapter 4 224

References 233

Chapter 1: Introduction

1.1 Supramolecular chemistry

More than 50 years after Fischer first introduced the lock-and-key analogy to explain the substrate association phenomena involving enzymes,[1,2] Pedersen's pioneering work on alkali metal binding crown ethers surfaced.[3] Soon after, Lehn and Cram reported the alkali metal cation binding motifs cryptands[4] and spherands,[5] paving the way for the 1987 Chemistry Nobel Prize *"for their development and use of molecules with structure-specific interactions of high selectivity"* (Figure 1.1). Their work garnered significant interest inspiring a multitude of research in the following years. In 2016, the advancements made in the supramolecular chemistry field were celebrated again when the Nobel Prize in Chemistry was awarded to Jean-Pierre Sauvage,[6] Fraser Stoddart[7] and Ben Feringa[8] for their trailblazing work on the *"the design and synthesis of molecular machines"*.

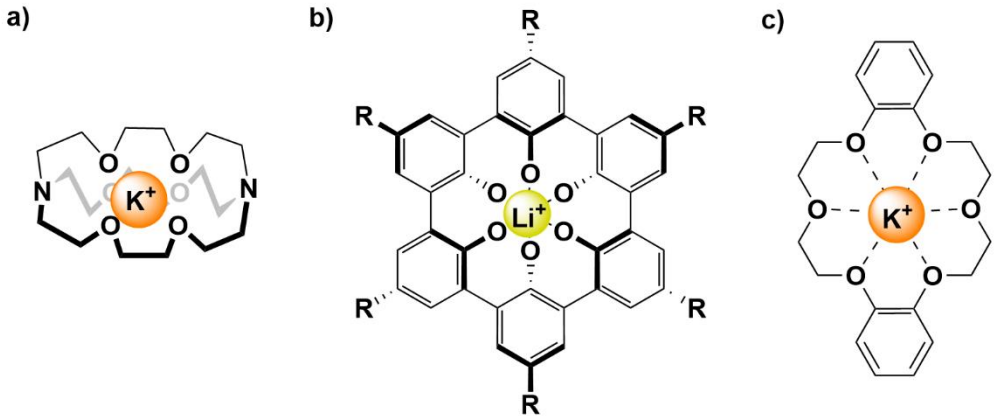


Figure 1.1. *Cation receptors: (a) Lehn's [2,2,2]cryptand,[4] (b) Cram's spherands[5] and (c) Pedersen's dibenzo-18-crown-6.[3]*

As described by Lehn in his Nobel Prize lecture, *"Supramolecular chemistry is the chemistry of the intermolecular bond, covering the structures and functions of the entities formed by association of two or more chemical species"*.[9] It is the study of non-covalent intermolecular interactions and their applications in the construction of multi-component molecular architectures and systems. These weak and reversible interactions include

electrostatic forces, van der Waals forces, π- π stacking interactions, solvophobic effects and sigma hole interactions.[10]

Two important aspects of supramolecular chemistry are self-assembly[11,12] and host-guest chemistry.[13] Self-assembly is the spontaneous association of small molecules into complex, larger structures using non-covalent interactions. Various examples of self-assembled biomolecules exist in nature such as the DNA strands which use hydrogen bonding interactions between their nucleotide bases to self-assemble into a double helical structure. On the other hand, host-guest chemistry is the selective recognition and binding between two chemical entities *via* reversible non-covalent interactions. Strong association between the receptor and guest species can be attained by complementary host-guest design[4] or by effecting preorganisation to maximise binding behaviour.[14] The latter is a well-defined and frequently employed concept that allows for the design of molecules with enhanced binding affinity and selectivity by optimising shape complementarity and geometric arrangements between the binding partners. A preorganised, rigid cavity reduces entropy loss upon binding which contributes to thermodynamic host-guest complex stability. Furthermore, preorganisation can also be used to effectively shield the binding pocket from the bulk solvent, thereby incurring a lower de-solvation penalty and enhancing host-guest interactions in polar protic solvents. These themes have inspired an enormous, broad myriad of supramolecular chemistry research finding applications in chemical, biological, medical and environmental sectors as well as in nanotechnology and materials design, including for example drug delivery systems, sensors, smart stimuli responsive materials and the environmental remediation of toxic pollutants.[15-20]

1.2 Non-covalent interactions

Non-covalent interactions refer to a broad category of reversible chemical interactions that occur between molecules or within molecules without the sharing or exchanging of any electrons between atoms.[21] The most common types of non-covalent interactions include:

1.2.1 Electrostatic interactions

Electrostatic interactions are attractive forces between two charged entities, such as ions or molecules with permanent dipoles.[22] They can be divided into three main categories depending on the charge and distance between the components: ion-ion, ion-dipole and dipole-dipole interactions (Figure 1.2).[23-25] The attractive forces between the components are governed by Coulomb's law and are therefore dependent on the charge and distance between the species. However, in solution, additional factors such as the dielectric constant of the solvent may inversely impact the interactions between the components.[26] Despite being strong interactions, they lack directionality which limits their use in the creation of specific host-guest binding systems.[27]

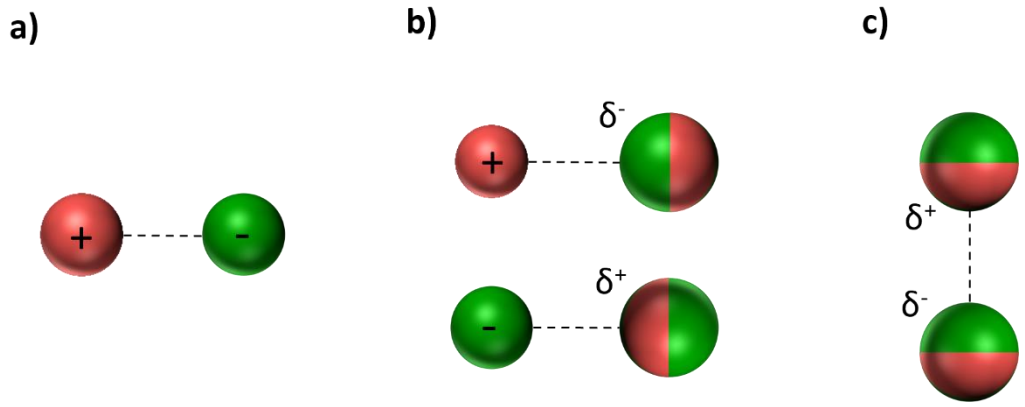


Figure 1.2. *Graphical representation of electrostatic interactions, a) ion-ion, b) ion-dipole and c) dipole-dipole.*

1.2.2 Hydrogen bonding

Hydrogen bonding (HB) interactions are generally denoted as R-H···B, where H is a hydrogen atom covalently attached to an electron-withdrawing group R (e.g., N, O, F) which leads to the formation of a permanent dipole. The resulting electron deficient hydrogen can then interact with a Lewis base B.[28] The strength of a hydrogen bond varies depending upon several factors such as the electronegativity difference and distance between the atoms, polarizability of the molecules, solvent effects and steric effects.[29] This leads to differences in the degrees of linearity and a large range of bond angles. Owing to its strength, directionality and readily accessible donor motifs, HB has proven to be the most common universal non-covalent interaction responsible for a variety of important biological and chemical phenomena such as affording stability to various proteins[30] as well as accounting for the unique physical properties of water.[31] Biological examples include complementary HB interactions between nucleotide base pairs in DNA[32] and sulphate[33] and phosphate oxoanion selective binding proteins[34] in bacteria (Figure 1.3).

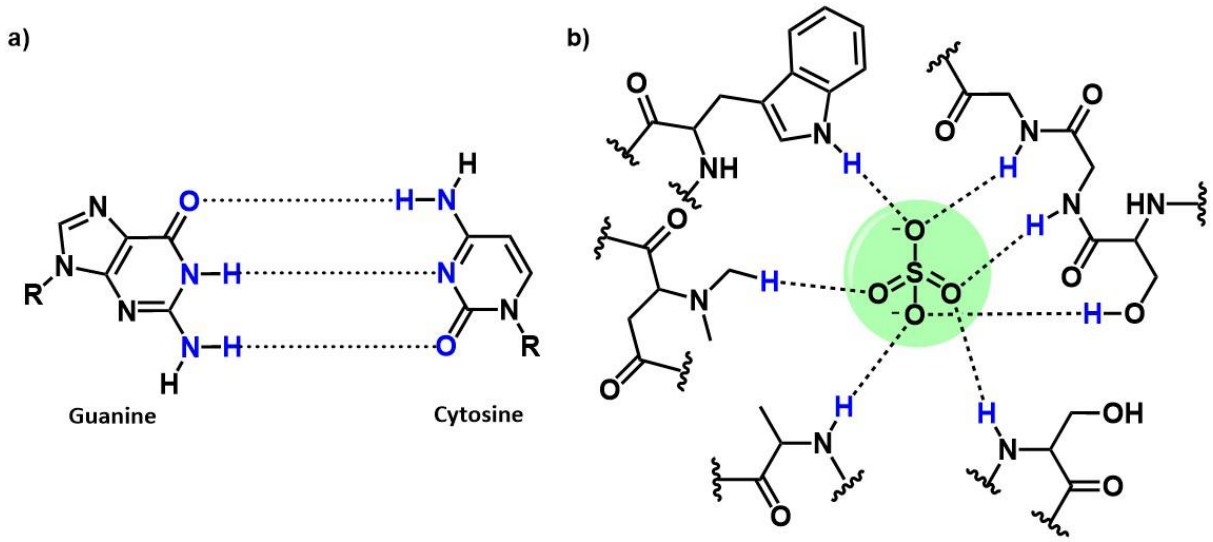


Figure 1.3. *a) Nucleotide guanine and cytosine base pair hydrogen bond formation[32] b) Convergent hydrogen bonding interactions in the anion binding pocket of sulphate binding protein (SBP) of Salmonella typhimurium.[33]*

1.2.3 Halogen bonding

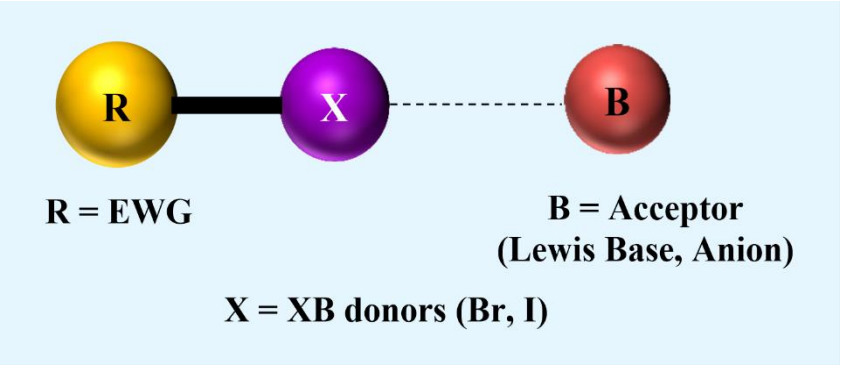


Figure 1.4. *Representation of a XB-interaction with a Lewis base (R = electron withdrawing groups, X=Cl, Br, I; B = Lewis base)*

A halogen bond is analogous to a hydrogen bond. The interaction is generally denoted as R-X···B, where X is a polarisable halogen atom, typically iodine, covalently attached to an electron-withdrawing group R and B is a Lewis base (Figure 1.4). The electron withdrawing group (R) causes an anisotropic distribution of the electron density of the halogen atom, creating a small region of localised, partial positive charge at the pole of halogen atom known as a sigma-hole.[35] Electrostatic surface potentials represent the electron density across the halogen atoms, where red surfaces highlight the regions of electron-deficient density wherein the halogen atom interacts with a Lewis base (Figure 1.5).[36]

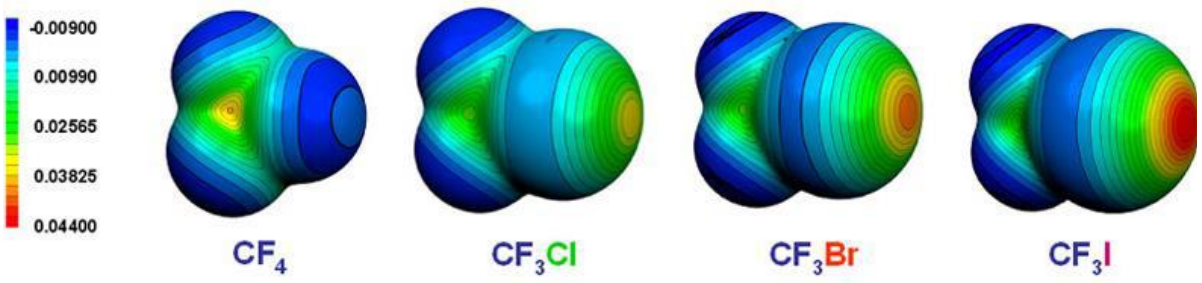


Figure 1.5. *Electrostatic surface potentials (adapted from[35,36])*

Consequently, halogen bonding (XB) interactions are highly directional, with the R-X···B bond angle close to 180°.[37] XB donor atoms are intrinsically more hydrophobic, aiding the desolvation of XB hosts in polar solvent media, which in particular benefits anion

recognition.[38] The strength of XB interactions are comparable to HB interactions (10-200 KJ/mol) and are enhanced with increasing the polarizability of the donor X atom (I>Br) or by using a more electronegative R group (sp> sp^2> sp^3).[39]

Similar sigma-hole formation is also observed in atoms belonging to other groups in the p-block when bonded to an electronegative atom. Like XB systems they too are capable of interacting with Lewis bases and are named after the groups they belong to such as chalcogen bonding (ChB)[40] for group 16, pnictogen bonding[41] for group 15 and tetral bonding[42] for group 14 elements.

1.2.4 Hydrophobic interactions

Hydrophobic interactions are the attractive forces between non-polar molecules in the presence of water. They are the key driving force in the formation and stability of various biological structures such as folding of proteins and formation of cell membranes.[43,44] They occur when, due to a difference in polarity, water molecules form a cage-like structure around the non-polar molecules forcing them to cluster together and interact to form micelles, lipid bilayers and other self-organised structures. This congregation of non-polar molecules is usually a consequence of an increase in entropy achieved upon exclusion of water molecules by the host systems (Classical Hydrophobic Effect).[45] However, recent reports citing enthalpic contributions as the major driving force behind these interactions have also been gaining interest (Non-classical Hydrophobic Effect).[46]

1.2.5 Ion-π interactions

Non-covalent interactions that arise from aromatic π-effects can be classified into cation-π and anion-π interactions. Cation-π interactions occur between a positively charged cation and

a π-electron cloud associated with an electron-rich aromatic system.[47] The strength of cation-π interactions is typically in the range of 10-50 kJ/mol and can be modulated by varying the size/charge density of the cation or aromatic unit as well as by changing the distance between the cation and the π-cloud.[48] They play a crucial role in various biological processes including protein-ligand binding (Figure 1.6a) and protein-protein interactions.[49,50]

Anion-π interactions arise as a result of electrostatic attractions between an anion and the π-delocalised electron density of an electron-deficient aromatic ring.[51] They are maximised with small anions in non-polar solvents enabling close proximity to the aromatic rings.[52] On account of being relatively weak (4-40 kJ/mol), these interactions are usually found in concert with other stronger interactions. Some well-known electron-deficient ring systems such as triazenes,[53] naphthalamide diamides (NDI)[54] and perfluoroarenes[55] have proven to serve as effective motifs for such interactions (Figure 1.6b).

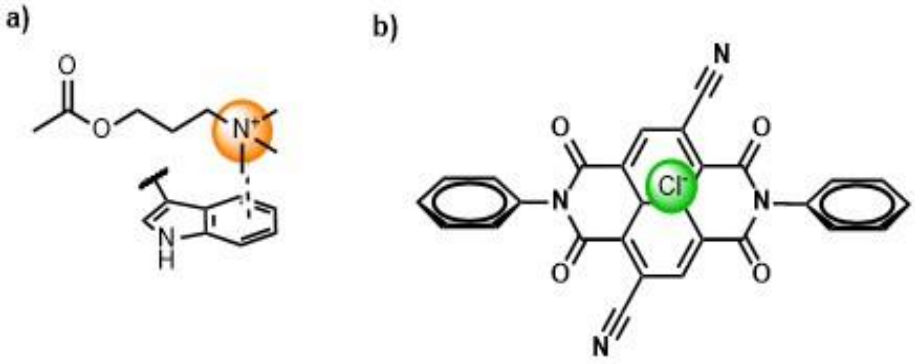


Figure 1.6. *a) Positively charged acetylcholine binding to a tryptophan residue,[56] b) Chloride interacting with an NDI unit.[54,57]*

1.3 Anion recognition

1.3.1 The importance of anion recognition

The pervasiveness of anions in almost every aspect of nature is evident from the fundamental roles they play in biological, medical, environmental, and industrial processes.[58-60] In biotic

systems, the majority of biomolecules are negatively charged and exist as polyanions under physiological conditions. These include genetically coded nucleic acids like DNA, RNA and energy building blocks like ATP.[61] The phagocytes in the immune system also produce highly-reactive superoxides as an oxidative protective mechanism against invading antigens.[62] Chloride is imperative for maintaining pH balance and blood-pressure within the body, and its mis-regulation can result in severe physiological diseases like cystic fibrosis and Alzheimer's disease.[63,64] Iodide plays an important role in the thyroid gland synthesising tyrosine-based hormones. Consequently, its deficiency has been one of the leading causes of thyroid cancer.[65] Additionally, anions can also participate in various chemical processes as catalysts as well as serve as key components in precipitation reactions, acid-base condensations and redox reactions.[66-68] Anion-based salt solubility and reactivity can be manipulated to effectively precipitate out precious materials or impurities.[69,70] For example, sulphates can form insoluble salts with metals mediating the extraction of heavy metals from wastewater.[71]

In the environment, anions play crucial roles in nutrient recycling and atmospheric chemistry. Anion concentrations are often used to monitor the health of ecosystems and detect environmental pollutants.[72] While nitrates and phosphates are key elements in fertilizers, their overuse disrupts aquatic wildlife ecosystems by causing eutrophication in lakes and rivers.[73] An excess of nitrates and sulphates in the air can aggravate problems such as global warming and acid rain.[74] Anions also play key roles in various industrial processes like wastewater treatment, mineral processing and chemical synthesis. However, industrial and manufacturing wastes if not disposed-of properly can lead to an accumulation of nitrates and perchlorates in soil water, poisoning the food source.[75-77] Transition metal oxoanions such as pertechnetate TcO_4^- from nuclear fuel reprocessing and manufacturing processes are highly dangerous and hazardous leaving behind radioactive residues for centuries.[78] Hence,

the need and importance of understanding the fundamental principles of anion recognition for developing host systems to help mitigate all the above anthropogenic problems cannot be overstated.

1.3.2 The challenges of anion recognition

Anions possess several intrinsic properties which make their recognition a formidable task. They exhibit a diverse range of geometries, ranging from simple spherical halides and trigonal planar anions like acetate, nitrate and carbonates to tetrahedral sulfates and octahedral transition metal complex anions (Figure 1.7). Moreover, biological anions such as dicarboxylates and nucleotide polyanions require intricate host receptor design for optimal shape and size complementarity. Even though this aspect opens up attractive avenues for selective host-cavity design, it is often synthetically demanding.[79]

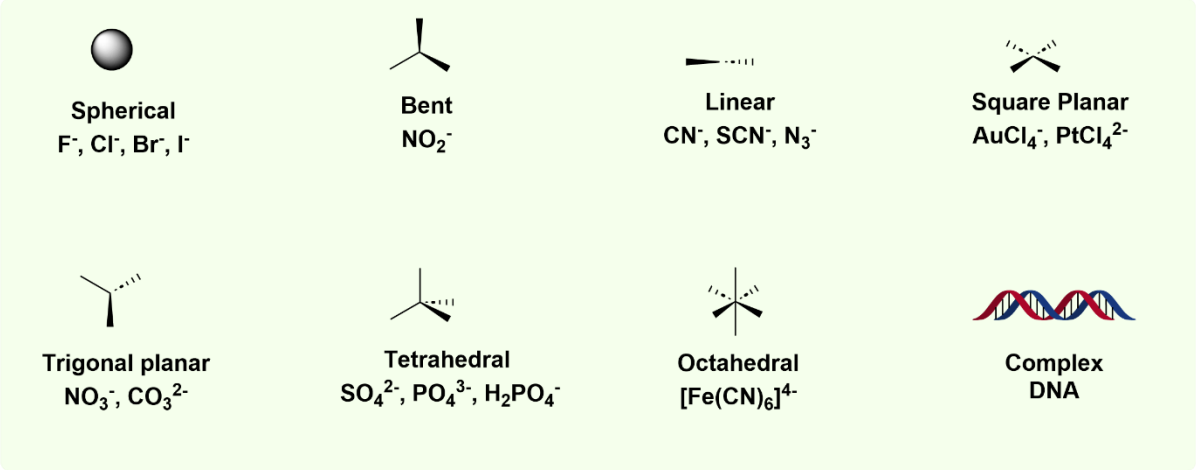


Figure 1.7. *Basic anion geometries*

Compared to isoelectronic cations, anions are larger in size thereby possessing a lower charge-to-size ratio than their cationic counterparts (Table 1.1). Consequently, they exhibit weaker electrostatic and ion-dipole interactions, potentially decreasing the affinity of a

receptor.[80] However, their larger size makes them highly polarisable, allowing favourable dispersion forces to have a greater effect in anion recognition.[81]

Table 1.1: *Ionic radii and free energies of hydration for anions and cations* [19,20]

Anion	Ionic radius (Å)	$\Delta G_{hydration}$ (kJ mol^{-1})	Cation	Ionic radius (Å)	$\Delta G_{hydration}$ (kJ mol^{-1})
F^-	1.33	-465	**Na^+**	1.02	-365
Cl^-	1.81	-340	**K^+**	1.38	-295
Br^-	1.96	-315	**Rb^+**	1.52	-
I^-	2.20	-275	**Cs^+**	1.67	-250

Many anions are also pH dependent, only existing within a certain pH window. Oxoanions such as phosphate for example, can exhibit multiple protonated species at a given pH value.[82] Polyammonium-based anion host systems are also pH dependent and as a consequence can only function within a narrow pH window, where the host remains

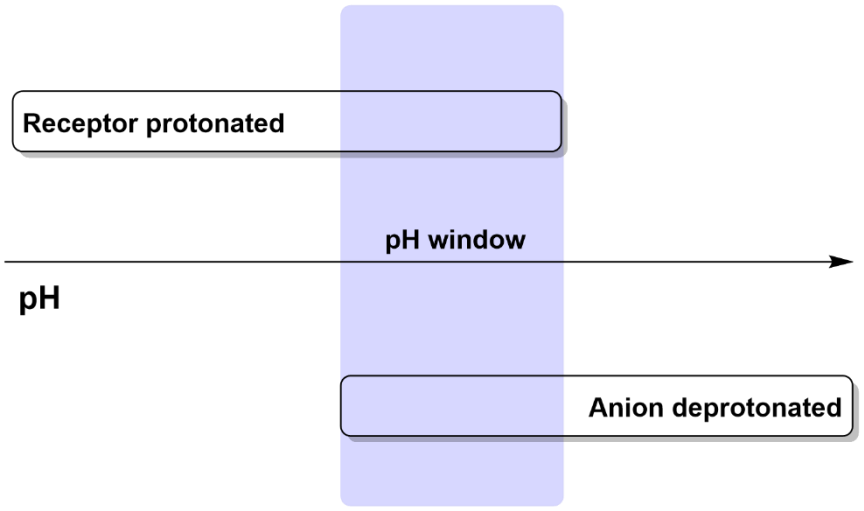


Figure 1.8. *Schematic illustration of the pH window in which anion recognition by a pH-dependent receptor may occur.*

protonated and the anion guest is present (Figure 1.8).[83,84] Moreover, highly basic anions like fluoride and cyanide commonly de-protonate acidic amide NH donor receptors in polar organic media like DMSO.[85,86]

Finally, anions exhibit higher free energies of solvation compared to cations of a similar size (Table 1.1) requiring them to overcome a greater de-solvation barrier in protic and aqueous solvent media.[87] Hence, the nature of the solvent plays an important role in anion binding affinity and selectivity. The Hofmeister series classifies anions of a given charge according to their hydrophobicity (Figure 1.9).[88] Smaller (hard) anions with a higher charge density such as fluoride are more heavily solvated compared to larger (soft) anions like iodide. This is due to hard anions generally stabilizing water-water interactions resulting in aggregation of hydrophilic molecules in solution, meanwhile softer anions have the tendency to disrupt water-water interactions thereby impeding hydration. In general, highly positively charged hosts have been employed for anion recognition in competitive protic media, whereas neutral host systems are primarily designed to function in aprotic organic solvents.

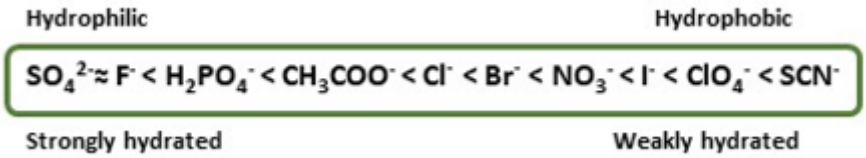


Figure 1.9. *Hofmeister series.*[88]

1.3.3 Receptors for anion recognition: Biotic/Natural receptors

The ubiquity of anions has promulgated nature's evolution of naturally occurring receptor proteins to bind anions with high selectivity and strength. A couple of well-known examples include the sulphate[33] and phosphate[34] binding proteins found in bacteria for the purpose of anion transport (Figure 1.10). Both proteins bind the oxoanion guest species with high

selectivity owing to convergent hydrogen bonding motifs completely encapsulating the anion at the recognition site. Single crystal XRD studies reveal that the sulphate binding protein makes use of seven hydrogen bonds contributed by five peptide NH groups, one serine OH and a NH donor from a tryptophan unit to stabilize the sulphate ion (K_a = 8.3 x 10^6 M^{-1}).[89] On the other hand, the phosphate binding protein employs twelve hydrogen bonds to achieve hydrogen phosphate recognition which are contributed by nine neutral peptide NH donors, two positively charged guanidinium motifs of the Arg-135 residue and one negatively charged carboxylate HB acceptor unit in Asp-56.[90] The negatively charged Asp-56 residue plays an important role in driving selectivity, as confirmed by the lower binding affinities obtained for a completely deprotonated anion such as sulphate. Such naturally occurring extensive protein networks capable of binding complex anions *via* complete encapsulation are still beyond the scope of synthetic chemists. However, they continue to serve as inspirations behind synthetic receptor design.

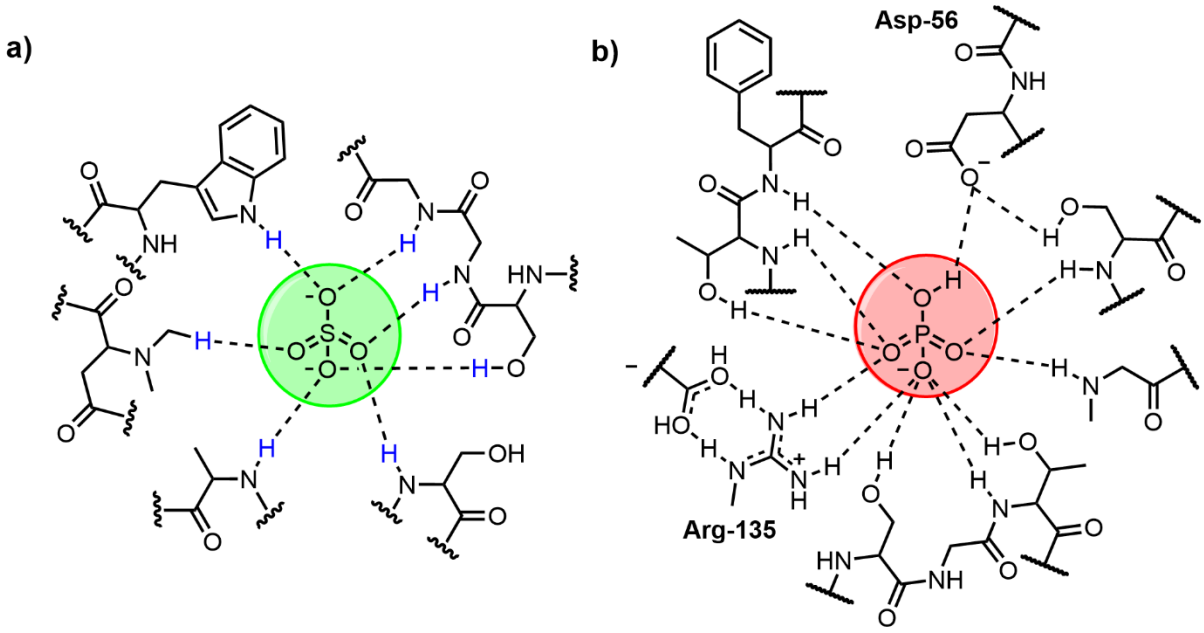


Figure 1.10. *Schematic representation of the array of hydrogen bonds which bind the anion in (a) sulfate[33] and (b) phosphate-binding proteins.[34]*

1.3.4 Receptors for anion recognition: Synthetic receptors

Mimicking the strategies employed by naturally occurring receptors for host-guest recognition have long since influenced synthetic host design. Successful approaches to guest recognition have focused on using the supramolecular host design principles of complementarity,[91] preorganization[92] and the macrocyclic effect[93] to maximise host-guest interactions. Hydrogen bonding has primarily been the non-covalent interaction of choice in synthetic anion design, while in more recent years sigma hole interactions like halogen bonding have proven to enhance the strength and selectivity of anion recognition. Categorised by the non-covalent interaction employed, the following section gives a brief overview of various synthetic anion receptors.

1.3.4.1 Hydrogen bonding receptors

Over the years, the popularity of hydrogen bonding receptors has exponentially increased owing to the HB's strength, directionality and increasing library of readily accessible donor motifs, making it the most universal non-covalent interaction responsible for a variety of important biological and chemical phenomena. Positively charged and neutral HB receptors that utilise N-H donors have dominated the anion recognition field, although C-H based HB donors have also emerged as suitable receptors especially for hydrophobic anions in the recent years.

1.3.4.1.1 Cationic HB receptors

1.3.4.1.1.1 N-H based polyammonium and guanidinium receptors

Positively charged hosts have been frequently used to enhance anion association and selectivity, especially in highly competitive polar protic solvents like water and methanol.

Polyammonium based receptors are the most established hosts to bind anions in aqueous solutions. Early examples include the pioneering work on polyammonium cages for halide recognition by Park and Simmons (Figure 1.11a)[94] and Lehn's polyammonium cryptand (Figure 1.11b)[95] capable of binding the fluoride anion with high affinity and selectivity in aqueous media under acidic conditions (log K_a = 10.6).

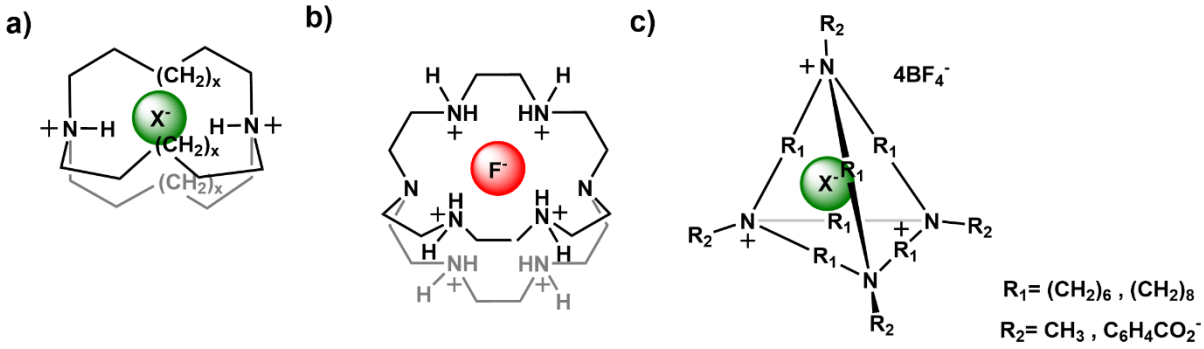


Figure 1.11. *a) Park and Simmon's katapinand receptor[94] b) Lehn's polyammonium cryptand[95] c) Schmidtchen's quaternary ammonium cages[96]*

In order to circumvent the narrow pH window in which these ammonium-based receptors operate, Schmidtchen came up with pH independent quaternary ammonium cages in 1977, wherein the cages bound halides and oxoanions in water and methanol *via* hydrophobic and electrostatic interactions only (Figure 1.11c).[96] Moreover, through zwitterionic functionalisation the neutral cage systems were able to mitigate the competitive

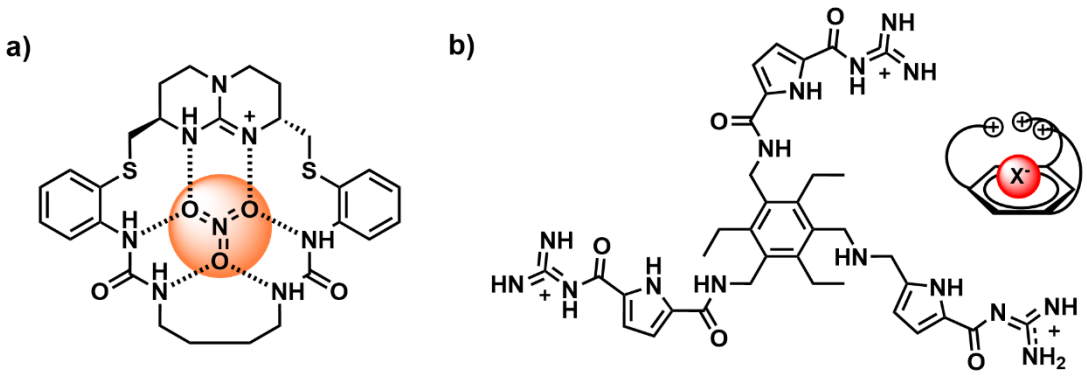


Figure 1.12. *a) Mendoza's tris-guanidinium macrocycle[97] b) Schmuck's tripodal guanidinium-carbonylpyrrole-based receptor.[98]*

effect of counter-anions, resulting in a 13-fold enhancement in chloride binding affinity (K_a = 2.7 x 10^2 M^{-1}) in water.

Due to their inherent ability to remain protonated across a wide pH range (pKa = 13.6), guanidinium motifs have also proven to be excellent HB donor motifs. For example, Mendoza's tris-guanidinium macrocycle strongly binds nitrate (K_a = 9.9 x 10^3) in acetonitrile *via* hydrogen bonds contributed by guanidium and urea moieties (Figure 1.12a).[97] Another striking example is Schmuck's tripodal guanidinium-carbonylpyrrole-based receptor which binds citrate selectively over other anions such as trifluoroacetate, chloride, tartrates and maleates in water, with impressively high binding affinities (K_a > 10^5 M^{-1}) (Figure 1.12b).[98] This is ascribed to dominating electrostatic interactions and charge complementarity.

1.3.4.1.1.2 C-H based imidazolium and triazolium receptors

The first example of an imidazolium-based acyclic receptor was reported by Sato and co-workers who made use of three convergent imidazolium motifs to bind halides in CD_3CN (Figure 1.13a).[99] Strong binding was achieved *via* a combination of C-H mediated hydrogen bonding and electrostatic interactions. Since then, numerous imidazolium-based receptors

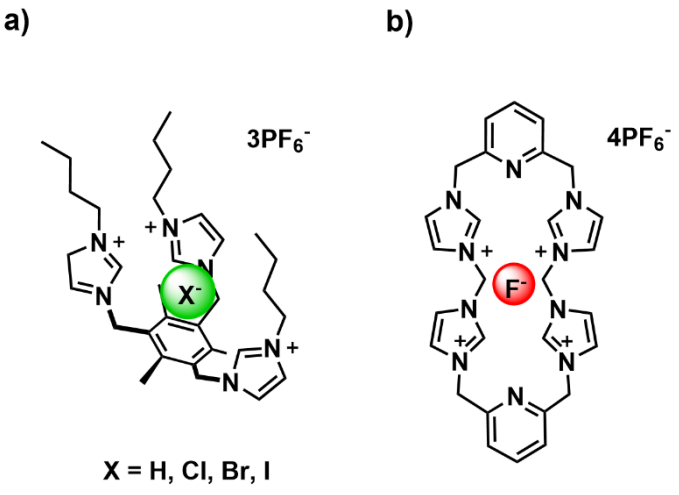


Figure 1.13. *a) Sato's imidazolium receptor[99] b) Kim's calix[4]imidazolium[2]pyridine fluoride receptor[100]*

have been reported including Kim's calix[4]imidazolium[2]pyridine macrocyclic receptor capable of strong and selective binding of fluoride (*Ka* = 28,900 M^{-1}) in competitive solvents like DMSO and acetonitrile, a result confirmed by ^{1}H NMR binding studies and single-crystal XRD data which showed all imidazolium motifs concertedly binding the fluoride anion (Figure 1.13b).[100]

Over recent years, triazole motifs have gained a lot of popularity owing to their relatively easy synthesis and incorporation into various structural host frameworks.[118,119] While they have been reported to show good binding capabilities in aprotic solvents as neutral receptors, further amplification of their binding abilities can be achieved by N-alkylation to form the cationic triazolium motif. An impressive example is Sessler's pyrrole-based triazolium-phane prepared *via* tetra-alkylation of a macrocycle originally synthesised using click chemistry (Figure 1.14).[101] ^{1}H NMR anion binding studies reveal that the receptor binds anions through charge assisted triazolium C-H and neutral N-H pyrrole HB interactions, exhibiting high affinities for oxoanions like HSO_4^-, $H_2PO_4^-$, and $HP_2O_7^{3-}$ (K_a = 9.88 ± 1.18 × 10^6) in methanol, a result further corroborated by single crystal XRD studies.

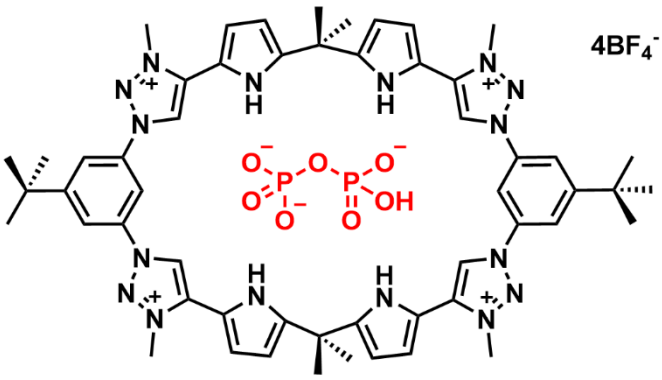


Figure 1.14. *Sessler's pyrrole-based triazolium-phane.*[101]

1.3.4.1.2 Neutral HB receptors

Compared to positively charged HB host systems, neutral HB receptors generally exhibit weaker intermolecular interactions with anions and are primarily designed to function in less competitive organic solvents.

1.3.4.1.2.1 N-H based amide, thioamide, urea, thiourea and pyrrole receptors

Attempts to emulate the naturally occurring sulphate binding protein found in bacteria such salmonella typhimurium led to the first amide-based HB receptor published in 1986 by Pascal and co-workers consisting of a cage-like structure capable of binding fluoride in d_6-DMSO (Figure 1.15a).[102] In the years that followed, a range of amide, urea, thiourea and squaramide HB donor motifs were incorporated into various acyclic and macrocyclic structures. Kubik's cyclo-peptide 'molecular oyster' receptor, which forms sandwich-like anion complexes using convergent HB interactions is a striking example of a neutral preorganised host impressively capable of binding iodide (K_{11} = 96 M^{-1}, K_{12} = 1270 M^{-1}) and sulphate (K_{11} = 24 M^{-1}, K_{12} = 6660 M^{-1}) ions in water/methanol 95:5 v/v solutions (Figure 1.15b).[103]

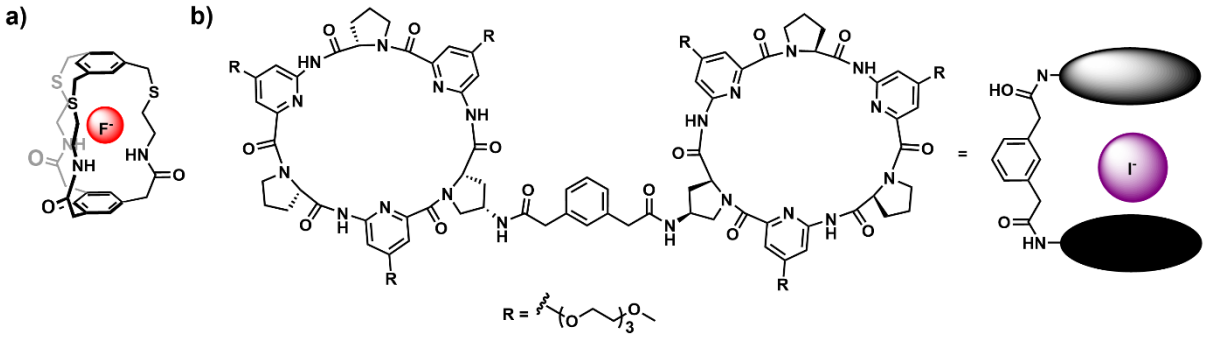


Figure 1.15. *a) Pascal's neutral amide cage-like receptor[102] b) Kubik's cyclo-peptide 'molecular oyster' receptor[103]*

Over the years, numerous urea and thio-urea based motifs have been employed to bind oxoanions, especially carboxylates due to their unique orientation and tuneable hydrogen bonding capabilities. A notable example of urea- and thiourea-based receptors

include Gale's macrocyclic host which displays remarkable acetate binding affinity (K_a = 5170 M^{-1}) in 95:5 DMSO:H_2O solvent media (Figure 1.16a).[104] Another example is Reinhoudt's

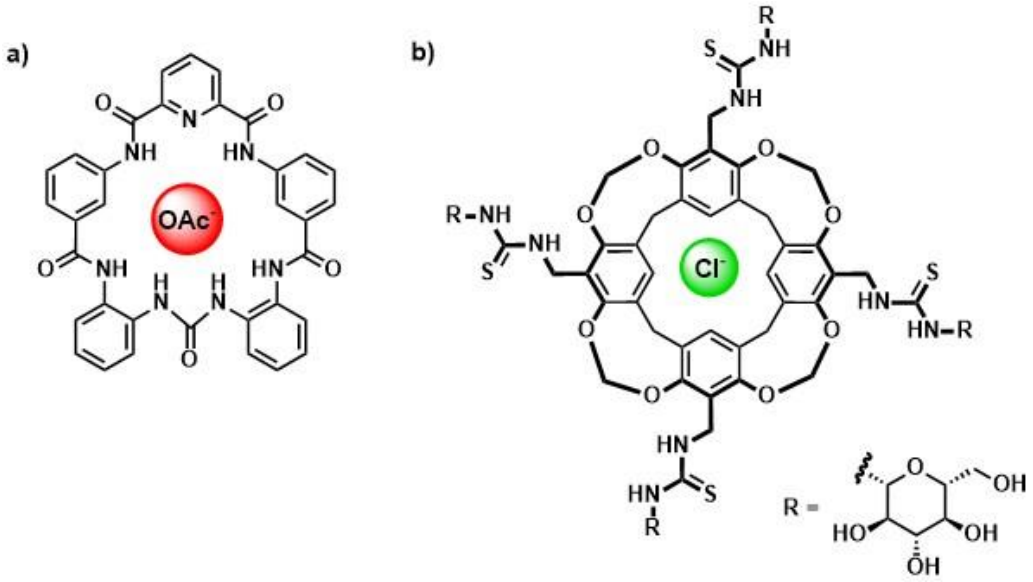


Figure 1.16. *a) Gale's amide and urea-based macrocyclic acetate receptor[104] b) Reinhoudt's thiourea-based cavitand.[105]*

thiourea-based cavitand host systems which demonstrated chloride selectivity (K_a = 1.5 x 10^4 M^{-1}) in 1:1 CH_3CN/H_2O solvent media upon (Figure 1.16b).[105] By conducting a series of ESI-MS titration studies and ITC experiments in CH_3CN/H_2O mixtures, the authors reported that the cavitand hosts bound anions in the following order of binding affinity: $Cl^->HSO_4^->NO_3^->Br^->I^->ClO_4^-$.

Squaramides are another class of neutral HB receptors that have rapidly gained interest owing to their unique chemical properties. They possess an aromatic ring-like structure with preorganised NH donors making them relatively more potent anion receptors than urea and thio-urea analogues (Figure 1.17).[106] These properties, as well as having HB acceptor capability *via* the carbonyl groups, has made them useful motifs across a wide variety of chemical and biological fields including bioconjugate chemistry, material science,

medicinal chemistry, molecular recognition, organometallic chemistry and organocatalysis.[107-112]

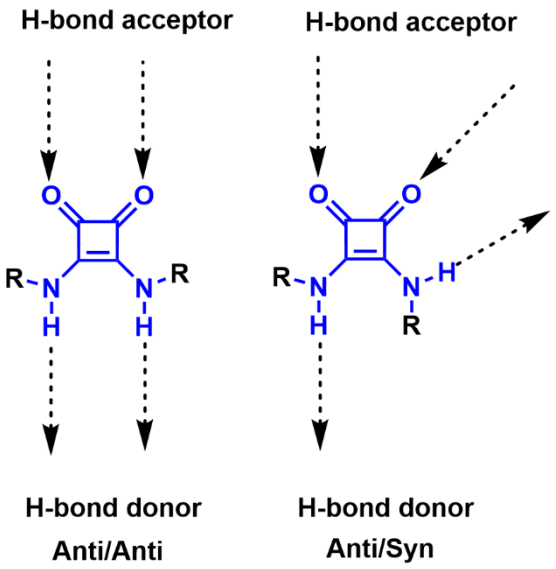


Figure 1.17. *Representations of the anti/anti- and anti/syn-conformations of bis-secondary squaramides.*

When integrated into acyclic and macrocyclic structural host frameworks squaramides have gained prominence as anion receptors even in highly polar organic and aqueous media.[113] The first example of a squaramide moiety being used in anion receptor design was reported by Costa and co-workers, wherein an acyclic receptor possessing pseudo-C_3

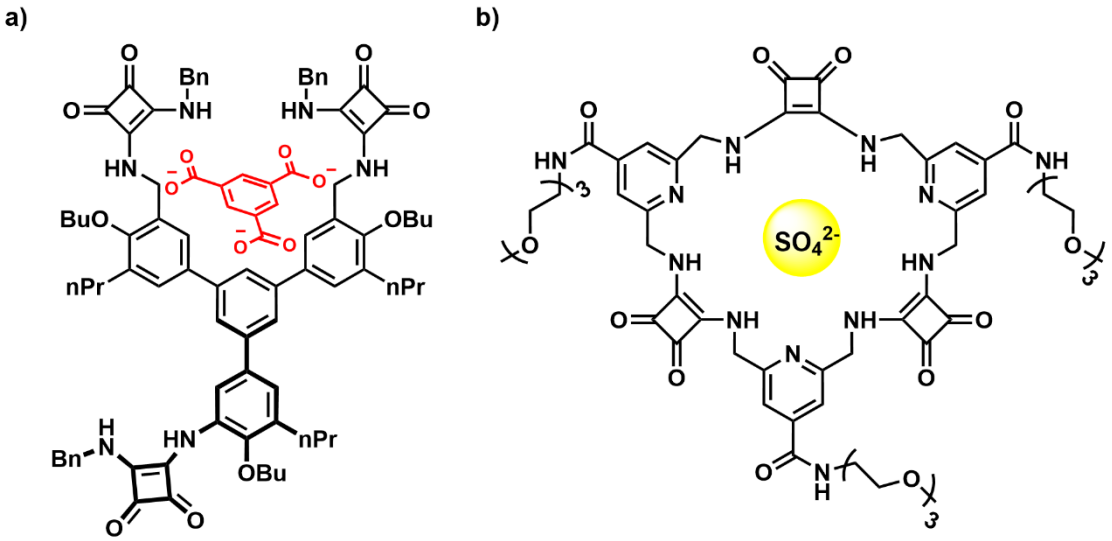


Figure 1.18. *a) Costa's neutral tricarboxylate detector[114] b) Qin's squaramide-based water-soluble macrocyclic receptors.[115]*

symmetry and composed of three squaramide moieties bound tricarboxylate ions (K_a = 7.7± 1.3 x 10^3 M^{-1}) in aqueous solutions (Figure 1.18a).[114] A recent report by Qin *et al.* detailed the synthesis of a family of water soluble macrocyclic squaramide-based anion receptors displaying a strong affinity for sulphate ions (K_a > 10^4 M^{-1}) in aqueous-DMSO mixtures across a wide pH range (3.2–14.1), making them potential candidates for plasma sulphate assays and sulphate extraction from nuclear waste (Figure 1.18b).[115]

More recently, Frontera, Morey and Anslyn reported a squaramide-functionalised quaternary ammonium tripodal receptor whose recognition properties towards a variety of aliphatic and aromatic carboxylate anions were studied using ITC experiments in competitive solvent media (3:1 EtOH/ H_2O) (Figure 1.19).[116] Association constants as high as 10^4-10^5 M^{-1} were obtained with a variety of tricarboxylate anions.

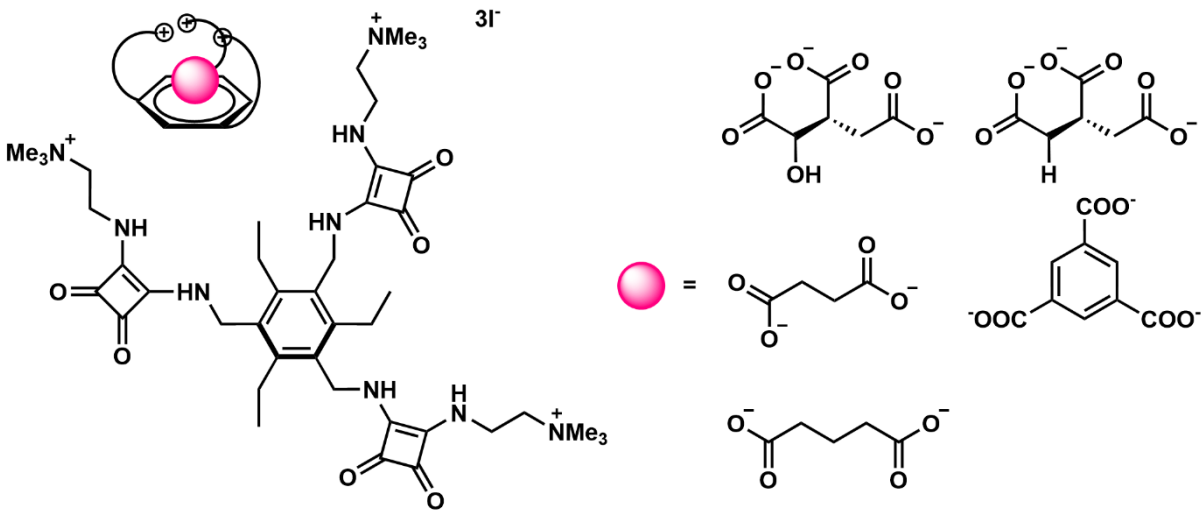


Figure 1.19. *Frontera, Morey and Anslyn's squaramide-functionalised quaternary ammonium tripodal receptor.*[116]

Aside from amide-based receptors, pyrroles are another class of HB donor motifs that have come up as valuable receptors in anion supramolecular chemistry. In 1996 Sessler and co-workers introduced the first calix[4]pyrrole system capable of strongly binding anions like fluoride (K_a = 1 x 10^4 M^{-1}) and phosphate (K_a = 1300 M^{-1}) in acetonitrile (Figure 1.20a).[117]

Since then, numerous examples of pyrrole-functionalised macrocycles have appeared in the literature including Kim and Sessler's strapped calix[4]pyrroles serving as neutral receptors for the linear azide anion in acetonitrile (Figure 1.20b).[118] Appending the pyrrole and naphtho-bipyrrole straps resulted in binding affinities two orders of magnitude higher than those obtained with the unfunctionalized calix[4]pyrrole macrocycle presumably due the additional N-H HB donors.

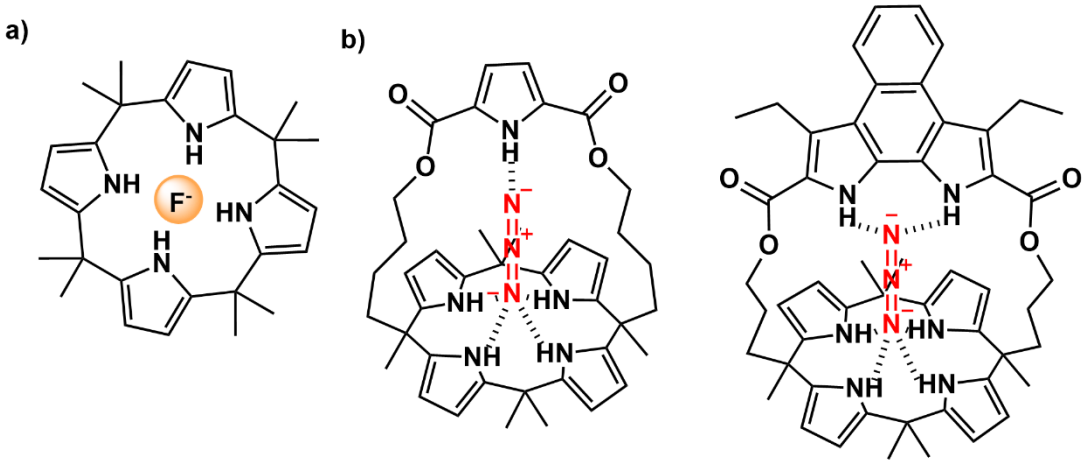


Figure 1.20. *a) Sessler's seminal calix-[4]pyrrole receptor[117] b) Kim and Sessler's strapped calix-[4]pyrrole azide receptors.[118]*

1.3.4.1.2.2 C-H based triazole receptors

As a consequence of their facile preparation using copper(I) catalysed 'click' alkyne-azide cycloaddition (CuAAC) synthetic methodology, triazoles have emerged as effective C-H mediated HB donors for anion recognition in a variety of aprotic and protic solvents. In a seminal publication, Flood and co-workers' described a preorganised macrocyclic tetrakis-triazole receptor which exhibits impressive chloride selectivity in DCM (K_a = 1.1 x 10^7 M^{-1}) (Figure 1.21a).[119] More recently, they also reported a triazole-functionalised cryptand-like cage receptor, wherein the 3-D triazole-directed C-H hydrogen bonding interactions in combination with the cryptand effect led to remarkably high binding constants (K_a = 10^8 M^{-1} for Cl^-) in DMSO (Figure 1.21b).[120] In addition to successfully extracting alkali metal chloride

salts from water into DCM, the cryptand was also able to inhibit brine-accelerated surface corrosion when coated onto mild-steel.

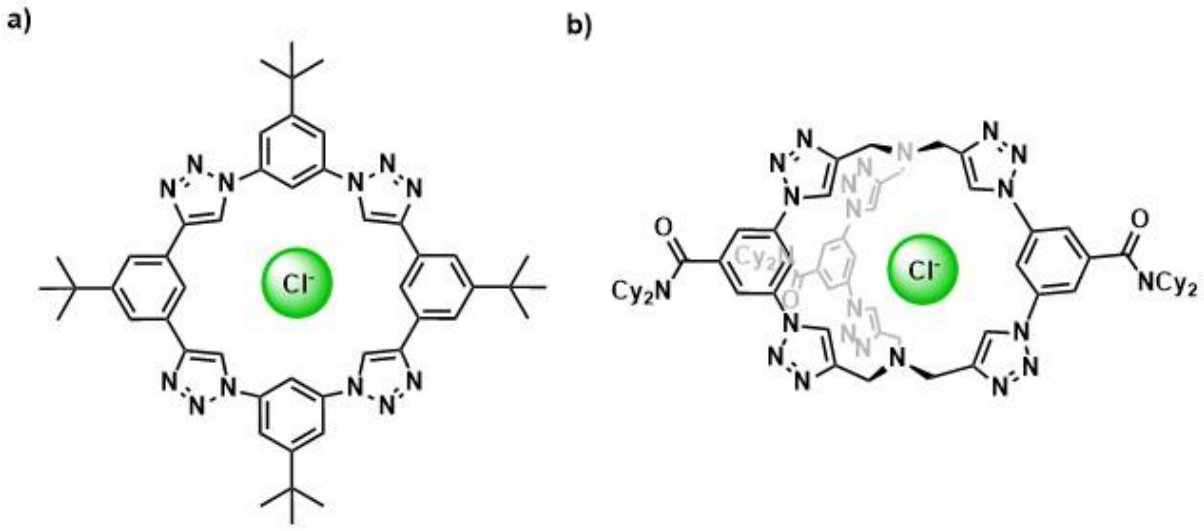


Figure 1.21. *a) Flood's macrocyclic tetrakis-triazole receptor[119] b) Flood's chloride binding cryptand cage-like receptor.[120]*

1.3.4.2 Halogen bonding receptors

Compared to hydrogen bonding, halogen bonding anion recognition still remains a relatively undeveloped field despite the numerous recent reports of XB host systems proving to be superior receptors than their HB analogues, particularly in highly polar solvent media, including aqueous solutions.

Akin to HB receptors, XB receptors can be classified into neutral receptors containing haloperfluoroarenes, halotriazoles and haloimidazoles, and positively charged XB assisted

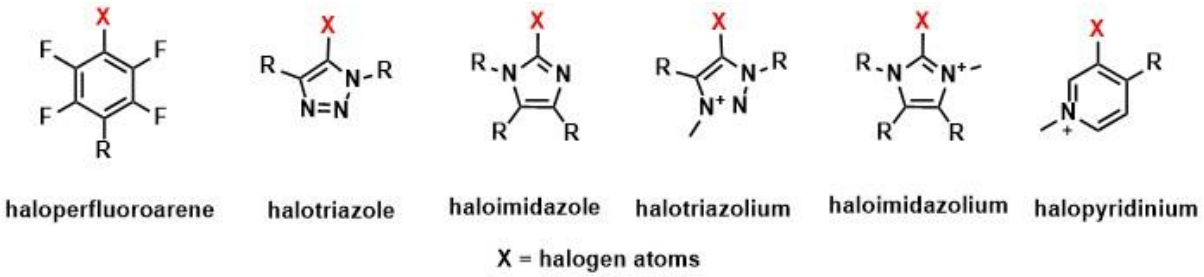


Figure 1.22. *Neutral and positively charged halogen bonding motifs for anion recognition.[121]*

receptors consisting of halotriazolium, haloimidazolium and halopyridinium motifs (Figure 1.22).[121]

1.3.4.2.1 Neutral XB receptors

Following Taylor's seminal work on tridentate iodoperfluorobenzene hosts capable of remarkably high chloride affinity (K_a = 1.9 x 10^4 M^{-1}) in d_6-acetone (Figure 1.23a),[122] halotriazoles have become a frequently used neutral XB donor motif due to their synthetic accessibility propelling their incorporation into various acyclic and macrocyclic structures. Beer and co-workers reported the first tetradentate XB iodo-triazole foldamer which exhibited a preference for heavier halides over acetate and dihydrogen phosphate in $CDCl_3$ (Figure 1.23b).[123] Importantly, the XB foldamer showed stronger association for all anions compared to its HB analogue highlighting the advantages of XB-functionalised receptor systems. Another notable example is Schubert's cleft-like receptors with varying spacer units

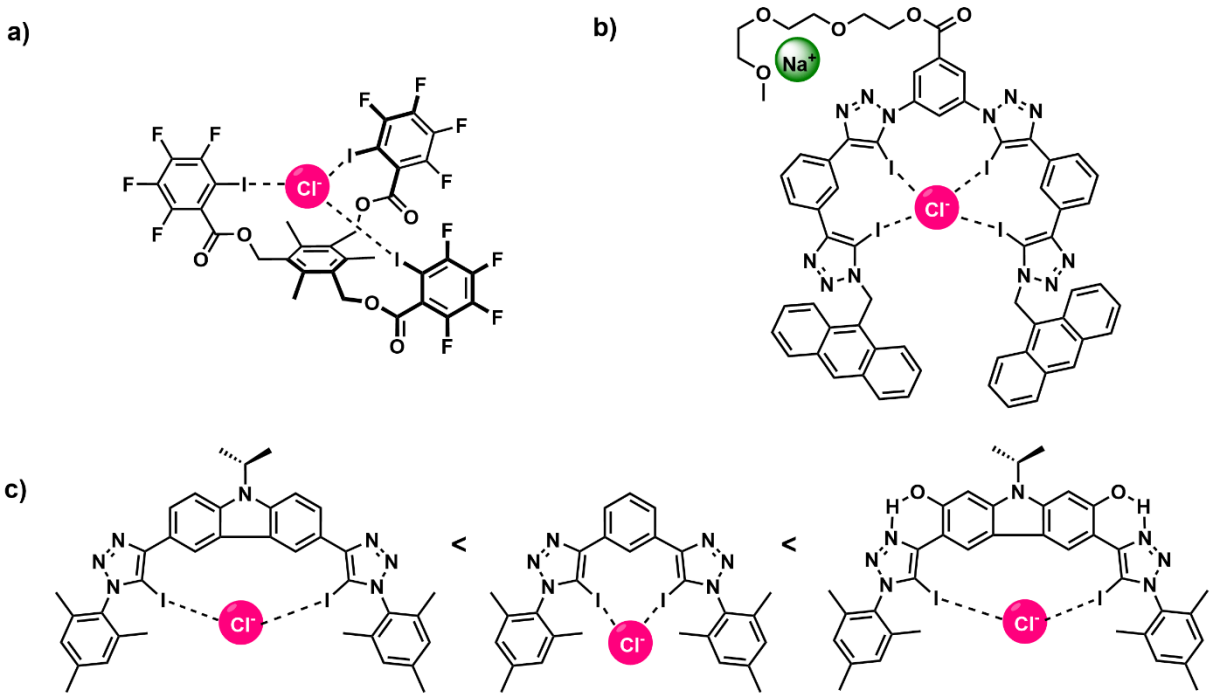


Figure 1.23. *a) Taylor's tridentate iodo-perfluorobenzene hosts[122] b) Beer's tetradentate XB foldamer[123] c) Schubert's cleft-like XB receptors.[124]*

between two iodotriazole XB donors (Figure 1.23c).[124] From ^{1}H NMR halide titration experiments and single crystal XRD studies, the authors analysed the effect of preorganised intramolecular carbazole hydroxyl-triazole interactions on the resulting bidentate XB chelating abilities of the receptors which were significantly enhanced for the hydroxy derivative owing to favourable preorganisation of the halogen donors due to conformationally restricted triazole units.

1.3.4.2.2 Positively charged halogen bonding receptors

Positively charge assisted XB receptors have the ability to enhance anion recognition, enabling strong XB-mediated binding in highly polar systems. Attaching an iodine halogen atom directly to a pyridinium motif has led to a potent class of charged XB systems. An excellent example is Berryman's acyclic XB bis-iodo-pyridinium receptor which exhibits strong perrhenate (ReO_4^-) binding (K_a = 8990 M^{-1}) in a 3:2 $CDCl_3$/ d_6-acetone solvent mixture (Figure 1.24a).[125] Alternatively, covalently linking the iodotriazole group to a pyridinium motif has

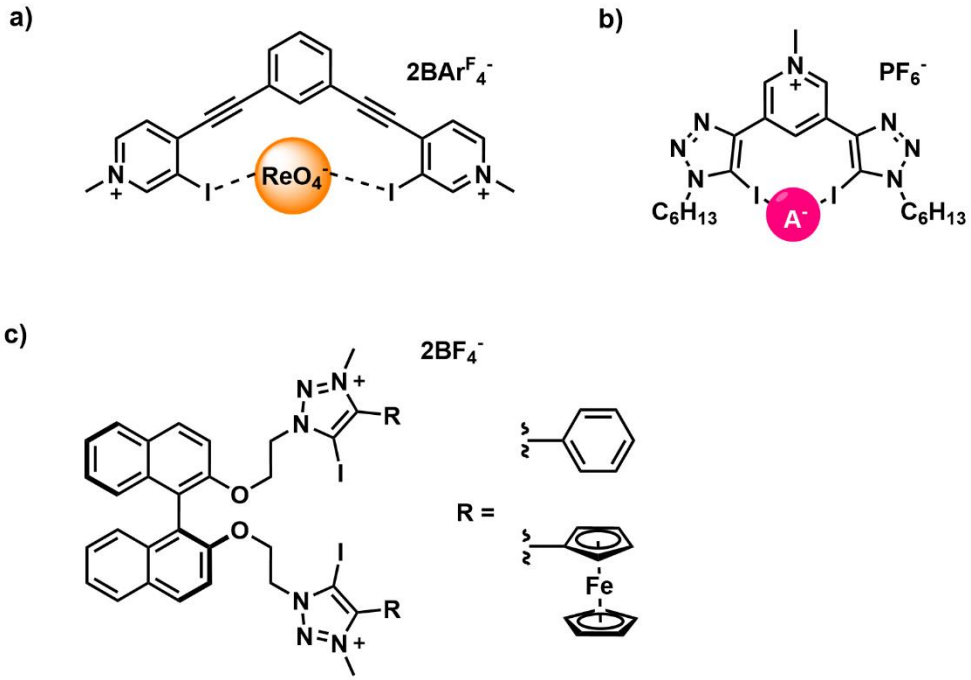


Figure 1.24. *a) Berryman's iodinated pyridinium receptor[125] b) Beer's iodo-triazole appended pyridinium receptor[126] c) Molina's BINOL bis-iodotriazolium receptor.[127]*

also generated powerful receptors as seen in Beer's bidentate acyclic receptor which displays a preference for acetate over halides in d_6-DMSO (Figure 1.24b).[126]

Direct alkylation of iodotriazole motifs produces even more potent cationic XB iodotriazolium donors. Molina and co-workers designed 1-1'-bi-2-naphthol (BINOL) bis-iodotriazolium receptors capable of binding oxoanions such as $HP_2O_7^{3-}$, $H_2PO_4^-$, and SO_4^{2-} (K_a > 10^3 M^{-1}) in competitive 9:1 CD_3CN/CD_3OD solvent media (Figure 1.24c).[127]

1.3.5 Anion sensing

The incorporation of reporter groups into anion host structural frameworks has led to potential anion sensor systems with the capability of detecting the anion recognition event *via* a macroscopic optical or electrochemical response. This section will detail these two types of anion sensors that have gained popularity in the field of anion sensing and the principles they are based on.

1.3.5.1 Optical sensors

Optical anion sensors are one of the most common types of anion sensors known. Based on their mode of signalling, these sensors can be classified into two major groups: fluorescent and colorimetric anion sensors.

1.3.5.1.1 Fluorescent/luminescent anion sensors

Fluorescent sensors are highly sensitive systems enabling anion detection at sub-micromolar concentrations. Commonly employed organic fluorophores include pyrenes, anthracenes and BODIPY dyes. Gunnlaugsson's thiourea-anthracene receptor (Figure 1.25a)[128] and Ashokkumar's BODIPY-appended amidothiourea receptors (Figure 1.25b)[129] are classic

examples of anion binding PET-induced fluorescent quenching in the presence of basic anions like acetates and fluorides in DMSO and DMSO/water mixtures respectively.

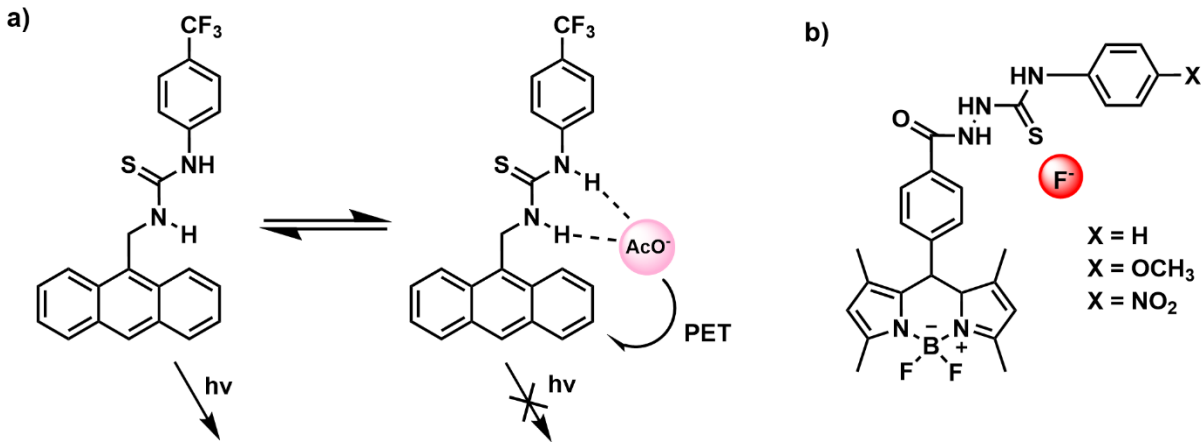


Figure 1.25. *a) Gunnlaugsson's thiourea-anthracene sensor that exhibits PET quenching upon recognising acetate[128] b) Ashokkumar's BODIPY-appended amidothiourea receptors for fluoride detection.[129]*

Alternatively, metal based optical sensors involving lanthanides have garnered significant interest owing to their unique luminescence properties. Faulkner's binuclear lanthanide(III) DOTA-based receptors are good examples of such systems which cooperatively bind and sense chloride in water and buffered media with association constants as high as 10^5 M^{-1}. The chloride is envisioned to be bound within the preorganised pockets formed between two lanthanide (Eu(III), Tb(III) and Yb(III)) centres (Figure 1.26).[130] Wherein sequential addition of KCl to the binuclear complexes in deionised water results in

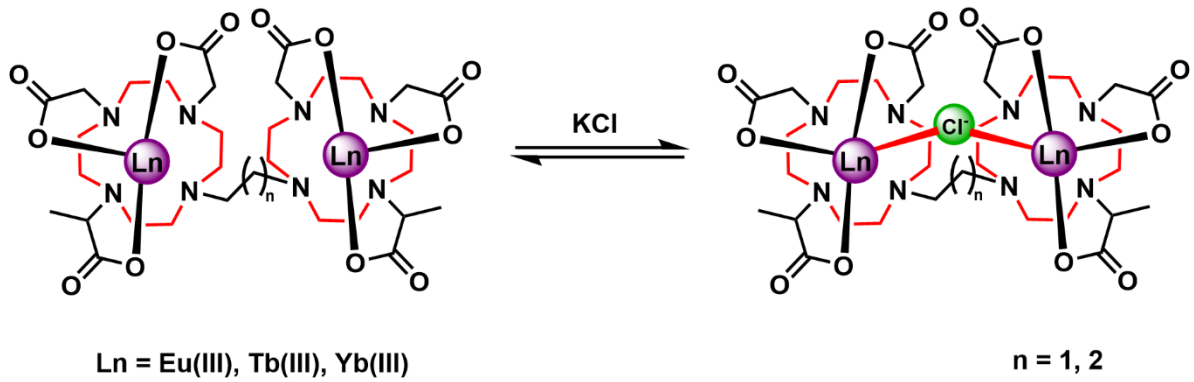


Figure 1.26. *Faulkner's lanthanide-based chloride sensor.[130]*

perturbations in the emission intensity of the lanthanide centres, tracked using luminescence titration experiments.

1.3.5.1.2 Colorimetric sensors

Colorimetric sensors rely on anion binding induced changes in a chromophore's electronic visible spectrum resulting in naked-eye detection. Such sensors are attractive from a practical standpoint since they eliminate the need for sensitive detection instruments. Sessler's series of calix[4]pyrrole hosts functionalised with an anthracene chromophore was one of the first examples of successful host-guest colorimetric sensors to be reported in 1999 (Figure 1.27a),[131] wherein the addition of excess equivalents of fluoride to the host elicited a dramatic change in colour going from yellow to red in DCM.

More recently, Lewis, James and co-workers demonstrated fluoride sensing using a relatively simple boron-containing azulene-based colorimetric sensor which selectively changed colour upon fluoride association. Using ^{11}B NMR experiments the authors confirmed the hybridisation change of the boron centre due to occupation of the vacant p-orbital by fluoride which causes the observed colour change (Figure 1.27b).[132] Furthermore, they also explored the effectiveness of the probe in ethanol/water (3:7) solvent media wherein a colour

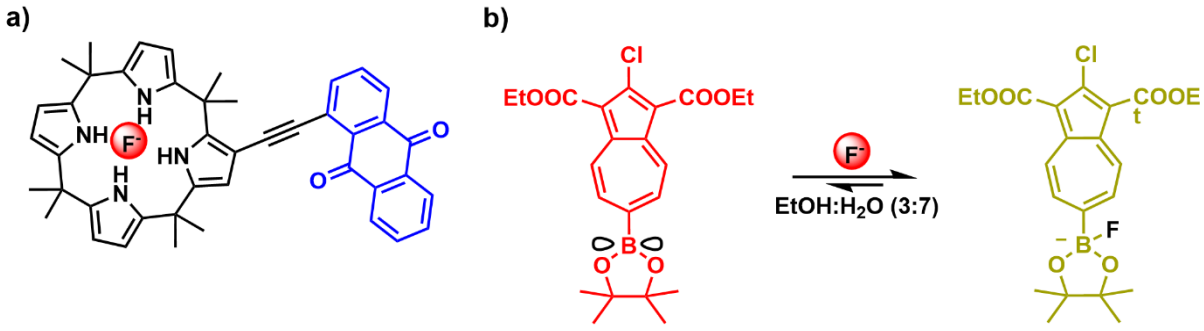


Figure 1.27. *a) Sessler's calix[4]pyrrole fluoride sensing hosts.[131] b) Lewis and James's boron-functionalised azulene-based fluoride sensor.[132]*

change was seen only upon addition of fluoride with a low limit of detection (LOD) of 5.75 mg/L.

1.3.5.2 Electrochemical sensors

Electrochemical-based sensors facilitate detection through changes in their voltage and current redox-properties to monitor guest species. Common redox-active groups integrated into an anion-host design include ferrocene and tetrathiafulvalene (TTF). A typical example is Becher's TTF-functioanlised calix[4]pyrrole receptor which exhibits a large cathodic perturbation of the TTF/TTF^{+} redox-couple (460 mV) upon chloride and bromide binding in acetonitrile (Figure 1.28a).[133]

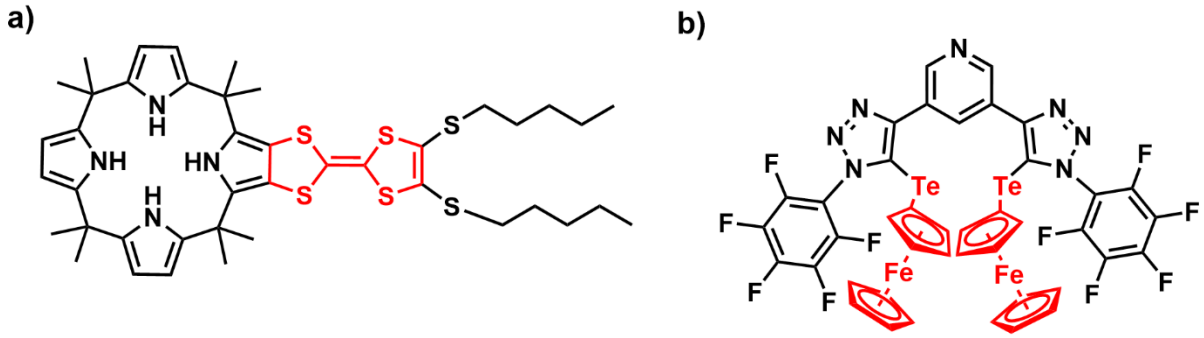


Figure 1.28. *a) Becher's TTF-functioanlised calix[4]pyrrole receptor[133] b) Beer's chalcogen-based ferrocene receptors.[135]*

Sigma-hole mediated anion binding has also emerged as an attractive means of achieving electrochemical anion sensing in polar solvent media. Building on their XB-based ferrocene receptor systems,[134] Beer and co-workers recently reported a chalcogen bonding(ChB)-based bis-ferrocene functionalised receptor (Figure 1.28b).[135] While the neutral reduced bis-ferrocene state of this ChB acyclic receptor displays weak anion association, electrochemical oxidation to the positively charged bis-ferrocenium oxidised state significantly enhances anion binding strength (up to 3 orders of magnitude), in effect

switching-on anion recognition in the 9:1 CH_3CN/H_2O electrolyte solvent system, with a noteworthy selectivity towards bromide.

1.4 Ion-pair recognition

As discussed in section 1.3, the ability to recognise charged species is crucial for the function of a variety of biological and chemical processes. Monotopic receptors designed to bind a specific anion or cation must however overcome the energy cost to separate the individual ion from its counter-anion, which serves to diminish the binding capabilities of the receptor. Heteroditopic receptors with binding sites for both the cation and anion offer a creative solution to this problem, whilst also opening up the possibility of favourable proximal cation-anion electrostatic interaction-induced cooperative binding. Their ability to bind ion-pairs has been exploited to extract ion-pair salt species in precious metal mining, toxic waste remediation,[136-139] aid inorganic salt solubilisation[140] and behave as effective agents for membrane transport[141] and sensors.[142]

Despite the aforementioned advantages, the field of ion-pair recognition still remains a relatively undeveloped area of research, mainly owing to the challenging design and synthesis of heteroditopic receptors. Investigating the complex equilibria involved in the

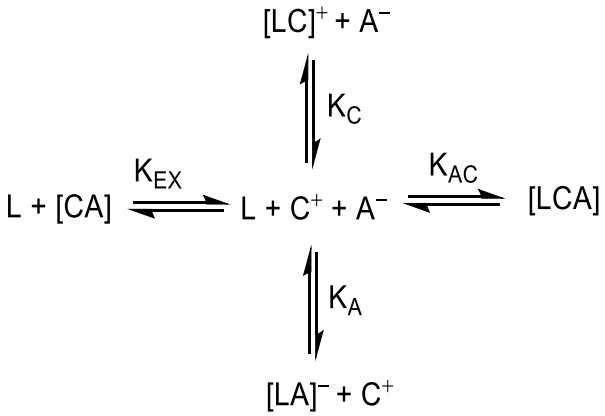


Figure 1.29. *Diagram illustrating the various equilibria that need to be considered in an ion-pair binding system. L = heteroditopic receptor, A = Anion, C = Cation.*

overall ion-pair binding process in such systems is also a challenge (Figure 1.29). This complexity becomes increasingly important in low polarity solvents due to competing strong ion-pairing effects. With a heteroditopic receptor, the ions can bind separately (K_C/K_A) or they can bind simultaneously as intended as an ion-pair (K_{AC}). Alternatively, the ions can also associate as an ion-pair external to the receptor (K_{EX}).

The common feature of all heteroditopic host systems is cooperativity, induced by proximal electrostatic interactions between the bound ions and/or conformational changes instigated by the binding event.[143] Cooperativity is deemed positive if the binding of an ion enhances the association of the counter-ion, and conversely negative if the apparent binding strength is diminished. Attempts to quantify cooperativity have proven highly challenging owing to the complex ion-pair binding equilibria already mentioned (Figure 1.29). However, it is common practice to report the calculation of the "cooperativity factor" which is simply the ratio of the ditopic host's affinity for a given ion in the presence and absence of the counter-ion.

1.4.1 Heteroditopic receptors for ion-pair recognition

Dependent upon the relative spatial positioning of the respective cation and anion recognition sites in a heteroditopic host design, the ion-pair binding modes of these systems can be broadly classified into contact ion-pair and separated ion-pair (Figure 1.30). When the binding sites are closely integrated, contact ion-pairing results, whereas solvent separated ion-pair binding can occur at greater separated distances.

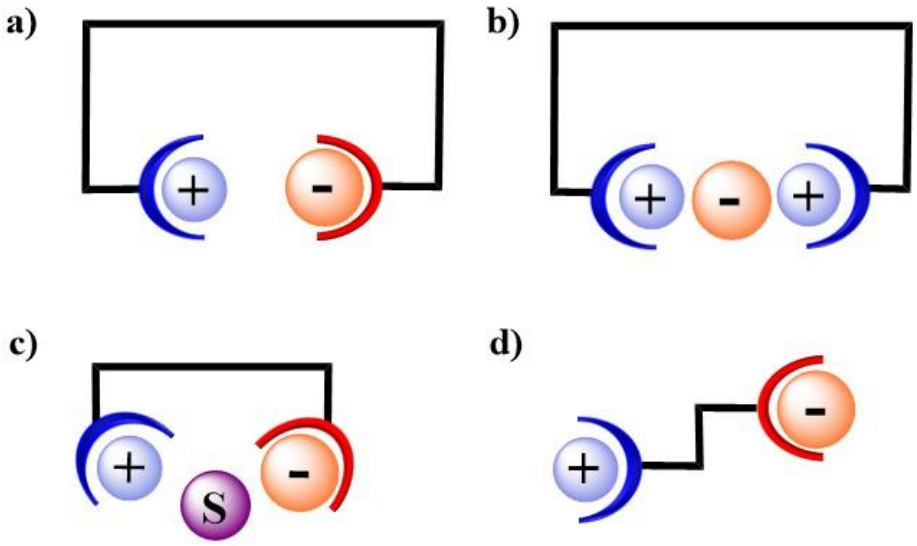


Figure 1.30. *Cartoon representations of general types of heteroditopic ion-pair receptors: a) contact ion-pair complex; b) cascade complex; c) solvent-separated ion-pair host and d) host-separated ion-pair.*

1.4.1.1 Heteroditopic receptors for separated ion-pair binding

An early report of a heteroditopic separated ion-pair receptor is Reinhoudt's urea- based calix[4]arene which was able to bind and extract the NaCl ion-pair in $CDCl_3$ (Figure 1.31a).[144] The work sought to highlight the importance of the calix lower-rim ester sodium cation binding playing a crucial role in preorganising the calix upper-rim urea groups to facilitate chloride recognition. Recently, Granda and co-workers designed a light-responsive azo-group linked heteroditopic receptor which exhibited reversible transport of ion-pairs by controlling the distance between the cation and anion binding units (Figure 1.31b).[145] The meta-stable *cis-azo* form showed a higher affinity and 74-fold higher extraction capabilities towards sodium halide ion-pairs in DCE compared to the thermodynamically stable *trans*-azo form.

Sessler's calix[4]pyrrole-calix[4]arene host is a rare example of a heteroditopic receptor that assumes different ion-pair binding modes depending on the nature of the counter-anion (Figure 1.31c).[146] They observe that caesium fluoride is bound selectively *via* a solvent-separated ion-pair recognition mode in 10% CD_3OD/ $CDCl_3$ solvent media, wherein

the presence of both ionic species is imperative to effect significant signal perturbation in the ^{1}H NMR spectrum, mimicking a cooperative *AND* logic gate. By contrast, in the case of CsCl and $CsNO_3$, the receptor binds the ion-pairs as a loosely/spatially separated ion-pair and contact ion-pair respectively as evidenced by single crystal X-ray structural analysis.

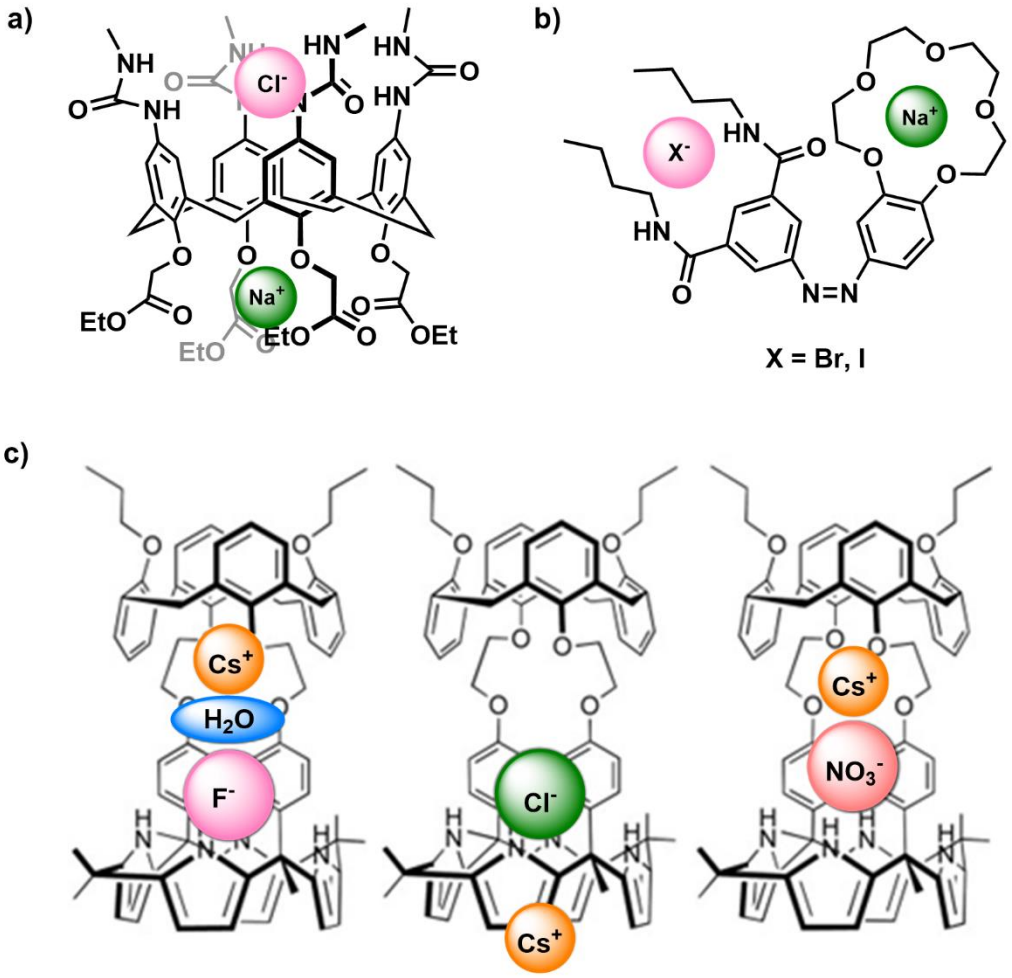


Figure 1.31. *a) Reinhoudt's urea-based calix[4]arene NaCl receptor[144] b) Granda's urea and crown-ether based cis-NaX receptor[145] c) Sessler's calix[4]pyrrole-calix[4]arene ion-pair receptor.[146]*

1.4.1.2 Heteroditopic receptors for contact ion-pair binding

Contact ion-pair recognition is an energetically favourable phenomenon since it minimises the penalty of separation of the two ions upon association with the receptor. One of the first examples described is Smith's ditopic macrocyclic receptor which selectively binds and extracts alkali metal halide ion pairs in d_6-DMSO *via* convergent isophthalamide HB anion

donors and diaza-18-crown-6-ether alkali metal cation recognition sites (Figure 1.32a).[147] Analogous systems have been designed by varying the anion binding site, as seen in Tuntulani's ferrocene-functionalised receptor which is also capable of electrochemically sensing the NaBr ion-pair in 95:5 $CD_3CN/CDCl_3$ (Figure 1.32b).[148]

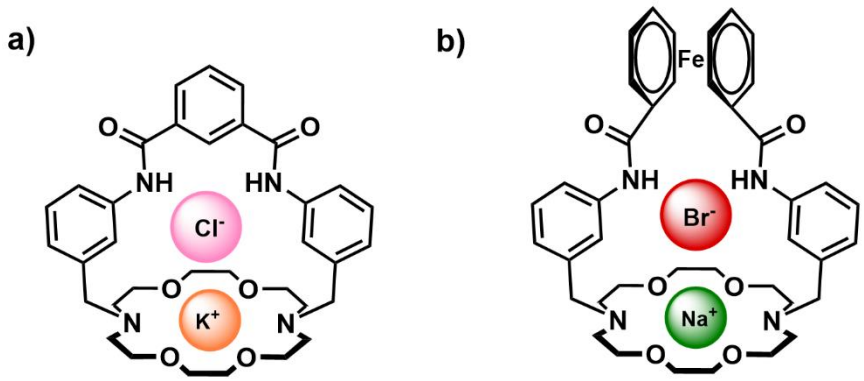


Figure 1.32. *a) Smith's macrocyclic ion-pair receptor[147] b) Tuntulani's ferrocene-based ion-pair receptor.[148]*

More recently Ballester and co-workers designed a series of diastereomeric heteroditopic receptors comprising a calix[4]pyrrole anion binding core attached to cation binding bis-phosphonate cavitands (Figure 1.33).[149] Upon addition of various phosphonium and ammonium chloride salts they found that the orientation of the cation and anion binding units in the receptor dictated the ion-pair binding modes, wherein diastereomer **A** bound the

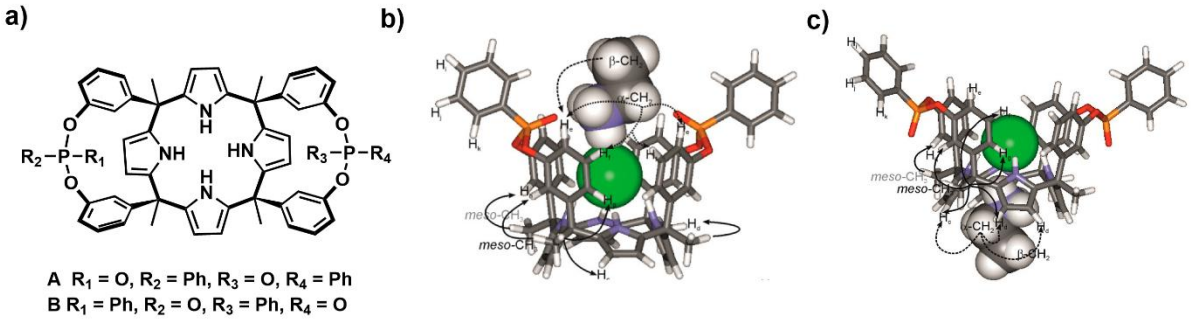


Figure 1.33. *a) Ballester's calix[4]pyrrole diastereomeric receptors b) CAChe energy minimised structure of diastereomer **A** complexed with alkylammonium cation c) CAChe energy minimised structure of diastereomer **B** complexed with alkylammonium cation.* [149]

ion-pairs in a 1:1 contact ion-pair arrangement. In contrast, its diastereomer **B** formed a separated arrangement with the salts in DCM and MeCN.

In 2008 Beer and co-workers reported a calix[4]-diquinone heteroditopic receptor that exhibited cooperative AND NH_4Cl ion-pair recognition in competitive solvent media like CD_3CN and 98:2 CD_3CN/D_2O (Figure 1.34).[150] They proposed that simultaneous binding of both the cation and anion was required to break the intramolecular hydrogen bonding between the quinone carbonyls and the isophthalamide N-H donors of the free ditopic receptor, resulting in a proximal arrangement of the cation and anion binding stations (Figure 1.34). Through solution and solid-state studies, they further confirmed that the individual cation and anion were unable to sufficiently overcome the intramolecular hydrogen bonding within the receptor accounting for their low affinity.

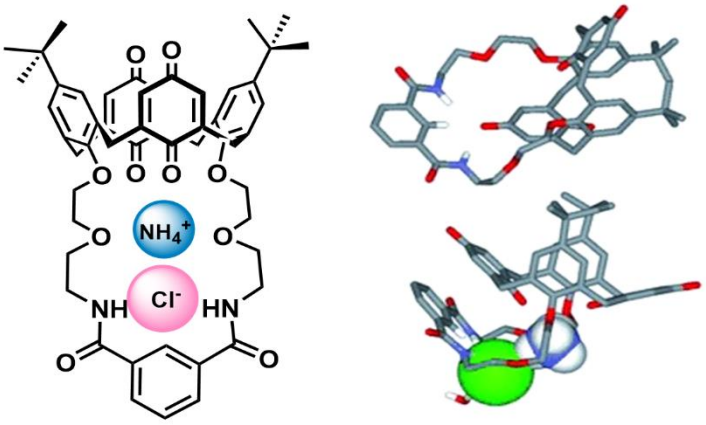


Figure 1.34. *Cooperative AND ion-pair receptor reported by Beer and co-workers, and X-ray crystal structures of the receptor in the absence (upper) and presence (lower) of a bound NH_4Cl ion pair.*[150]

1.4.1.3 Heteroditopic receptors for cascade ion-pair binding

Heteroditopic receptors can also be designed in such a way that the anion is sandwiched between bound cations forming a cascade complex (Figure 1.30b). These cascade complexes can sometimes be viewed as model systems for biotic-inorganic complexes. For example, haemocyanins are proteins responsible for transporting oxygen in molluscs and anthropods

(Figure 1.35a).[151] These metalloproteins bind oxygen between two histidine coordinated copper(I) binding sites resulting in a dicopper(II)-O_2-ligand bridged cascade assembly. An abiotic example of cascade complexation is Wiess's [24-ane-N_2S_4] macrocycle which forms a cascade complex with azide anions perched between two SNS-Cu(II) binding sites (Figure 1.35b).[152]

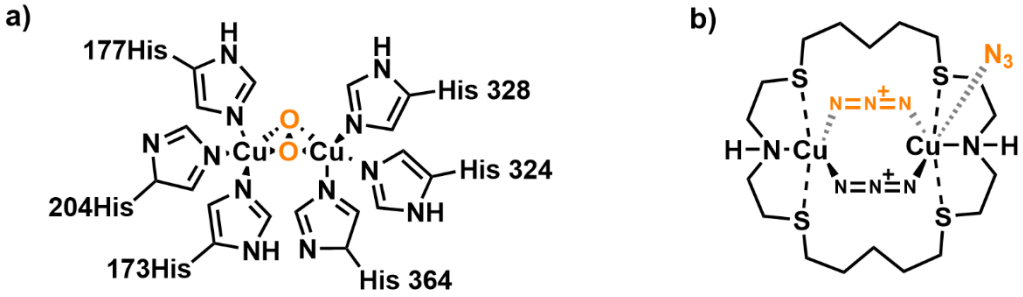


Figure 1.35. *a) Structure and binding mode of Haemocyanins[151] b) Wiess's [24-ane-N_2S_4] azide binding macrocycle.[152]*

1.4.2 Applications of heteroditopic receptors

1.4.2.1 Salt extraction

Salt extraction is an important and environmentally relevant application of heteroditopic receptors. With potential applications in transition metal extraction from mineral ores, White *et al.* designed a series of salen-based ligands capable of effectively extracting almost 100% of $CuSO_4$ from a pH 3.8 aqueous solution into chloroform (Figure 1.36a).[153] Another recent example includes Dobrzycki's squaramide-based receptors equipped with a crown-ether unit to extract potassium salts such as K_2SO_4 from aqueous to organic phases (Figure 1.36b).[154]

Over the years the extraction and removal of harmful radioactive charged species has garnered significant interest across various countries and communities around the world. Beer's tren-based heteroditopic receptor demonstrates a remarkable 20-fold enhancement in perrhenate binding in the presence of sodium cation in $CDCl_3$ (Figure 1.36c).[155] Structural

similarities between perrhenate and radioactive pertechnetate anion, a major water pollutant from nuclear fuel processing, prompted aqueous-chloroform liquid-liquid extraction studies with sodium pertechnetate salt, which the receptor was able to successfully extract into the organic solvent phase.

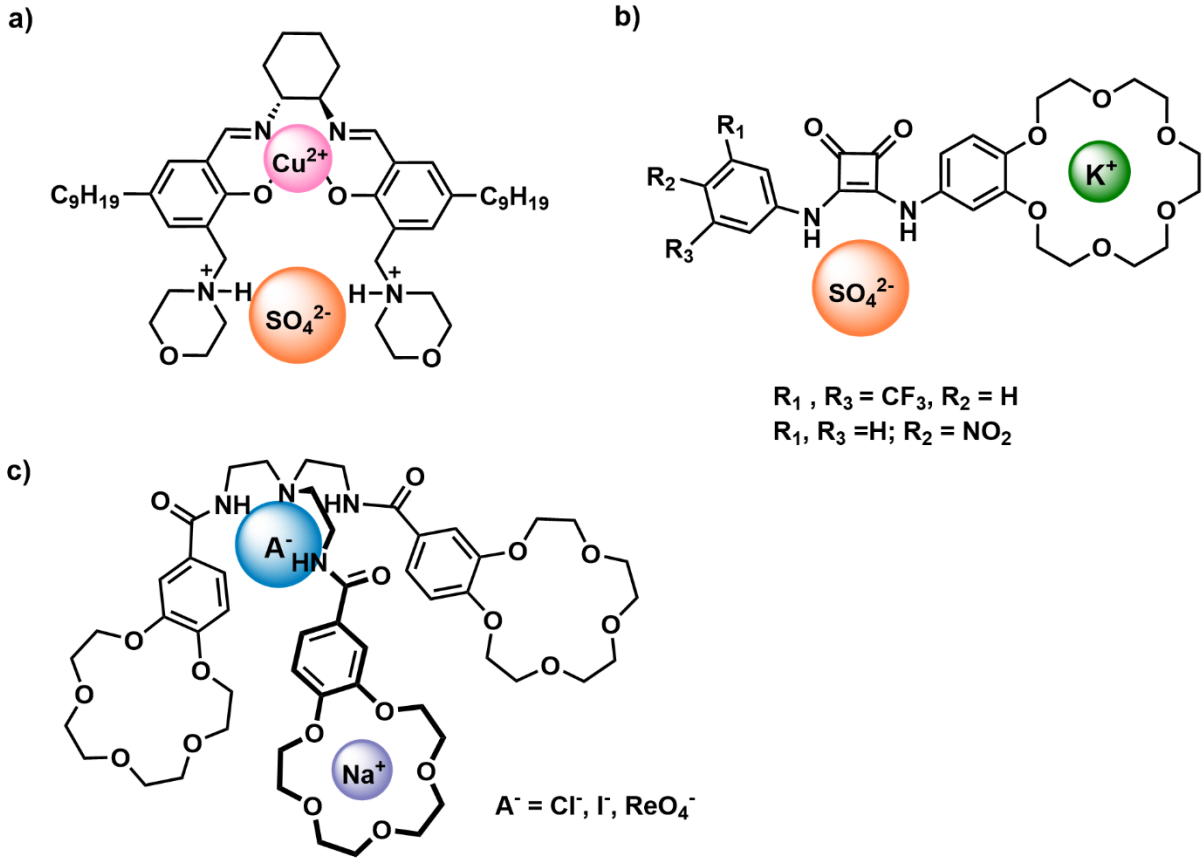


Figure 1.36. *a) White's salen derivatives for $CuSO_4$ ion-pair extraction[153] b) Dobrzycki's squaramide-based KX ion-pair receptors[154] c) Beer's tren-based heteroditopic receptor.[155]*

1.4.2.2 Membrane transport

Membrane transport generally refers to the movement of ions, molecules or other substances across cellular membranes in order to maintain a chemical balance and local charge neutrality within living cells. These processes play a critical role in various biological processes such as signal transduction, gland secretion, nutrient uptake, waste removal and maintenance of cellular homeostasis. While numerous examples of anion and cation

transport have been reported in literature, the field of ion-pair co-transport has only recently started witnessing progress. A notable example is a series of urea-based aza-crown ether derivatives designed by Jeong and co-workers which selectively bound and transported alkali metal salts *via* a M^+/Cl^- symport across a POPC (palmitoyl-2-oleoyl-sn-glycero-3-phosphocholine, a phospholipid used for biophysical experiments) membrane (Figure 1.37a).[156] ^1H NMR titration experiments in competitive 9:1 CD_3CN/ CD_3OD solvent media and single-crystal XRD data confirmed that addition of alkali cations to the heteroditopic receptors cooperatively enhanced anion binding *via* formation of a contact ion-pair.

Jabin and Barktik reported the first tris(thio)urea calix[6]arene-based transporters that behaved as efficient carriers for Cl^-/NO_3^- antiport while also facilitating the co-transport of primary and bulky *t*-butyl ammonium chloride salts across a lipid bilayer (Figure 1.37b).[157] Fluorescence-based transport experiments with primary ammonium salts highlighted the advantages of utilising a cavity-based transporter to make the co-transport of ion-pair salts

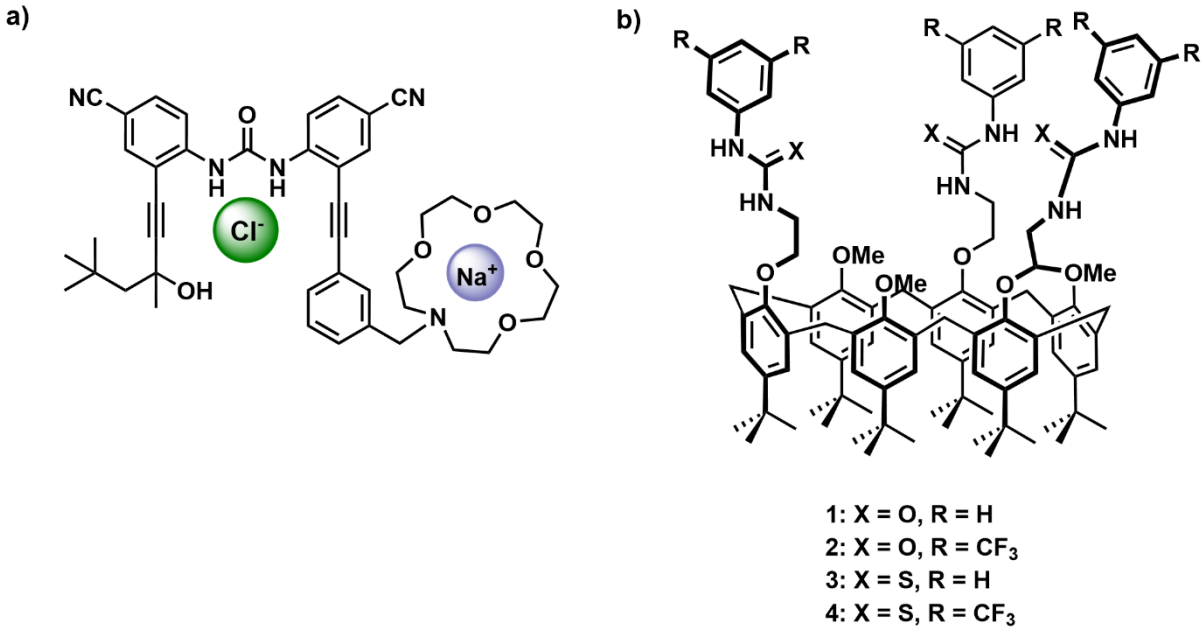


Figure 1.37. *a) Jeong's urea-based aza-crown ether derivatives for alkali metal salts transport across a POPC membrane[156] b) Jabin and Barktik's tris(thio)urea calix[6]arene-based transporters.[157]*

more favourable than the Cl^-/NO_3^- antiport. Conversely, analogous experiments with bulkier ammonium salts failed to produce a similar preference for co-transport owing to the large size of the bulkier ammonium salts precluding complexation within the calix cavity.

1.4.2.3 Sensors

Akin to monotopic receptors, sensing of ion-pairs also requires the incorporation of suitable optical or electrochemical reporter units in the receptor. Compared to monotopic sensors, however, development of heteroditopic sensors has been limited. Examples of ion-pair sensors include ferrocene-imidazopyrene receptor designed by Otón *et al.* in 2011, which upon binding with the $Zn(H_2PO_4)_2$ salt showed cathodic shifts of the ferrocene/ferrocenium redox couple as well as changes in the emission spectra owing to the presence of both optical and electrochemical transducers within the receptor (Figure 1.38).[158]

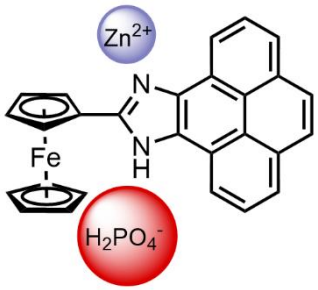


Figure 1.38. *Otón's ferrocene-imidazopyrene ion-pair receptor.*[158]

1.5 Mechanically interlocked molecules

Although the concept of chemical bonds has been the subject of interest since the earliest chemical research, another class of bonding has been gaining popularity for some time now: the mechanical bond. While covalent bonding exists between atoms sharing electrons, mechanical bonds are associated with molecular entities called component parts. Defined in the seminal book by Bruns and Stoddart, "The Nature of the Mechanical Bond: From

Molecules to Machines", a mechanical bond is as "*an entanglement of space between two or more component parts such that they cannot be separated without breaking or distorting the chemical bonds between atoms*". The two quintessential examples of mechanically interlocked molecules (MIMs) are rotaxanes and catenanes which continue to garner widespread interest due to their unique topologies and diverse functionalities. The names of both these systems are derived from Latin, catenane coming from the Latin word *catena* meaning chain and representing two or more linked macrocyclic components. Derived from the word *rota* for wheel and *axis* for axle, a rotaxane consists of a macrocycle through which a linear component, the axle, remains threaded owing to bulky terminating groups. During the past 40 years since Sauvage's seminal report for synthesising a [2]catenane in a noteworthy yield,[172] many more types of MIMs have come into existence such as knots, Boromean rings, Solomon links and more recently clippanes (Figure 1.39).

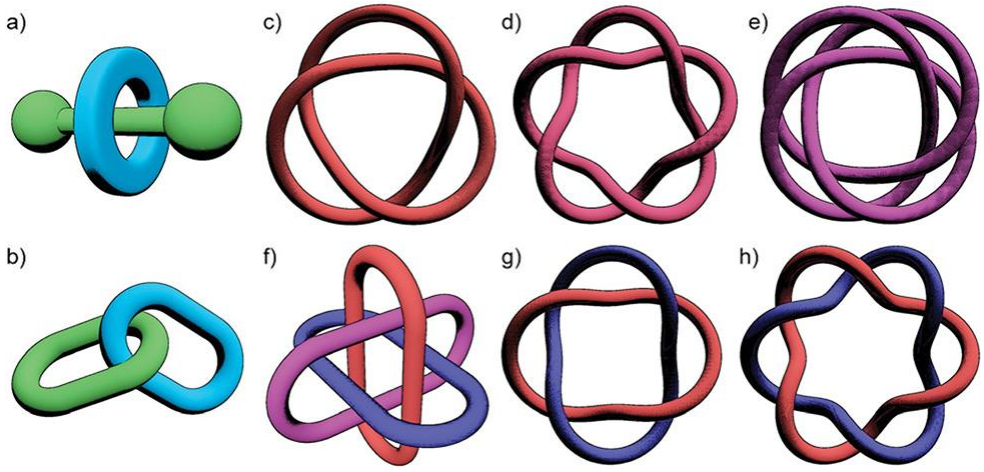


Figure 1.39. *Examples of mechanically interlocked molecules: a) [2]rotaxane[159] b) [2]catenane[160] c) trefoil knot[161] d) pentafoil knot[162] e) 8_{19} knot[163] f) Borromean rings[164] g) Solomon link (double-braided [2]catenane)[165] h) Star of David [2]catenane (621 link)[166]-adapted from [167]*

1.5.1 Synthesis of mechanically interlocked molecules

Molecules with non-trivial topologies started attracting interest as soon as the synthesis of medium-sized molecular rings became viable in 1912.[168] However, it was not until the syntheses of catenanes and rotaxanes in the 1960s did the idea of mechanical bonds start gaining ground.[169] While the seminal works of Ed Wasserman and Gottfried Schill are the cornerstones behind MIMs,[170,171] it was the pioneering discovery of the synthesis of interlocked molecules using templating methods by Sauvage that turned the tide around for MIM chemistry.[172] Since then the field of MIMs synthesis has grown exponentially with researchers coming up with robust, high yielding synthetic methodologies to prepare such systems.

1.5.1.1 Template directed synthesis of MIMs

1.5.1.1.1 Cation template: passive cation templation

Dietrich, Buchecker and Sauvage's 1983 transformative publication on the synthesis of [2]catenanes using a copper(I) metal template[172] set into motion widespread research leading to a plethora of examples employing transition metals as templates for the synthesis of MIMs. In their work they exploited the tetrahedral coordinative stereochemistry of the Cu(I) cation in preorganising two phenanthroline units in an orthogonal arrangement, followed by a

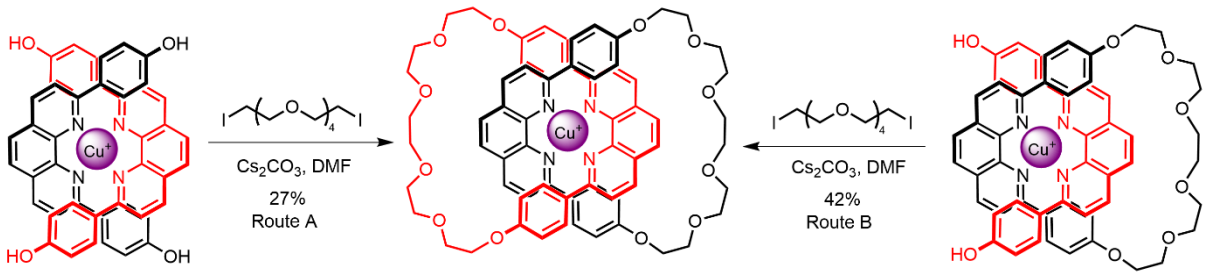


Figure 1.40. *Formation of Sauvage's metallo-[2]catenane using a passive metal template.*[172]

Williamson ether double macrocyclisation to afford the desired [2]catenane in 27% yield (Figure 1.40). Interestingly, solid state single crystal XRD analysis revealed that the metal-free [2]catenane possessed a dramatically altered conformation from the demetallated structure alluding to possible circumrotation of the macrocycles in the absence of copper.

Notably, in this case the copper(I) cation serves as a passive templating agent since it only plays a role in arranging the components in a favourable manner while not being involved in the catenane formation step. Passive transition metal cation templates have since been utilised to make a variety of MIMs exploiting diverse coordination geometries offered by different transition metals like Au^{+} (linear)[173], Pd^{2+} (square planar),[174] Zn^{2+} (trigonal bipyramidal)[175] and Co^{3+}, Ni^{2+}, Fe^{2+} (octahedral).[176-178] In particular, Leigh and co-workers have reported various interlocked systems made using passive metal templates. A notable example is the square planar coordinating palladium(II)-template directed synthesis of a hetero[2]catenane (78% yield) wherein by varying the order of cyclization reactions they successfully isolated the [2]catenane, its topological [2+2]macrocyclic isomer and the two constituent macrocycles (Figure 1.41).[174]

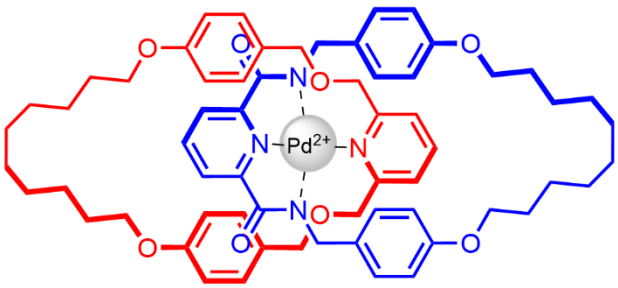


Figure 1.41. *Leigh's examples of MIMs formed via passive metal template with palladium.*[174]

Another impressive example is their cobalt(II)-template directed synthesis of a [2]rotaxane and homo[2]catenanes where the cobalt(II) cation binds the tridentate dianionic pyridine-2,6-dicarboxamido ligands in an octahedral geometry (Figure 1.42).[176] Interestingly,

while it is Co^{2+} that thermodynamically assembles the components together, oxidation to Co^{3+} is essential for kinetically trapping the components to afford cyclization. Reduction of the template thereafter generates the neutral [2]rotaxanes and [2]catenanes.

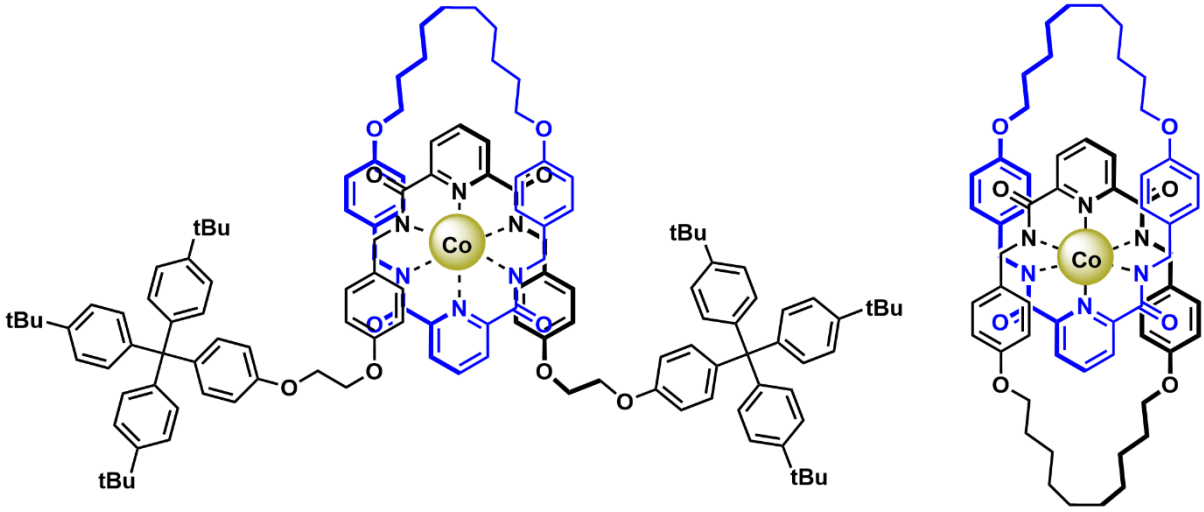


Figure 1.42. *Leigh's examples of MIMs formed via passive metal template with cobalt.*[176]

Besides transition metals, lanthanides have also been utilised to prepare interlocked species. The first example of a lanthanide-directed [2]rotaxane synthetic strategy was reported by Zapata *et al.* which involved the initial formation of a pseudorotaxane between

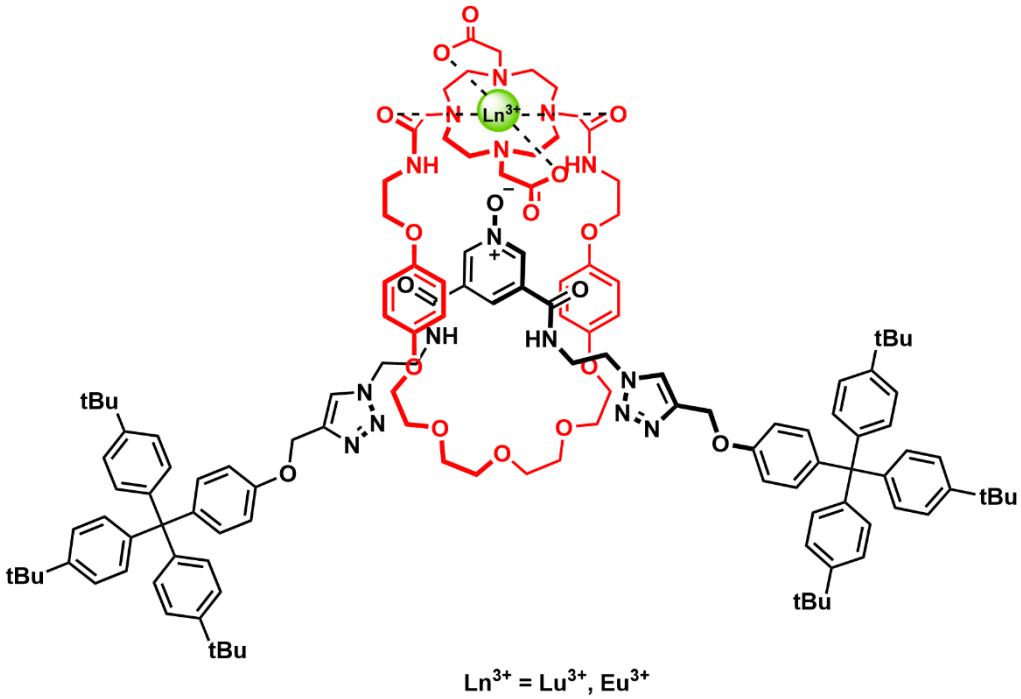


Figure 1.43. *Zapata's [2]rotaxane synthesised using a lanthanide metal template.*[179]

a lanthanide coordinating DOTA based macrocycle and a pyridine N-oxide thread followed by successive CuAAC click reactions to stopper the ends (Figure 1.43).[179]

Alkali metals (Li^+, Na^+, K^+) and alkaline earth metals (Ca^{2+}, Ba^{2+}) have also been used as successful templates to synthesise MIMs. Examples include Sanders's lithium-directed [2]catenane formation where the lithium cation preorganises the components by coordinating with the oxygens in the polyether macrocycle and pyromellitic diimide thread.[180] Subsequent Grubbs' (II) catalysed ring closing metathesis macrocyclization affords the [2]catenane in 60% yield (Figure 1.44a). Another noteworthy example is Chiu's sodium cation-template directed [2]catenane synthesis where they use a sodium cation to orthogonally arrange two diamine ethylene glycol-based precursors which undergo subsequent Schiff base condensation reactions to form the [2]catenane (Figure 1.44b).[181]

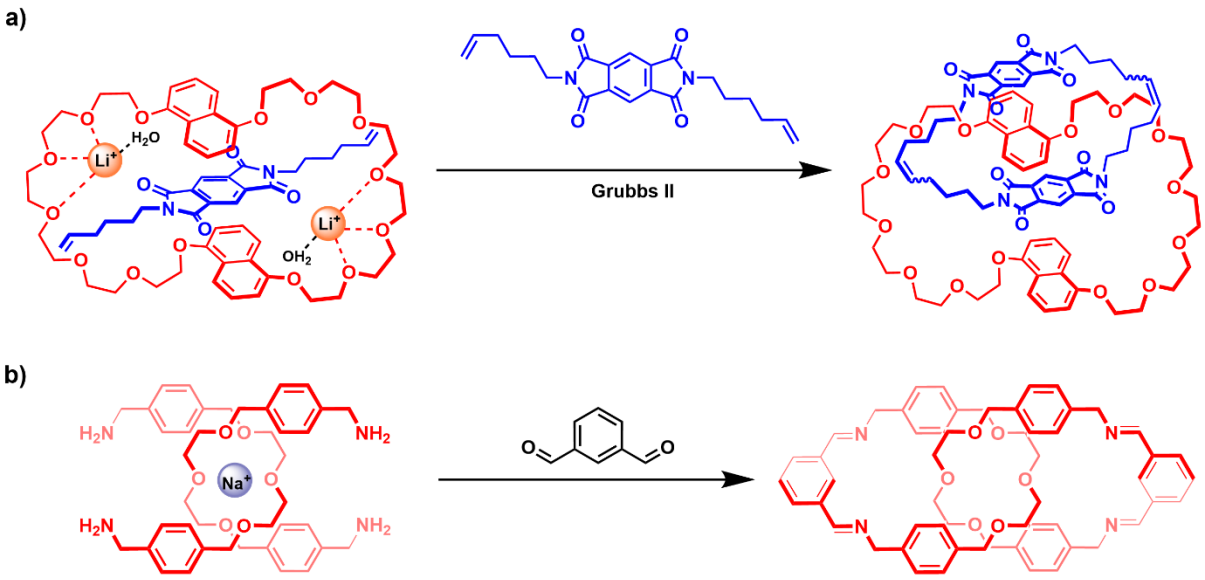


Figure 1.44. *a) Sander's Li^+-templated [2]catenane[180] b) Chiu's sodium template directed synthesis of a [2]catenane.[181]*

1.5.1.1.2 Cation template: Active Metal Templation

While passive transition metal template synthesis has served as an effective method to construct interlocked systems, it fails to exploit the full potential of transition metal ions by using them only as assembling and organising agents. Building on the well-documented catalytic behaviour of transition metals, in 2006 Leigh and co-workers first introduced the active metal template (AMT) approach as an effective method to synthesise MIMs (Figure 1.45).[182] It involved a catalytically active metal centre, copper(I), bound endotopically within the cavity of a macrocycle, which mediates the formation of a new covalent bond through the ring to form the interlocked species, in this case a triazole bond *via* a CuAAC click reaction. The metal involved therefore behaves both as an active templating agent as well as a catalyst during the formation of the interlocked final product. Consistent with catalytic processes, AMT also occurs under kinetic control as opposed to passive metal template which relies on the formation of a thermodynamically stable complex. In recent years various transition metal-catalysed reactions have been used to synthesize rotaxanes and catenanes involving metals such as Cu(I),[183-188] Pd(II)[189-191] Ni(II),[192,193] and Zn(II).[194] Among these the Cu(I)

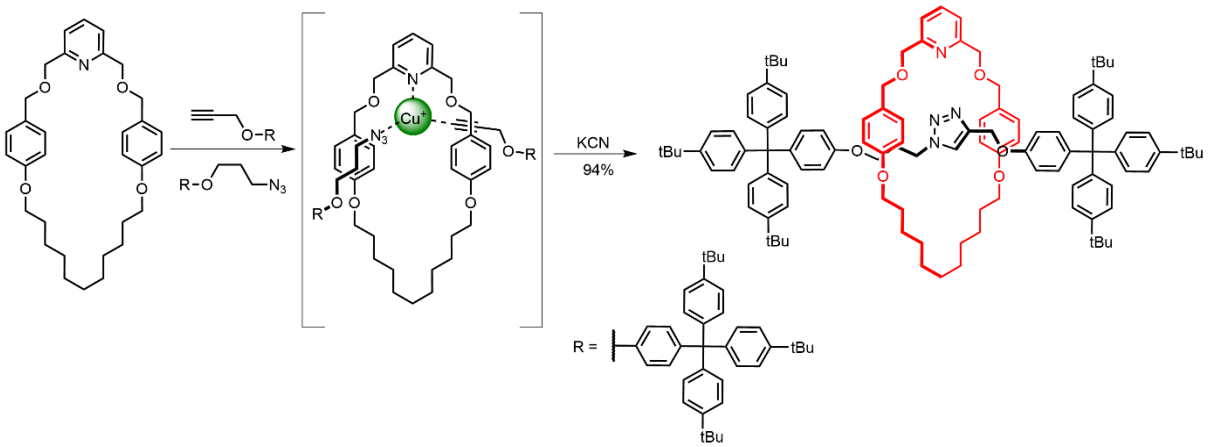


Figure 1.45. *Leigh's [2]rotaxane formed via AMT with proposed monometallic intermediate shown.*[182]

catalysed CuAAC click reaction has gained considerable popularity owing to mild reaction conditions, functional group compatibility and high yielding nature of the reaction.[195]

Recently, Lewis *et al.* designed Sauvage-type molecular shuttles by employing sequential Cu(I) catalysed click reactions on ethynyl pyridyl derivatives threaded through bipyridine macrocycles in impressive 52% yields (Figure 1.46).[196] ^{1}H NMR and ^{1}H-^{1}H ROESY NMR studies were conducted to investigate the dynamic co-conformational behaviour of the shuttle by simply varying the binding cation causing macrocyclic translocation across the axle component.

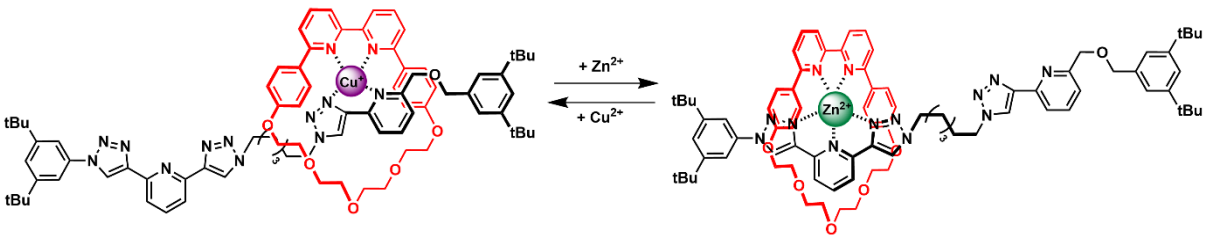


Figure 1.46. *Lewis's Sauvage-type molecular shuttle synthesised using Cu(I) catalysed click reactions.*[196]

1.5.1.1.3 Anion template synthesis of MIMs

Through exploiting the various HB and XB recognition motifs of acyclic and macrocyclic anion receptors (see section 1.3.4), various anion templates have been used in MIM construction. In 1999 Vögtle reported the first anion templated [2]rotaxane synthesis which employed the NH hydrogen bond donor capabilities of a tetralactam macrocycle in capturing an anionic phenolate stopper unit (Figure 1.47).[197] Subsequent reaction with a bromo-functionalised half-axle unit afforded the [2]rotaxane in an impressive yield of 95%.

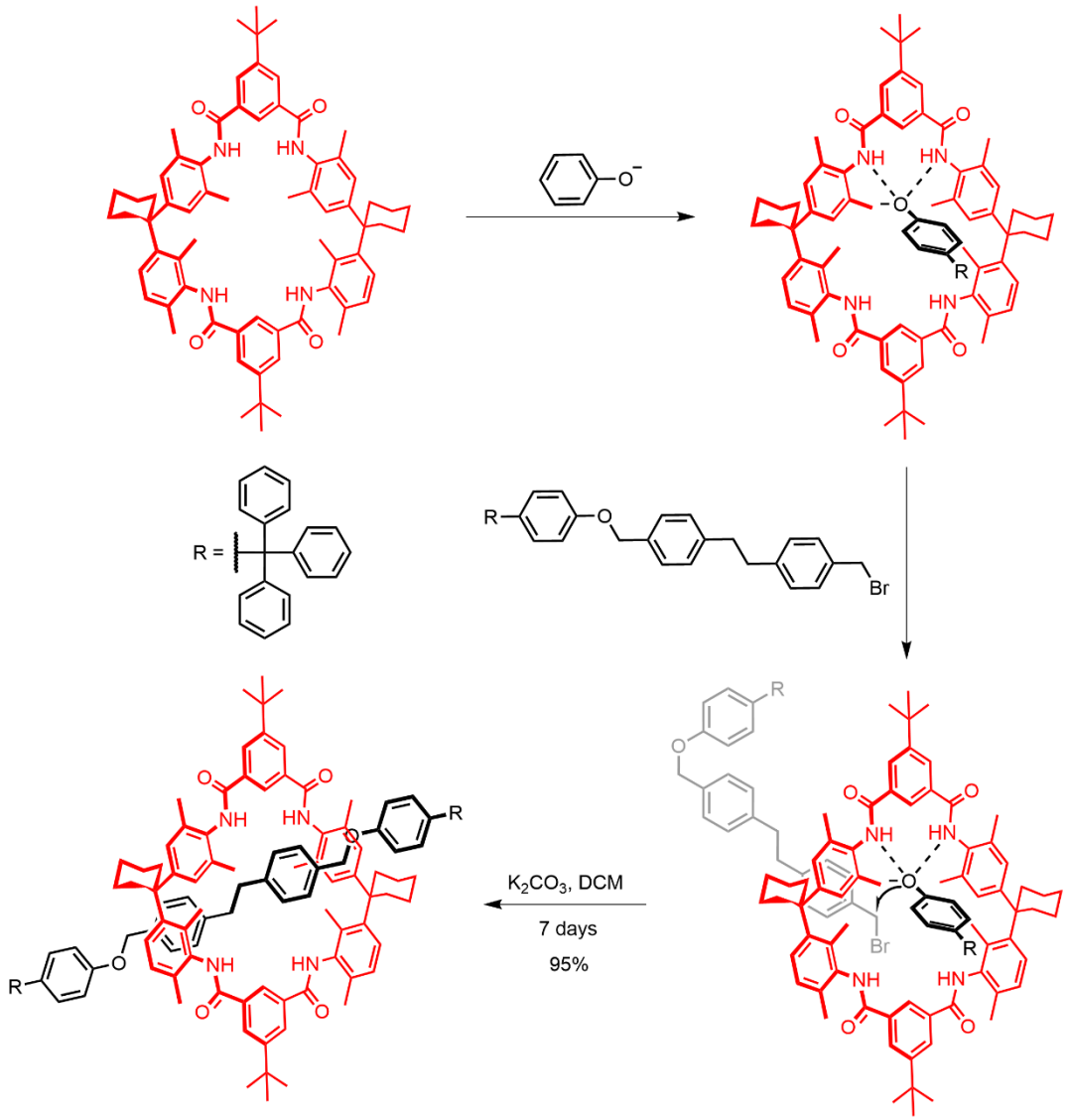


Figure 1.47. *Vögtle's [2]rotaxane formed using an anionic template.*[197]

The use of discrete inorganic anions as templating units was unprecedented until in 2001 Beer and co-workers reported the chloride templated pseudorotaxane assembly between a bis-amide-3,5-pyridinium threading unit and a neutral isophthalamide based acyclic thread (Figure 1.48a).[198] The chloride anion template was envisaged to be complexed between the two components in an orthogonal arrangement stabilised by four NH-Cl^- hydrogen bonds and two CH-Cl^- interactions contributed by the phenyl and pyridinium units. Applying this methodology to construct interlocked structures resulted in the first chloride template directed [2]rotaxane synthesis reported by Beer *et al.* in 2002 (Figure 1.48b).[199]

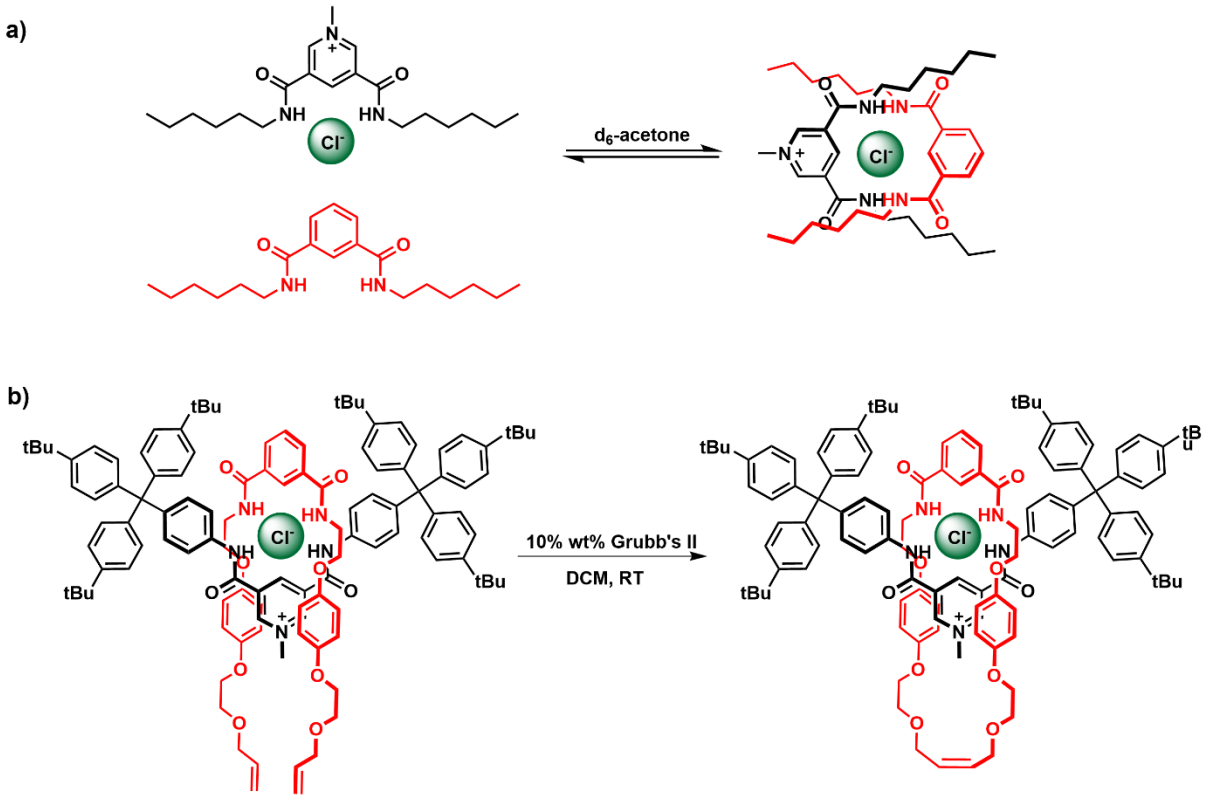


Figure 1.48. *a) Orthogonal association of hydrogen bonding acyclic motifs around a chloride anion template[198] b) Chloride anion-templated [2]rotaxane synthesis via ring closing metathesis.[199]*

Recently, Beer and co-workers succeeded in constructing neutral [2]rotaxanes using a chloride template wherein the chloride was simultaneously bound to the axle's potent iodotriazole XB donors and macrocycle precursor's amine HB donors. Subsequent

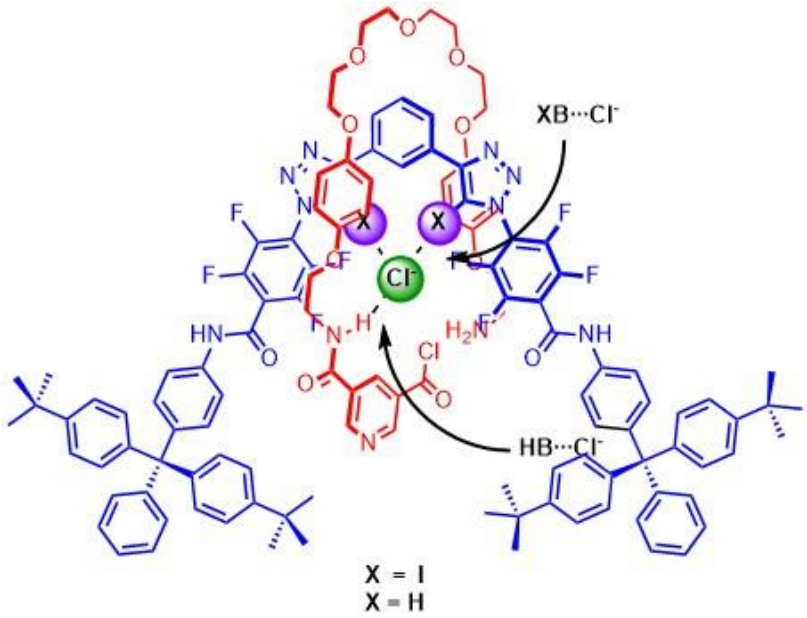


Figure 1.49. *Beer's neutral XB [2]rotaxanes synthesised via chloride anion templation.[200]*

macrocyclization *via* amide condensation afforded the XB-functionalised [2]rotaxane in 37 % yield (Figure 1.49).[200]

Besides chloride, anions such as nitrite, nitrate, sulfate and bromide also have been used for the purpose of MIMs synthesis.[201-203] In 2010 Beer and co-workers reported the first bromide-templated XB [2]rotaxane host system containing an iodo-triazolium motif in the axle (Figure 1.50).[203] Following bromide template removal, anion recognition investigations revealed that the [2]rotaxane's unique interlocked host cavity displayed impressive iodide selectivity (K_a = 2228 M^{-1}) in highly polar solvent mixtures (45:45:10 $CDCl_3/CD_3OD/D_2O$).

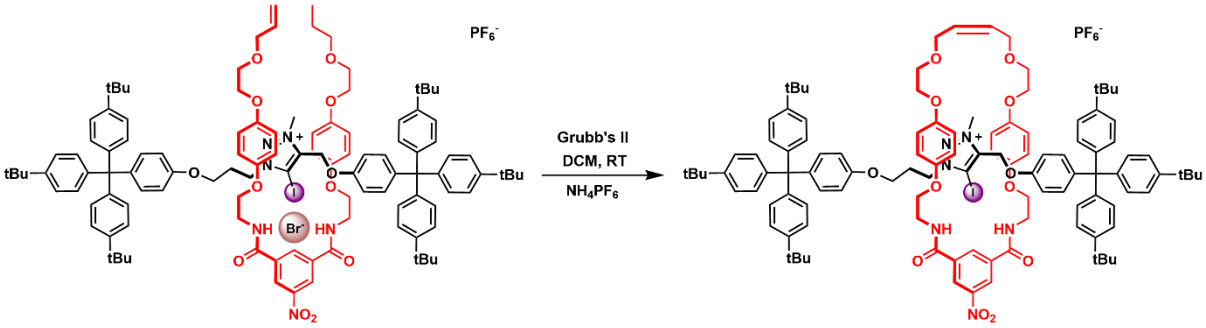


Figure 1.50. *Beer's bromide anion templated [2]rotaxane.*[203]

1.5.2 Applications of mechanically interlocked molecules

The presence of mechanical bonds confer unique properties to MIMs opening up a wide range of potential applications as sensors, molecular shuttles, switches, pumps and machines.

1.5.2.1 MIMs for host-guest recognition and sensing

The unique and elaborate preorganised three-dimensional binding cavities found in mechanically interlocked molecules coupled with effective shielding of the binding site from the bulk solvent makes them excellent receptors for cation and anion guest recognition.[204,205] Incorporation of photo-active or redox groups in MIMs also facilitates anion sensing.[206,207] Following Sauvage's revolutionary work on copper(I) coordinating phenanthroline-based

[2]catenanes,[172] in 1996 Swager introduced a metal-free polyrotaxane functionalised with bipyridine and phenanthroline units in the axle and macrocycle respectively. The work detailed how transition metal cation (copper(II), zinc(II)) binding to the poly[2]rotaxane induces an optical response resulting in significant red shifts of the UV-vis absorption spectrum in CH_2Cl_2 (Figure 1.51).[208]

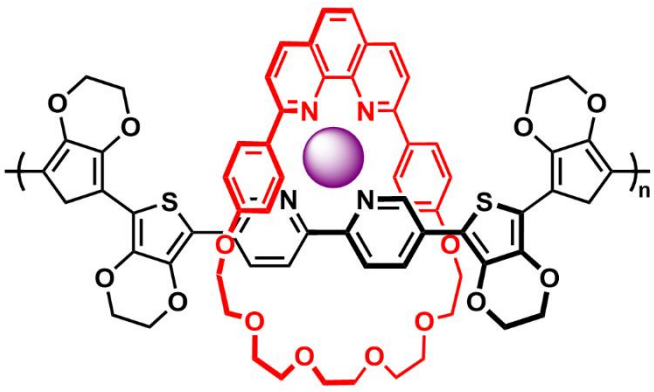


Figure 1.51. *Swager' polyrotaxane Cu(I) receptor*[208]

More recently, Roessler and Goldup reported a series of [2]rotaxanes, synthesised using Cu(I) catalysed AMT click reactions, containing varying numbers of heterocyclic nitrogen-donors (Figure 1.52).[209] The cation binding affinities of these multidentate rotaxanes and their non-interlocked components were investigated with a number of first-row transition metal ions such as Co(II), Ni(II), Cu(II) and Zn(II). Optical and electrochemical studies revealed that the mechanical bond played an essential role in stabilizing and altering the properties of different transition metal guest cations, resulting in various geometries and spin states. For example, the nickel(II) cation only formed a stable, five-coordinated complex with

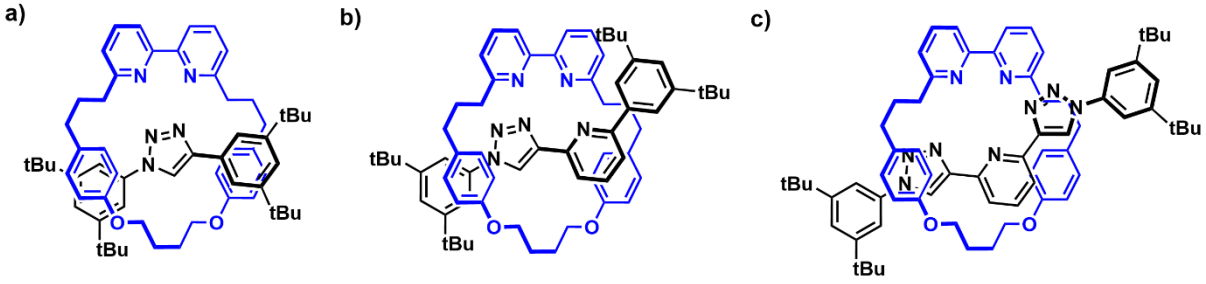


Figure 1.52. *Roessler and Goldup's [2]rotaxane with a) three, b) four, c) five nitrogen donors.*[209]

the pentadentate rotaxane, as confirmed *via* solid-state single-crystal XRD analyses. Electrochemical studies showed that the rotaxane-Ni^{2+} complex underwent reduction to form the Ni^{+} complex, while the corresponding Co^{2+} complex existed in a mixture of both high and low spin states. Furthermore, the high positive redox potential recorded for the Cu(II)/ Cu(I) redox couple when bound to the tetradentate rotaxane confirmed the rotaxane's binding pocket to be an ideal ligand for Cu(I), consistent with the high Cu(I) binding affinities observed with analogous binding pockets generated in Sauvage's bis-phenanthroline based [2]catenanes.

Langton *et al.* reported the first XB [2]rotaxane host capable of selectively binding and sensing iodide (K_a= 6300 M^{-1}) in pure water (Figure 1.53).[210] Upon iodide anion complexation the macrocycle component's ruthenium(II) bipyridyl complex motif's MLCT emission band was enhanced owing to rigidification of the MIM receptor.

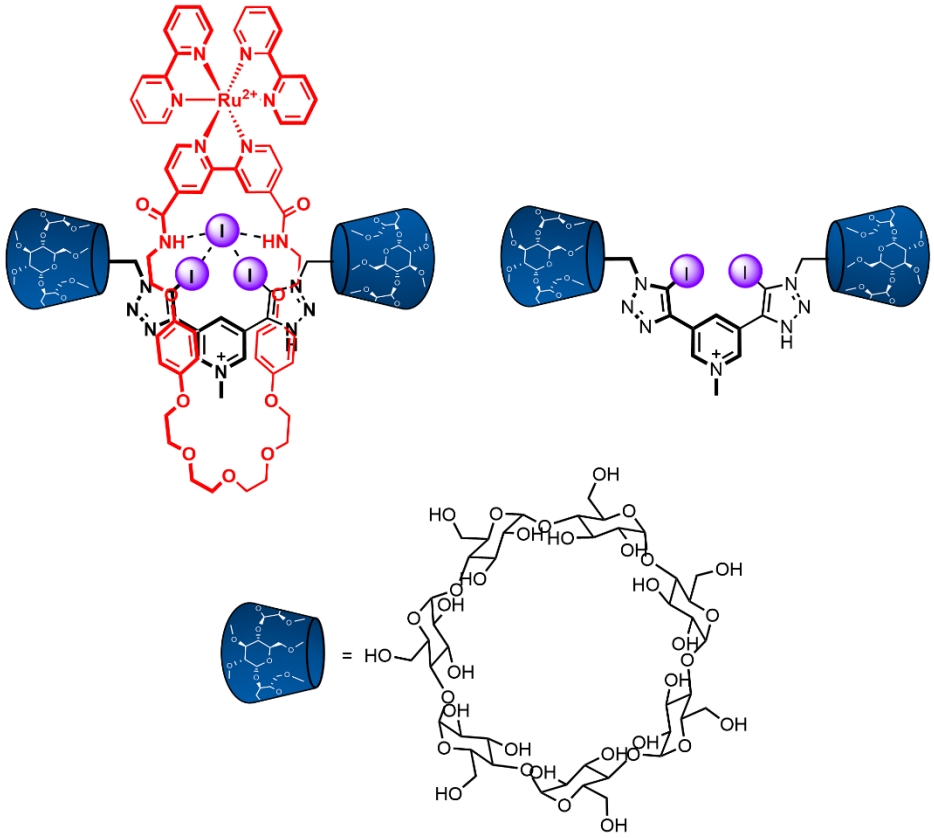


Figure 1.53. *Langton's XB [2]rotaxanes with a Pyridinium and Ruthenium- bipyridyl complex.*[210]

A good example of a colorimetric MIM anion sensor is Smith's squaraine-containing [2]rotaxane host system consisting of a deep-red fluorescent squaraine dye residing within a tetralactam macrocycle that completely quenches the dye's fluorescence (Figure 1.54).[211] ^{1}H NMR and fluorescence studies conducted with the [2]rotaxane in chloroform revealed that upon addition of TBACl the halide displaces the squaraine axle motif, resulting in macrocyclic translocation which causes a 3-fold enhancement in fluorescence emission visible to the naked eye. The reversibility of the colorimetric [2]rotaxane sensor was confirmed by addition of $NaBAr^F_4$ which resulted in the precipitation of NaCl causing the macrocycle to shuttle back to the squaraine station and quenching of the deep-red fluorescence.

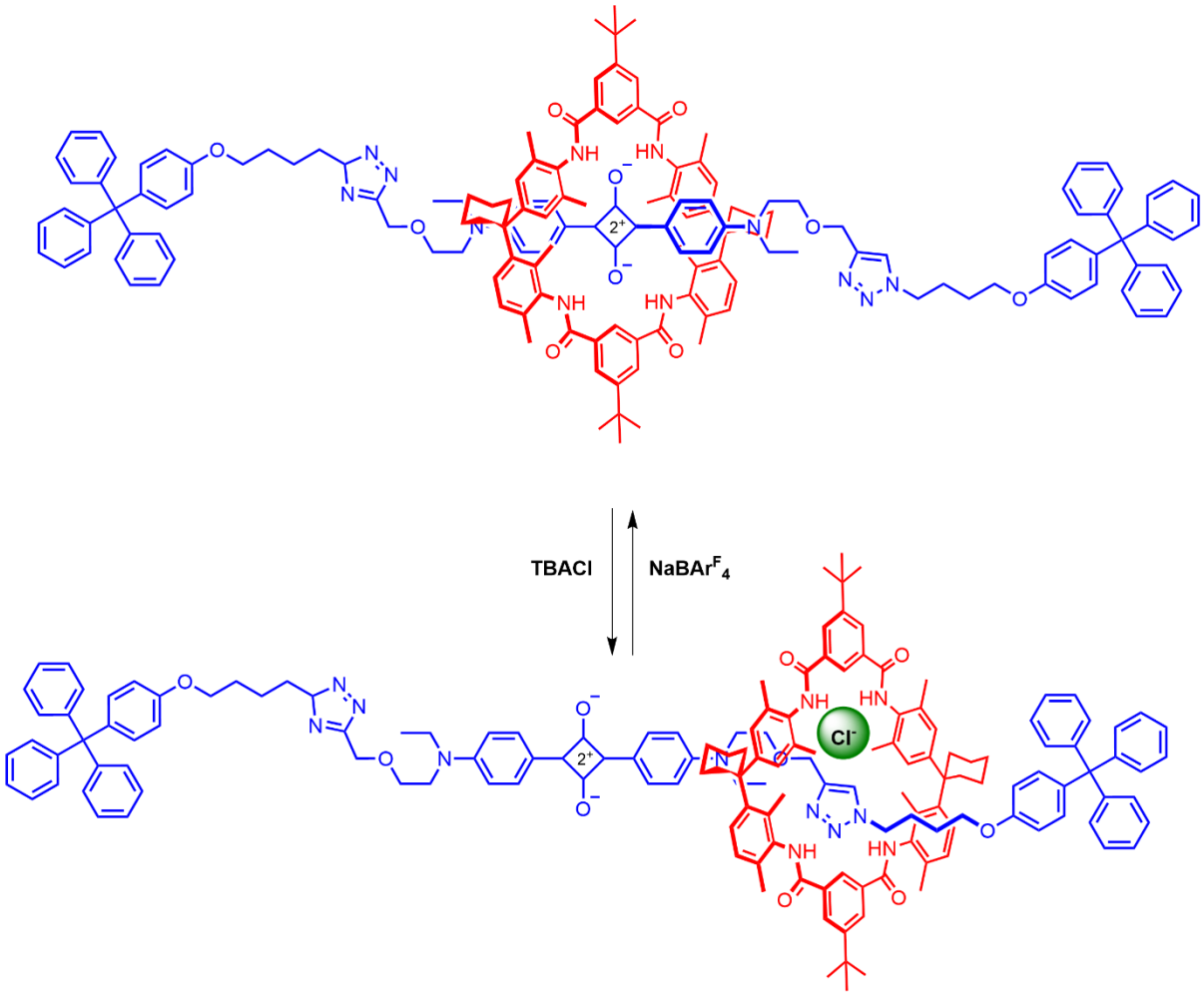


Figure 1.54. *Smith's chloride sensing [2]rotaxane.*[211]

Lin's diketopyrrolopyrrole (DPP) based [2]rotaxane is another example of a MIM host that undergoes macrocyclic translocation upon selective anion binding, in this case with fluoride in DMSO (Figure 1.55).[212] The authors posit that the initial addition of fluoride to the system leads to fluoride binding within the cavity of the rotaxane, which is tracked using both fluorescence-based and electrochemical experiments. However, further addition of the basic fluoride anion results in deprotonation of the amide donors, causing macrocyclic translocation to the DPP core inciting a colour change and quenching of fluorescence.

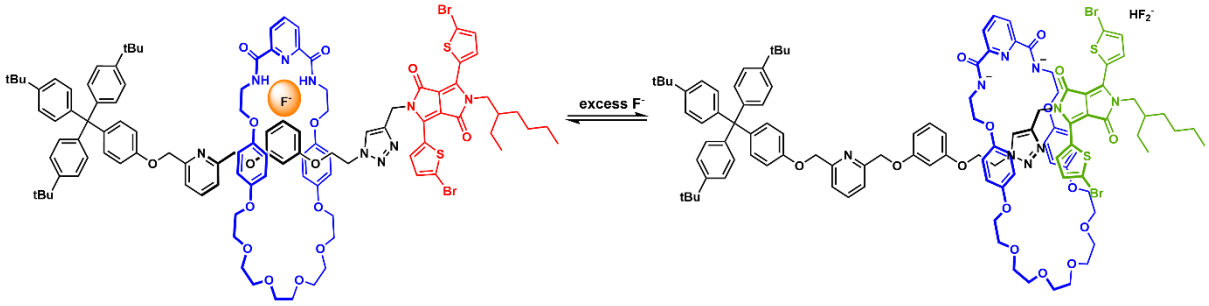


Figure 1.55. *Lin's DPP based [2]rotaxane fluoride receptor.*[212]

1.5.2.2 MIMs for membrane transport

Mechanically interlocked molecules have proven to be attractive candidates for synthetic molecular machines in part owing to the stochastic Brownian motion of the macrocycle component along the axle in a dynamic [2]rotaxane. This behaviour has rendered applications in biological fields including drug delivery and passive ion-transport across cell membranes. An example of the latter includes Smithrud's arginine-derivatized dibenzo-24-crown-8 (DB24C8) [2]rotaxane host system furnished with a benzo-18-crown-6 (B18C6) blocking group capable of transporting alkali and alkaline earth metal cations from aqueous environments across a chloroform phase membrane. While the DB24C8 site serves to enable effective binding in aqueous environments by contracting and forming salt-bridges, the B18C6 blocking

group is responsible for the binding of the metal cations (Figure 1.56).[213] As corroborated by their previous work with such systems,[214] the [2]rotaxanes were cytotoxic in the low micromolar range when incubated with SKOV-3 ovarian cancer cells. Upon addition of cations such as Ca^{2+} and Mg^{2+}, an increase in the cytotoxicity of the [2]rotaxanes indicated that intracellular cation binding and transport could be employed to trigger cell death by apoptosis.

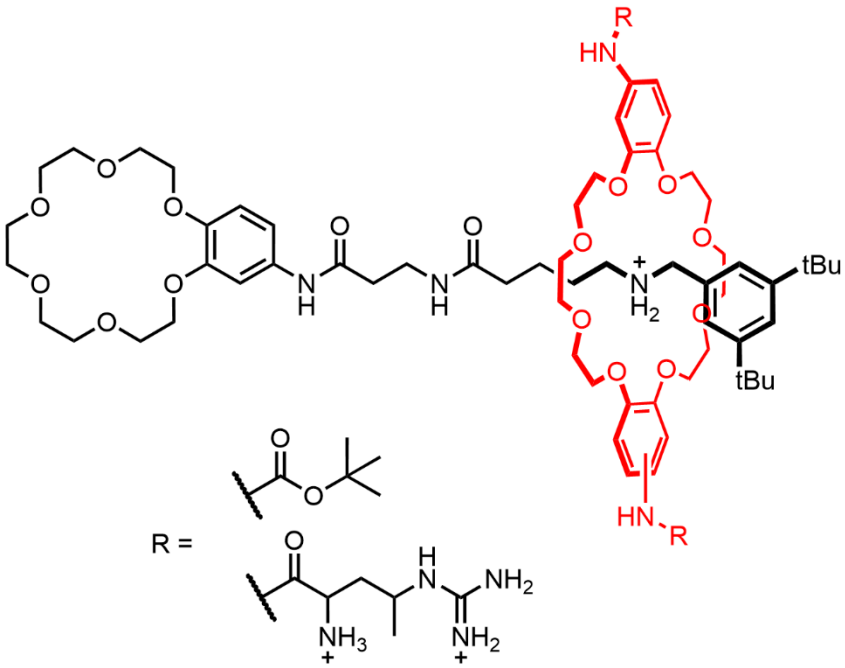


Figure 1.56. *Smithrud's host-[2]rotaxane for transport of alkaline metal cations.*[213]

A more recent example of a MIM-based [2]rotaxane ion-channel K^+/Cl^- co-transporter was reported by Pang *et al.* They showed that the introduction of an appended B18C6 crown-ether motif to the B24C8 macrocycle component and axle triazole units in the [2]rotaxane membrane spanning structure enabled strong ion-pair binding such that macrocyclic translocation facilitated K^+/Cl^- co-transport across the lipid bilayer (Figure 1.57).[215]

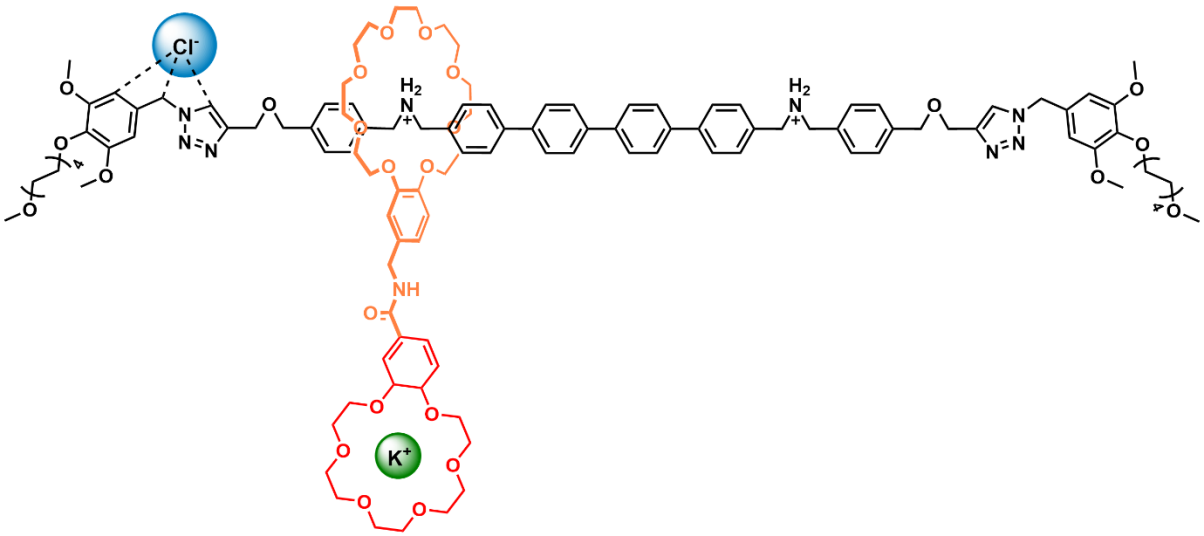


Figure 1.57. *Pang's [2]rotaxane ion-pair receptor and co-transporter.*[215]

1.5.2.3 Catalysis

Interlocked molecules have been frequently utilised as catalysts for organic synthesis, fuel cells and environmental remediation applications. Leung in 2016 described a fluorescent [2]rotaxane containing amine and thiourea axle stations, wherein the position of the macrocycle dictated which site mediated the selective catalysis of substrates in a multi-component system (Figure 1.58).[216] In a mixture containing the rotaxane, substrates A or B with a nitro-styrene C and aldehyde D, the thiourea of the rotaxane when de-shielded activated the nitro-olefin, whilst upon addition of base the exposed axle secondary amine brought about the iminium catalysis of substrate A/B with aldehyde D. The two co-conformational station macrocycle occupation modes of the rotaxane resulted in remarkable yields of the desired Michael addition products, with only trace amounts of the competing by-product alluding to the highly selective and effective nature of the rotaxane-based organocatalyst.

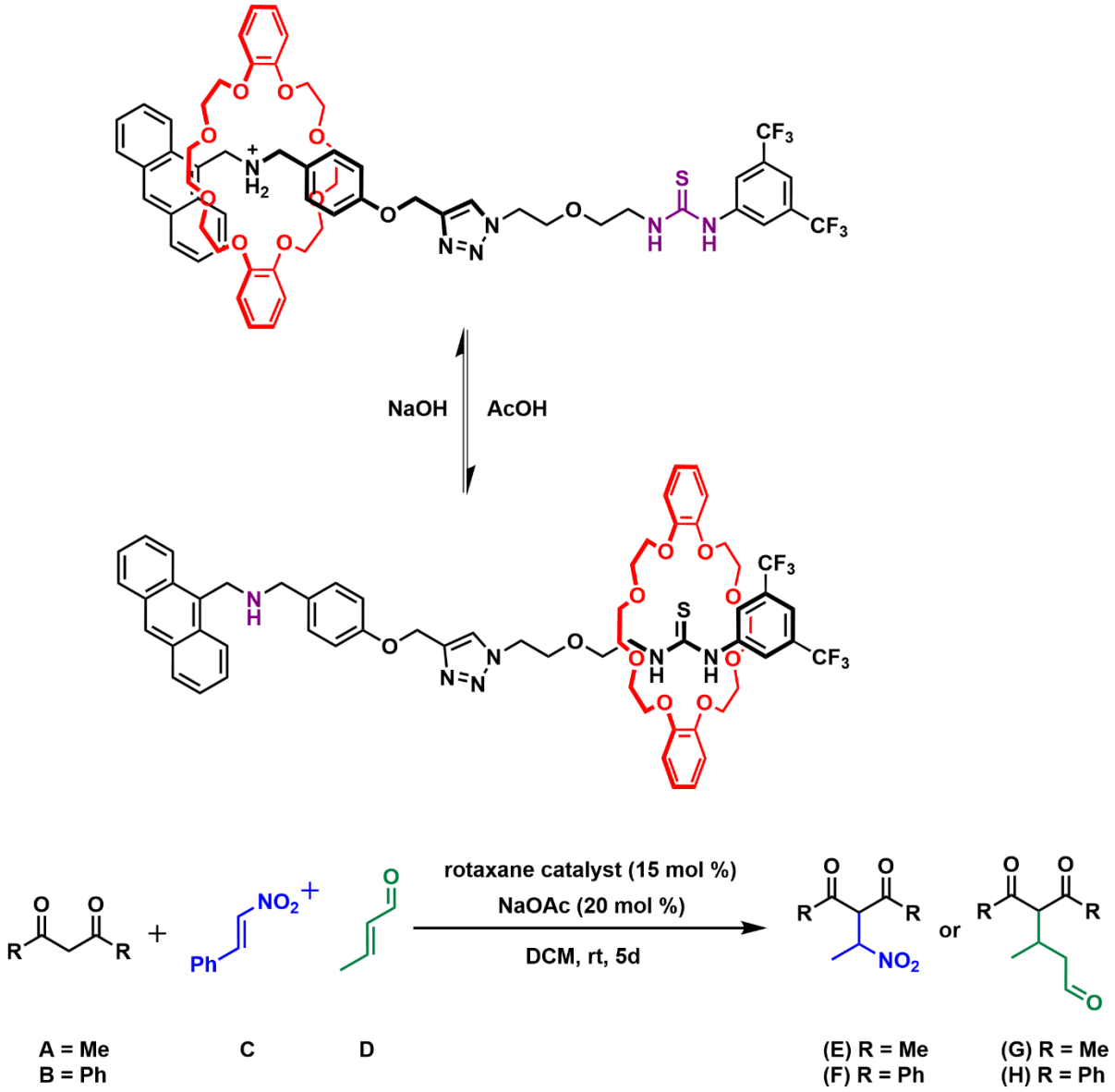
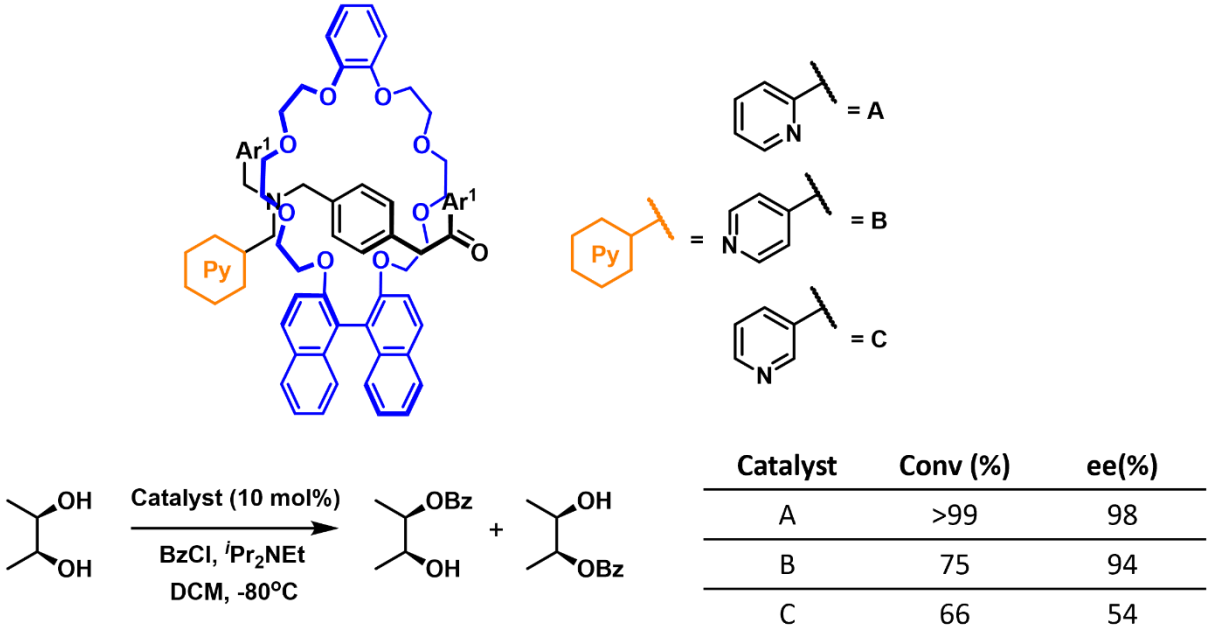


Figure 1.58. *Leung's acid-base mediated switchable [2]rotaxane catalyst.*[216]

In addition to catalysing reactions, MIMs can also serve as chiral catalytic carriers capable of transmitting their chiral information *via* asymmetric catalysis. A notable example is Takata's [2]rotaxanes containing a BINOL-based crown ether macrocycle and a nucleophilic pyridyl axle (Figure 1.59).[217] The influence of altering the position of the nitrogen in the pyridine unit relative to the linker was investigated by employing the [2]rotaxanes as catalysts in the o-benzoylation of *meso*-1,2-diphenylethane-1,2-diol. Studies revealed that while the

ortho and meta-pyridyl groups afford excellent stereoselectivities (94-98% *ee*), the para-pyridyl analogue results in only 54% *ee* formation.



Catalyst	Conv (%)	ee(%)
A	>99	98
B	75	94
C	66	54

Figure 1.59. *Takata's chiral rotaxanes with pyridine-groups.[217] Enantiomeric excess given for (1R-2S)-isomer.*

1.6 Project aims and objectives

The integration of squaramides into acyclic and macrocyclic host frameworks has shown enormous promise in the anion recognition field, with binding affinities typically surpassing those of traditional HB donors like urea and thiourea (See section 1.3.4.1.2.1). Surprisingly however, reports of incorporating such motifs into MIMs are rare with only a handful of examples known. Moreover, no instances of squaramide containing interlocked structures capable of host-guest recognition had been reported prior to the work carried out in this thesis. Exploiting the mechanical bond effect for charged guest recognition, the overall thesis project aim and objective was to design and construct novel squaramide-based MIM host molecules for anion, cation and ion-pair guest recognition.

Chapter 2 describes a series of asymmetrical squaramide-based heteroditopic [2]rotaxanes for lithium halide ion-pair recognition, synthesised *via* an active metal template approach. Extensive ^{1}H NMR titration studies are carried out to elucidate the anion and ion-pair recognition properties of these receptors. Solid-liquid extraction studies are also conducted to explore the [2]rotaxanes capability of extracting lithium halide salts into organic media.

Chapter 3 reports a series of symmetrical squaramide-based heteroditopic [2]rotaxanes for the purpose of sodium halide ion-pair recognition. An alkali metal cation template-directed approach is utilised for the synthesis of the target interlocked receptors. Quantitative ^{1}H NMR titration studies are carried out to determine their anion and ion-pair recognition properties in competitive organic solvent mixtures. Additionally, solid-liquid extraction studies are carried out to explore the sodium halide salt extraction capabilities of the [2]rotaxanes.

Chapter 4 details a series of mono- and bis-squaramide-based [2]rotaxanes synthesised using Cu(I) catalysed active metal template methodology. The halide and oxoanion binding properties of the [2]rotaxanes are examined *via* quantitative ^{1}H NMR titration experiments to investigate the impact of multiple squaramide motifs on the anion binding capabilities of the receptors.

Chapter 2: Squaramide-based Heteroditopic [2]Rotaxanes for Lithium Halide Ion-pair Recognition and Extraction

2.1 Introduction

2.1.1 MIMs for heteroditopic ion pair recognition

As discussed in the introductory chapter, section 1.4, heteroditopic ion-pair receptors containing discrete recognition sites for cations and anions offer a useful solution to circumventing the energy cost expended by monotopic receptors in trying to separate the target guest ion from its counter-ion. Moreover, heteroditopic host systems further bring into focus the interplay between the co-bound ions and its effect on host-guest association strength. This effect, better known as cooperativity usually occurs as a result of favourable coulombic electrostatic interactions between the co-bound ions and/or conformational allosteric effects instigated by the ion-pair binding event. While the area of ion-pair recognition has seen extensive advancement over the years, heteroditopic receptor examples have mostly been dominated by acyclic or macrocyclic receptors. A good example is Smith's ditopic macrobicyclic receptor that cooperatively binds and extracts alkali metal halide ion pairs *via* convergent HB donors as anion binding sites and crown-ether based alkali metal cation recognition sites, exhibiting up to a 9-fold enhancement in the chloride association

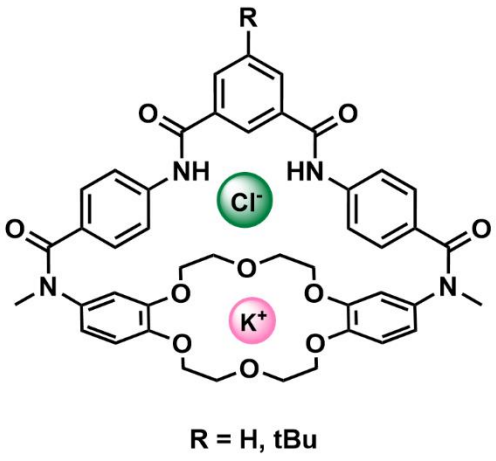


Figure 2.1. *Smith's ditopic macrocyclic ion-pair receptor.*[218]

constant value in the presence of one equivalent of potassium tetraphenylborate salt in 3:1 DMSO/MeCN solvent mixture (Figure 2.1).[218]

Despite the advantages of their unique topologies and preorganised interlocked cavities that have in particular been shown to enhance anion recognition capabilities (see section 1.5.1.2), examples of heteroditopic MIMs remain scarce. The first example of such a system, a heteroditopic [2]rotaxane, was only reported in 2014 by Knighton *et al.*, wherein coordination of alkali metal cations (Li^+, Na^+ and K^+) to the calix[4]diquinone unit in the macrocycle in concert with the axle's pyridyl N-oxide motif induced pirouetting of the MIM components resulting in preorganisation of the rotaxane's axle amide hydrogen bond donors for anion recognition (Figure 2.2).[219] This favourable cation-induced preorganisation of the anion recognition site was consistent with the significant enhancement witnessed in the chloride binding strength, with the largest enhancement observed in the presence of Na^+ (15-fold for Cl^- in 4:1 $CDCl_3/CD_3OD$ solvent mixture).

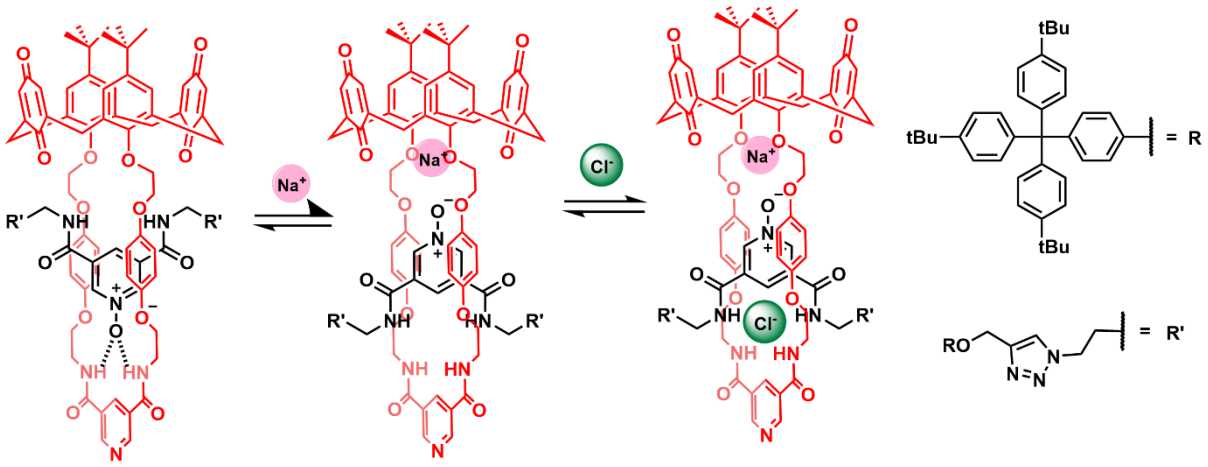


Figure 2.2. *Knighton's calix[4]diquinone-based [2]rotaxane exhibiting ion-pair binding.*[219]

Even since then only a handful of heteroditopic MIMs have subsequently appeared including Beer's [2]catenane consisting of a pyridine N-oxide macrocycle and a pyridinium bridged calix[4]diquinone macrocycle operating as a macrocycle-separated ion-pair receptor

(Figure 2.3).[220] Synthesised using an unprecedented sodium cation-template activated ester amide condensation clipping methodology, the resulting [2]catenane was serendipitously isolated with a NaCl ion-pair endotopically bound within the binding cavities separated by the macrocycles, characterised by single crystal X-ray structural analysis.

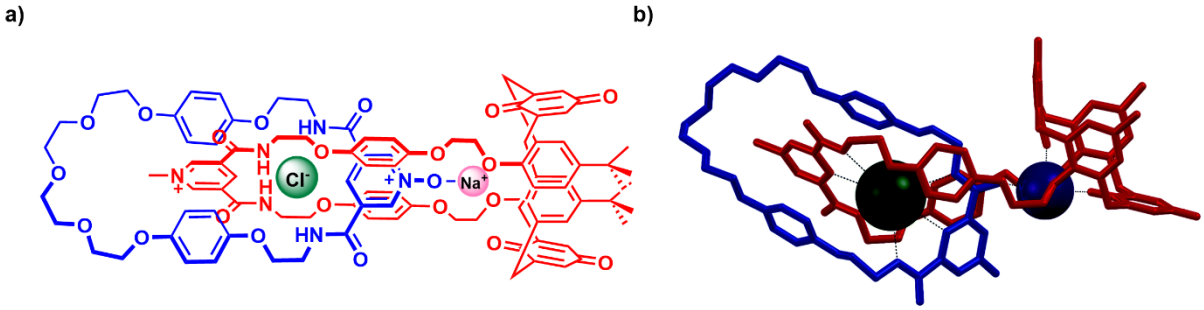


Figure 2.3. *a) Beer's macrocycle-separated heteroditopic [2]catenane NaCl ion-pair complex; b) Single-crystal X-ray structure of [2]catenane ·NaCl (stick representation).*[220]

Valderrey *et al.* recently described a bis-calix[4]pyrrole containing [2]rotaxane which strongly bound tetraalkylammonium salts of Cl^-, OCN^- and NO_3^- in a 1:1 binding stoichiometry in chloroform (Figure 2.4).[221] Quantitative ITC titration experiments revealed that the interlocked system demonstrated a preference for TBANCO ($7.9\times10^5\ M^{-1}$) over $TBANO_3$ ($4\times10^4\ M^{-1}$) and TBACl ($5\times10^4\ M^{-1}$) in $CDCl_3$ likely due to host-guest size complementarity between the cylindrical cavity and linear NCO^- anion. Furthermore, replacing the organic cation to methyltrioctylammonium (MTO^+) resulted in a 20-fold increase in the binding of MTOCl relative to TBANCO, presumably due to better encapsulation of the cation within the calix[4]pyrrole unit.

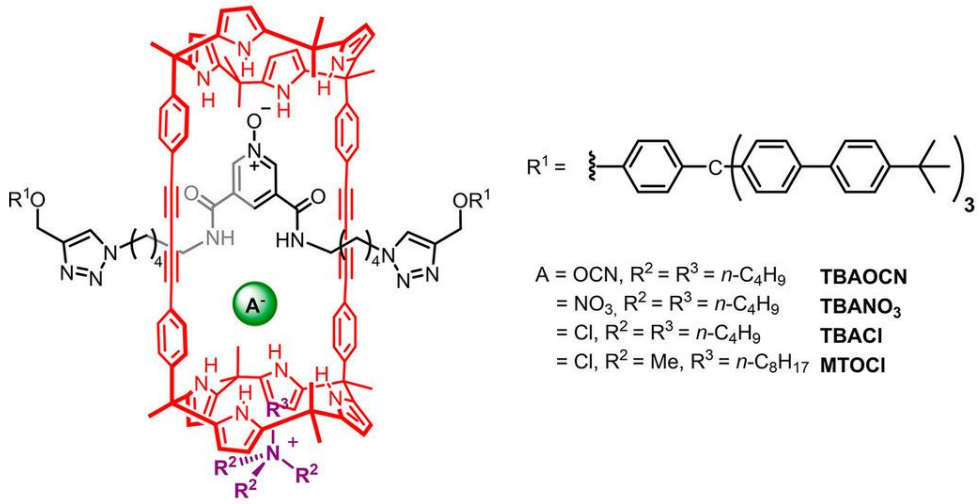


Figure 2.4. *Valderrey's [2]rotaxane for the recognition of quaternary ammonium salts.*[221]

Another example is Goldup's [2]rotaxane which binds an ion-pair *via* pH stimulated macrocyclic translocation (Figure 2.5).[222] Their work emphasises the importance of a H^+ cation in shuttling the macrocycle away from the urea unit in the axle, consequently enabling anion recognition at the urea station in 1:1 $CDCl_3/CD_3CN$ solvent mixtures ($K_a(Cl^-) > 10^4$, $K_a(Br^-) = 4.7 \times 10^3$, $K_a(HSO_4^-) = 2.3 \times 10^3$).

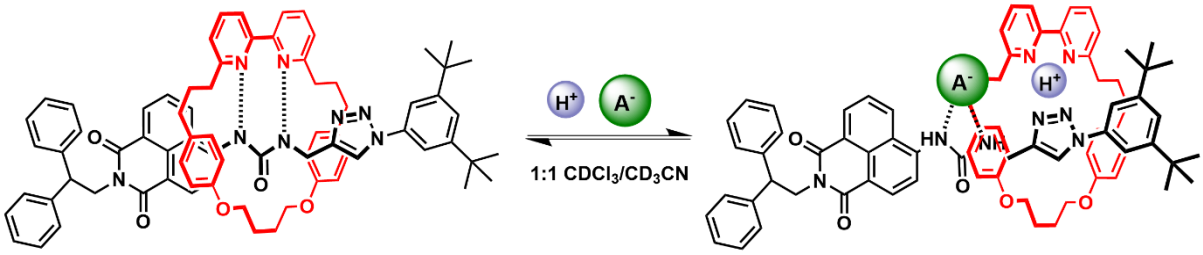


Figure 2.5. *Goldup's proton pH mediated ion-pair receptor.*[222]

More recently, Beer and co-workers reported a series of XB and HB functionalised heteroditopic [2]rotaxanes for lithium halide ion-pair recognition (Figure 2.6).[223] Wherein lithium cation-coordination to the pyridyl binding site of the [2]rotaxane instigated a notable increase in the binding of halides like bromide and iodide in polar organic solvent media. Moreover, the XB furnished [2]rotaxane exhibited remarkably stronger LiBr/LiI ion-pair

affinities compared to the HB [2]rotaxane analogue underscoring the superiority of XB-halide sigma-hole interactions.

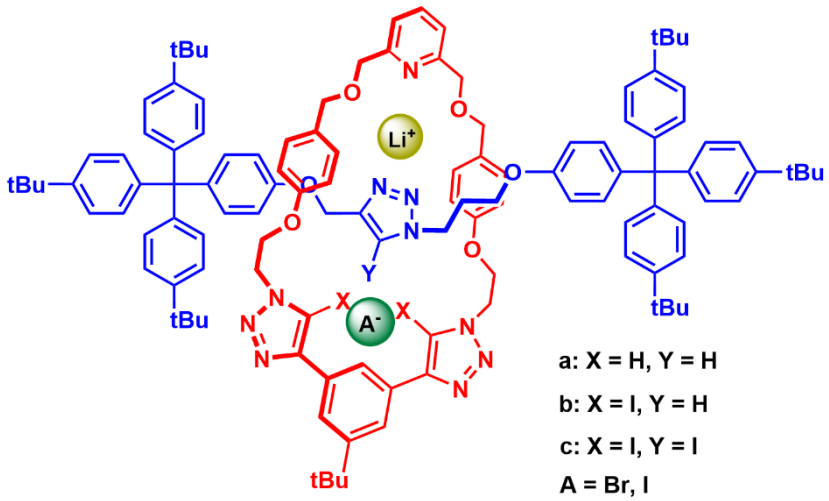


Figure 2.6. *Beer's heteroditopic [2]rotaxanes for lithium halide ion-pair recognition.*[223]

Drawing inspiration from Chiu's [2]catenane synthesis involving sodium cation templated polyether precursors,[181] Beer and co-workers designed XB heteroditopic [2]catenanes for ion-pair recognition and extraction. Using a sodium cation template to preorganise polyether-based precursors, subsequent CuAAC bis-azide-bis-iodoalkyne click cyclisation reactions afforded a series of potent heteroditopic catenanes (Figure 2.7).[224] Single

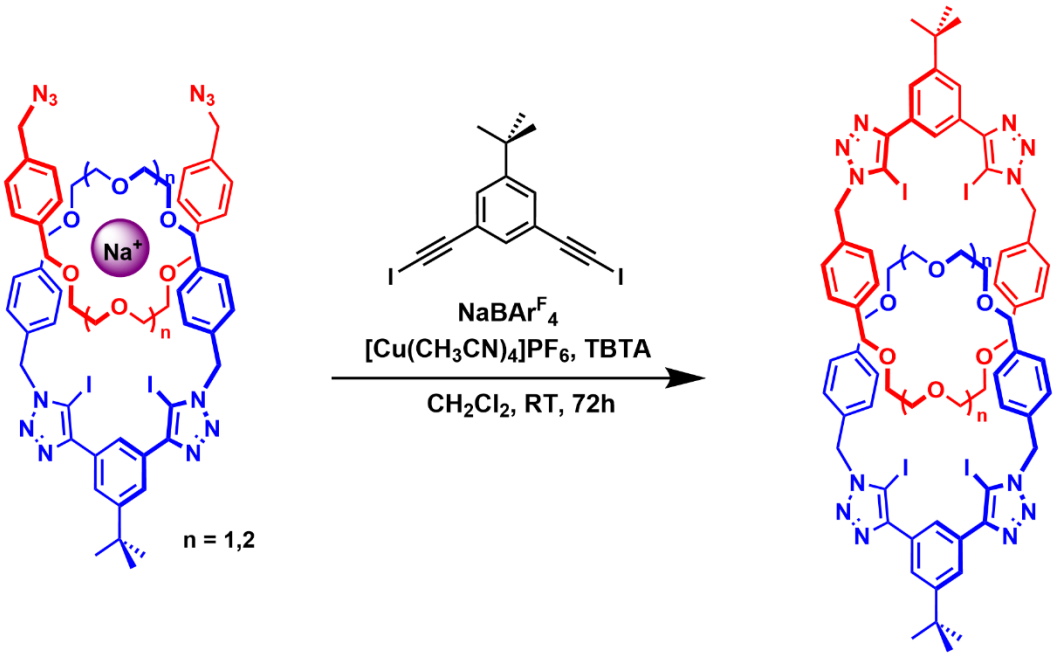


Figure 2.7. *Beer's heteroditopic [2]catenane alkali metal halide receptors.*[224]

crystal XRD structural analysis and ^{1}H NMR studies in 1:1 $CD_3CN/CDCl_3$ solvent media revealed the addition of sodium or potassium alkali metal cations induced co-conformational changes in the interlocked macrocycle components, favourably preorganising the XB anion binding sites and effecting a significant enhancement in halide anion binding affinities.

2.1.2 Squaramide containing MIMs

Section 1.3.4.1.2.1 detailed the effective use of squaramides in acyclic and macrocyclic frameworks for the purpose of anion recognition, with their binding affinities often surpassing those of traditional N-H directed HB donor analogues like urea and thiourea even in competitive polar solvents. Reports of integrating squaramides into MIMs however are surprisingly rare with only a couple of examples known.

The first example of a squaramide-functionalised [2]rotaxane was reported by Leigh and co-workers in 2015. Their switchable [2]rotaxane organocatalyst contained a secondary

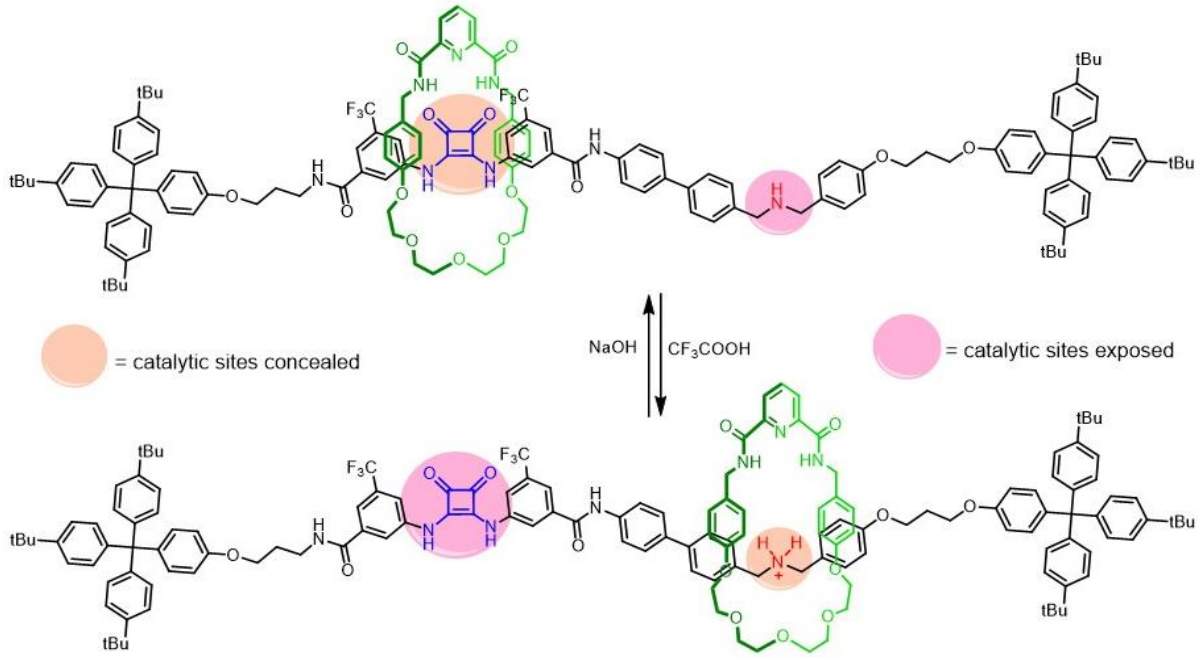


Figure 2.8. *Leigh's acid-base mediated switchable rotaxane catalyst.*[225]

amine and squaramide active site, each promoting a different chemical transformation *via* acid-base mediated macrocyclic translocation (Figure 2.8)[225]

More recently, Spicer *et al.* reported a series of chiral [2]rotaxanes furnished with either a urea or squaramide motif in which addition of chloride instigated macrocyclic shuttling across the axle component along with changes in the expression of mechanical chirality of the interlocked systems (Figure 2.9).[226] Both phenomena were reversed upon addition of $NaBAr^{F}{}_{4}$ owing to the extraction of chloride *via* salt precipitation.

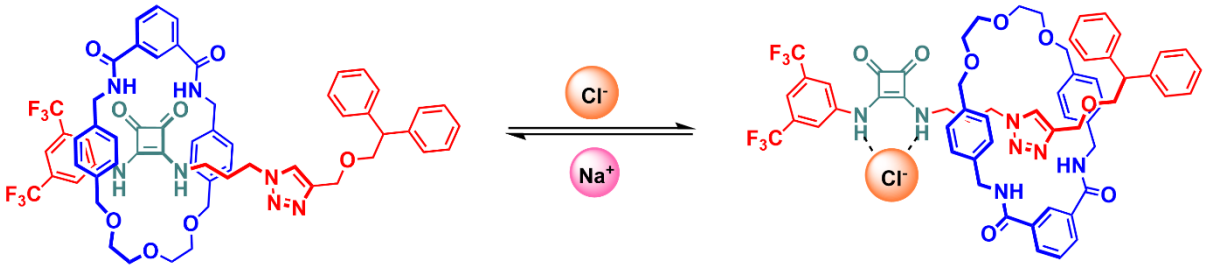


Figure 2.9. *Spicer's squaramide containing chiral [2]rotaxane.*[226]

2.2 Chapter objectives

Despite squaramides being well-known for their bidentate N-H hydrogen bond donors for anion recognition applications, the Lewis basicity of their carbonyl groups for potential metal

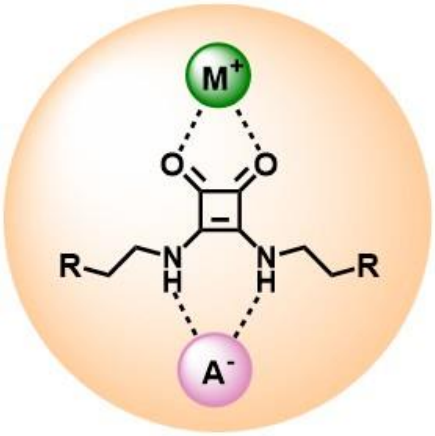


Figure 2.10. *Potential of the squaramide motif for ion-pair recognition highlighting its ambidentate coordination mode utilised in this work. M^{+} = Alkali metal cation, and A^{-} = Halide anion.*

cation binding has surprisingly not been exploited. With this in mind, the overall theme of this thesis was to design and integrate squaramide-functionalised synthons into heteroditopic MIM host frameworks for the purposes of ion-pair recognition. Wherein it was envisioned that the squaramide motif would simultaneously bind a metal cation *via* bidentate chelation of the carbonyl groups and an anion through the NH donors (Figure 2.10).

Specifically for this chapter's project, lithium halide salt ion-pair recognition was targeted. Over the past few decades, the demand for lithium salts has witnessed a sharp increase owing to their ever-increasing use in lithium-ion batteries, metallurgy and manufacturing in automotive and renewable energy sectors, in addition to applications in pharmaceuticals and the nuclear industry.[227-230] However, despite their importance in modern life, lithium salts pose significant biological risks causing irreversible neurological impairments including dementia, Parkinson's disease and peripheral neuropathies in humans.[231,232] Recent reports have revealed an alarming increase in lithium concentration in streams and soil due to irresponsible mining practices and injudicious disposal of batteries and salt-extraction effluents.[233] Lithium salt recognition is therefore becoming increasingly crucial for the sake of technological advancement and mitigation of its adverse biological and environmental effects.

The aim of this project was to design and synthesise a series of novel squaramide-based heteroditopic [2]rotaxanes for lithium halide ion-pair recognition (Figure 2.11). To this end, soluble asymmetrical, squaramide-based axle precursor synthons and appropriate halogen bonding (XB) and hydrogen bonding (HB) macrocycle components were initially prepared for integration into rotaxane MIM structural frameworks.

Extensive ^{1}H NMR titration studies were carried out to elucidate cation, anion and ion-pair recognition properties of these receptors, as well as solid-liquid extraction studies with lithium halide salts. Additionally, the incorporation of photo-active coumarin motifs into the rotaxane's axle component enabled preliminary ion-pair sensing investigations to be undertaken.

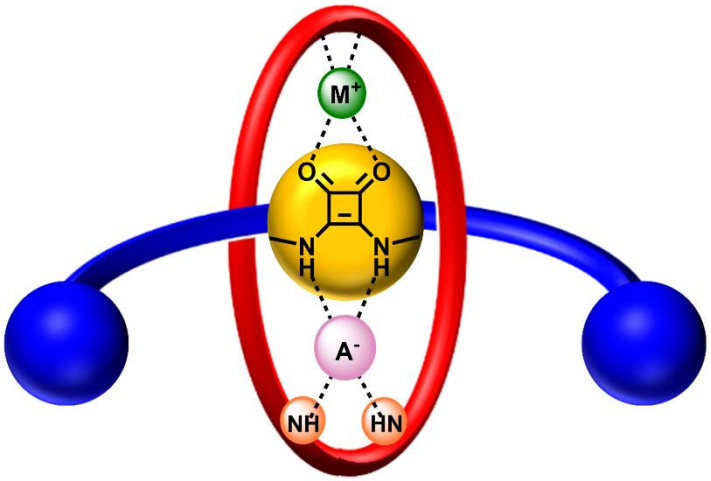


Figure 2.11. *Cartoon representation of ion-pair binding with a squaramide containing rotaxane. M^+ = Lithium cation, and A^- = Halide anion.*

2.3 Synthesis and characterisation

Section 1.5.1.1.2 of the introductory chapter detailed the use of the active metal template (AMT) methodology as a powerful and versatile tool for synthesizing interlocked structures like rotaxanes and catenanes. A typical AMT MIM synthetic protocol employs a copper(I) catalysed stopper terminal alkyne-azide cycloaddition (CuAAC) reaction where Cu(I) is endotopically bound within the cavity of a macrocycle to catalyse triazole mechanical bond formation.

The synthetic strategy utilised to prepare the target heteroditopic squaramide-based [2]rotaxanes adapted this AMT--CuAAC methodology which required the initial preparation

of appropriate azide functionalised squaramide axle precursor synthons and pyridyl containing XB/HB macrocycles.

2.3.1 Synthesis of squaramide axle precursor synthons

The initial design of the acyclic squaramide axle precursor synthon lent inspiration from Leigh's switchable pH-modulated [2]rotaxane catalyst discussed in section 2.1.2 (Figure 2.12).[225] The electron withdrawing CF_3 groups were expected to impart hydrophobicity and strong anion recognition capabilities to the receptor. Additionally, the azide functional groups were incorporated to enable participation in copper (I) catalysed azide-alkyne cycloaddition (CuAAC) click reactions with stopper alkynes in attempts to form the target interlocked structures.

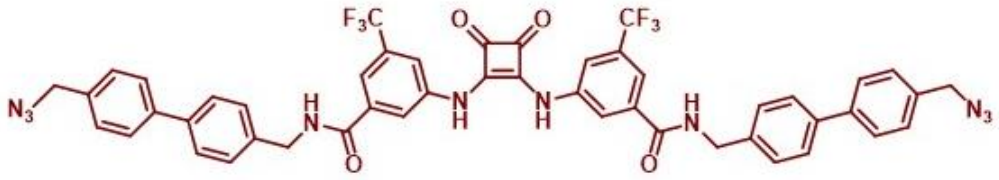
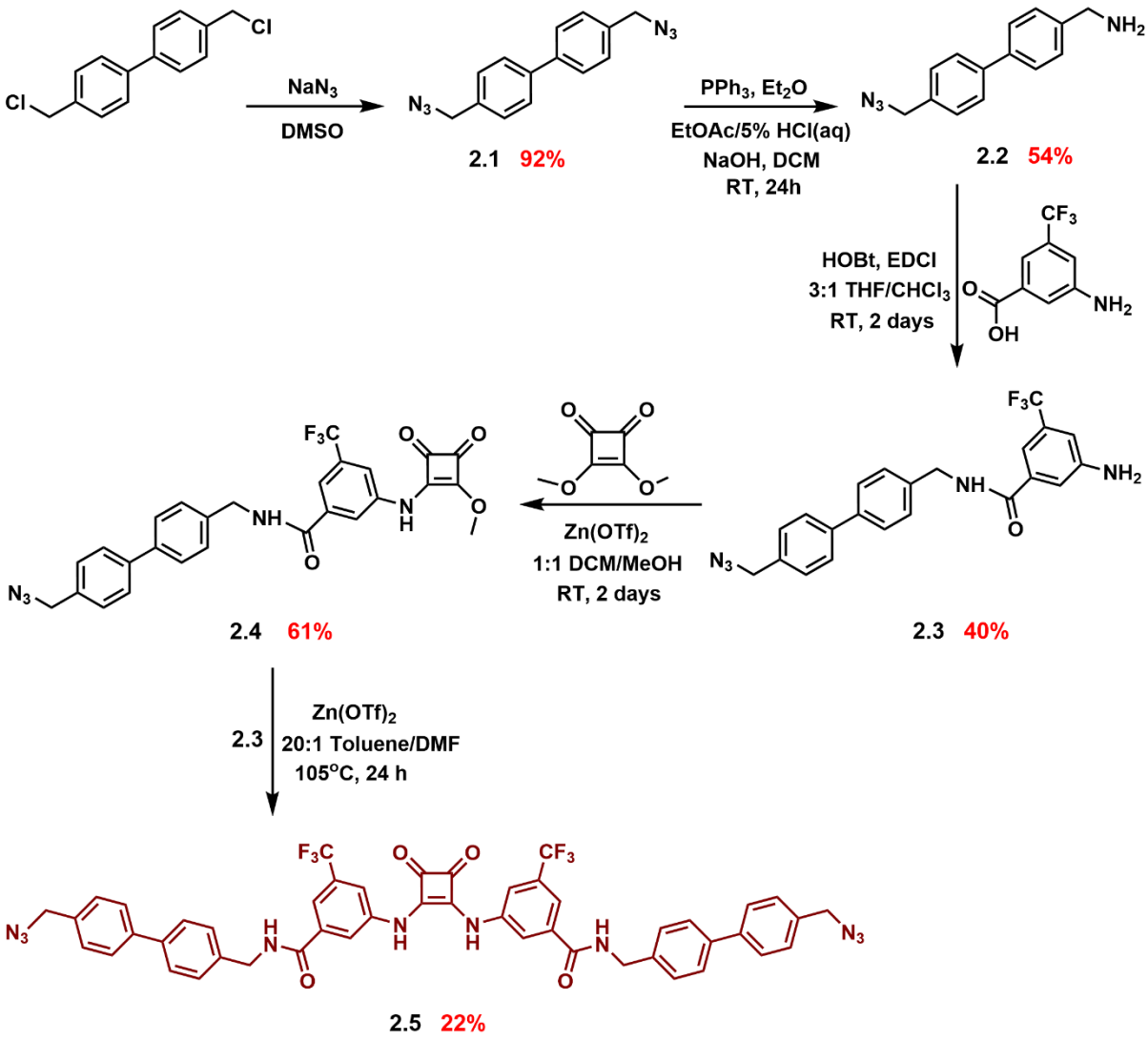


Figure 2.12. *Target acyclic squaramide axle precursor synthon.*

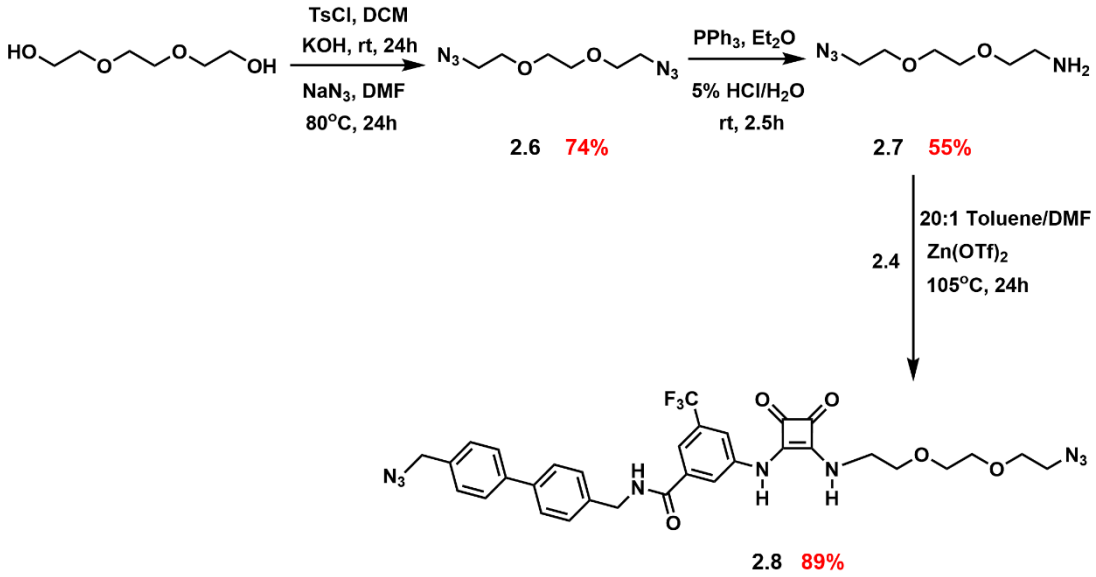
The synthesis of the target molecule (Scheme 2.1) began with the preparation of bis-azide **2.1** using a known literature procedure,[234] which upon monoreduction with triphenylphosphine in the presence of 5% HCl in ethyl acetate/diethyl ether solvent mixture gave **2.2** in a 54% yield. Condensation of **2.2** with 3-amino-5-(trifluoromethyl) benzoic acid afforded **2.3** in a 40% yield which was subsequently mono-coupled with methyl-squarate ester in the presence of zinc triflate. Due to poor solubility, the reaction was carried out in multiple small-scale setups to give a final yield of 61%. The second coupling was carried out under harsher conditions in a 20:1 toluene:DMF solvent mixture heated to 105^{o}C to produce **2.5** in a 22% yield following purification using preparatory TLC in a 2% MeOH/DCM solvent

system. This low yield of **2.5** may be attributed to the compound's poor solubility in common organic solvents, a phenomenon frequently observed with squaramide-based derivatives due to hydrogen bonding induced intermolecular stacking in relatively less polar organic solvents. Unfortunately, the poor solubility of **2.5** precluded attempts to incorporate the motif into interlocked structures.



Scheme 2.1. *Synthesis of target molecule* ***2.5****.*

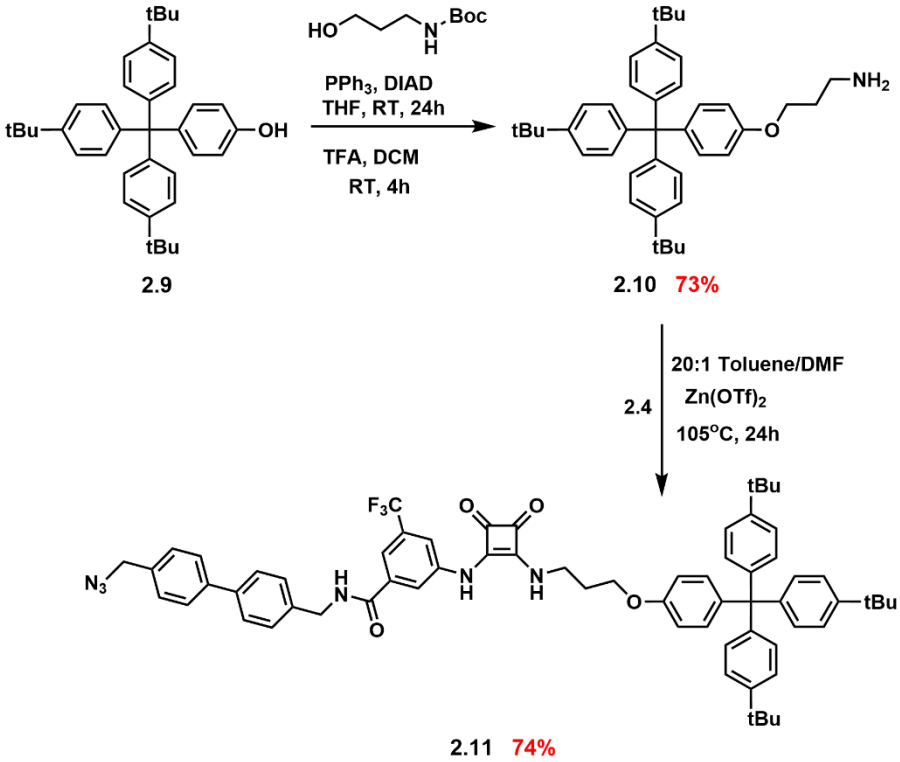
To overcome the issue of poor solubility, a series of asymmetric, potentially more soluble synthons **2.8** and **2.11** were designed. Tosylation of triethylene glycol, followed by reaction with sodium azide afforded bis-azide **2.6** in 74% overall yield (Scheme 2.2).



Scheme 2.2. *Synthesis of synthon* ***2.8***

Monoreduction with triphenylphosphine in the presence of 5% HCl gave **2.7** in 55% yield. Previously prepared compound **2.4** was then condensed with **2.7** to afford **2.8** in 89% yield.

Alternatively, asymmetrical squaramide axle precursor synthon **2.11** was designed by introducing a tertiary butyl terphenyl appended stopper to improve solubility. Previously



Scheme 2.3. *Synthesis of synthon* ***2.11****.*

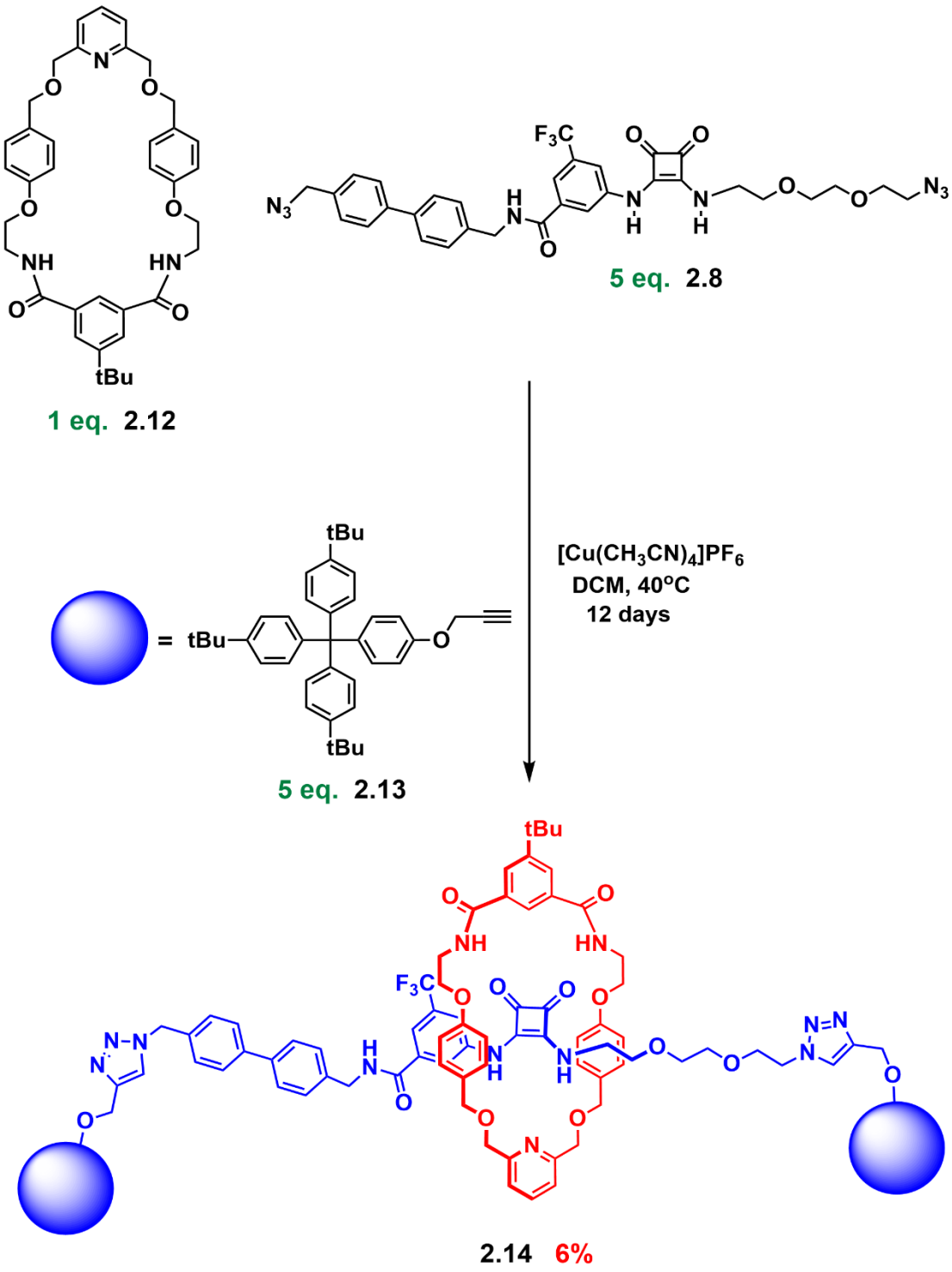
synthesized stopper precursor, **2.9**,[235] was reacted with Boc-protected 3-aminopropanol following a reported procedure,[236] to form, after TFA Boc-deprotection, amine functionalised stopper **2.10** in 73% yield (Scheme 2.3). Condensation of **2.10** with **2.4** in the presence of zinc triflate afforded **2.11** in 74% yield.

2.3.2 Synthesis of HB/XB macrocycles for AMT-directed [2]rotaxane preparation

Following the synthesis of soluble squaramide-based axle precursors, the preparation of HB macrocycle **2.12** and XB macrocycle **2.16** was undertaken following previously reported multi-step procedures.[223] Both macrocycles **2.12** and **2.16** contained a pyridyl motif unit to facilitate the AMT-- CuAAC rotaxane synthesis.

2.3.3 Synthesis of squaramide-functionalised HB [2]rotaxane

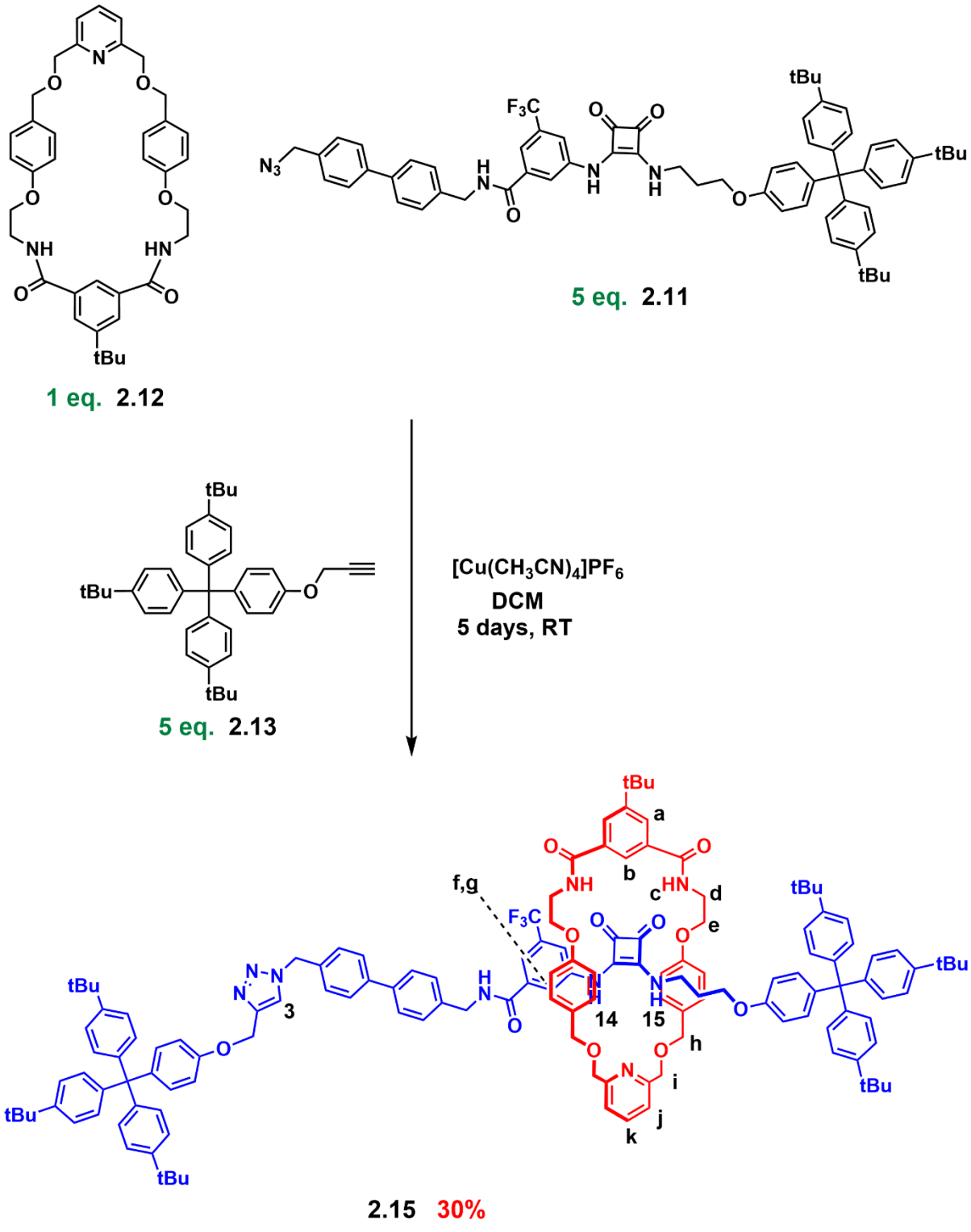
Employing typical AMT conditions, an equimolar mixture of macrocycle **2.12** and $Cu(CH_3CN)_4PF_6$ in dichloromethane was combined with five equivalents of stopper alkyne **2.13** and bis-azide **2.8**. The reaction was left to stir at room temperature for seven days, during which monitoring the reaction using TLC revealed no evidence of the desired product. However, heating to 40^{o}C for the next five days led to reaction products as indicated by TLC analysis. Purification by preparative TLC afforded [2]rotaxane **2.14** (Scheme 2.4) in a modest isolated yield of 6%. which was characterised by ^{1}H NMR and ESI-HRMS. The low yield of the [2]rotaxane precluded characterisation using ^{13}C NMR analysis.



Scheme 2.4. *Synthesis of [2]rotaxane* ***2.14****.*

An analogous AMT rotaxane synthesis was undertaken with mono-stoppered azide axle precursor synthon **2.11**, macrocycle **2.12** and stopper alkyne **2.13** in the presence of $Cu(CH_3CN)_4PF_6$ in dichloromethane at room temperature (Scheme 2.5). The reaction mixture

was monitored for 5 days by TLC, following which an aqueous work-up and purification using preparative TLC resulted in a significantly improved 30% yield of [2]rotaxane **2.15**. The novel rotaxane was characterised using ^{1}H NMR, ^{13}C NMR and ESI-HRMS.



Scheme 2.5. *Synthesis of [2]rotaxane* ***2.15.***

Successful formation of [2]rotaxane **2.15** was evidenced by comparison of its ^{1}H NMR spectrum with those of its macrocycle and axle components in $CDCl_3$ (Figure 2.13). Diagnostic upfield shifts of the macrocycle's aryl protons, $H_{f,g}$ owing to donor-acceptor interactions between the macrocycle's electron-rich aromatic groups and electron-deficient squaramide axle component were indicative of mechanical bond formation. Also of note were the downfield shifts of the internal macrocycle isophthalamide cavity protons H_b and H_c, likely due intercomponent HB interactions between the amide HB donors of the macrocycle and squaramide Lewis basic carbonyl groups in the axle.

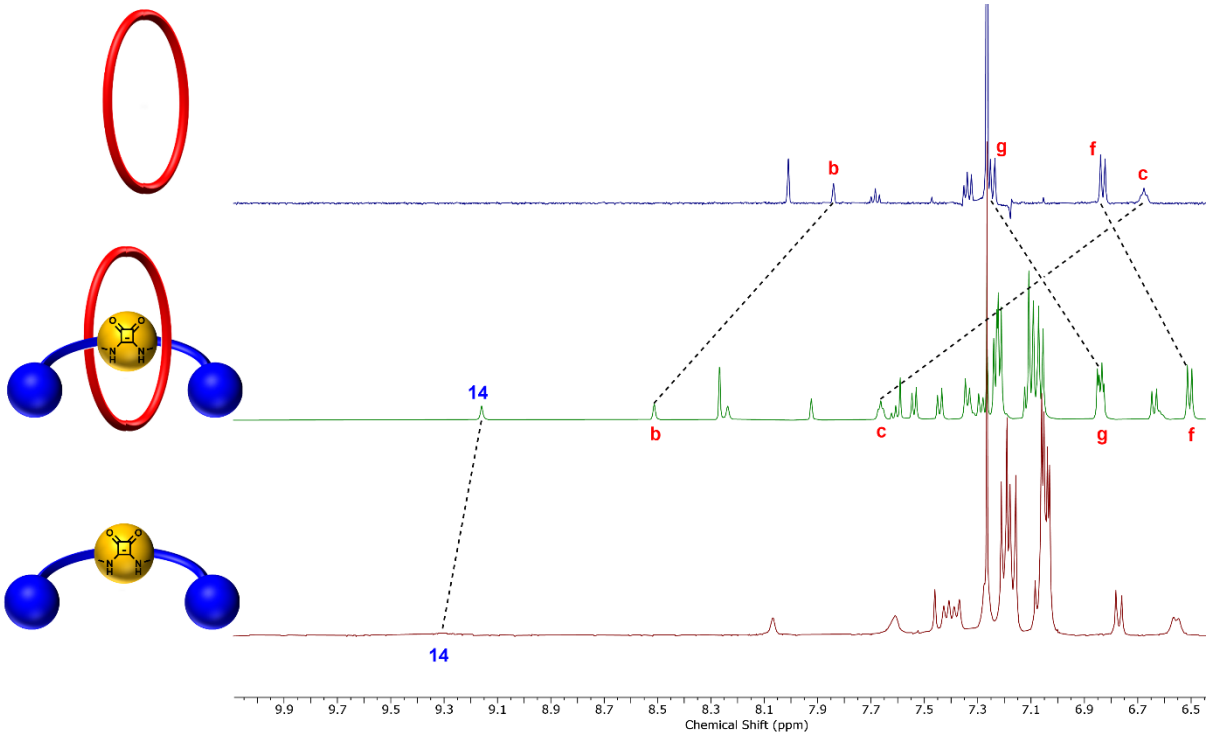


Figure 2.13. *Truncated stacked ^{1}H NMR spectra of i) macrocycle **2.12** ii) [2]rotaxane **2.15** and iii) axle component **2.15a** ($CDCl_3$, 500 MHz, 298K).*

Interestingly, the ^{1}H-^{1}H ROESY NMR study in $CDCl_3$ revealed through space coupling between the axle squaramide NH protons and the macrocycle protons while none was observed between the axle's triazole proton and the protons of the macrocycle (Figure 2.14). This suggested that the macrocycle resides at the squaramide centre of the axle likely due to

favourable intercomponent hydrogen bonding interactions between the axle-squaramide HB NH donors and pyridyl group of the macrocycle.

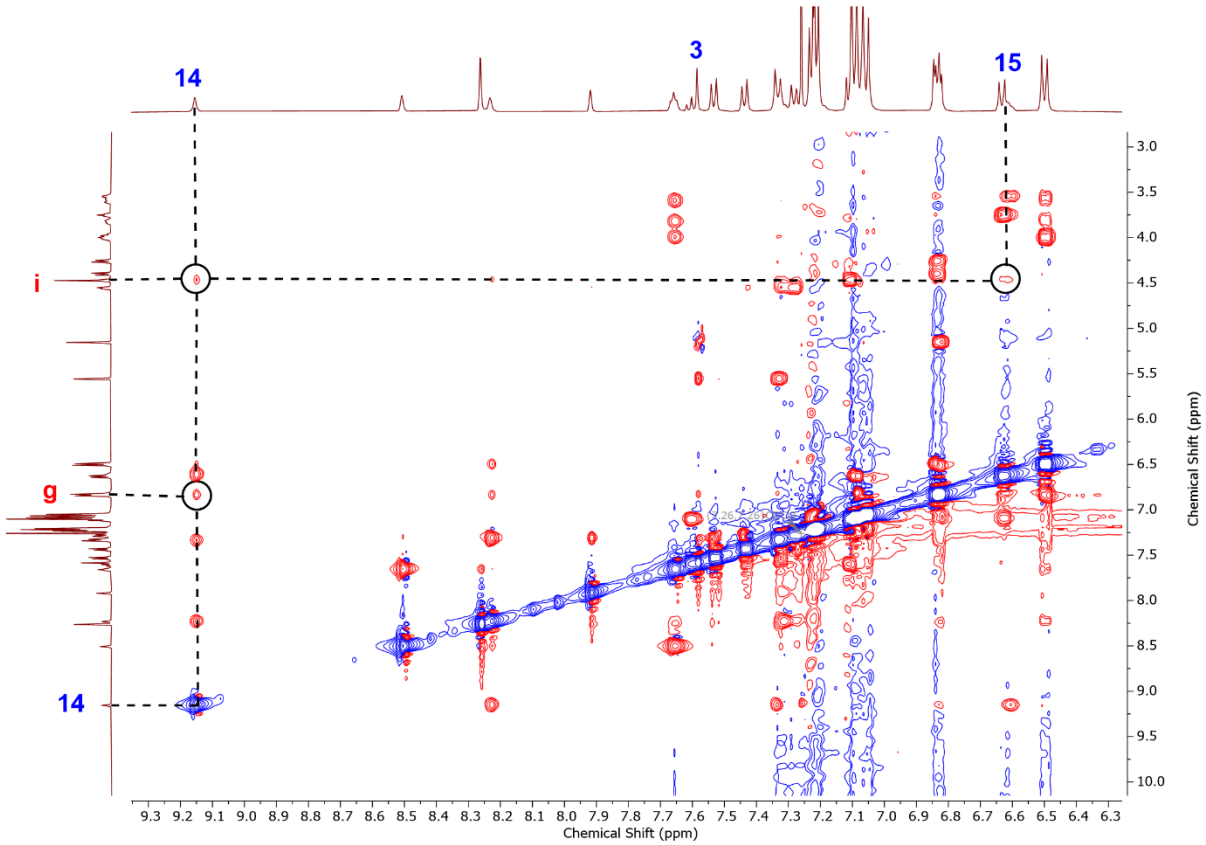
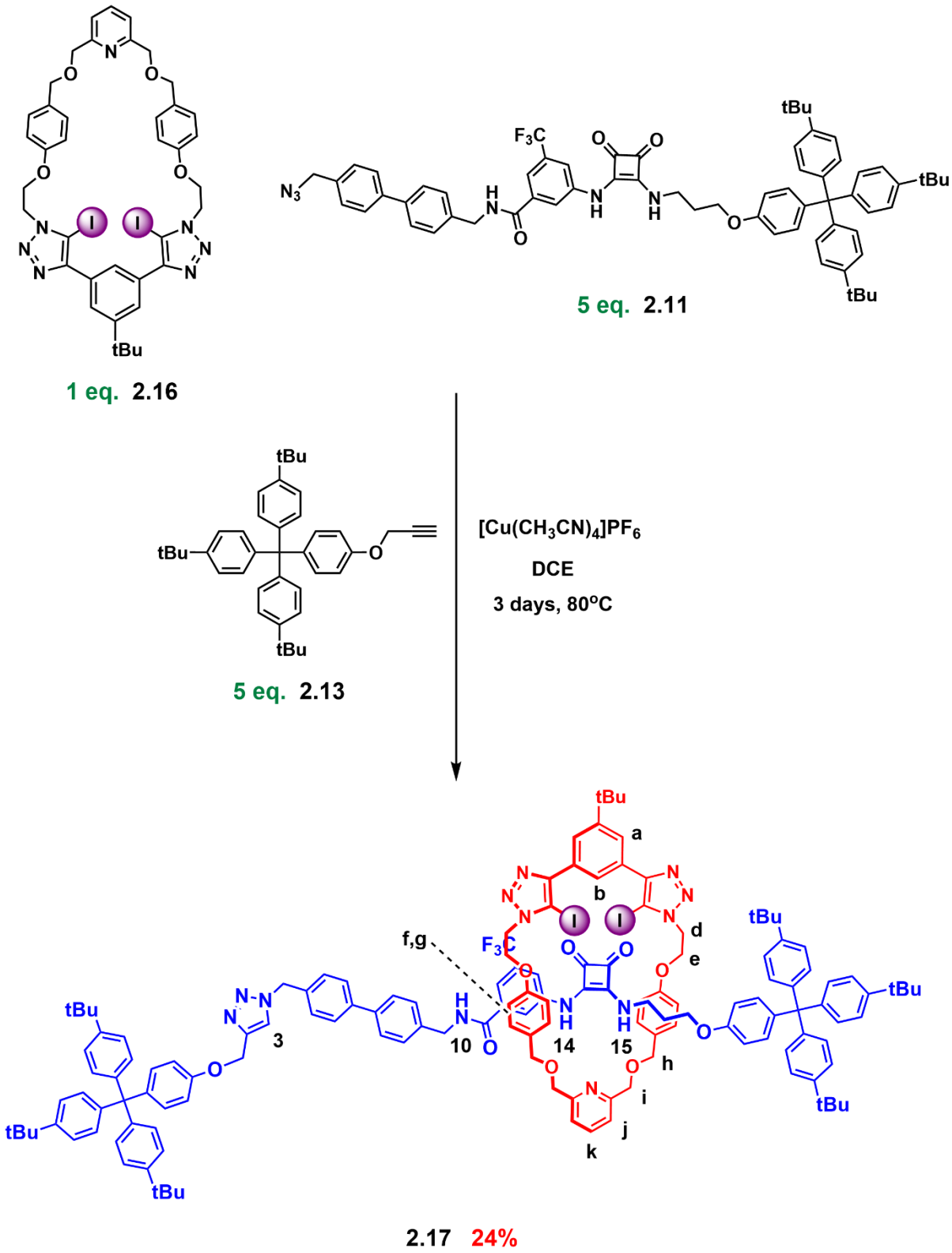


Figure 2.14. *Truncated ^{1}H-^{1}H ROESY NMR spectrum of [2]rotaxane* ***2.15*** *in $CDCl_3$.*

2.3.4 Synthesis of squaramide-functionalised XB [2]rotaxane

An equimolar mixture of macrocycle **2.16** and $Cu(CH_3CN)_4PF_6$ in dichloroethane was combined with five equivalents of stoppered alkyne **2.13** and mono-stoppered azide **2.11** (Scheme 2.6). The reaction was left to stir at 80°C for 3 days. Purification by preparative TLC afforded [2]rotaxane **2.17** in 24% yield. The novel rotaxane was characterised by ^{1}H NMR, ^{13}C NMR and ESI-HRMS.



*Scheme 2.6. Synthesis of [2]rotaxane **2.15**.*

Successful formation of [2]rotaxane **2.17** was evidenced by comparison of its ^{1}H NMR spectrum with those of its macrocycle and axle components in $CDCl_3$ (Figure 2.15). ^{1}H-^{1}H

ROESY NMR study in $CDCl_3$ revealed similar intercomponent axle-squaramide NH donor-pyridyl group interactions as in [2]rotaxane **2.15** (Figure 2.16).

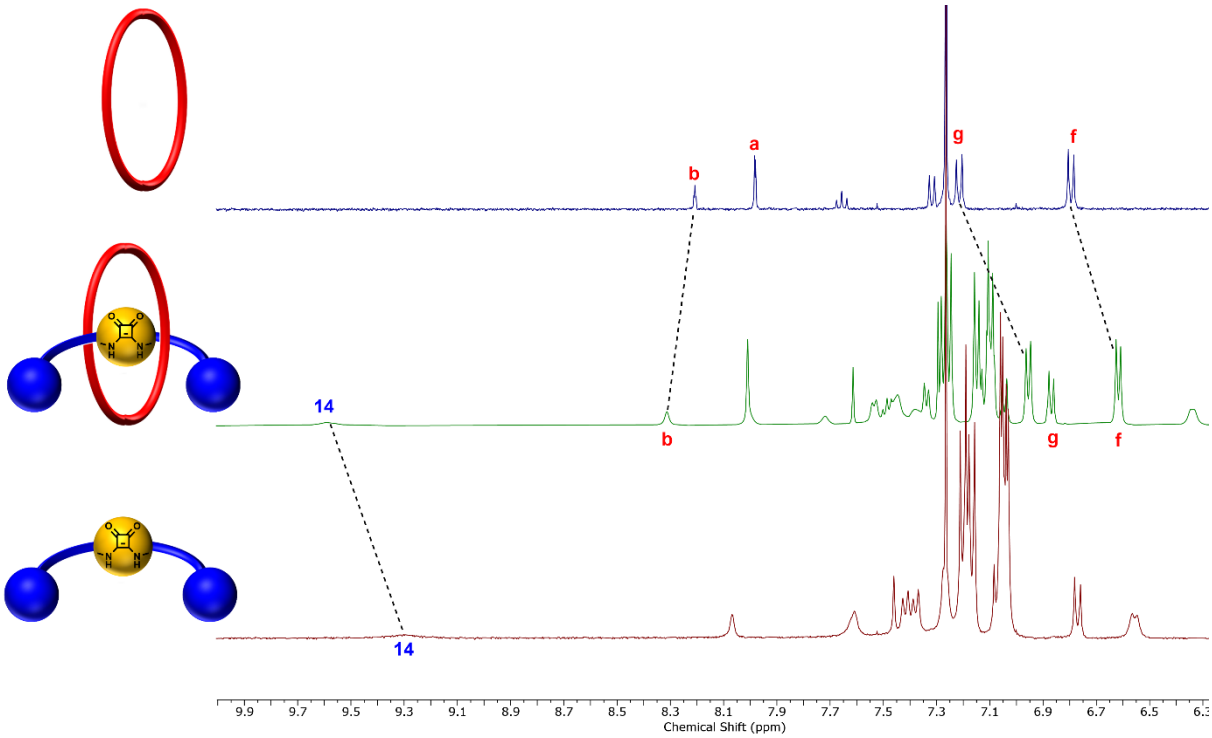


Figure 2.15. *Truncated stacked ^{1}H NMR spectra of i) macrocycle **2.16** ii) [2]rotaxane **2.17** and iii) axle component **2.17a** ($CDCl_3$, 500 MHz, 298K).*

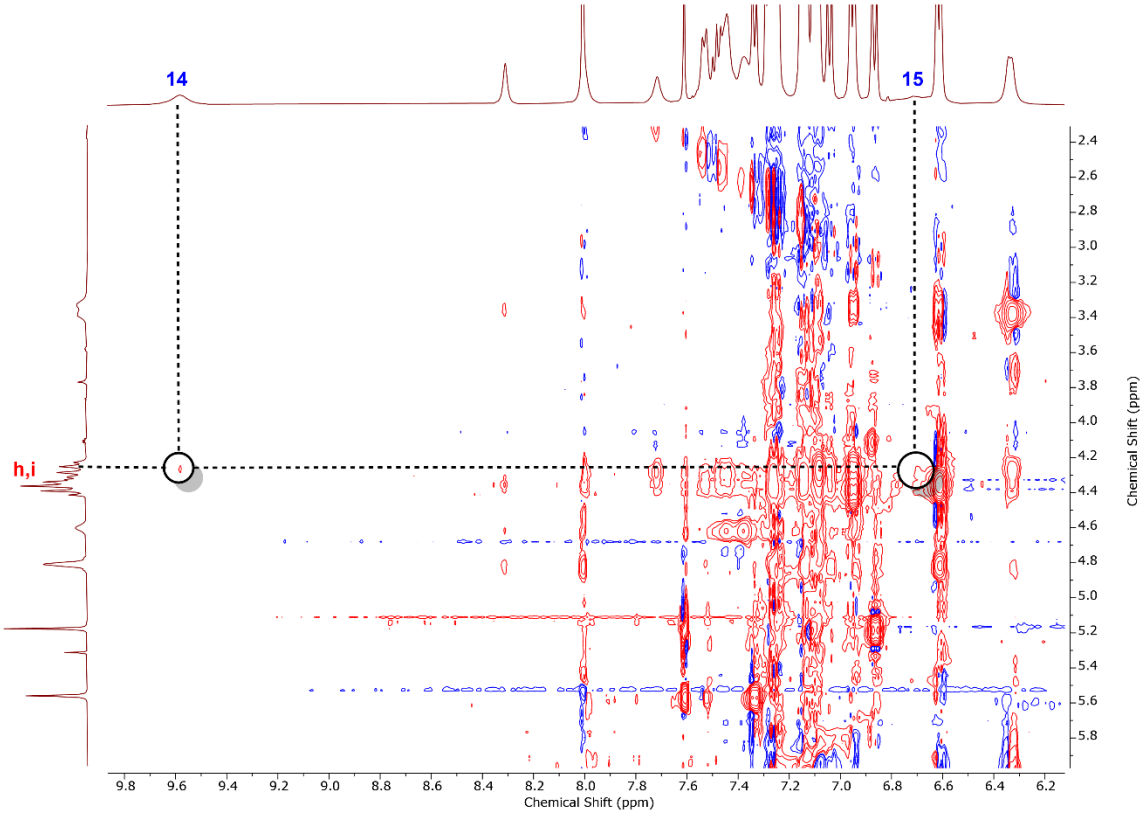


Figure 2.16. *Truncated ^{1}H-^{1}H ROESY NMR spectrum of [2]rotaxane **2.17** in $CDCl_3$.*

2.4 Host-guest recognition studies

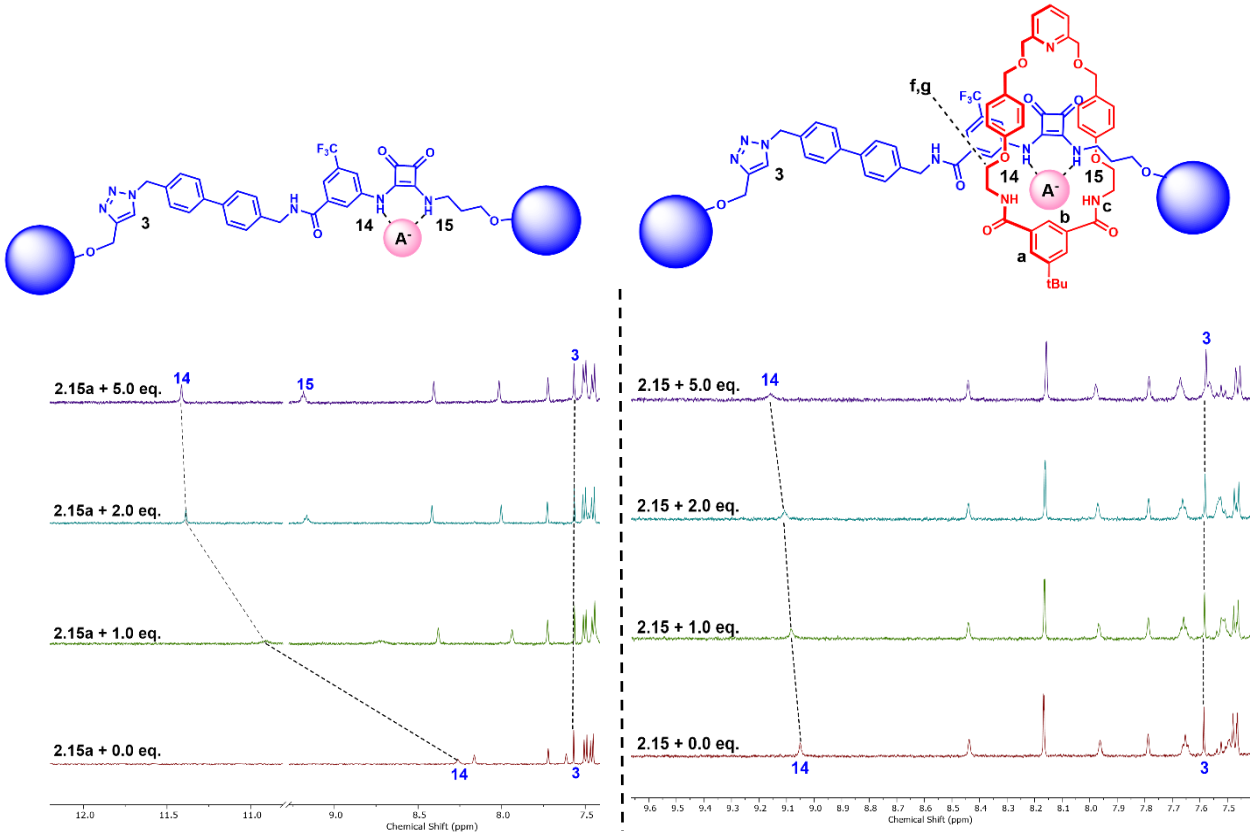


Figure 2.17. *Truncated ^{1}H NMR spectra of axle* ***2.15a*** *and [2]rotaxane* ***2.15*** *with increasing equivalents of TBACl in 1:9 $CD_3CN/CDCl_3$ (500MHz, 298K).*

2.4.1 Preliminary anion binding studies

Following the successful synthesis of [2]rotaxanes **2.15** and **2.17** efforts were directed towards investigating their anion, cation and ion-pair recognition properties. In a preliminary study involving [2]rotaxane **2.15** and its axle **2.15a**, the halide anion binding properties of the squaramide containing mechanically interlocked molecule relative to its non-threaded axle component were first compared *via* ^{1}H NMR titration experiments in 10% CD_3CN-$CDCl_3$ solvent media.

Sequential addition of TBA halide salt aliquots to the axle component, **2.15a** resulted in significant downfield shifts of the squaramide N-H protons H_{14} while imperceptible

perturbations of the triazole proton H_3 indicated it does not participate in the anion binding event (Figure 2.17). In stark contrast analogous halide ^{1}H NMR titration experiments with [2]rotaxane **2.15** resulted in much smaller downfield perturbations in the chemical shifts of the rotaxane's cavity protons namely H_{14} and H_b.

Bindfit[237] analysis of the titration isotherms obtained by monitoring the squaramide proton, H_{14} determined 1:1 host-guest stoichiometric halide association constants summarised in Table 2.1. Consistent with the respective proton chemical shift perturbation magnitudes observed in the ^{1}H NMR titration experiments, the halide association constant values for [2]rotaxane **2.15** were significantly diminished compared to the axle component **2.15a**, despite the presence of additional macrocycle component HB donors in the interlocked system. This comparative reduction in rotaxane halide binding strength may be attributed to competing intercomponent macrocycle pyridyl-axle squaramide and macrocycle amide-squaramide carbonyl hydrogen bonding interactions, evidence of which was noted in both the one dimensional ^{1}H NMR and two dimensional ^{1}H-^{1}H ROESY NMR spectra of [2]rotaxane **2.15** (Figures 2.13 and 2.14).

Table 2.1: *Halide anion association constants K_a (M^{-1}) for axle **2.15a** and [2]rotaxane **2.15** [1.0 mM] in 1:9 $CD_3CN/CDCl_3$ at 298 K.[a]*

Anion	Axle **2.15a**	[2]Rotaxane **2.15**
Cl^-	2700	188
Br^-	$>10^4$	73
I^-	5700	254

[a] K_a values calculated using Bindfit[237] software using a 1:1 host-guest binding model by monitoring squaramide proton H_{14}. All anions added as their TBA salts; Error percentages less than 10% unless specified.

In order to overcome the competing rotaxane's intercomponent HB interactions and instigate preorganisation of the anion recognition site, one equivalent of lithium perchlorate

salt was added to [2]rotaxane **2.15**. Concomitant with the upfield perturbations of the internal benzene proton H_b, the introduction of lithium cation elicited downfield shifts in the external pyridine proton, H_k suggesting disruption of the intercomponent HB, importantly

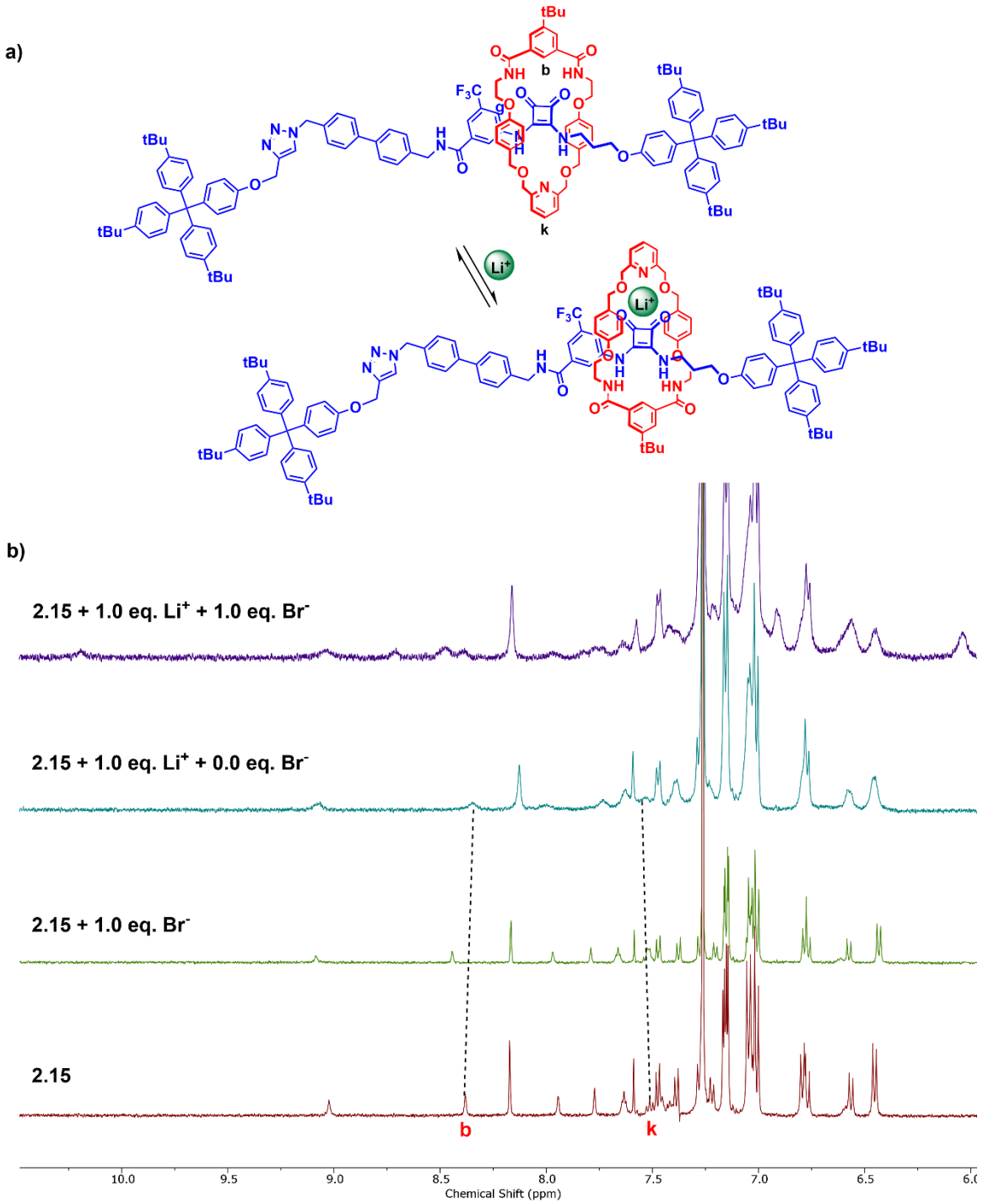


Figure 2.18. *a) Proposed macrocyclic preorganisation occurring in [2]rotaxane* ***2.15*** *upon addition of one equivalent of $LiClO_4$. b) Truncated ^1H NMR spectra of [2]rotaxane* ***2.15*** *with one equivalent of TBABr in the absence and presence of one equivalent of $LiClO_4$ in 10% CD_3CN-$CDCl_3$ (500 MHz, 298 K).*

highlighting the rotaxane's co-conformational change that occurs to enable the metal cation being cooperatively bound between the macrocycle pyridyl and axle squaramide carbonyl oxygen donors (Figure 2.18a). Interestingly, subsequent halide addition made the monitoring of chemical shift perturbations of the cavity protons exceedingly difficult due to binding being *slow* on the NMR timescale, indicative of very strong halide recognition (Figure 2.18b). This ion-pair binding cooperativity effect may be attributed to favourable proximal metal cation-anion electrostatic interactions and macrocyclic preorganisation induced in the presence of a co-bound lithium cation. Attention was thereafter directed towards using a more competitive solvent medium to enable quantitative determination of association constant data.

2.4.2 Quantitative ^{1}H NMR halide binding titration studies

Halide anion titrations were conducted by adding aliquots of TBA halide salts to a 1mM solution of each rotaxane in the more competitive 3:7 $CD_3CN/CDCl_3$ solvent mixture. With increasing anion concentration, macrocycle amide protons H_c, internal benzene proton H_b and axle squaramide N-H protons $H_{14,15}$ of [2]rotaxane **2.15** moved progressively downfield, indicating that halide anion binding occurs in the interlocked cavity of the [2]rotaxane (Figure 2.19). Bindfit[237] analysis of the titration isotherm data determined 1:1 stoichiometric host-guest binding constants summarised in Table 2.2. As expected, [2]rotaxane **2.15** displayed weak halide association with a modest preference for iodide.

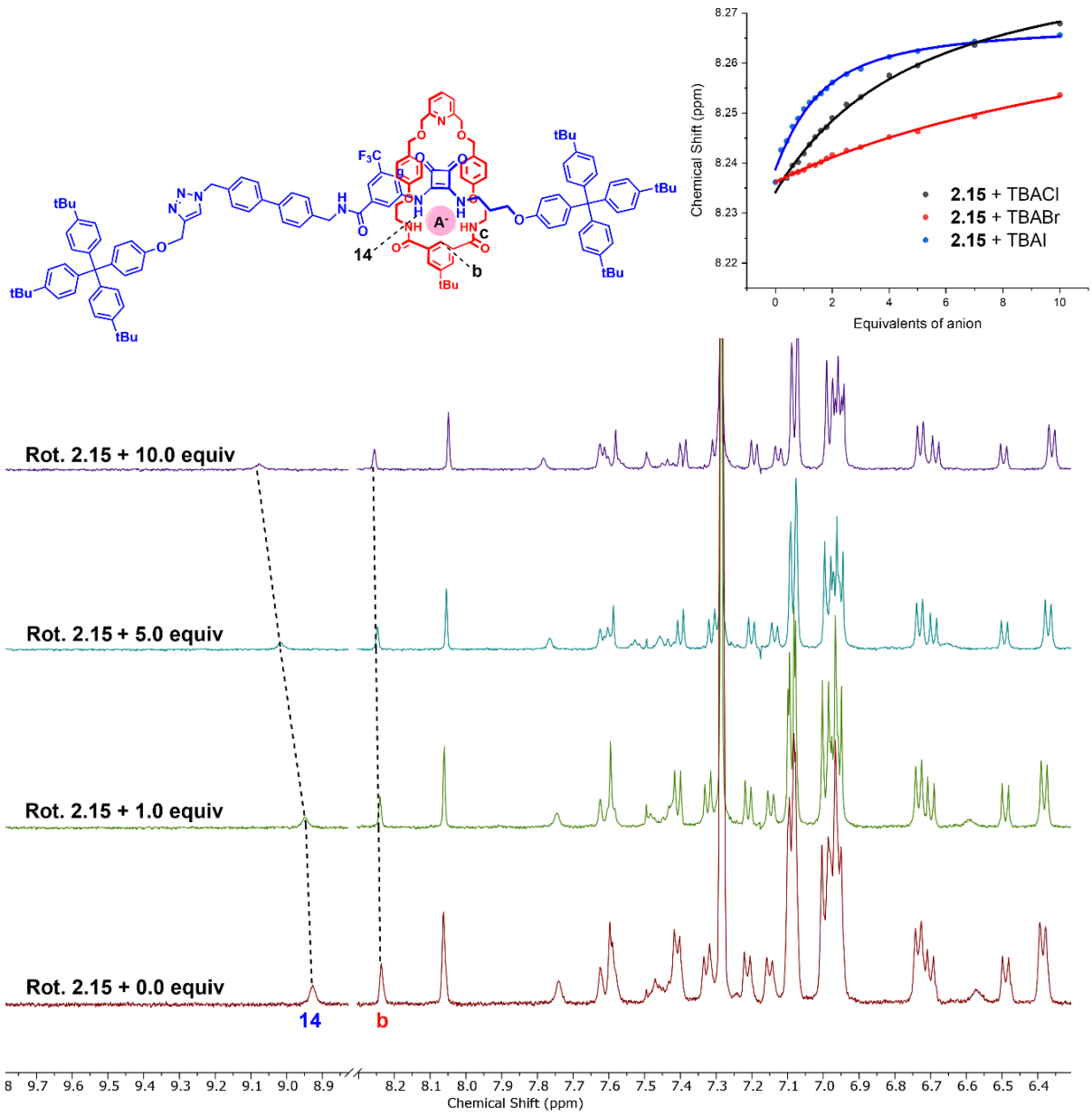


Figure 2.19. *^{1}H NMR spectra of [2]rotaxane **2.15** upon addition of 1, 5 and 10 equivalents of TBABr (500 MHz, 298 K, 7:3 $CDCl_3$/CD_3CN). Inset: Binding isotherms showing changes in chemical shift of internal benzene proton b upon increasing equivalents of halide anions.*

Interestingly, this trend was reversed for the XB functionalised rotaxane **2.17**, which exhibited a preference for the charge dense chloride. Upon gradual addition of the TBA halide salts to a 1mM solution of [2]rotaxane **2.17** significant downfield shifts of the axle squaramide N-H protons $H_{14,15}$ and upfield shifts of the internal benzene proton H_b were observed (Figure 2.20). This indicated that the halide anion was bound in the vicinity of the rotaxane XB anion binding donors. Additionally, the noteworthy downfield shifts of the axle methylene spacer

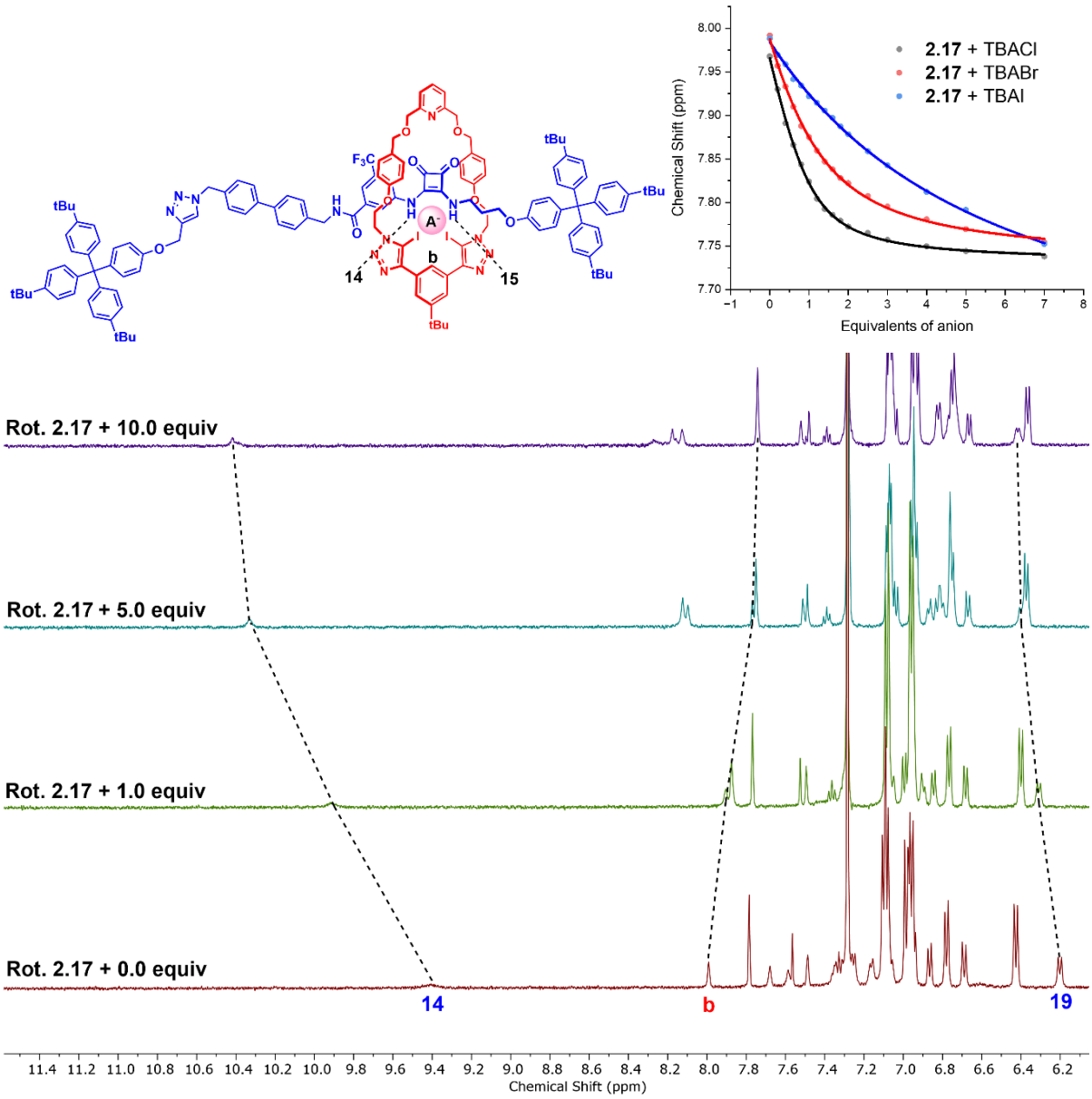


Figure 2.20. *^{1}H NMR spectra of [2]rotaxane **2.17** upon addition of 1, 5 and 10 equivalents of TBABr (500 MHz, 298 K, 7:3 $CDCl_3/CD_3CN$). Inset: Binding isotherms showing changes in chemical shift of internal benzene proton b upon increasing equivalents of halide anions.*

protons $H_{16,18}$ and stopper protons H_{19} suggested that the guest anion was perched between the plane of the macrocycle and one of the stopper groups.

Importantly, Table 2.2 shows that XB [2]rotaxane **2.17** exhibited strikingly larger halide binding constant values relative to HB [2]rotaxane **2.15**, with *ca.* 30- and 40-fold enhancement in the case of chloride and bromide respectively, highlighting the improved binding and

selectivity profiles offered by sigma-hole halogen bond donors over their traditional hydrogen bonding analogues.

Table 2.2: *Halide anion association constants K_a (M^{-1}) for [2]rotaxanes **2.15** and **2.17** [1.0 mM] in 3:7 $CD_3CN/CDCl_3$ at 298 K.[a]*

Anion	[2]Rot. **2.15**	[2]Rot. **2.17**
Cl^-	128	3894
Br^-	33	1375
I^-	175	194

[a] K_a values calculated using Bindfit[237] software using a 1:1 host-guest binding model by monitoring internal benzene proton H_b. All anions added as their TBA salts. Error percentages less than 10% unless specified.

2.4.3 Quantitative ^{1}H NMR alkali metal cation binding titration studies

To investigate the potential of the [2]rotaxanes to complex alkali metal cations, quantitative ^{1}H NMR titrations were conducted by adding aliquots of alkali metal cation salts such as $NaBAr^F{}_4$ and $LiClO_4$ to a 1mM solution of the respective rotaxanes in 30% CD_3CN-$CDCl_3$ solvent media. For both rotaxane systems, with increasing metal cation concentration, perturbations in the proton signals neighbouring the pyridyl group of the macrocycles namely H_h, H_i, H_k were observed indicating that the alkali metal cation binding occurs *via* the pyridyl group of the macrocycle (Figure 2.21 and 2.22). Additionally, qualitative ^{13}C-NMR cation binding studies with the [2]rotaxanes in $CDCl_3$ revealed that the addition of an equivalent of alkali metal cation salt results in the upfield shifts of the cyclobutenedione peaks at 180 ppm and 160 ppm suggesting that the squaramide carbonyls participate in cation binding in concert with the macrocycle's pyridyl motif. The determined binding constants were calculated with Bindfit[237] using a 1:1 stoichiometric host-guest binding model summarised in Table 2.3. Inspection of the binding data revealed that while both rotaxanes displayed modest cation association

constants, they both demonstrated a preference for lithium over sodium, most likely due to better size-complementarity and steric properties of the formed cavity.

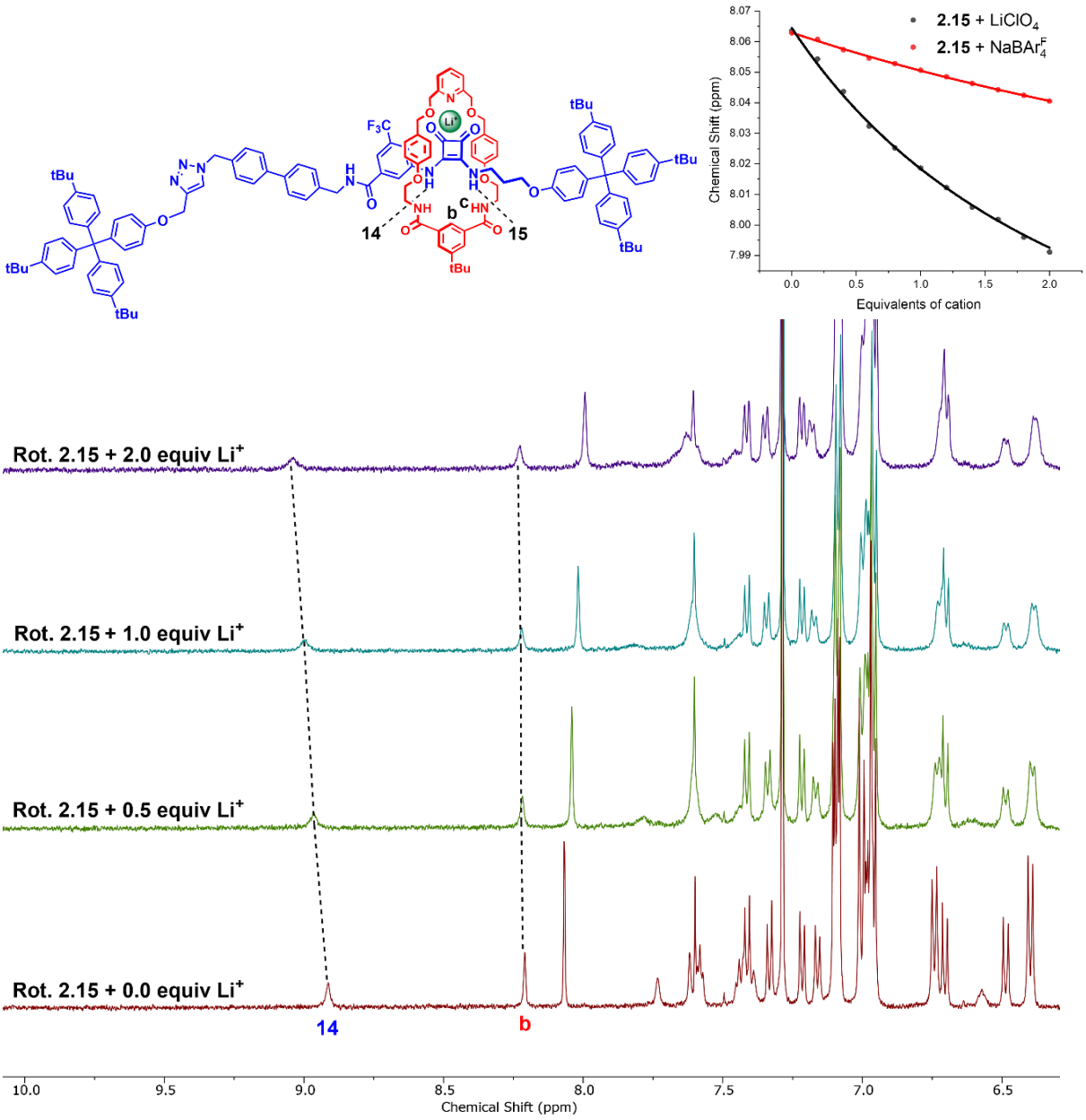


Figure 2.21. *^{1}H NMR spectra of [2]rotaxane* ***2.15*** *upon addition of 0.5, 1 and 2 equivalents of $LiClO_4$ (500 MHz, 298 K, 7:3 $CDCl_3$/CD_3CN). Inset: Binding isotherms showing changes in chemical shift of internal benzene proton b upon increasing equivalents of alkali metal cations.*

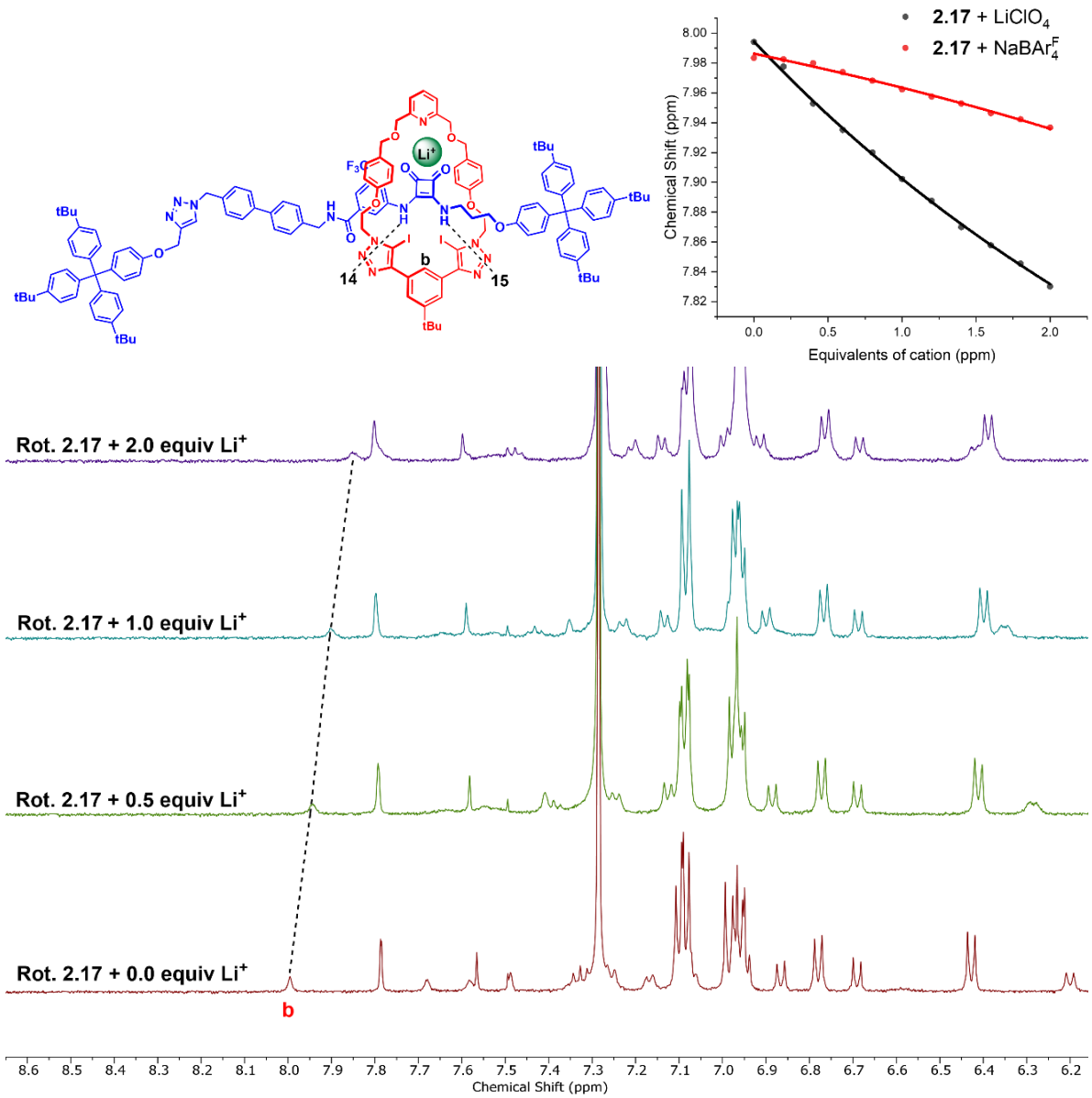


Figure 2.22. *^{1}H NMR spectra of [2]rotaxane **2.17** upon addition of 0.5, 1 and 2 equivalents of $LiClO_4$ (500 MHz, 298 K, 7:3 $CDCl_3/CD_3CN$). Inset: Binding isotherms showing changes in chemical shift of internal benzene proton b upon increasing equivalents of alkali metal cations.*

Table 2.3: *Cation association constants K_a (M^{-1}) for [2]rotaxanes **2.15** and **2.17** [1.0 mM] in 3:7 $CD_3CN/CDCl_3$ at 298 K.[a]*

Cation	[2]Rot. **2.15**	[2]Rot. **2.17**
Li^+	279	253
Na^+	146	156

[a] K_a values calculated using Bindfit[237] software using a 1:1 host-guest binding model by monitoring internal benzene proton H_b. Lithium and sodium added as $LiClO_4$ and $NaBAr^F_4$. Error percentages less than 10% unless specified.

2.4.4 Quantitative ^{1}H NMR ion-pair binding titration studies

After establishing the efficacy of the [2]rotaxane systems to separately bind Li^+ cation and halide anions, their ability to bind lithium halide ion-pairs were investigated by adding aliquots of TBA halide salts to a 1 mM solution of each rotaxane pre-complexed with 1 equivalent of lithium perchlorate in the 3:7 $CD_3CN/CDCl_3$ solvent media.

With increasing halide anion concentration, the squaramide N-H protons $H_{14,15}$ and internal benzene proton H_b of [2]rotaxane **2.15** broadened and moved downfield consistent with anion binding occurring in the macrocycle's bis-amide anion binding cleft and interlocked cavity of the [2]rotaxane (Figure 2.23). Monitoring these proton shifts by Bindfit[237] analysis determined apparent 1:1 host: guest stoichiometric association constants summarised in Table 2.4. As was hoped, the presence of co-bound lithium cation led to a significant enhancement of halide anion binding affinities, with up to an 8-fold enhancement seen in the case of bromide.

Table 2.4: *Apparent association constants K_a (M^{-1}) for [2]rotaxanes **2.15** and **2.17** [1.0 mM] in the presence of 1 equiv. $LiClO_4$ in 3:7 CD3CN/CDCl3 at 298 K.[a]*

Host	Cation	% cation bound	Anion	K_a (M^{-1})
[2]Rot. **2.15**	Li^+ (1 eq.)	19%	**Cl^-**	-[b]
			Br^-	273
			I^-	300(10)
[2]Rot. **2.17**	Li^+ (1 eq.)	17%	**Cl^-**	5766
			Br^-	3076
			I^-	559

[a] K_a values calculated using Bindfit[237] software using a 1:1 host-guest binding model by monitoring internal benzene proton H_b. Lithium cation added as $LiClO_4$. All anions added as their TBA salts. Error percentages less than 10% unless specified. [b] Salt recombination.

In the case of chloride, however, the addition of TBACl to the lithium-complexed [2]rotaxane **2.15** led to salt recombination resulting in LiCl precipitation, suggesting that ion-pair binding could not overcome the high lattice enthalpy of the alkali metal salt. Consistent with the anion binding results obtained in section 2.4.2, lithium cation-complexed [2]rotaxane **2.15** displayed a preference for iodide.

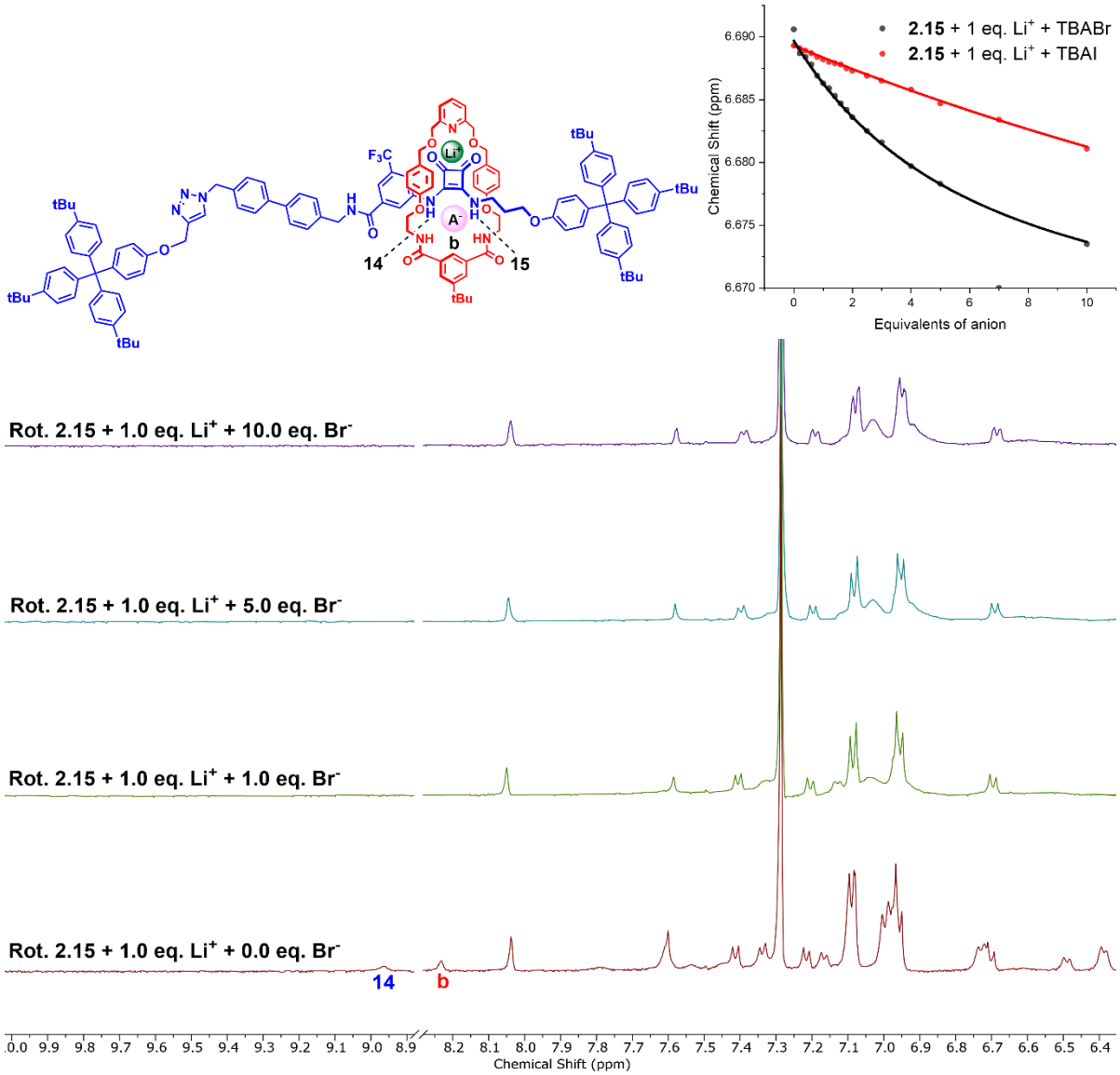


Figure 2.23. *^{1}H NMR spectra of [2]rotaxane **2.15** upon addition of addition of 1, 5 and 10 equivalents of TBABr in the presence of 1 equivalent of $LiClO_4$ (500 MHz, 298 K, 7:3 $CDCl_3/CD_3CN$). Inset: Binding isotherms showing changes in chemical shift of internal benzene proton b upon increasing equivalents of halide anions.*

Conversely, a reversal in halide selectivity was again observed for the lithium-complexed XB functionalised [2]rotaxane **2.17**. Sequential addition of halides to the pre-complexed [2]rotaxane **2.17** led to downfield shifts of the axle squaramide N-H protons $H_{14,15}$ and upfield shifts of the internal benzene proton H_b indicative of anion binding being mediated by both axle squaramide HB donors and macrocycle XB donors in the [2]rotaxane cavity (Figure 2.24). As expected, the presence of co-bound lithium cation augmented the

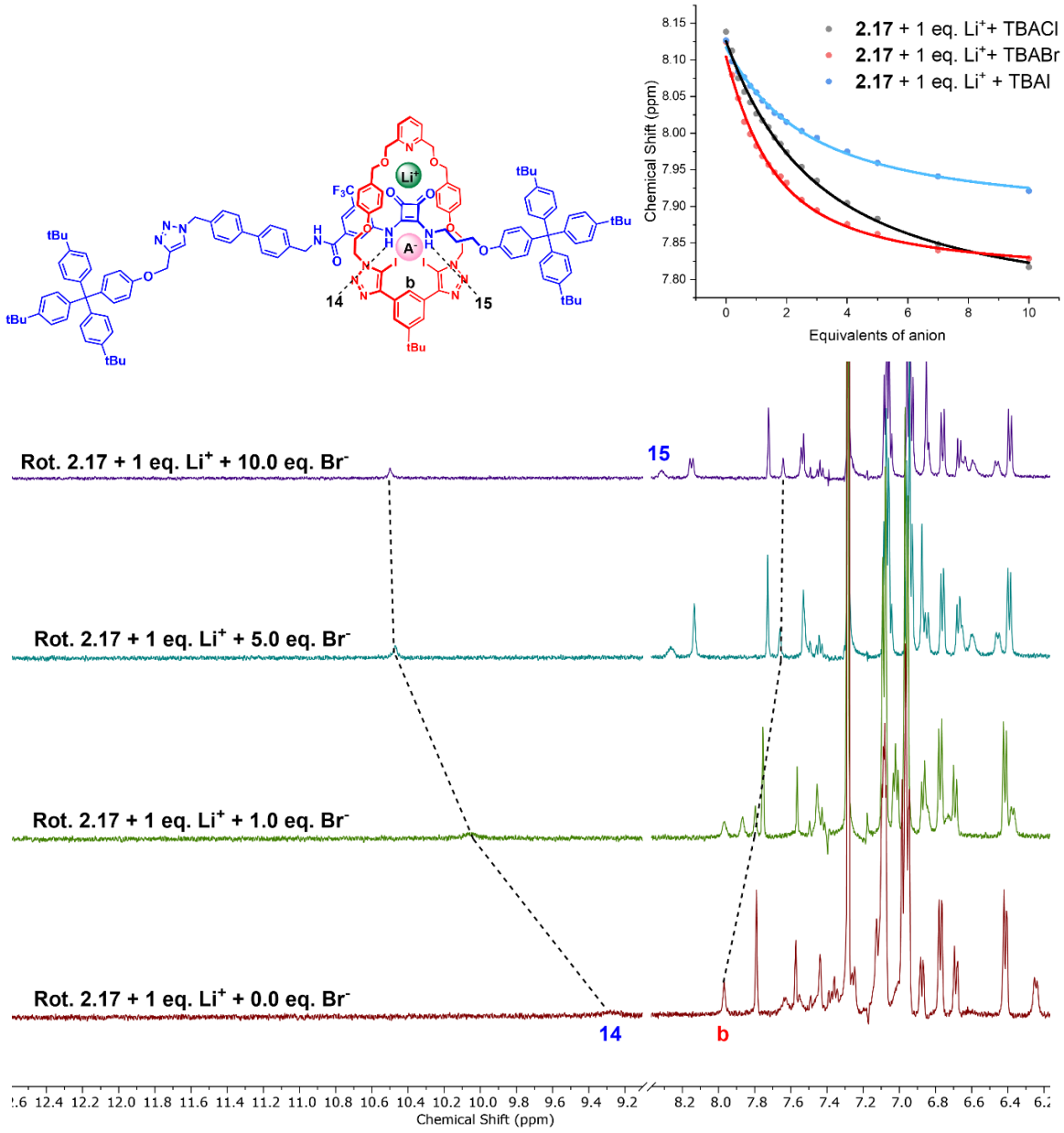


Figure 2.24. *^{1}H NMR spectra of [2]rotaxane **2.17** upon addition of addition of 1, 5 and 10 equivalents of TBABr in the presence of 1 equivalent of $LiClO_4$ (500 MHz, 298 K, 7:3 $CDCl_3/CD_3CN$). Inset: Binding isotherms showing changes in chemical shift of internal benzene proton b upon increasing equivalents of halide anions.*

anion binding affinities of the receptor emphasizing the advantages of positive cooperative electrostatic effects on heteroditopic host-guest recognition.

Notably, TBACl addition to the cation-complexed [2]rotaxane did not result in LiCl salt precipitation, presumably due to strong binding and stabilization of chloride in the rotaxane cavity. Furthermore, under the titration conditions used in this study involving the addition of one equivalent $LiClO_4$, the previously obtained lithium cation association constant values can be used to estimate the % metal cation bound to the rotaxanes (Table 2.4). This impressively indicates that despite the relatively low % of Li^+ bound (*ca.* 20%), the XB heteroditopic rotaxane **2.17** is still capable of strong LiX halide ion-pair binding, notably overcoming even the high lattice enthalpy of LiCl recombination.

2.4.5 Solid-liquid extraction studies

Prompted by the promising ion-pair binding results, the ability of the heteroditopic [2]rotaxanes to extract lithium halide ion-pairs into organic media was explored by conducting preliminary solid-liquid extraction studies. In a typical experiment, a 1mM solution of each rotaxane in $CDCl_3$ was sonicated with excess (*ca.* 5-fold) microcrystalline samples of LiX salts for 20 minutes, following which the solution was filtered and its ^1H NMR recorded.

Comparison of the pre- and post-extraction spectra revealed that both [2]rotaxanes were able to successfully extract LiBr and LiI, with complexation induced shifts (CIS) in the proton signals being consistent with those observed during ion-pair binding studies discussed in section 2.4.4 (Figures 2.25 and 2.26). Notably, while [2]rotaxane **2.15** was unable to extract LiCl as a result of the salt's high lattice enthalpy, [2]rotaxane **2.17** successfully extracted LiCl into $CDCl_3$, corroborating the solution phase ion-pair binding results obtained in section 2.4.4

and further underlining the enhanced binding and selectivity behaviour displayed by XB systems over their HB analogues.

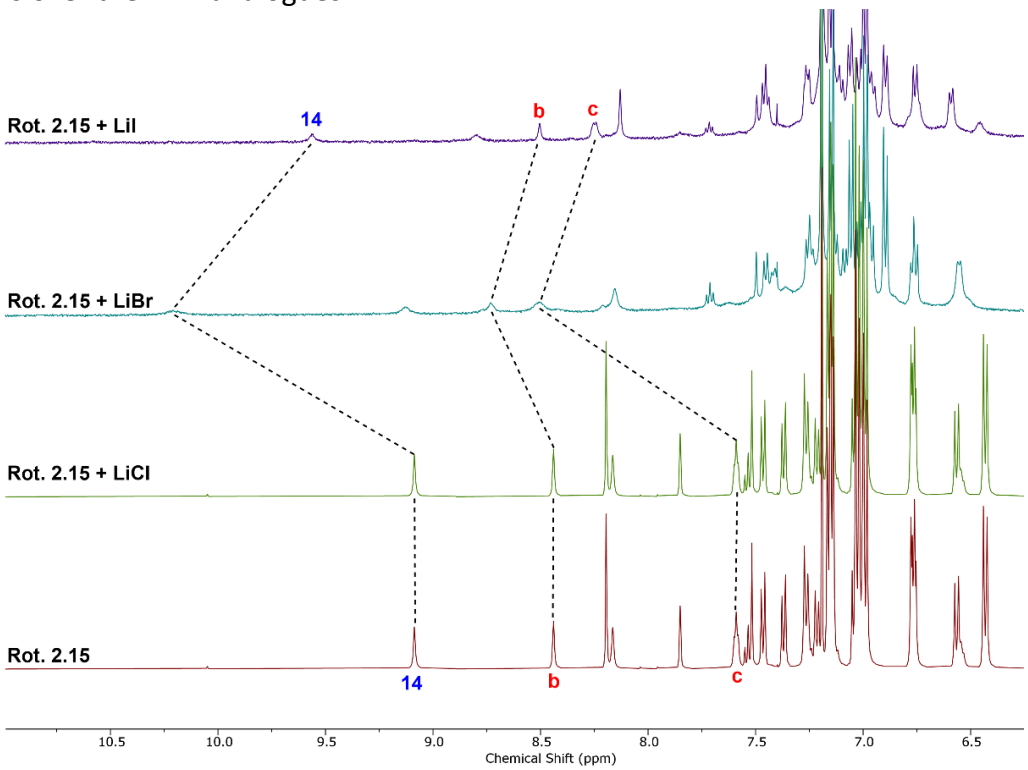


Figure 2.25. *Pre- and post-extraction ^{1}H NMR spectra of [2]rotaxane* ***2.15*** *with excess LiCl, LiBr and LiI ($CDCl_3$, 500MHz, 298K).*

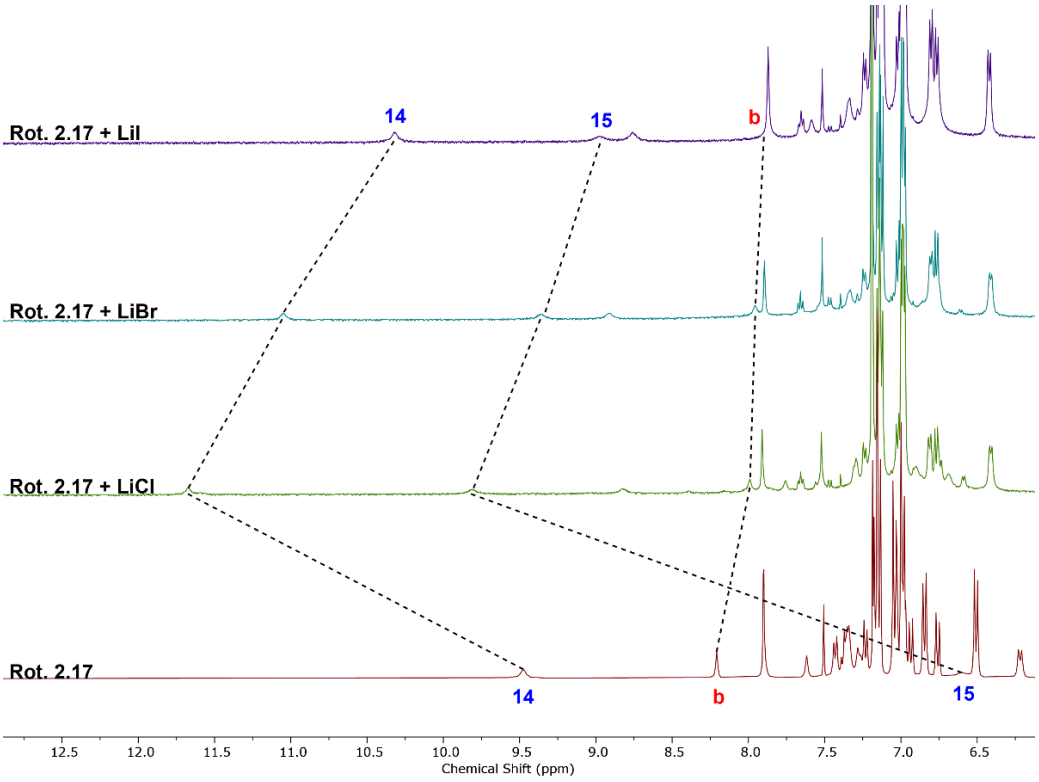


Figure 2.26. *Pre- and post-extraction ^{1}H NMR spectra of [2]rotaxane* ***2.17*** *with excess LiCl, LiBr and LiI ($CDCl_3$, 500MHz, 298K).*

2.4.6 Conclusions

To summarise, two novel squaramide-based heteroditopic [2]rotaxanes containing XB and HB anion binding donors were synthesised using active template methodology. Extensive ^{1}H NMR titration studies revealed that the XB-functionalised [2]rotaxane **2.17** was a remarkably better halide anion receptor compared to its HB analogue **2.15**, displaying up to *ca.* 30-fold larger chloride binding constant magnitude, underscoring the superiority of sigma-hole XB interactions to enable strong anion recognition in polar organic solvents. The introduction of one equivalent of lithium perchlorate the [2]rotaxane systems led to significant enhancements of their halide binding affinities, despite the relatively low % of lithium cation co-bound, highlighting the efficacy of mechanical bond positive cooperativity in ion-pair recognition. Notably, XB functionalised [2]rotaxane **2.17** exhibited superior lithium halide ion-pair binding over its HB analogue, overcoming even the high lattice enthalpy of the "hard" LiCl salt. Furthermore, preliminary solid-liquid extraction studies revealed that both rotaxanes were able to successfully extract LiBr and LiI, in addition to [2]rotaxane **2.17** being able to extract LiCl as well, consistent with their solution-phase ion-pair recognition properties.

2.5 Coumarin containing [2]rotaxane analogues

Section 1.3.5.1 of the introduction detailed the use of fluorescent reporter groups to enable optical sensing of anion guest species. Coumarins are an example of a frequently utilised

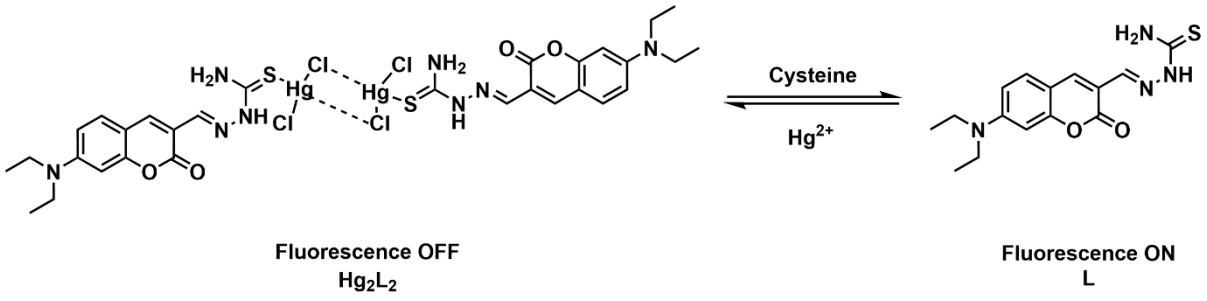


Figure 2.27. *Wang's reversible coumarin-based fluorescent probe.* [239]

family of fluorophores comprising a central 1-benzopyran-2-one motif.[238] They have widely been used in the field of supramolecular host-guest sensing chemistry owing to their high fluorescent yields, tuneable emission wavelengths and high sensitivity. An interesting example includes Wang's reversible coumarin-based fluorescent probe which exhibits selective detection of mercapto biomolecules namely CyS, Hcy and GSH in 1:99 DMSO/water solution (Figure 2.27).[239] Addition of Cys to the Hg^{2+} coordinated receptor results in ligand exchange and switching-on of fluorescence (emission at 525 nm) which can subsequently be quenched upon introduction of Hg^{2+}. Such reversible ON/OFF complexation/decomplexation behaviour is shown to be reproducible and is also confirmed by solid-state single crystal structural analysis.

Examples of systems capable of *sensing* ion-pair species remain scarce. Page and Sessler's copolymeric system comprising strapped calix[4]pyrroles or secondary ammonium

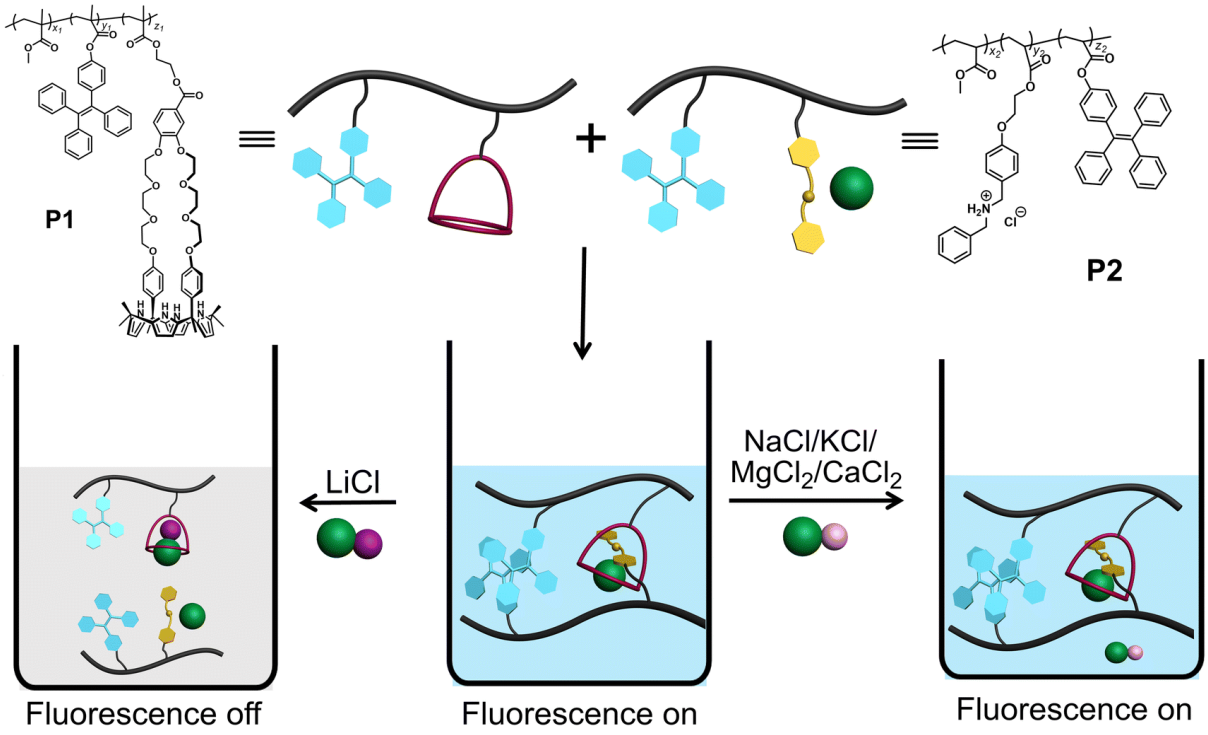


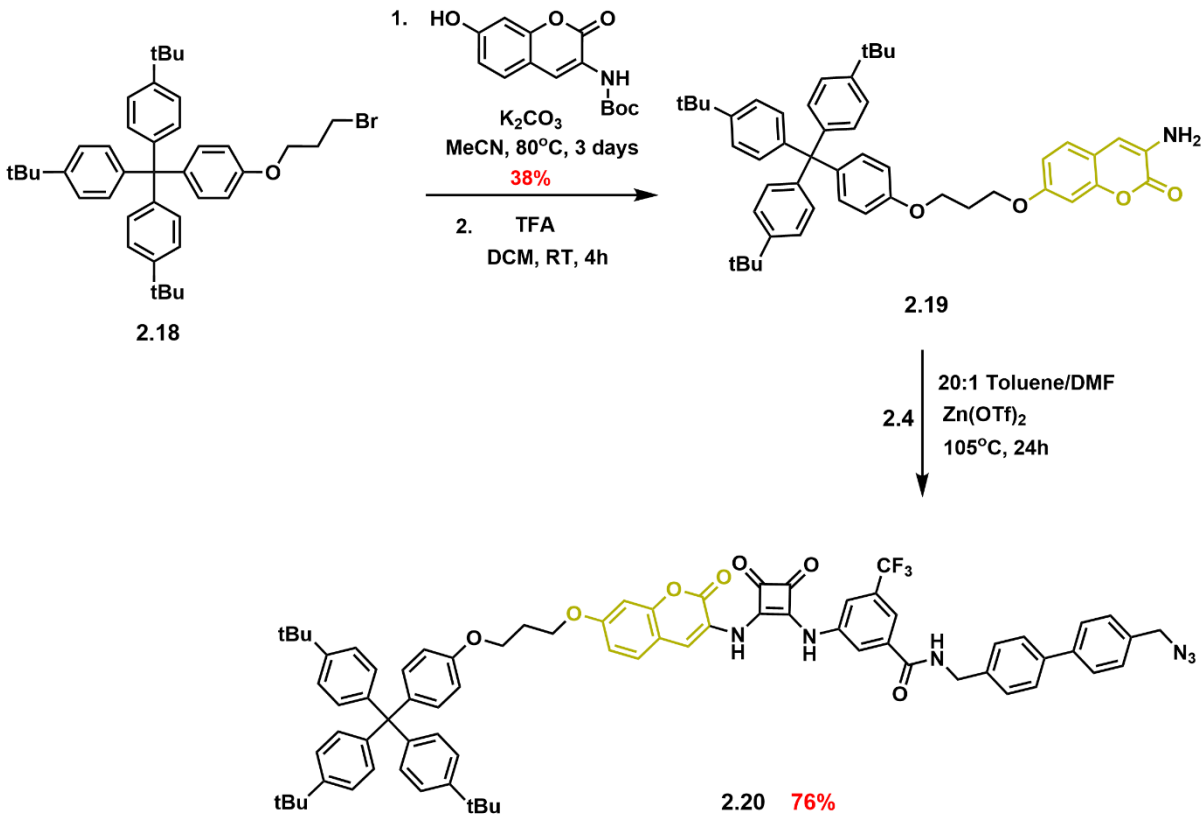
Figure 2.28. *Page and Sessler's copolymeric fluorescent LiCl sensor.* [243] *P1 = Polymer 1, P2 = Polymer 2. Adapted from* [240]

groups furnished with pendent triphenylethylene (TPE) motifs to induce aggregate induced emission (AIE) upon self-assembly, is a rare example of a heteroditopic fluorescent LiCl sensor (Figure 2.28).[240] Addition of LiCl to the copolymeric system in acetonitrile results in the disruption of host-guest crosslinks between the strapped calix[4]pyrrole/ secondary ammonium polymeric chains effecting disaggregation and diminution of TPE emission. In contrast, addition of NaCl, KCl, $MgCl_2$, $CaCl_2$ salts incite insignificant changes in TPE emission.

The synthesis of coumarin axle functionalised analogues of heteroditopic rotaxanes **2.15** and **2.17** was undertaken, where it was anticipated that in addition to fluorescent LiX ion-pair sensing capability, the incorporated coumarin motif may potentially augment ion-pair recognition *via* its carbonyl group for cation binding and an anion through its C-H hydrogen bond donors.

2.5.1 Synthesis of coumarin functionalised squaramide axle precursor

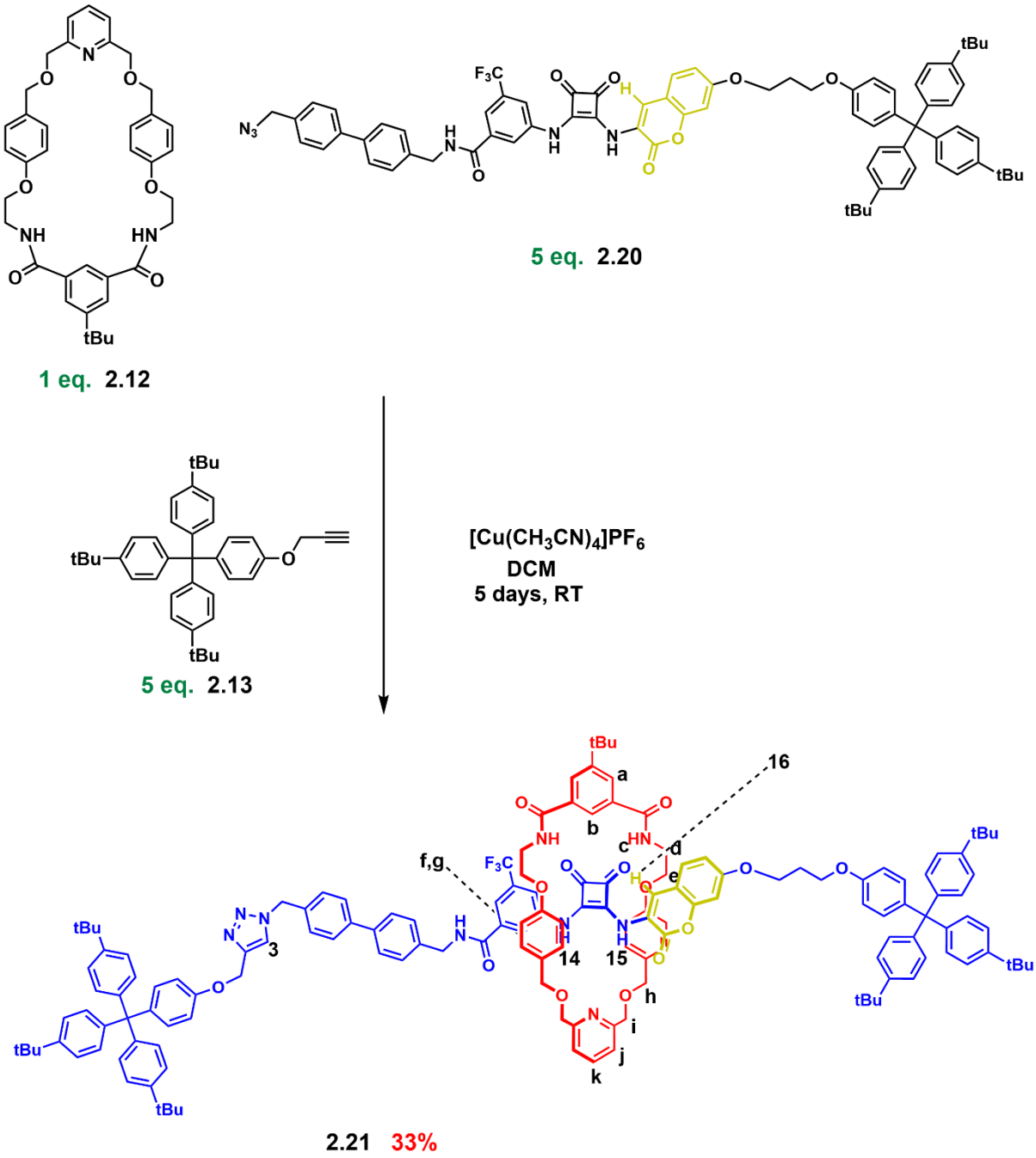
In order to synthesise the target coumarin containing [2]rotaxanes, the appropriate coumarin-based squaramide axle azide precursor was initially prepared (Scheme 2.7). Using modified literature procedures, Boc-protected coumarin amine[241] was reacted with terphenyl stopper bromide, **2.18** in acetonitrile under basic conditions to afford the Boc-protected coumarin stopper amine, **2.18a** in 38% yield. Deprotection of the amino group in the presence of trifluoroacetic acid (TFA) in DCM at room temperature produced the stopper appended coumarin amine **2.19** in quantitative yields. Coupling with **2.4** in the presence of zinc triflate in a 20:1 toluene:DMF solvent mixture gave the desired azide **2.20** in 76% yield, characterised by ^{1}H NMR, ^{13}C NMR spectroscopy and ESI-HRMS.



Scheme 2.7. *Synthesis of synthon* ***2.20****.*

2.5.2 Synthesis of coumarin-squaramide HB [2]rotaxane

Using typical AMT conditions described in section 2.3.3, an equimolar mixture of macrocycle **2.12** and $Cu(CH_3CN)_4PF_6$ in dichloromethane was combined with five equivalents of stopper alkyne **2.13** and azide **2.20** (Scheme 2.8). The reaction was left to stir at room temperature for five days following which the reaction mixture was subjected to an aqueous work-up with



Scheme 2.8. *Synthesis of [2]rotaxane* ***2.21****.*

basic EDTA/NH_4OH. Purification by preparative TLC afforded [2]rotaxane **2.21** in 33% yield, characterised by ^1H NMR, ^{13}C NMR and ESI-HRMS.

Evidence of successful formation of rotaxane **2.21** was observed by comparison of the ^1H NMR spectra of the [2]rotaxane with its non-interlocked axle and macrocycle components in $CDCl_3$ (Figure 2.29). In general, upfield shifts of the xylene protons $H_{f,g}$ were consistent with the donor-acceptor interactions between the electron-rich aromatic units in the macrocycle and the electron-deficient squaramide units in the axle indicative of mechanical bond formation. Of note were the downfield shifts of the macrocycle protons H_b and H_c which could be ascribed to possible intercomponent hydrogen bonding interactions between the HB donor groups in the macrocycle and the Lewis basic squaramide carbonyl groups in the axle, akin to observations previously witnessed in the non-coumarin containing rotaxanes **2.15** and **2.17** as well. Additionally, upfield shifts of the coumarin proton H_{16} and squaramide amide

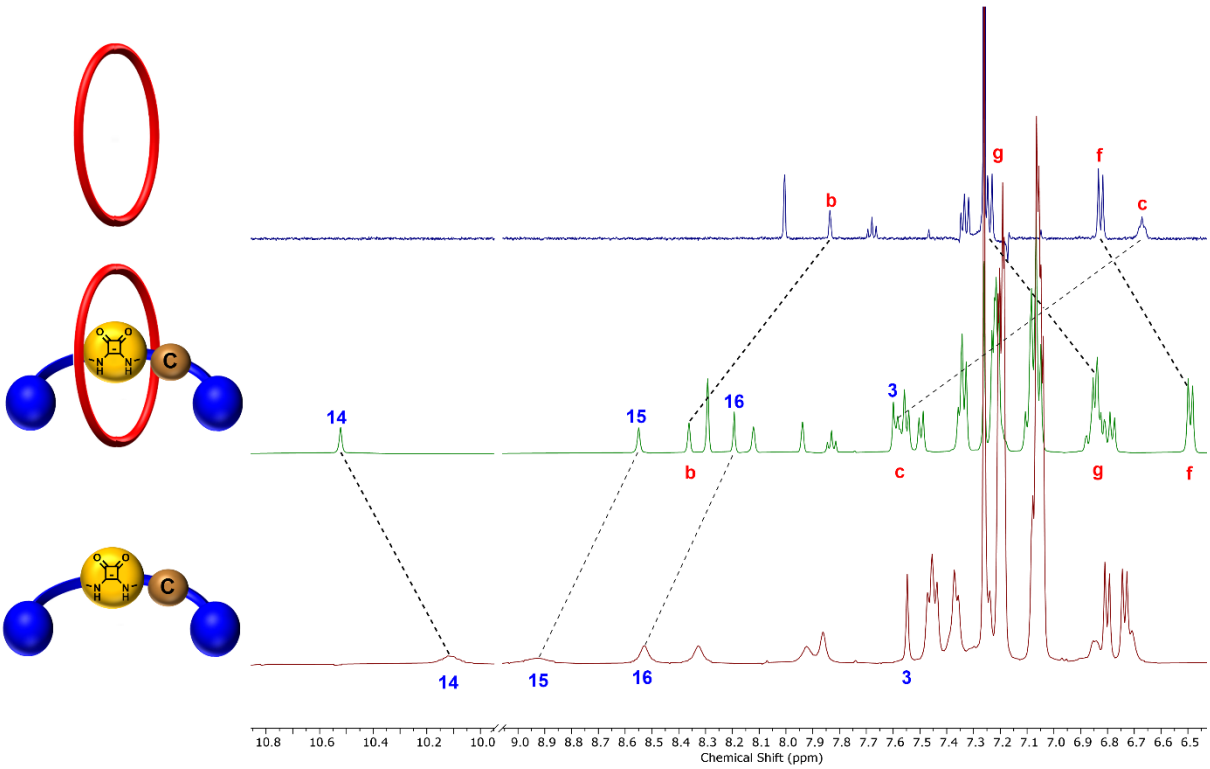


Figure 2.29. *Truncated stacked ^1H NMR spectra of i) macrocycle **2.12** ii) [2]rotaxane **2.21** and iii) axle component **2.21a** ($CDCl_3$, 500 MHz, 298K).*

proton H_{15} were also observed, and were likely a result of the weakening of HB interactions between the axle squaramide motif and the coumarin unit owing to the competing HB NH donor and acceptor units introduced by the macrocycle.

In order to investigate this further, a ^{1}H-^{1}H ROESY NMR study was conducted in $CDCl_3$ which evinced through-space intercomponent macrocycle pyridyl-axle squaramide interactions similar to those observed with rotaxanes **2.15** and **2.17** (Figure 2.30). Additionally, through-space coupling interactions were also observed between coumarin protons $H_{16,17}$ and protons neighbouring the amide region of the macrocycle namely $H_{d,e}$ suggesting possible coumarin proton-squaramide carbonyl HB interactions.

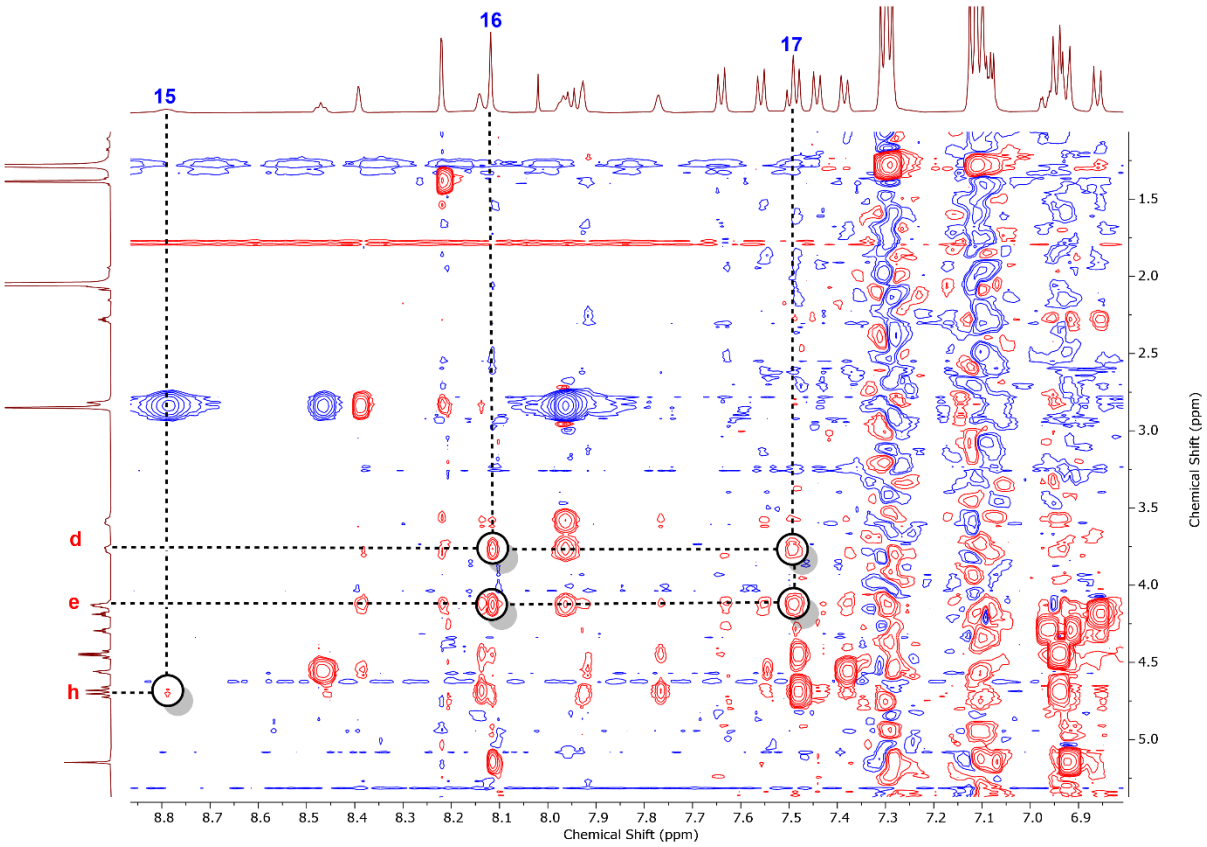
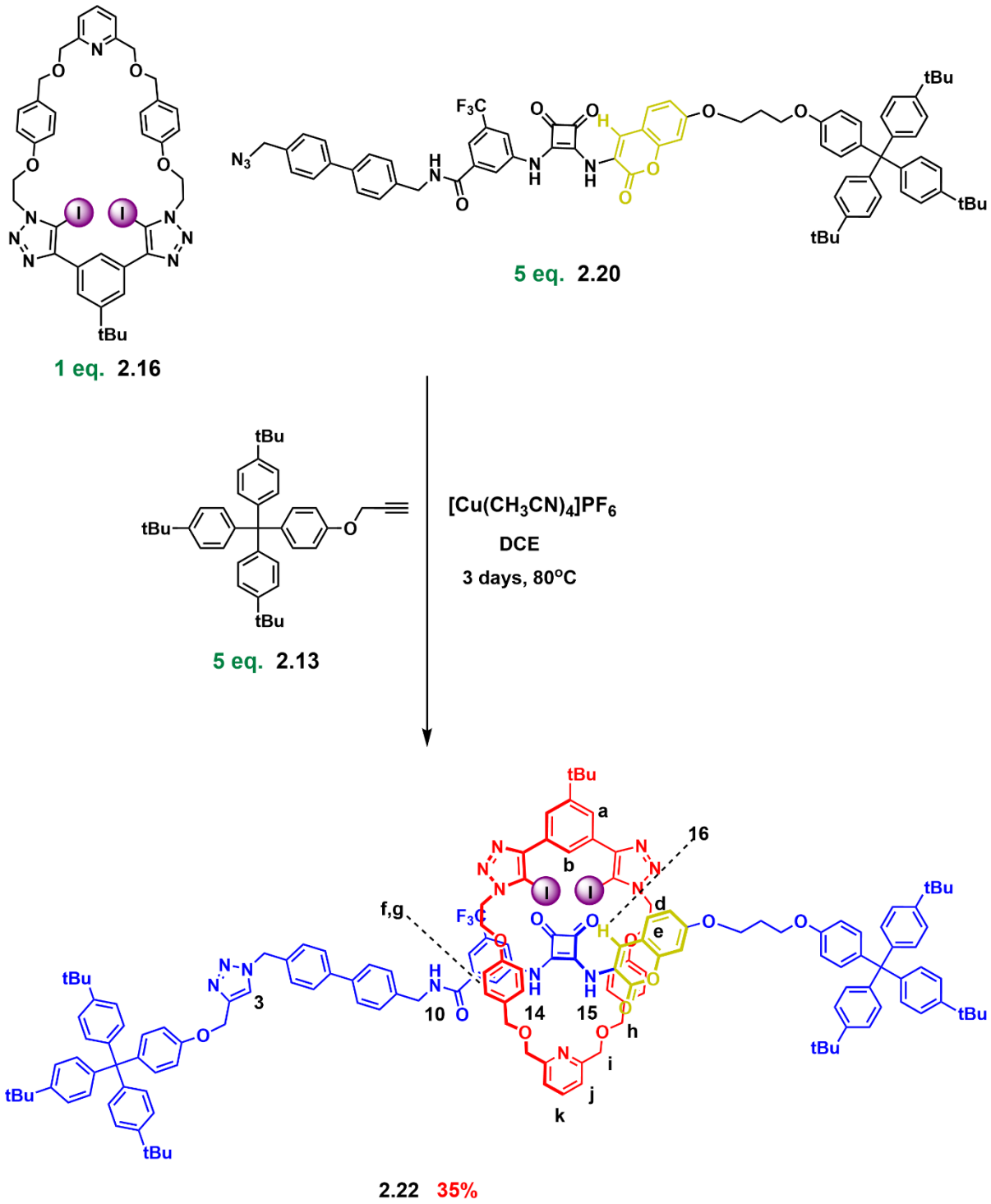


Figure 2.30. *Truncated ^{1}H-^{1}H ROESY NMR spectrum of [2]rotaxane* ***2.21*** *in $CDCl_3$.*

2.5.3 Synthesis of coumarin-squaramide XB [2]rotaxane

Using AMT conditions discussed in section 2.3.4, macrocycle **2.16** and $Cu(CH_3CN)_4PF_6$ in dichloroethane were combined with five equivalents of stopper alkyne **2.13** and azide **2.20**



Scheme 2.9. *Synthesis of [2]rotaxane* ***2.22****.*

(Scheme 2.9). The reaction was left to stir at 80°C for 3 days. After an aqueous work-up and purification using preparative TLC, [2]rotaxane **2.22** was isolated in 35% yield (Scheme 2.9). The novel rotaxane was also characterised by ^{1}H NMR, ^{13}C NMR and ESI-HRMS.

A comparison of the ^{1}H NMR spectra of [2]rotaxane **2.22** with its non-interlocked components revealed diagnostic upfield shifts of the aromatic protons $H_{f,g}$ of the macrocycle in line with the shielding effect arising from the formation of a mechanical bond (Figure 2.31). Moreover, downfield shift of the internal benzene proton of the macrocycle namely H_b was reminiscent of inter-component HB interactions between the macrocycle HB donors and axle squaramide carbonyl motifs previously noted in the case of rotaxanes **2.15**, **2.17** and **2.21**. As discovered in the case of rotaxane **2.21**, interlocked structure synthesis resulted in the upfield shifts of the coumarin proton H_{16} and the squaramide proton H_{15} alluding to possible weakening of HB interactions between the coumarin unit and squaramide motif of the axle

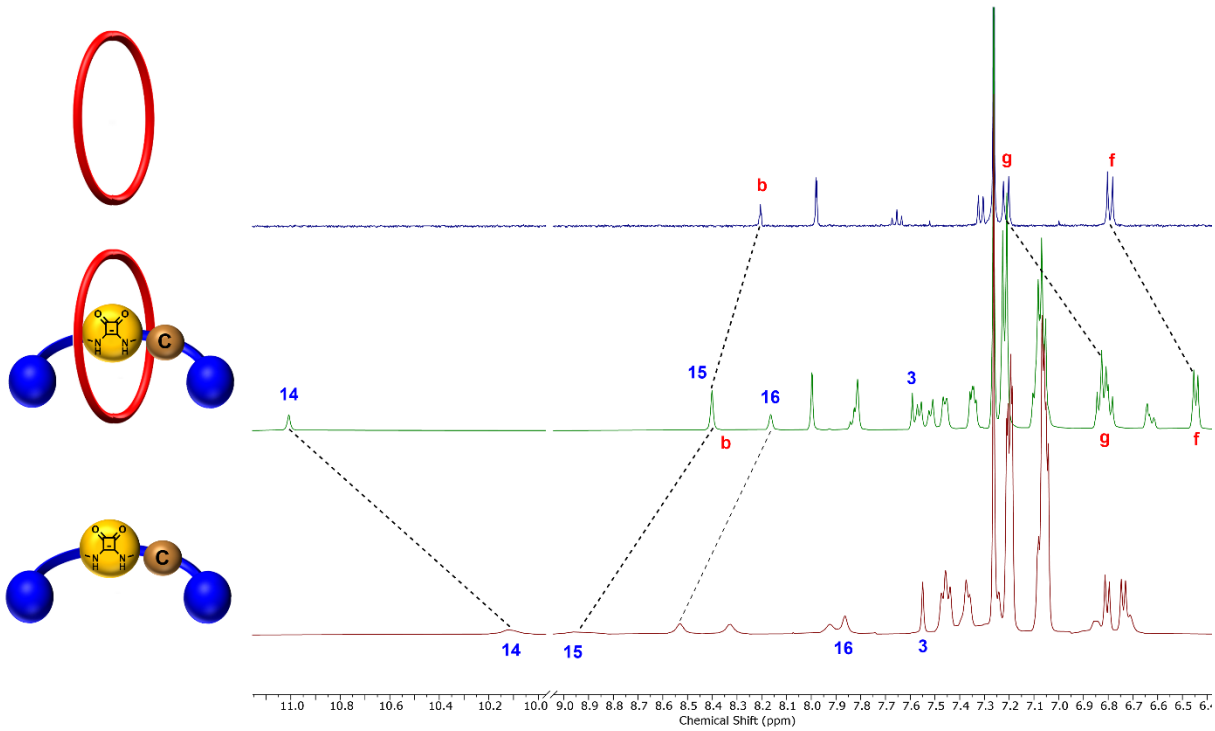


Figure 2.31. *Truncated stacked ^{1}H NMR spectra of i) macrocycle **2.16** ii) [2]rotaxane **2.22** and iii) axle component **2.22a** ($CDCl_3$, 500 MHz, 298 K).*

as a result of interlocked structure synthesis. ^{1}H-^{1}H NMR ROESY experiments in $CDCl_3$ were further corroborative of such intercomponent interactions (Figure 2.32).

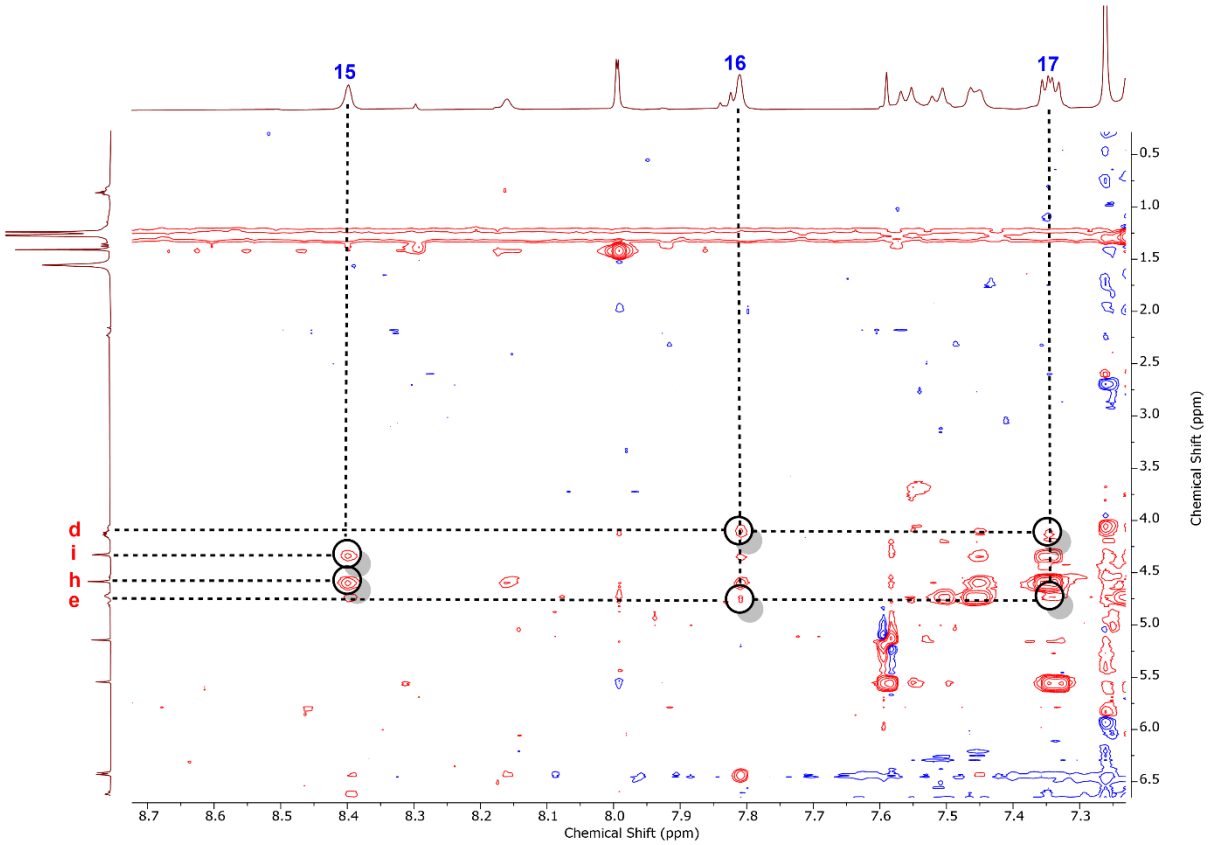


Figure 2.32. *Truncated ^{1}H-^{1}H ROESY NMR spectrum of [2]rotaxane* ***2.22*** *in $CDCl_3$.*

2.6 Host-guest recognition studies

2.6.1 Quantitative ^{1}H NMR halide binding titration studies

To assess the halide binding properties of the coumarin based [2]rotaxanes, ^{1}H NMR anion titration experiments were conducted with TBA halide salts in 3:7 $CD_3CN/CDCl_3$ solvent mixture. In the case of [2]rotaxane **2.21**, sequential addition of chloride to a 1mM solution of the receptor resulted in downfield perturbations of internal benzene protons H_b and axle squaramide N-H protons $H_{14,15}$ indicative of chloride being bound within the amide anion binding cleft of the [2]rotaxane (Figure 2.33). Analogous titration experiments with bromide and iodide, conversely, induced upfield shift of squaramide N-H proton H_{14} and downfield

shifts of the other squaramide N-H proton H_{15} and internal benzene proton H_b, suggesting that larger anions may be favouring an exotopic coordination mode. Notably, imperceptible perturbations in the coumarin proton H_{16} suggested it does not participate in anion binding. Bindfit[237] analysis of the titration isotherm data obtained *via* monitoring the internal benzene proton H_b determined 1:1 stoichiometric host-guest binding constants summarised in Table 2.5. Inspection of the binding data revealed that while HB rotaxane **2.21** exhibited a similar

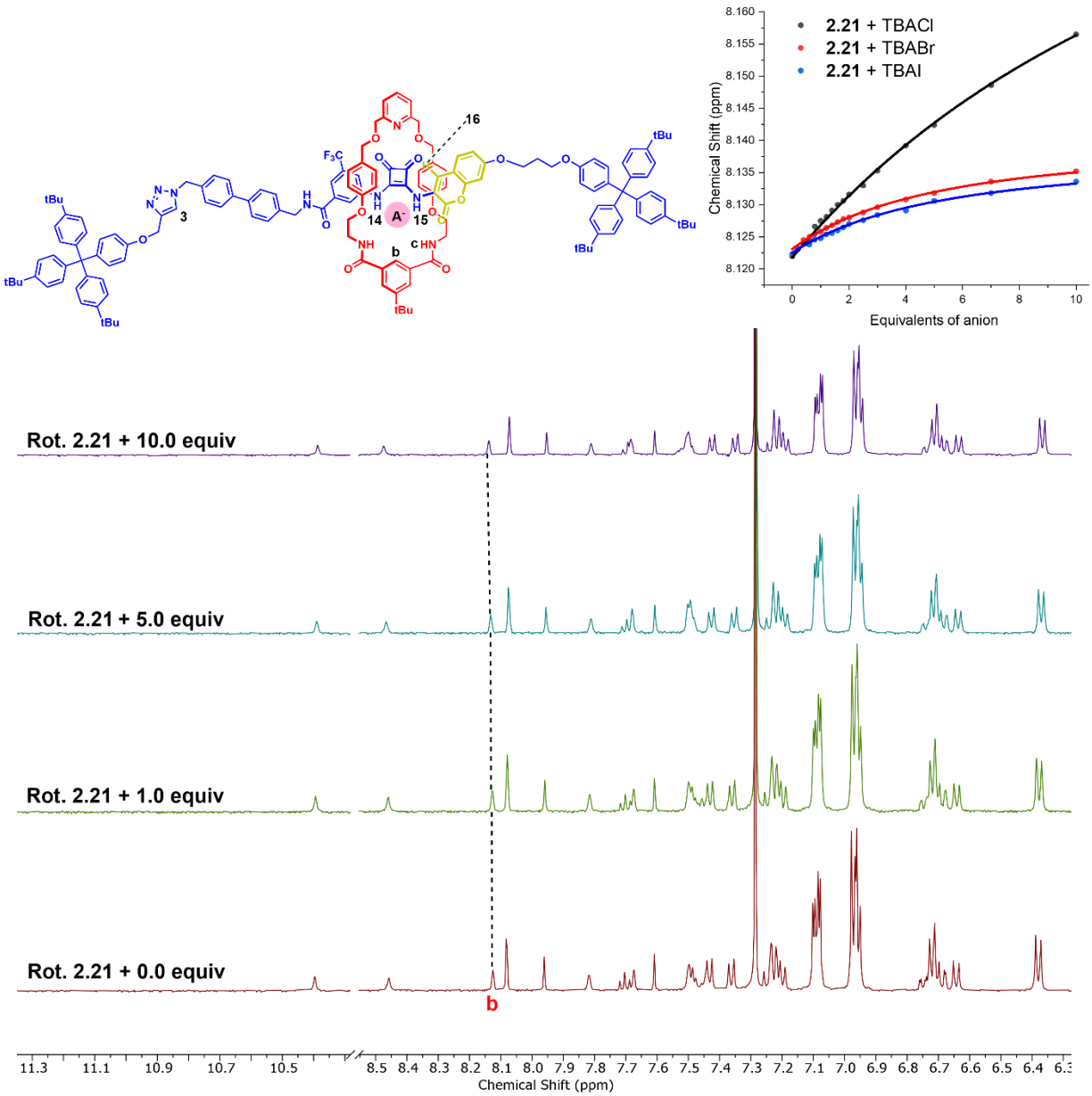


Figure 2.33. *^{1}H NMR spectra of [2]rotaxane **2.21** upon addition of 1, 5 and 10 equivalents of TBABr (500 MHz, 298 K, 7:3 $CDCl_3/CD_3CN$). Inset: Binding isotherms showing changes in chemical shift of internal benzene proton b upon increasing equivalents of halide anions.*

preference for iodide, as seen in the case of HB rotaxane **2.15** (Table 2.2), the magnitudes of the calculated association constants of the coumarin-appended analogue were notably lower. This may be attributed to the relative steric inaccessibility of the anion binding donors and reduced size of the anion binding cavity as a consequence of the coumarin motif, forcing larger anions to prefer an exotopic coordination mode.

Table 2.5: *Halide anion association constants K_a (M^{-1}) for [2]rotaxanes **2.21** and **2.22** [1.0 mM] in 3:7 $CD_3CN/CDCl_3$ at 298 K.*[a]

Anion	[2]Rot. **2.21**	[2]Rot. **2.22**
Cl^-	26	238
Br^-	100	69
I^-	130	36

[a] K_a values calculated using Bindfit[237] software using a 1:1 host-guest binding model by monitoring internal benzene proton H_b. All anions added as their TBA salts. Error percentages less than 10% unless specified.

Similar to the selectivity trends witnessed with XB rotaxane **2.17**, coumarin-containing XB [2]rotaxane **2.22** also demonstrated a preference for chloride upon being subjected to analogous titration conditions. Following addition of chloride and bromide salts to the rotaxane receptor, downfield shifts of the axle squaramide N-H protons $H_{14,15}$ and upfield shift of the internal benzene proton H_b were noted indicating that the anions were bound endotopically within the [2]rotaxane cavity (Figure 2.34). Additionally, the proton resonances of the coumarin motif namely H_{16} also experienced noticeable downfield shifts alluding to the possible preorganisation and eventual participation of the coumarin unit in anion binding. Interestingly, as seen with [2]rotaxane **2.21**, the addition of a larger halide such as iodide ensued upfield shifts of one of the axle squaramide N-H protons suggesting exotopic binding of the larger anion. Importantly, in contrast to XB rotaxane **2.17**, XB rotaxane **2.22** also demonstrated significantly lower binding affinities (*ca.* 16- and 20-fold reduction in the case

of chloride and bromide respectively). This dramatic diminution in binding constant values can be ascribed to the penalty involved in disrupting the coumarin mediated axle-macrocycle intercomponent HB interactions in addition to the relatively rotaxane smaller binding pocket.

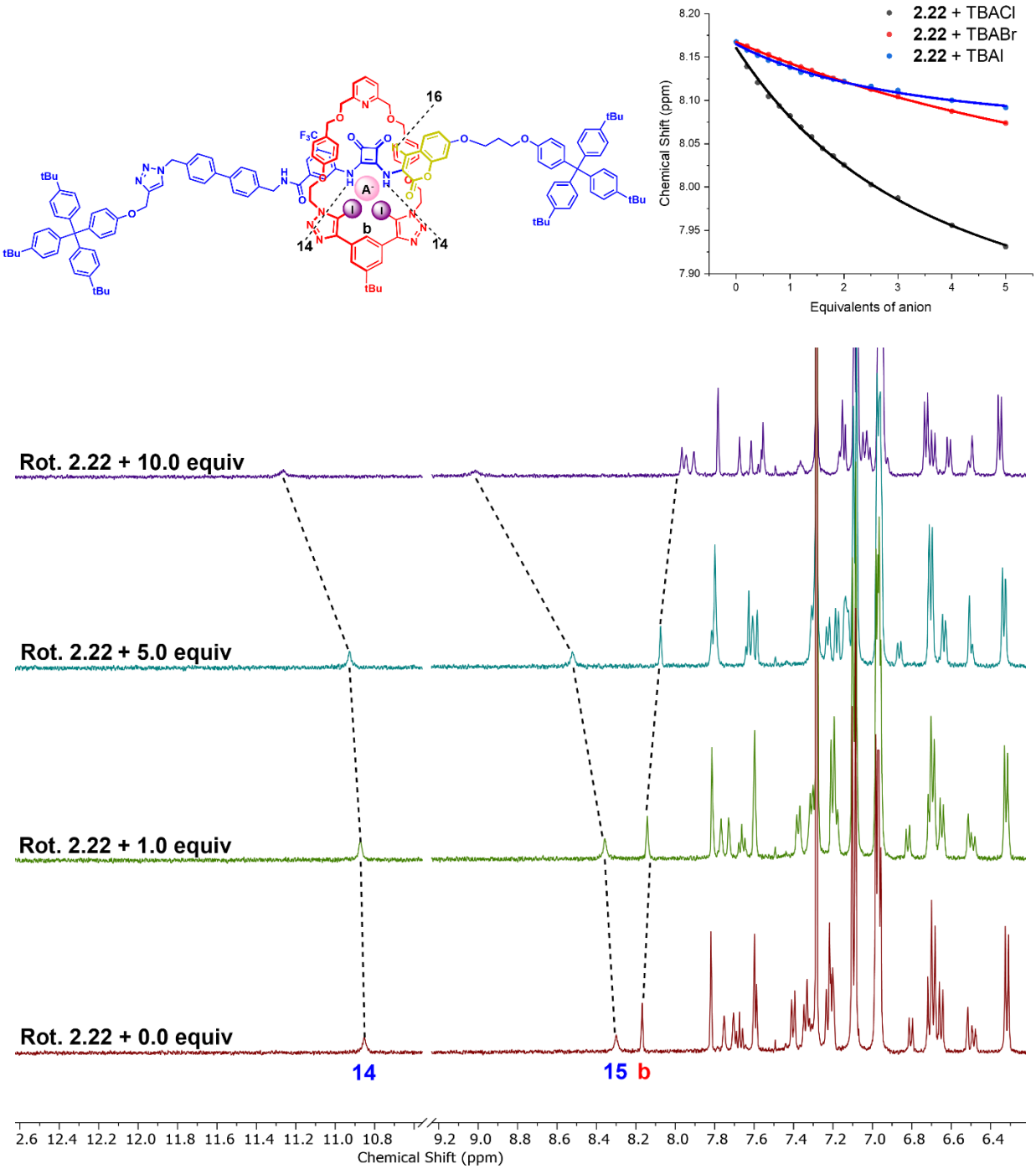


Figure 2.34. *^{1}H NMR spectra of [2]rotaxane **2.22** upon addition of 1, 5 and 10 equivalents of TBABr (500 MHz, 298 K, 7:3 $CDCl_3/CD_3CN$). Inset: Binding isotherms showing changes in chemical shift of internal benzene proton b upon increasing equivalents of halide anions.*

2.6.2 Quantitative ^{1}H NMR alkali metal cation binding titration studies

To investigate the capability of the coumarin appended rotaxanes, **2.21** and **2.22** to complex alkali metal cations, ^{1}H NMR titrations were conducted by adding aliquots of lithium perchlorate and sodium BAr^F, alkali metal cation salts to a 1mM solution of each rotaxane in 30% CD_3CN-$CDCl_3$ solvent media. For both rotaxanes, gradual downfield shifts of the protons in the vicinity of the macrocycle component pyridyl group namely Hk, H_h and H_i were observed. Additionally, increasing cation concentration also resulted in upfield shifts of the coumarin proton H_{16}, suggestive of possible disruption of the coumarin proton-squaramide carbonyl HB interactions and subsequent co-conformational preorganisation of the coumarin carbonyl for cation binding (Figure 2.35 and 2.36). By monitoring the chemical shifts of the aforementioned proton resonances, Bindfit[237] analysis of the resulting titration isotherms using a 1:1 host-guest stochiometric binding model determined the cation association constants summarised in Table 2.6.

Table 2.6: *Cation association constants K_a (M^{-1}) for [2]rotaxanes **2.21** and **2.22** [1.0 mM] in 3:7 $CD_3CN/CDCl_3$ at 298 K.[a]*

Cation	[2]Rot. **2.21**	[2]Rot. **2.22**
Li^+	177	84
Na^+	76	47

[a] K_a values calculated using Bindfit[237] software using a 1:1 host-guest binding model by monitoring internal benzene proton H_b. Lithium and sodium added as $LiClO_4$ and $NaBAr^F_4$. Error percentages less than 10% unless specified.

As evident from the binding data, both coumarin functionalised rotaxanes bound lithium more strongly compared to sodium, presumably due to lithium's smaller size-complementarity with the cation-binding cavity. Interestingly, the binding strength of both cations was markedly lower for the coumarin-based rotaxanes **2.21** and **2.22** compared to

their non-coumarin rotaxane analogues **2.15** and **2.17.** The respective sterically crowded cation binding cavity and additional competing coumarin based intercomponent rotaxane interactions may be responsible for the observed diminished cation affinities.

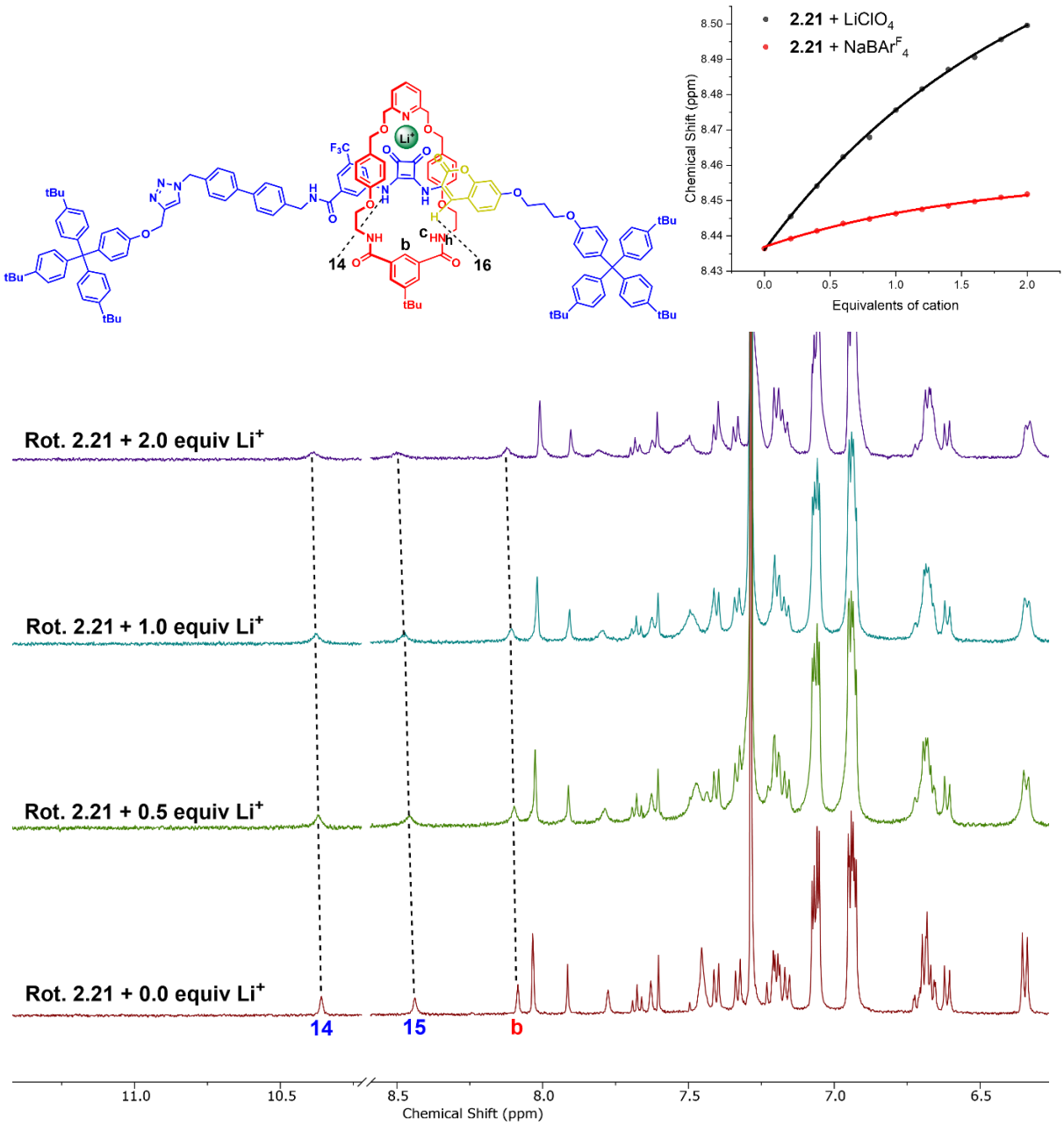


Figure 2.35. *^{1}H NMR spectra of [2]rotaxane **2.21** upon addition of 0.5, 1 and 2 equivalents of $LiClO_4$ (500 MHz, 298 K, 7:3 $CDCl_3/CD_3CN$). Inset: Binding isotherms showing changes in chemical shift of internal benzene proton 14 upon increasing equivalents of lithium cations.*

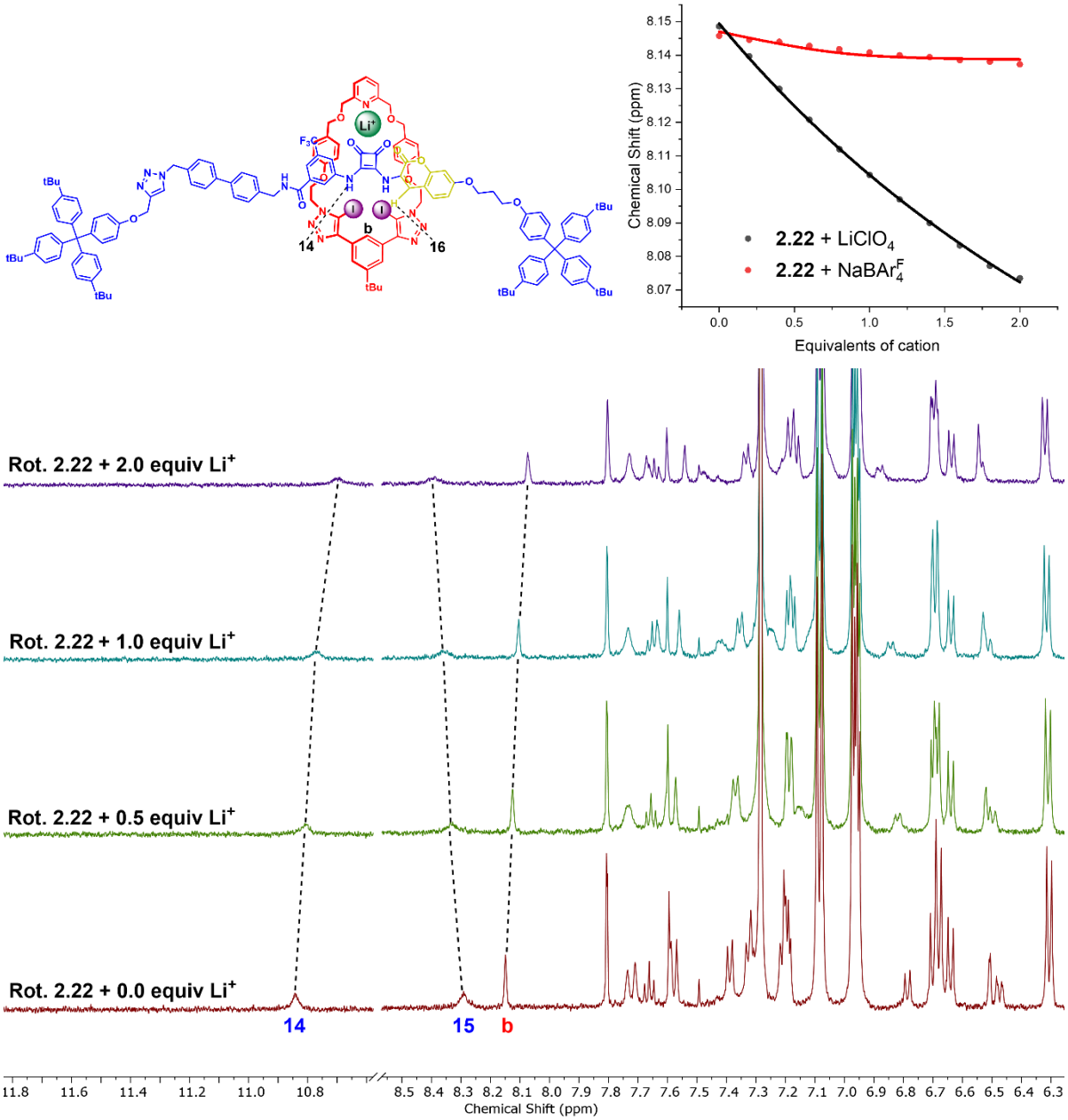


Figure 2.36. *^{1}H NMR spectra of [2]rotaxane **2.22** upon addition of 0.5, 1 and 2 equivalents of $LiClO_4$ (500 MHz, 298 K, 7:3 $CDCl_3$/CD_3CN). Inset: Binding isotherms showing changes in chemical shift of internal benzene proton b upon increasing equivalents of halide anions*

2.6.3 Quantitative ^{1}H NMR ion-pair binding titration studies

The previous ^{1}H NMR ion-pair binding titration protocol was undertaken again to assess the potential of the coumarin-containing rotaxanes to simultaneously bind lithium halide ion-pairs, wherein aliquots of TBA halide salts were added to a 1 mM solution of each rotaxane in the presence of 1 equivalent of lithium perchlorate in 3:7 $CD_3CN/CDCl_3$ solvent media.

Considering first the LiX ion-pair binding properties of HB rotaxane **2.21,** addition of bromide to the lithium-complexed rotaxane caused squaramide NH protons $H_{14,15}$ and internal benzene proton H_b to broaden and move downfield consistent with anion binding occurring in the bis-amide anion binding cleft and interlocked cavity of the [2]rotaxane (Figure 2.37). Addition of TBAI on the other hand induced upfield shifts of squaramide N-H proton H_{14} and downfield shifts of N-H proton H_{15} and internal benzene proton H_b, thereby suggesting that the larger anion may be favouring an exotopic coordination mode. Notably, addition of TBACl led to decomplexation of the metal cation and LiCl precipitation confirming that ion-pair binding could not overcome the lattice energy of the alkali metal salt. In all cases, addition of halides elicited negligible shifts in the proton resonances corresponding to the coumarin motif indicating it does not participate in anion binding.

By monitoring these proton shifts as a function of anion concentration, binding isotherms for the titrations with bromide and iodide in the presence of 1 equivalent of $LiClO_4$ were obtained. Analysis of the apparent ion-pair binding data summarised in Table 2.7 revealed that the presence of co-bound lithium only evoked a relatively small enhancement in halide binding affinities with HB rotaxane **2.21**, displaying a modest preference for iodide.

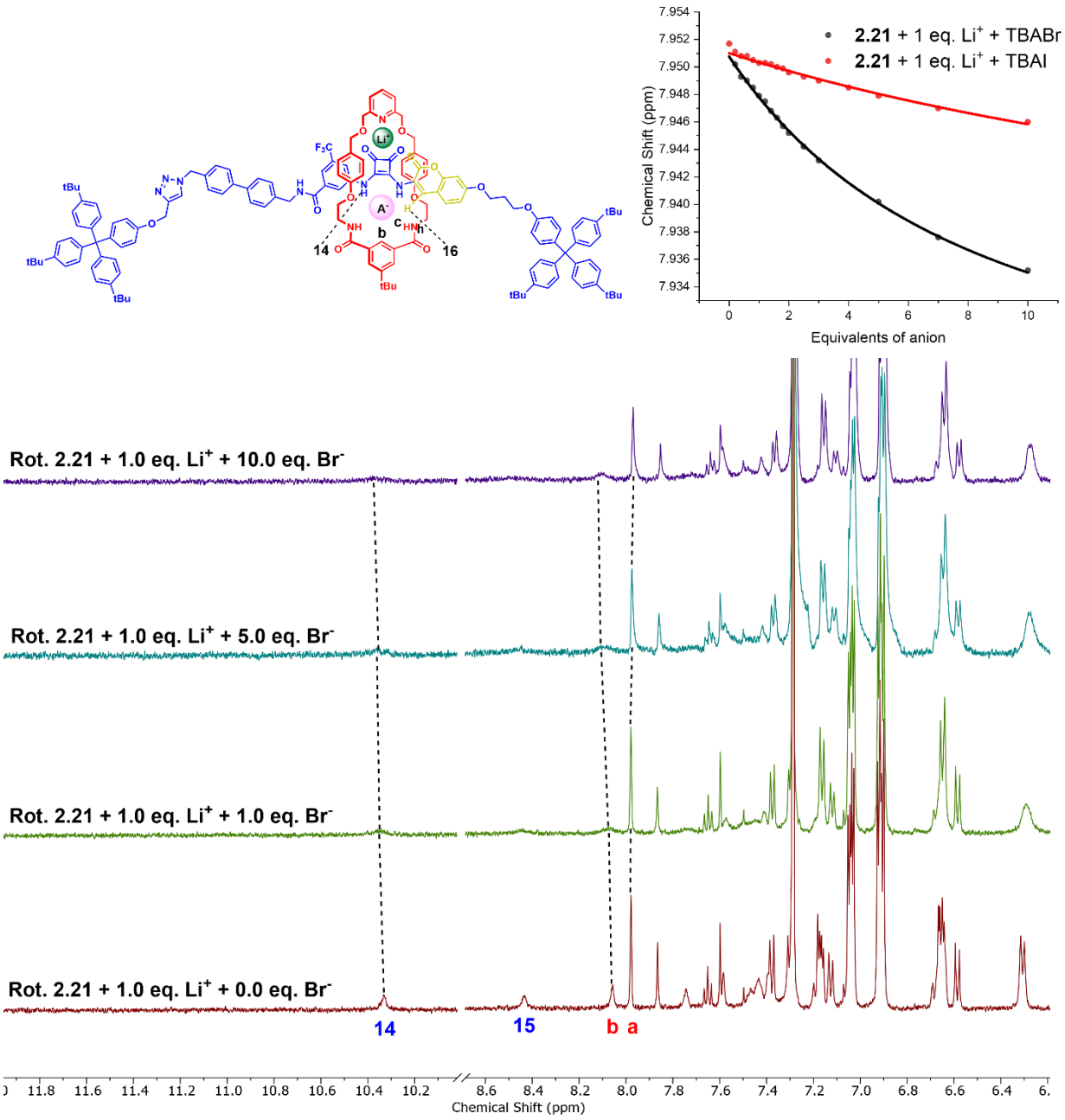


Figure 2.37. *^{1}H NMR spectra of [2]rotaxane **2.21** upon addition of addition of 1, 5 and 10 equivalents of TBABr in the presence of 1 equivalent of $LiClO_4$ (500 MHz, 298 K, 7:3 $CDCl_3/CD_3CN$). Inset: Binding isotherms showing changes in chemical shift of external benzene proton a upon increasing equivalents of halide anions.*

Alternatively, addition of chloride and bromide halide salts to the pre-complexed XB [2]rotaxane **2.22** elicited significant downfield shifts of the axle squaramide N-H protons $H_{14,15}$ and coumarin proton H_{16} and upfield shifts of the internal benzene proton H_b indicative of binding occurring within the interlocked cavity of the [2]rotaxane *via* a combination of the axle's various HB donors and macrocycle XB donors (Figure 2.38). The only exception to this

behaviour was observed during the addition of TBAI to the lithium-complexed [2]rotaxane **2.22** which engendered one of the squaramide NHs to shift upfield instead. This behaviour was consistent with iodide favouring an exotopic coordination mode when binding to these coumarin-based rotaxanes.

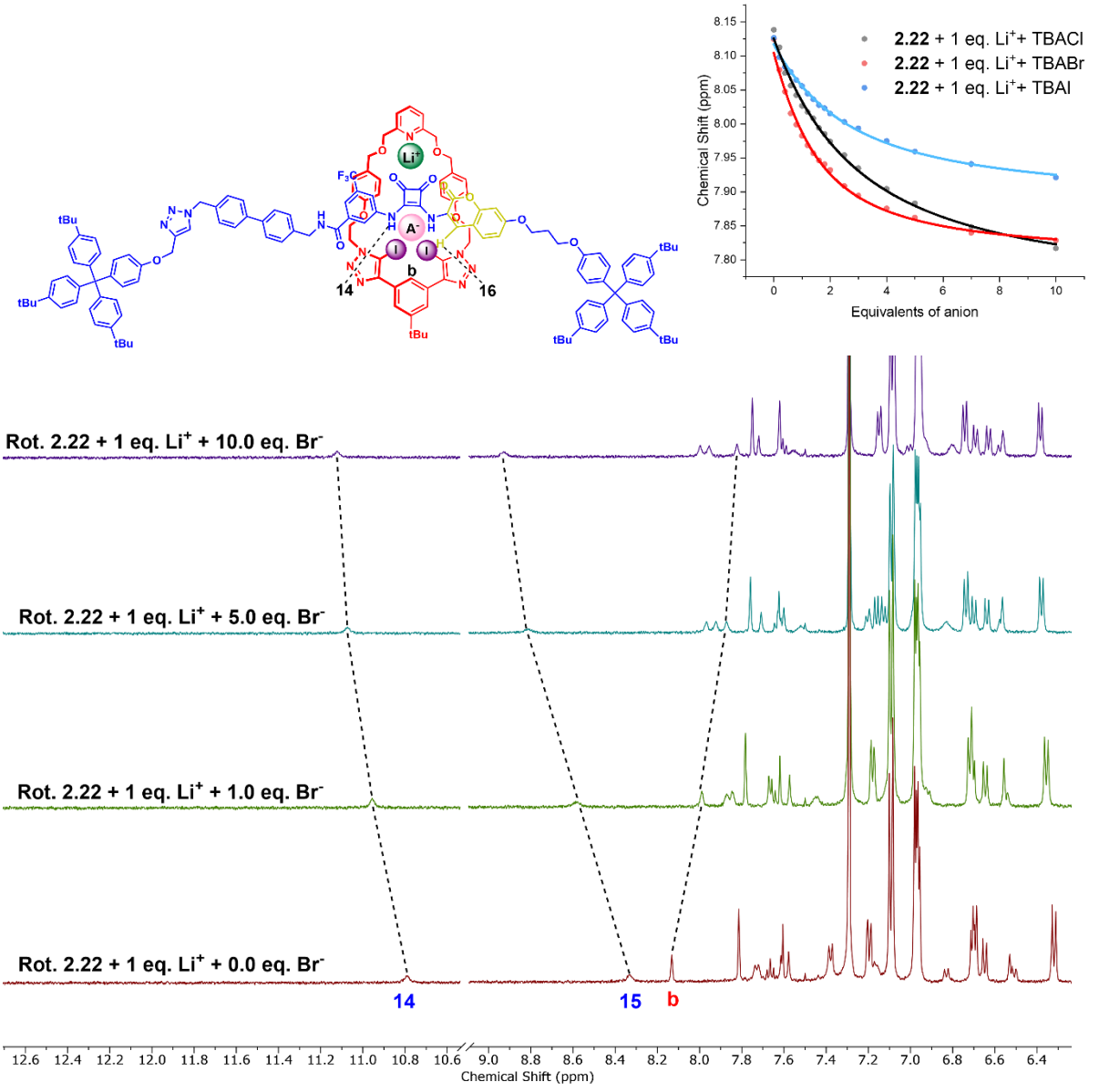


Figure 2.38. *^{1}H NMR spectra of [2]rotaxane **2.22** upon addition of addition of 1, 5 and 10 equivalents of TBABr in the presence of 1 equivalent of $LiClO_4$ (500 MHz, 298 K, 7:3 $CDCl_3$/CD_3CN). Inset: Binding isotherms showing changes in chemical shift of internal benzene proton b upon increasing equivalents of halide anions.*

Inspection of the binding data in Table 2.7 was revelatory of coumarin XB [2]rotaxane **2.22** impressively binding the LiCl ion-pair, possibly owing to the strong binding and

stabilization of chloride in the XB-functionalised rotaxane cavity. However, the magnitude for the apparent LiCl association constant was much diminished compared to XB rotaxane **2.17.** Moreover, lithium-complexed coumarin XB rotaxane **2.22** was seen to exhibit a preference for bromide, demonstrating an up to *ca.* 23-fold larger bromide constant magnitude compared to the free receptor. This is in contrast to the trends observed with XB rotaxane **2.17**, a deviation attributed to XB coumarin rotaxane **2.22** being a weaker anion binding host compared to its non-coumarin analogue.

Table 2.7: *Apparent association constants K_a (M^{-1}) for [2]rotaxanes **2.21** and **2.22** [1.0 mM] in the presence of 1 equiv. $LiClO_4$ in 3:7 CD3CN/CDCl3 at 298 K.[a]*

Host	Cation	% cation bound	Anion	K_a (M^{-1})
[2]Rot. **2.21**	Li^+ (1 eq.)	13%	**Cl^-**	-[b]
			Br^-	108
			I^-	200
[2]Rot. **2.22**	Li^+ (1 eq.)	7%	**Cl^-**	405
			Br^-	1552
			I^-	471

[a] K_a values calculated using Bindfit[237] software using a 1:1 host-guest binding model by monitoring internal benzene proton H_b. Lithium cation added as $LiClO_4$. All anions added as their TBA salts. Error percentages less than 10% unless specified. [b] Salt recombination.

In summary, disappointingly the ion-pair association constants obtained with coumarin-appended rotaxanes are markedly lower than those obtained with the non-coumarin rotaxane analogues. This can be rationalised by consideration of the significantly lower individual cation and anion binding affinities of the coumarin-containing rotaxanes possibly due to sterically inaccessible binding cavities and competing intercomponent HB interactions introduced by the coumarin unit.

2.6.4 Preliminary optical studies

The photophysical properties of the photo-active coumarin-based [2]rotaxane receptors, **2.21** and **2.22** were investigated in 3:7 $CH_3CN/CHCl_3$ solvent media using UV-visible absorption and fluorescence spectroscopy (Figure 2.39) and the photophysical data is summarised in Table 2.8.

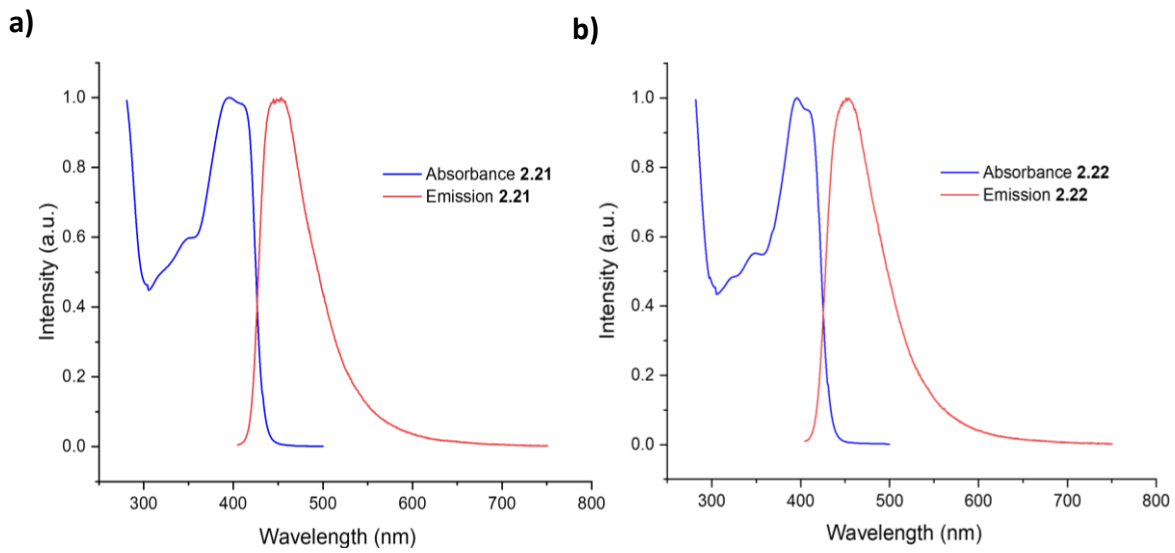


Figure 2.39. *a) Normalised emission and absorption spectra for [2]rotaxane **2.21** b) Normalised emission and absorption spectra for [2]rotaxane **2.22**. Concentration of receptors = 100 µM. Solvent=3:7 CD3CN/CDCl3 at 293 K.*

Table 2.8: *Wavelengths of maximum absorption and emission for [2]rotaxanes **2.21** and **2.22** in 3:7 $CD_3CN/CDCl_3$.*

Receptor	**Absorbance λ_{abs} (nm)**	**Emission λ_{ems} (nm)**	**Stokes shift (nm)**
[2]Rot. **2.21**	385	453	68
[2]Rot. **2.22**	385	453	68

Emission wavelength excited at $\lambda_{max\ abs}$, in 3:7 $CD_3CN/CDCl_3$ at 293 K. Concentration of receptors: 100 µM

Additionally, in order to understand and rationalise the differences in the adopted co-conformations and interactions between the squaramide and coumarin donor groups upon

ion association, the absorption spectra of the non-coumarin rotaxanes were overlayed with those of their coumarin-based analogues, which revealed two distinct absorption bands corresponding to the squaramide and coumarin motifs (Figure 2.40). This indicated that while the two moieties potentially interacted with each other, the interactions were not strong enough to significantly change the electronic properties of the two donor groups.[242]

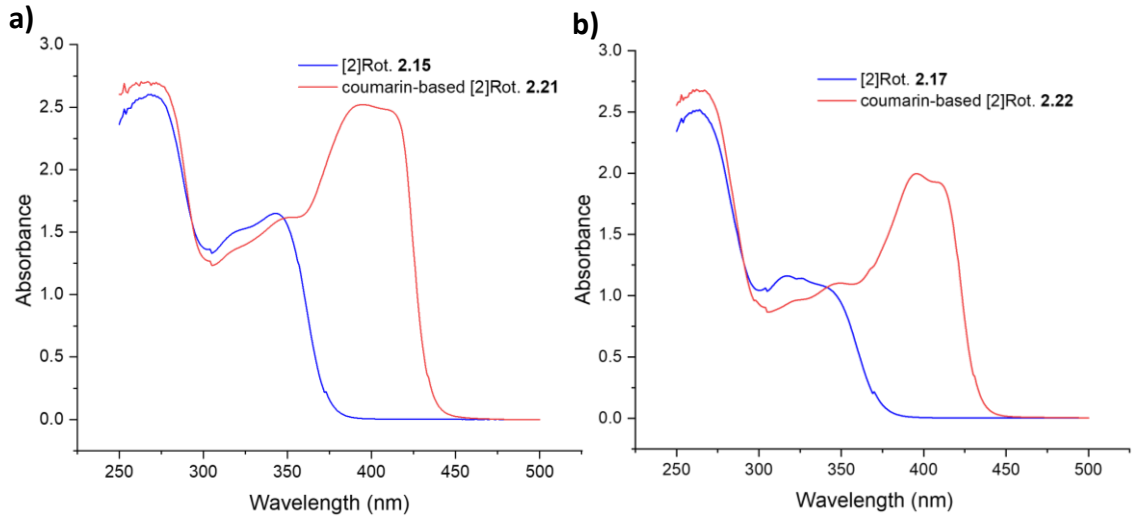


Figure 2.40. *a) Comparison of absorption spectra of [2]rotaxanes **2.15** and **2.21** b) Comparison of absorption spectra of [2]rotaxanes **2.17** and **2.22**. Concentration of receptor: 100 µM. Solvent=3:7 $CD_3CN/CDCl_3$ at 293 K.*

Preliminary qualitative absorption and fluorescence titration studies were undertaken in the same solvent system to investigate the anion, cation and ion-pair photo-active sensing properties of the coumarin-based rotaxanes, **2.21** and **2.22**. For the purposes of this study, $LiClO_4$ and TBABr were chosen as the cation and anion salt sources owing to reasonable respective ion binding affinities demonstrated by the receptors during ^{1}H NMR titration experiments (Table 2.5 and 2.6).

Upon addition of solid TBABr to a 100 µM solution of the free HB coumarin rotaxane **2.21** negligible changes in the absorption and emission spectra (λ_{ex} = 385 nm) suggested that anion binding instigated small variations in the optical properties of the receptor (Figure

2.41a), consistent with the squaramide and coumarin donor units not being preorganised to bind the anion, as previously concluded during ^{1}H NMR titration studies (Section 2.6.1). Addition of solid $LiClO_4$ to the solution thereafter engendered perturbations in both the coumarin and squaramide bands in the absorption spectrum, indicative of likely receptor preorganisation and consequent ion-pair binding. Furthermore, a remarkable increase and red-shift in the fluorescence intensity was also observed, attributable to potential rigidification of the binding cavity and consequent reduction of non-radiative decay processes upon cooperative LiBr ion-pair binding.[243] Upon reversing the order of the addition of ions, addition of solid $LiClO_4$ to the free rotaxane first induced changes in the regions of the

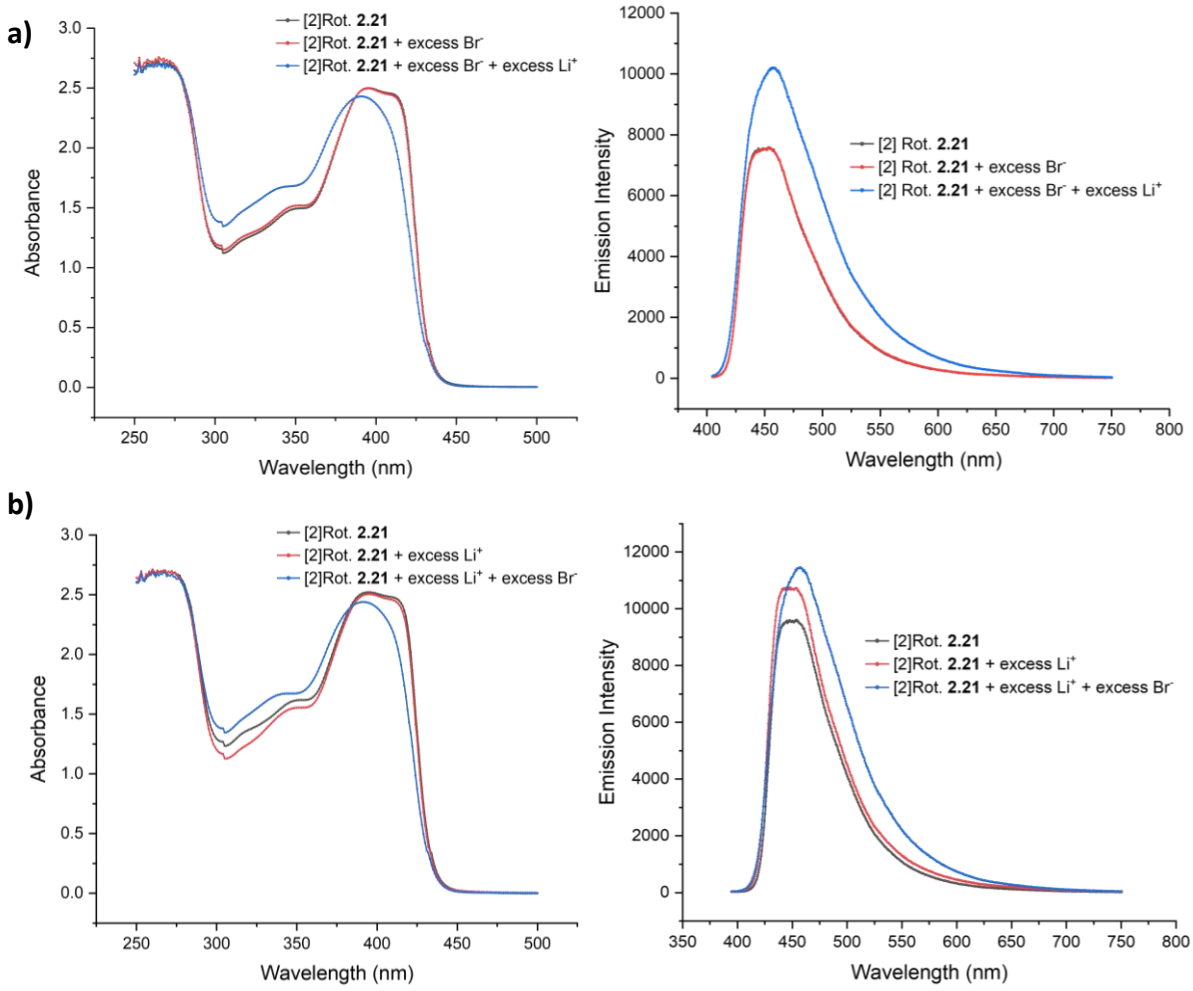


Figure 2.41. *Changes in the absorption and fluorescence emission intensity of receptor* ***2.21*** *upon addition of a) excess TBABr followed by the addition of excess $LiClO_4$ b) excess $LiClO_4$ followed by the addition of excess TBABr. Concentration of receptor= 100 µM. Solvent=3:7 $CD_3CN/CDCl_3$ at 293 K.*

absorption curve attributed to the squaramide motif alluding to the squaramide carbonyls complexing the lithium cation (Figure 2.41b). This was also accompanied with an increase in fluorescence intensity due to likely rigidification of the MIM binding cavity. Subsequent addition of TBABr to the lithium complexed [2]rotaxane resulted in a further increase and red-shift of the fluorescence intensity of the emission spectra in concert with drastic changes in the absorption spectra ascribed to concomitant cation and anion association by the heteroditopic rotaxane receptor.

In the case of XB [2]rotaxane **2.22**, initial addition of solid TBABr to a 100 μM solution of the free receptor under analogous conditions (λ_{ex} = 385 nm) led to a notable decrease in fluorescence intensity (Figure 2.42a). This was indicative of anion association involving the XB iodotriazole donors, known for instituting a heavy atom constituted fluorescence quenching effect.[244] Changes were also observed in both the squaramide and coumarin regions of the absorption spectra indicating possible co-conformational changes instigated upon anion binding. Addition of excess $LiClO_4$ to the bromide complexed system resulted in a further decrease in fluorescence intensity and changes in the absorption spectra owing to the cooperative binding of the LiBr ion-pair.

Alternatively, upon addition of excess $LiClO_4$ to the free receptor, a similar decrease in the coumarin fluorescence was observed (Figure 2.42b), suggestive of lithium cation binding disrupting the intercomponent interactions within the receptor. Slight perturbations were also seen in the absorption spectra due to potential preorganisation of the cation binding site. Thereafter addition of excess TBABr led to a significant decrease in fluorescence intensity in concert with changes in the absorption spectral regions of both the squaramide and coumarin units, credited to the strong LiBr ion-pair association with the XB [2]rotaxane.

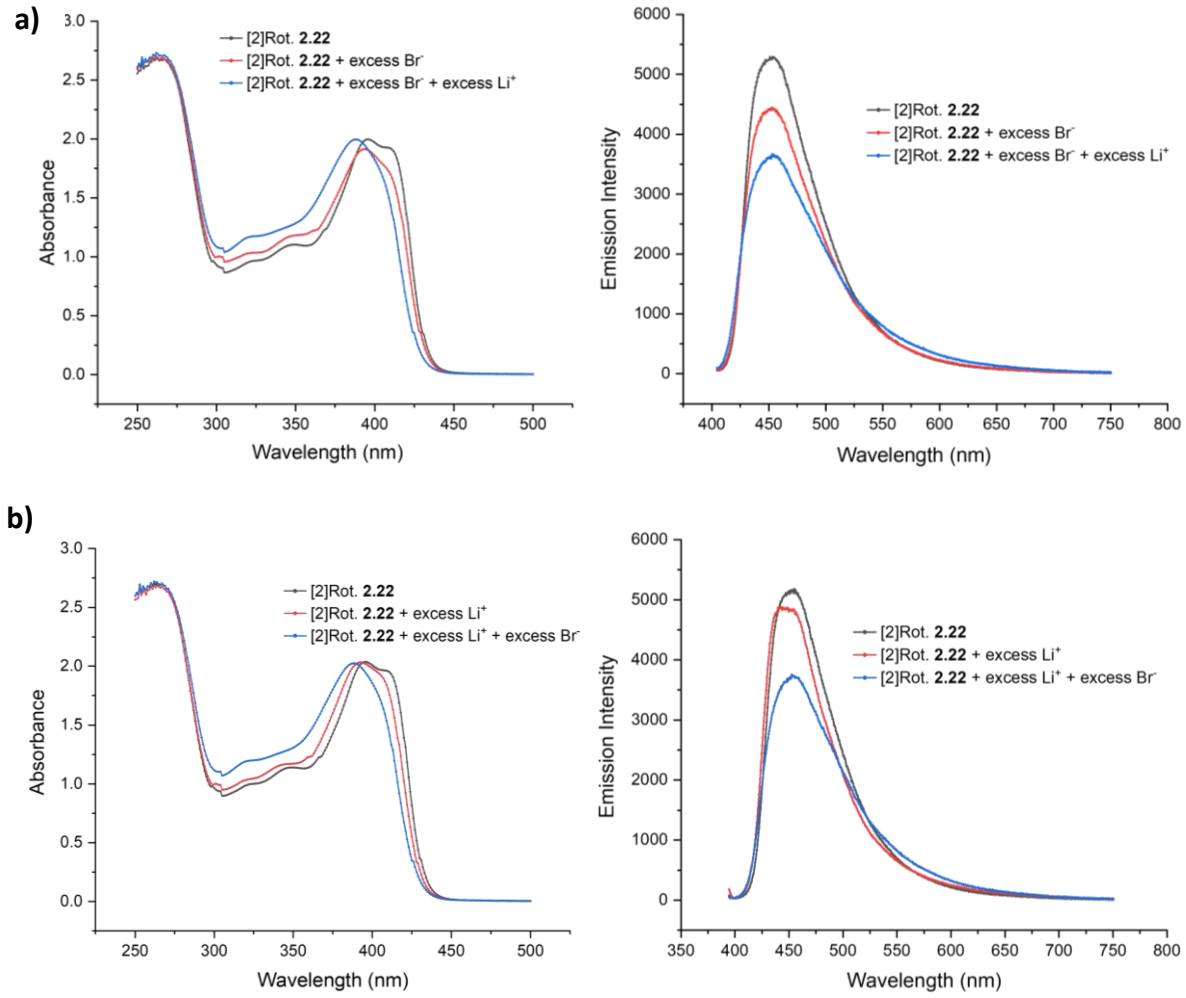


Figure 2.42. *Changes in the absorption and fluorescence emission intensity of receptor* ***2.22*** *upon addition of a) excess TBABr followed by the addition of excess $LiClO_4$ b) excess $LiClO_4$ followed by the addition of excess TBABr. Concentration of receptor: 100 µM. Solvent=3:7 $CD_3CN/CDCl_3$ at 293 K.*

2.6.5 Solid-liquid extraction studies

The potential of these coumarin-containing rotaxanes to function as lithium halide salt extractants was evaluated by carrying out some preliminary ^{1}H NMR solid-liquid extraction studies. In a typical experiment, an excess of a solid lithium salt (LiCl, LiBr, LiI) was added to 1.0 mM a solution of the receptor in $CDCl_3$ (700 µL) and the mixture was sonicated for 20 min. The excess salt was subsequently removed by filtration.

Inspection of the post-extraction spectra of HB rotaxane **2.21** showed that the receptor was able to successfully extract LiBr and LiI into organic solution with the complexation induced shifts (CIS) being consistent with those observed during solution-phase ion-pair titration studies (Figure 2.43). Specifically, in the case of LiBr, downfield shifts of the internal benzene proton H_b and protons in the vicinity of the pyridyl unit of the macrocycle, H_h and H_i alluded to the co-binding of the ion-pair. Conversely, LiI addition resulted in a system which remained in slow exchange between the fully complexed and free receptor. In contrast, no extraction of LiCl was observed, which was ascribed to the high lattice enthalpy of the LiCl salt.

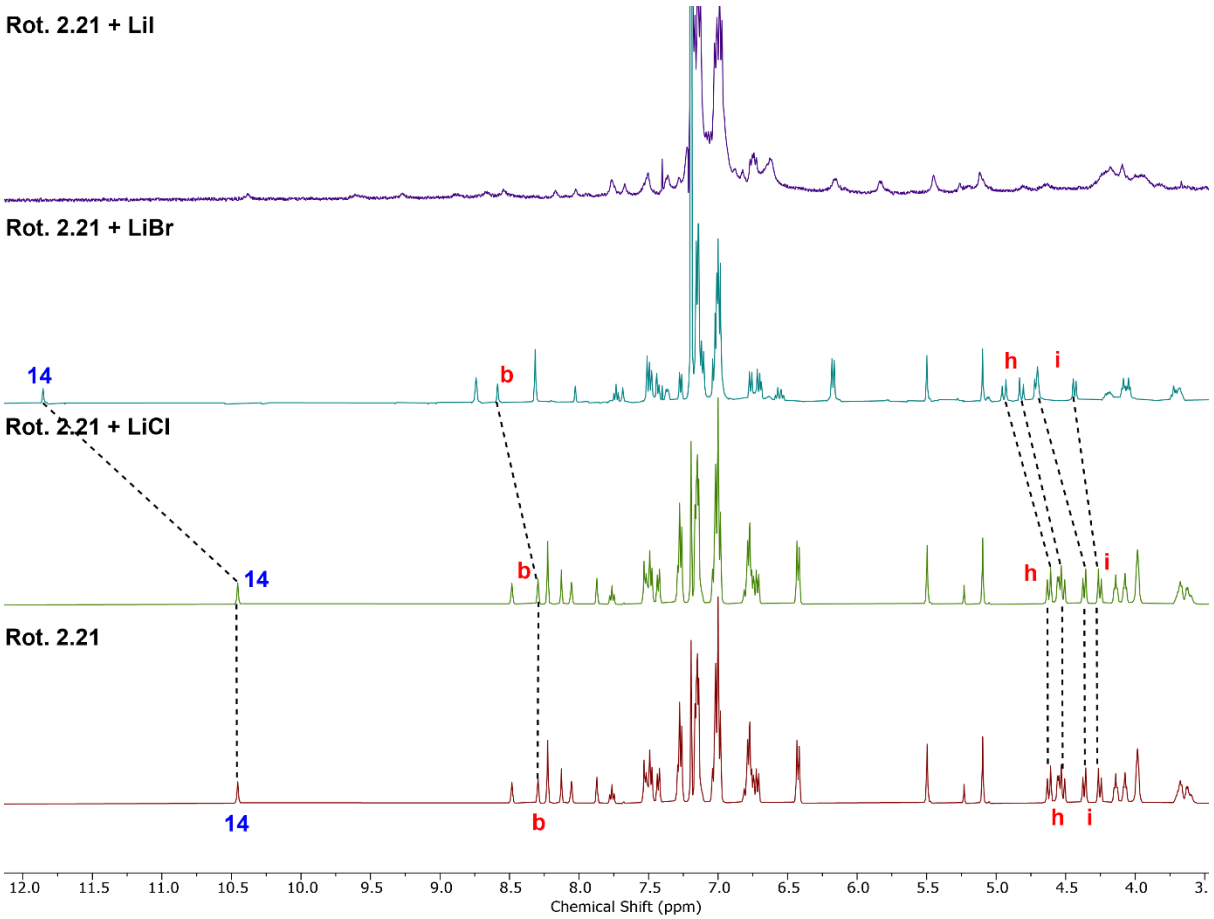


Figure 2.43. *Pre- and post-extraction ^{1}H NMR spectra of [2]rotaxane **2.21** with excess LiCl, LiBr and LiI ($CDCl_3$, 500MHz, 298K).*

In the case of XB [2]rotaxane **2.22**, comparison of the post- and pre-extraction ^{1}H NMR spectra revealed that the receptor was able to successfully extract LiCl and LiBr into $CDCl_3$ wherein chemical shift perturbations corresponding to the proton resonances neighbouring the anion and cation binding cavities namely, H_b and $H_{h,i}$ respectively were indicative of concomitant binding of the LiCl and LiBr ion-pair (Figure 2.44). Interestingly, addition of LiI salt to a solution of XB rotaxane **2.22** resulted in the formation of an insoluble complex in $CDCl_3$. This was evidenced by the lack of proton peaks in the ^{1}H NMR spectrum in $CDCl_3$ and further confirmed by dissolving the filtered residue in DMSO which recovered the free rotaxane.

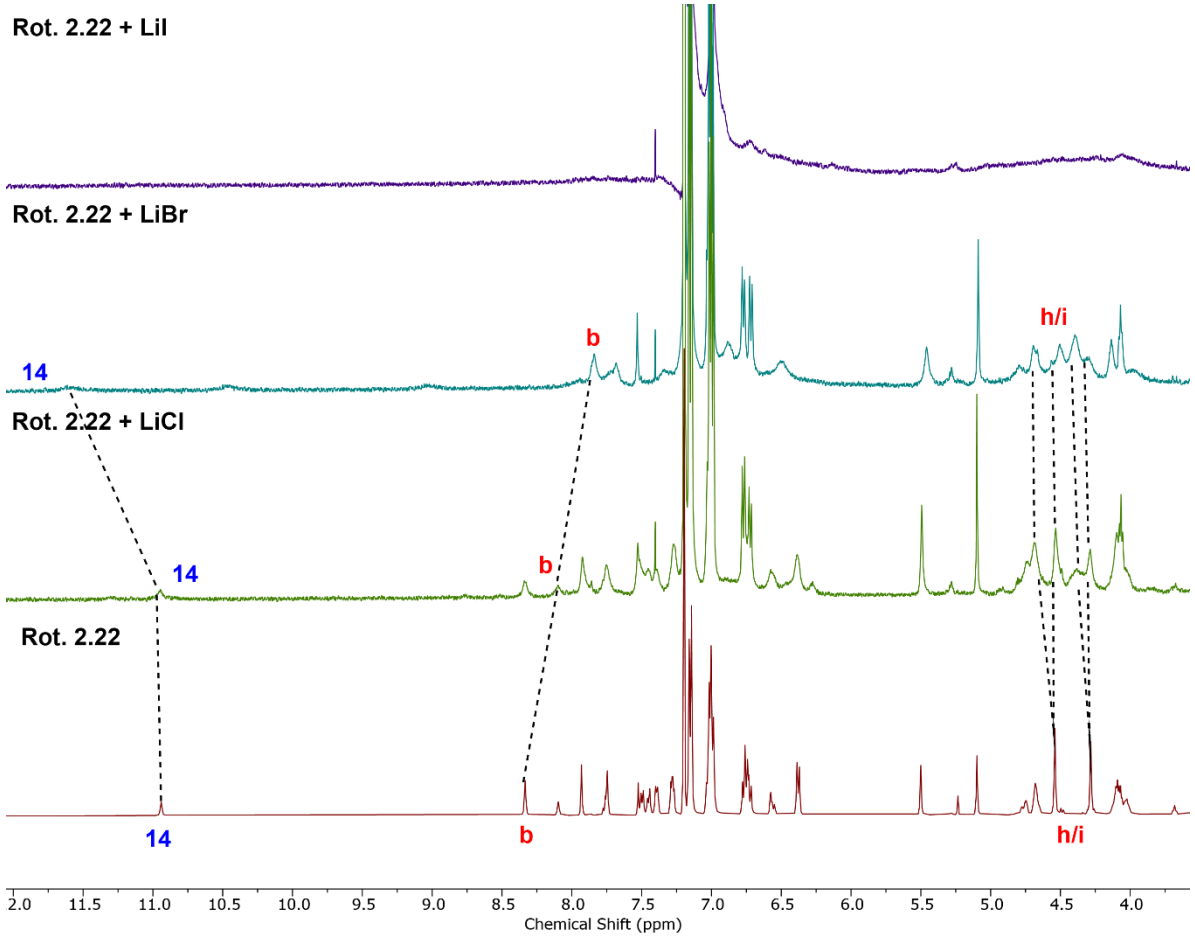


Figure 2.44. *Pre- and post-extraction ^{1}H NMR spectra of [2]rotaxane **2.22** with excess LiCl, LiBr and LiI ($CDCl_3$, 500 MHz, 298K).*

2.7 Conclusions and Future work

In conclusion, four novel squaramide-based heteroditopic [2]rotaxanes functionalised with XB and HB anion binding donors were prepared using active template methodology. Quantitative ^{1}H NMR host-guest titration studies revealed that a co-bound lithium metal cation led to notable enhancements of halide binding strengths of the [2]rotaxane receptors, highlighting the advantages of positive cooperative electrostatic effects instigated by heteroditopic designed MIM host structures. Importantly, both XB functionalised receptors **2.17** and **2.22** exhibited superior ion-pair binding properties in comparison to their HB rotaxane analogues **2.15** and **2.21**, underpinning the improved selectivity and binding profiles offered by sigma-hole XB systems. In particular it is noteworthy that they were also able to impressively bind the LiCl ion-pair, showcasing the significance of strong, simultaneous cation and anion association in enabling ion-pair recognition. Introduction of a coumarin motif in the axle unfortunately led to a diminution in halide binding affinity, possibly due to steric inaccessibility of the anion binding site, causing the larger halide anions to even prefer an exotopic coordination mode and competing coumarin-based intercomponent MIM HB interactions. Qualitative optical studies conducted with the coumarin-based [2]rotaxanes under analogous solvent conditions showed significant ion-pair binding mediated alterations in the absorbance and fluorescence properties of the coumarin receptors, suggesting promising prospects in the development of future MIM-based heteroditopic optical sensors. Preliminary solid-liquid extraction studies receptors revealed all four rotaxanes extracted LiBr into organic media in addition to XB rotaxanes **2.17** and **2.22** also successfully extracting the LiCl ion-pair.

In light of the promising ion-pair binding and extraction results, especially those pertaining to the XB [2]rotaxanes, future work could entail the incorporation of other sigma-hole donors including chalcogen bonding and pnictogen bonding motifs into similar interlocked host systems (Figure 2.45). A detailed study into the exploration and comparison of their ion-pair binding capabilities relative to XB and HB analogues, to recognise alkali metal salts as ion-pairs could lay the foundation for the future design of sigma-hole functionalised multitopic MIMs. Furthermore, the incorporation of chromophore/fluorophores other than coumarin like BODIPY into the heteroditopic MIM host structural framework could open up avenues for optical ion-pair sensing analysis (Figure 2.46).

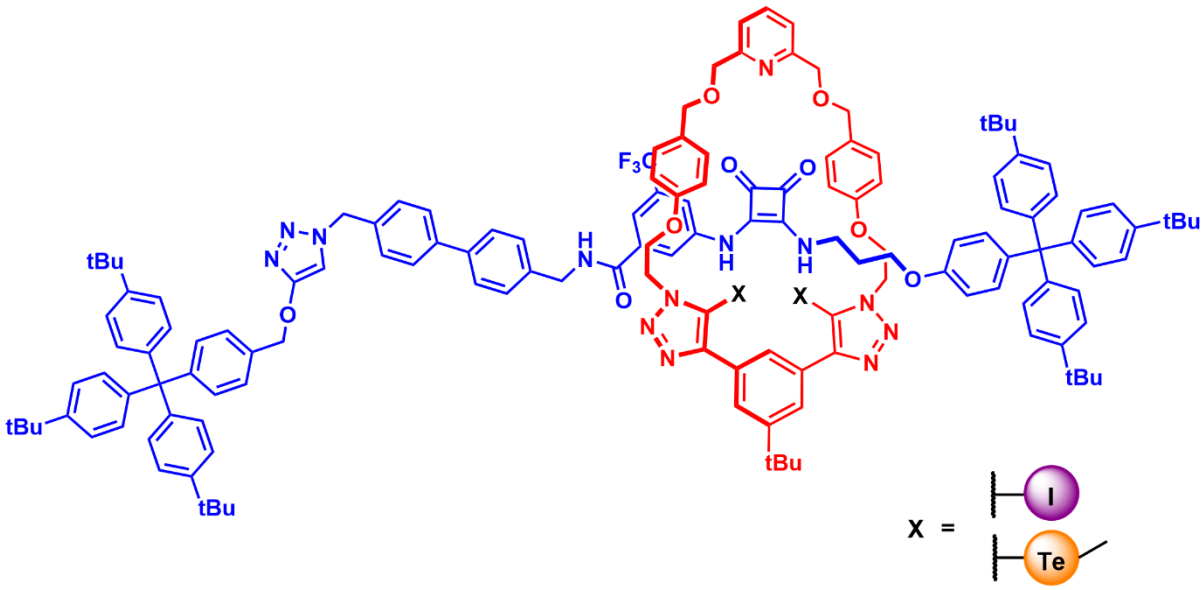


Figure 2.45. *A squaramide functionalised XB and ChB [2]rotaxane.*

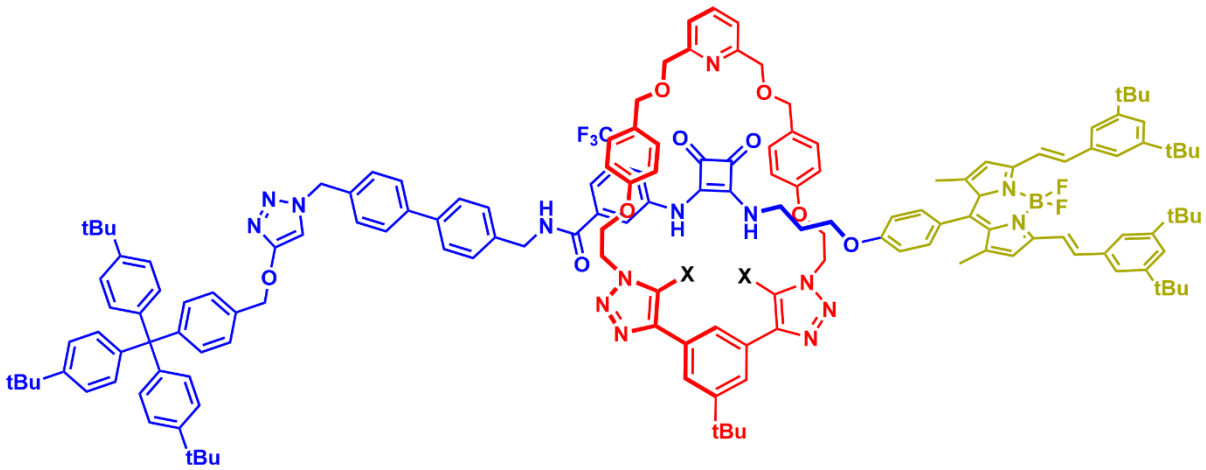


Figure 2.46. *A BODIPY functionalised squaramide [2]rotaxane.*

Chapter 3: Squaramide-based Heteroditopic [2]Rotaxanes for Sodium Halide Ion-pair Recognition and Extraction

3.1 Introduction

As discussed in the previous chapters, heteroditopic receptors possess the ability to simultaneously bind both anions and cations, a capability that confers them superiority and selectivity over their monotopic analogues largely owing to tuneable cooperative enhancements evinced as a consequence of proximal electrostatic and positive allosteric effects instigated by co-bound oppositely charged species.[245-249]

Sodium salts are ubiquitous, playing fundamental roles in wide-ranging biological, medical, environmental, and industrial processes.[250-252] Water scarcity, an ever-present humanitarian need in many developing countries, exacerbated by unpredictable climate change, has brought into focus the urgent need to recycle and reuse wastewater as well as develop methods to desalinise seawater. Heteroditopic receptors have proven uniquely capable of extracting alkali metal salts, even those possessing large lattice enthalpies such as sodium chloride, a key technological challenge to the anthropogenic generation of portable water. While multitopic receptors have shown promise in this area, they have mostly been restricted to crown-ether based recognition sites for sodium binding and convergent amide HB functionalised cavities for halide anion recognition.[253,254]

An interesting example is Beer's *tren*-based heteroditopic receptor consisting of a tripodal amide-based anion recognition site and benzo-15-crown-5 functionalised cation binding sites, which displays significant cooperative binding of chloride, iodide and perrhenate anions in the presence of a sodium cation in $CDCl_3$ (Figure 3.1).[155] Encouraged by a 20-fold enhancement in perrhenate binding in the presence of sodium, liquid-liquid extraction studies are conducted with the structurally similar pertechnetate counter-anion

TcO_4^-, a well-known radioactive pollutant found in nuclear waste streams,[255] which the receptor successfully extracts from aqueous media into chloroform.

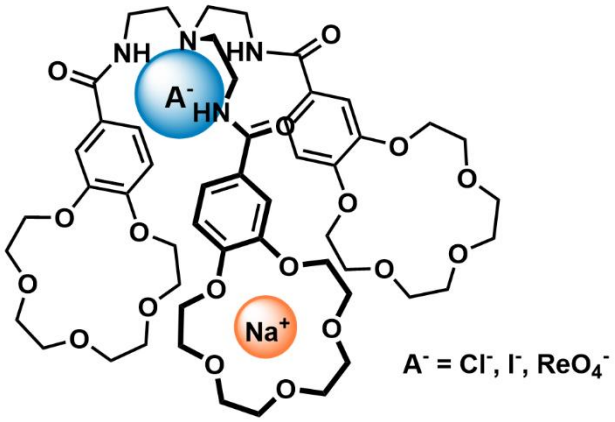


Figure 3.1. *Beer's tren-based heteroditopic receptor.*[155]

Recently, Romanski and co-workers reported an acyclic squaramide functionalised benzo-15-crown-5 receptor which successfully binds a variety of sodium salt ion-pairs through squaramide NH anion donors and crown-ether based cation donors in 9:1 acetonitrile/water mixtures (Figure 3.2).[256] Furthermore, comparative ^1H NMR extraction studies revealed that the ditopic receptor extracted the NaCl ion-pair with a 22% extraction efficiency from water into nitrobenzene, in contrast to urea-based derivatives and crown-ether lacking analogues which proved incapable of extracting the sodium halide salt (Figure 3.2).

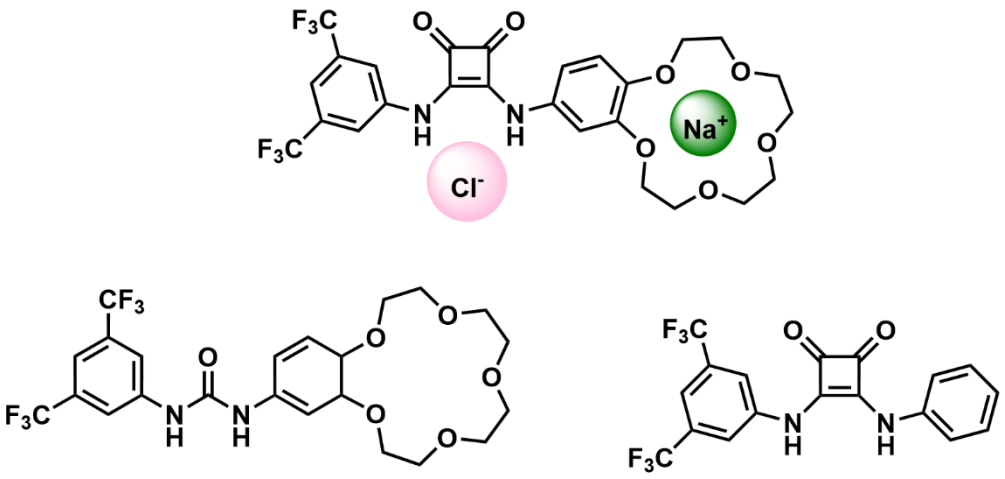


Figure 3.2. *Romanski's squaramide-based NaCl heteroditopic receptor and the urea-based derivatives and crown-ether lacking analogues used as control systems.*[256]

Whilst mechanically interlocked host frameworks have proven effective for the purpose of anion recognition, recent advances have revealed their promising utilisation in the field of ion-pair recognition,[218-225] as further illustrated in the previous chapter. Beer and co-workers have reported various interlocked structures capable of binding sodium salts including a neutral [2]catenane synthesised using a chloride templated strategy (Figure 3.3).[257] Solid-state X-ray structural analysis of the serendipitously isolated NaCl salt revealed the metal cation is coordinated to the pyridine nitrogen of one macrocycle in concert with the polyether oxygens of the other macrocycle.

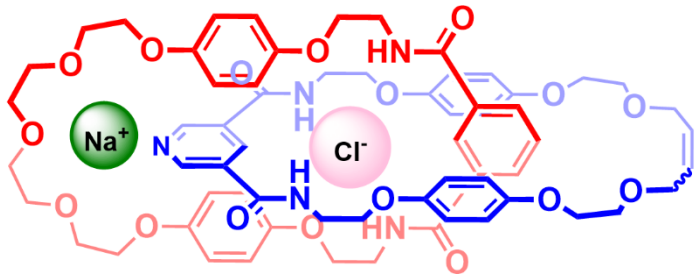


Figure 3.3. *Beer's NaCl binding [2]catenane receptor.*[257]

More recently, Beer and co-workers reported a series of XB functionalised [2]rotaxane systems prepared using an alkali metal template directed approach.[181] Quantitative ^{1}H NMR ion-pair recognition studies highlighted an impressive mechanical bond induced cooperative enhancement of halide anion binding affinities (*ca.* 8-10 fold enhancement for NaI and KI ion-pairs) in 1:1 $CD_3CN/CDCl_3$ solvent media(Figure 3.4).[258] Notably, the determined apparent ion-pair association constant values were of greater magnitude than those of previously studied XB heteroditopic [2]catenane analogues.[225] This was ascribed to the greater co-conformational flexibility afforded by the rotaxane receptors over 'mechanical bond isomeric' catenane structures.

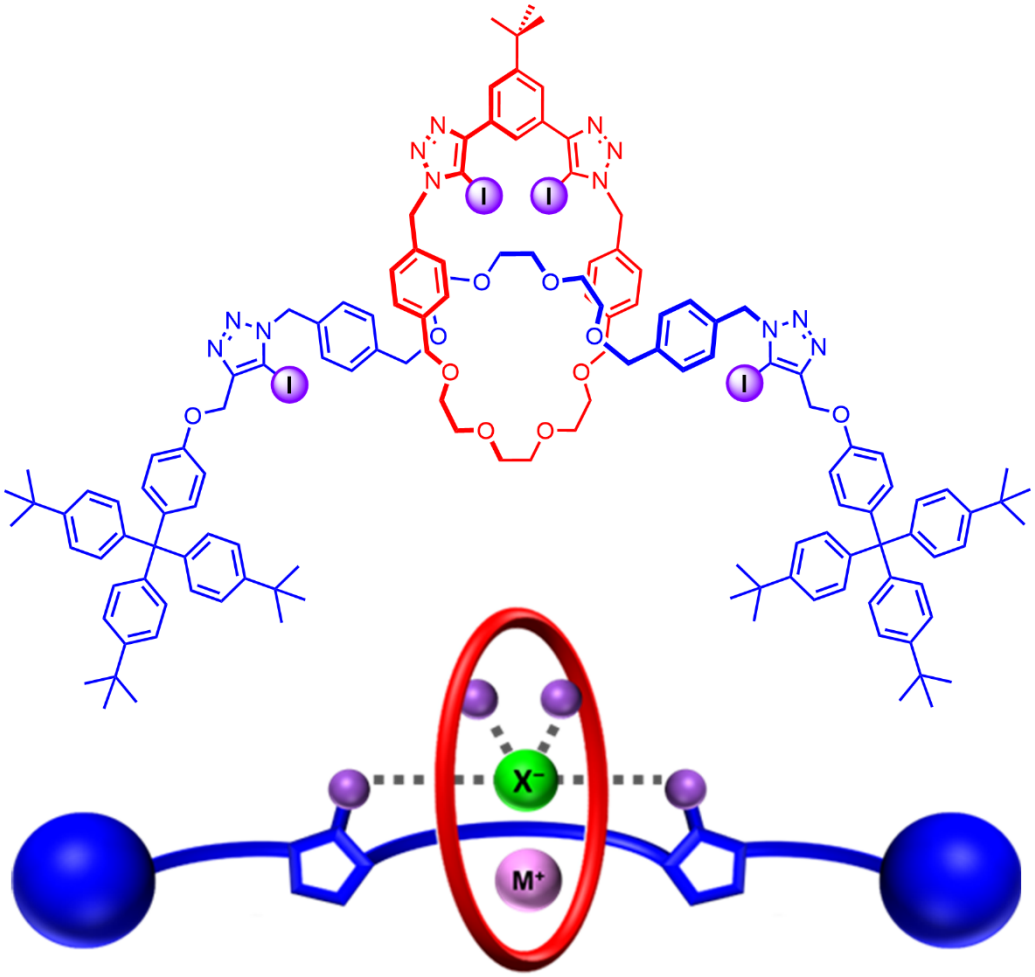


Figure 3.4. *Beer's heteroditopic [2]rotaxanes capable of alkali metal halide recognition.*[258]

3.2 Chapter objectives

As discussed in Chapter 2, despite their well-known anion recognition potency, the integration of the squaramide motif into mechanically interlocked molecules still remains scarce, with only a few examples documented.[226,227]

Building on the promising results of Chapter 2, detailing a series of heteroditopic squaramide-based interlocked structures capable of lithium halide salt recognition and extraction, the work described in this chapter seeks to design a series of squaramide-containing [2]rotaxanes for the purpose of sodium halide ion-pair recognition. Notably, this

chapter describes the further exploitation of the squaramide carbonyls in an unprecedented sodium cation alkali metal template-directed strategy to construct MIMs for sodium halide ion-pair recognition and extraction.

3.3 Synthesis and characterisation

3.3.1 Pseudo-rotaxane studies

Drawing inspiration from Chui's alkali metal template directed approach for MIM synthesis,[181] heteroditopic squaramide containing [2]rotaxanes were prepared using an unprecedented sodium cation template-directed coordination of a squaramide axle precursor-macrocycle polyether pseudo[2]rotaxane assembly, which subsequently underwent double stoppering to afford the target [2]rotaxanes (Figure 3.5).

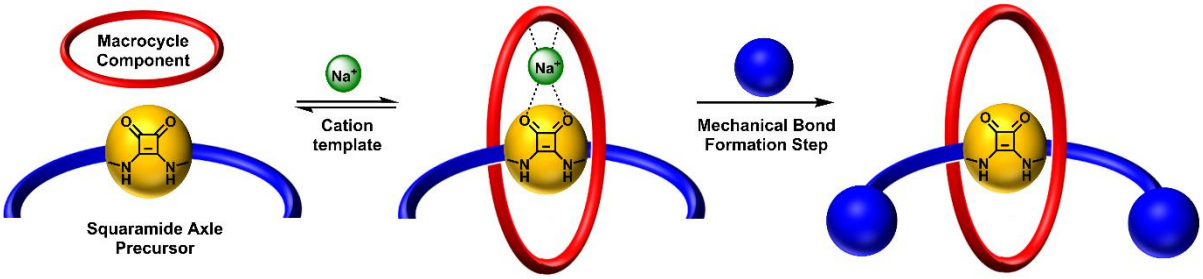
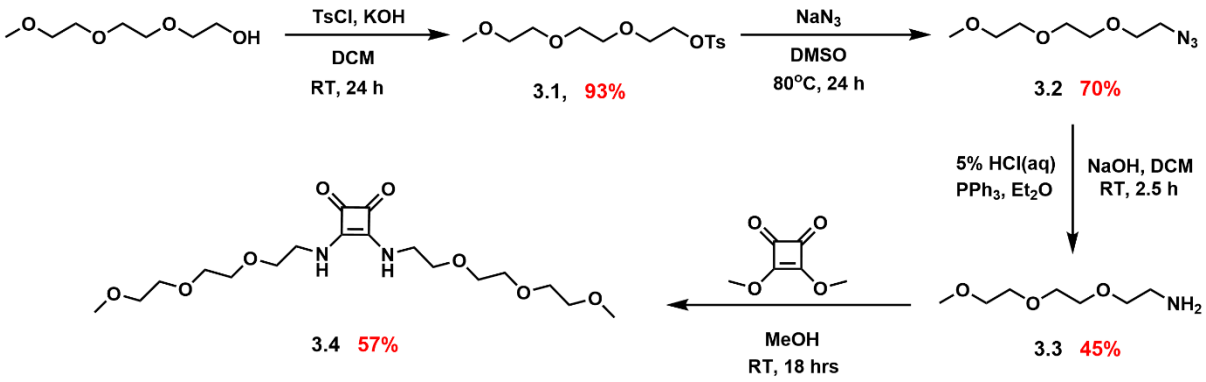


***Figure 3.5**. Schematic showing synthesis of the squaramide-based [2]rotaxane host systems.*

To this end, preliminary ^{1}H NMR pseudo[2]rotaxane assembly investigations were initially undertaken with the simple ethylene glycol-furnished squaramide axle precursor **3.4** (Scheme 3.1). It's synthesis began with the preparation of the tosylated precursor **3.1** which subsequently underwent azidation in DMF to form the mono-azide **3.2** in 70% yield. Staudinger reduction of **3.2** with triphenylphosphine in the presence of 5% HCl in diethyl ether thereafter gave the amine precursor **3.3** in 45% yield. Condensation of **3.3** with methyl-

squarate ester in methanol at room temperature for 18 hours afforded the target axle precursor **3.4** in 57% yield.



Scheme 3.1. *Synthesis of synthon* ***3.4***

Three potentially suitable macrocycles containing either crown ether-like arrangements of oxygen donor atoms as in **3.5**,[259] or mixed polyether and pyridyl isophthalamide cyclic linkages in **3.6**[260] and **3.7**[261] respectively were prepared using previously reported multi-step literature procedures (Figure 3.6).

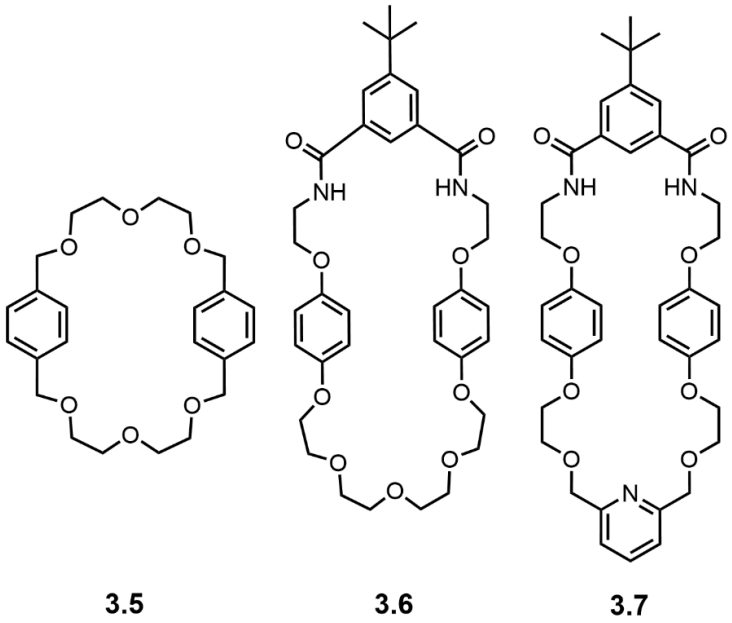


Figure 3.6. *Macrocycles chosen for the pseudo-rotaxane studies.*

Thereafter, quantitative ^{1}H NMR pseudo[2]rotaxane titration investigations were carried out to determine the stability and association affinities of sodium-cation template

mediated interpenetrative pseudo[2]rotaxane assemblies between squaramide axle precursor **3.4** and macrocycles, **3.5**, **3.6** and **3.7**. Accordingly, aliquots of **3.4** were gradually added to a 2mM solution of the respective macrocycle in the absence and presence of one equivalent of $NaBAr^F_4$ in $CDCl_3$. Representative ^1H NMR titration spectra are shown for macrocycle **3.7** (Figures 3.7 and 3.8, in the absence and presence of $NaBAr^F_4$ respectively). Upon successive additions of **3.4** to the sodium-complexed macrocycles, significant shifts in the aromatic protons of the macrocycle and the axle methylene protons were observed, indicative of pseudo-rotaxane formation. By contrast, **3.4** addition in the absence of a sodium cation template resulted in considerably smaller perturbations in the proton signals, suggesting much weaker association of the MIM precursor components. This was confirmed by quantitative Bindfit[237] analysis of the respective binding isotherms to determine the 1:1 stoichiometric host-guest association constants shown in Table 3.1.

Assessment of the binding data in Table 3.1 revealed that in the presence of sodium, crown-ether like macrocycle **3.5** demonstrated a modest association with the axle precursor. Meanwhile, isophthalamide-containing macrocycles **3.6** and **3.7** exhibited markedly larger K_a values of 1278 M^{-1} and 1849 M^{-1} respectively. Notably, in the absence of sodium, no ^1H NMR evidence of interpenetration was observed for macrocycle **3.5** and only weak K_a values (< 50 M^{-1}) were recorded for macrocycles **3.6** and **3.7** which may be attributed to HB interactions

Table 3.1: *Apparent association constants K_a (M^{-1}) of macrocycles **3.5**, **3.6** and **3.7** with **3.4** in absence or presence of one equiv. of $NaBAr^F_4$ in 7:3$CDCl_3$/CD_3CN at 298K.[a]*

Anion	Template	Mac. **3.5**	Mac. **3.6**	Mac. **3.7**
	-[b]	-[c]	36	16
SQ thread 3.4	$NaBAr^F_4$	189	1278 (14)	1849 (21)

[a] K_a values calculated using Bindfit[237] software using a 1:1 host-guest binding model. Error percentages less than 10% unless specified. Global fit performed for all systems. [b] No template. [c] No binding.

between the Lewis basic squaramide carbonyls and the macrocyclic isophthalamide HB donors.

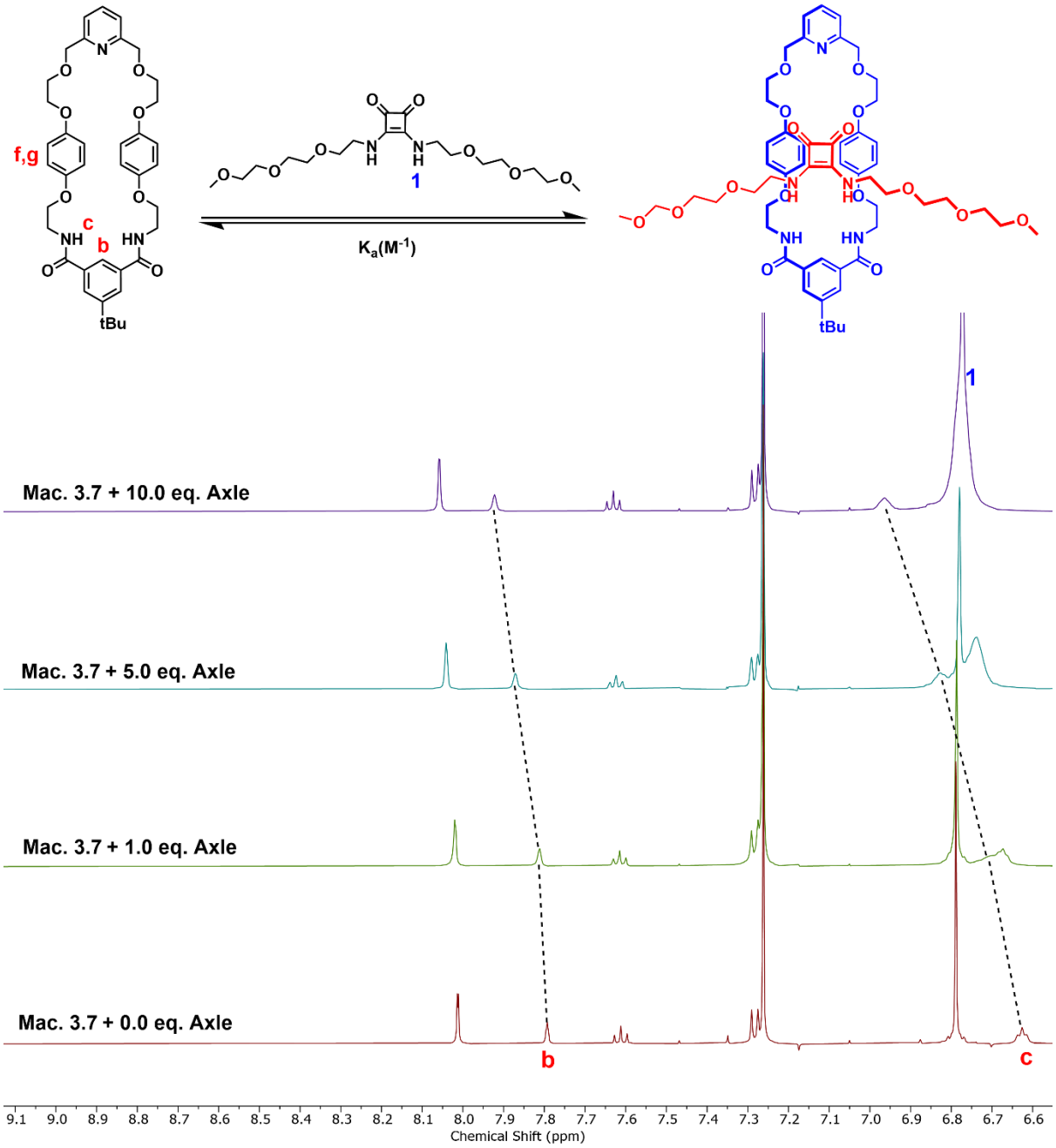


Figure 3.7. *Truncated ^1H NMR titration spectra of macrocycle* ***3.7*** *upon addition of 1, 5 and 10 equivalents of axle precursor* ***3.4*** *(500 MHz, 298 K, 7:3 $CDCl_3/CD_3CN$, [Receptor] = 2.0 mM).*

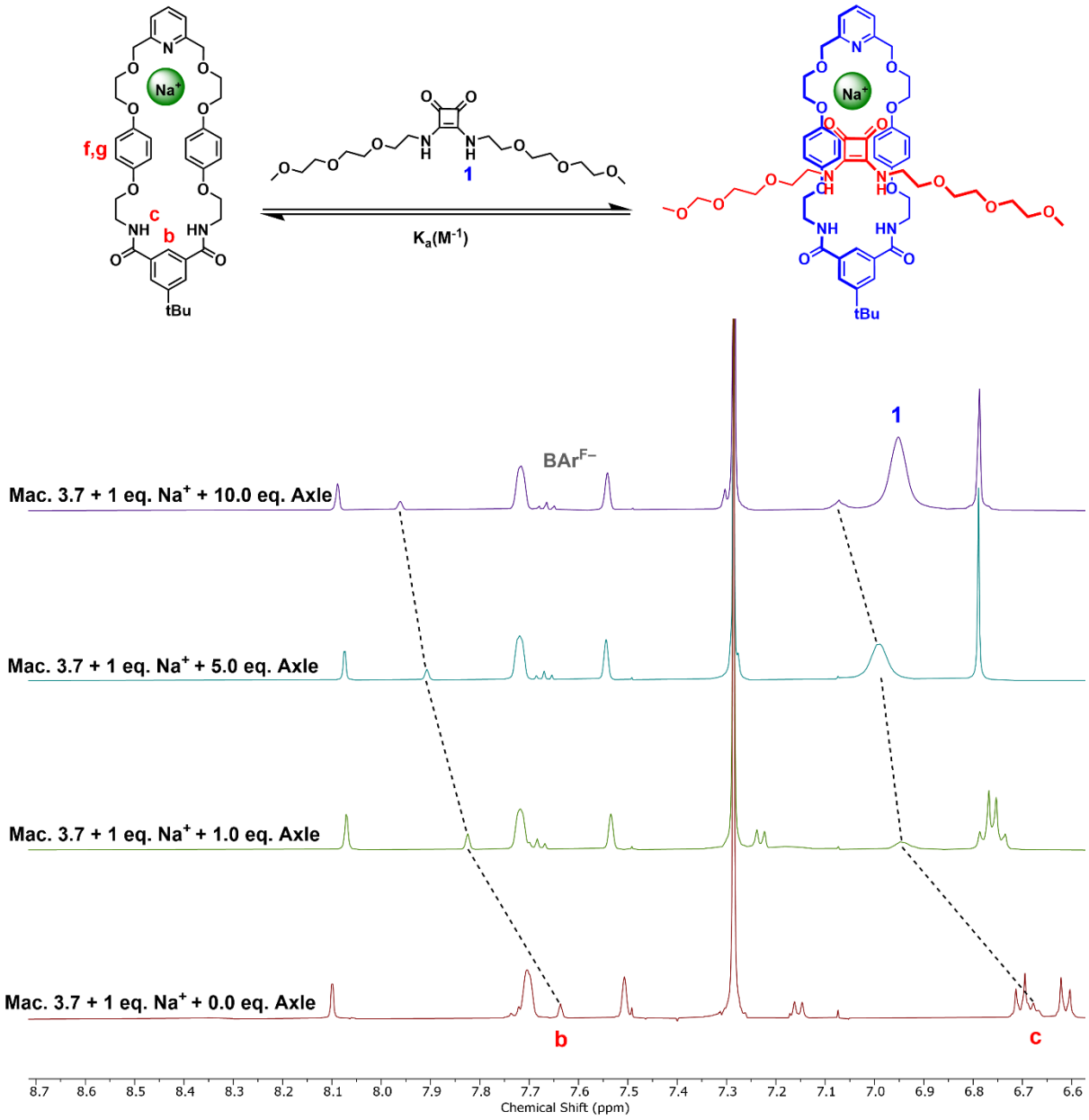
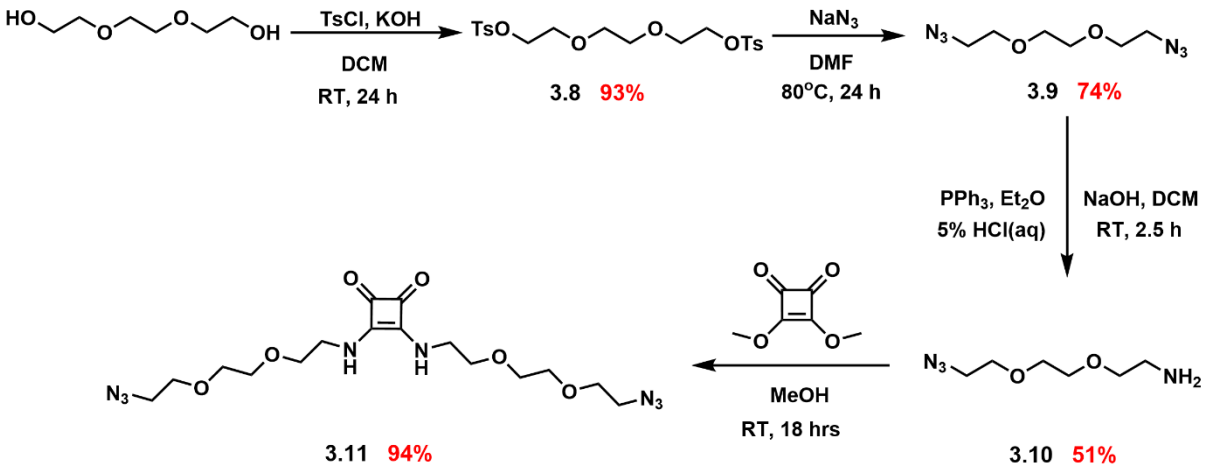


Figure 3.8. *Truncated ^{1}H NMR titration spectra of macrocycle **3.7** upon addition of 1, 5 and 10 equivalents of the axle precursor **3.4** in the presence of 1 equivalent of $NaBAr^{F}{}_{4}$ (500 MHz, 298 K, 7:3 $CDCl_3/CD_3CN$, [Receptor] = 2.0 mM).*

3.3.2 Synthesis of acyclic squaramide-based bis-azide precursor

Having established confirmation of pseudo[2]rotaxane formation upon sodium template complexation, the synthesis of the target [2]rotaxanes was envisaged using a Cu(I) catalysed alkyne-azide cycloaddition-mediated double stoppering strategy. Accordingly, a suitable squaramide-based bis-azide axle precursor, **3.11** was prepared wherein commercially

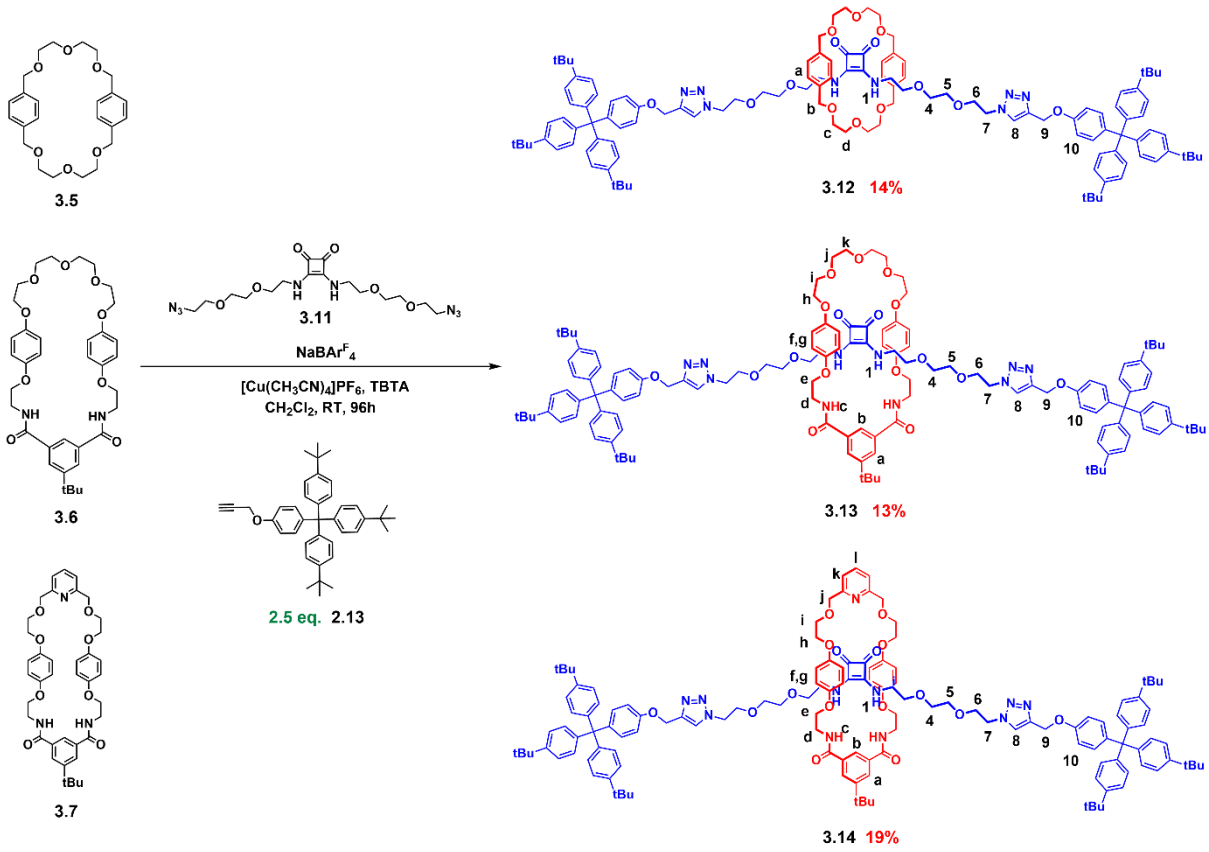
available triethylene glycol first underwent tosylation followed by azidation to give the bis-azide **3.9** in 74% yield (Scheme 3.2). Monoreduction of **3.9** with triphenylphosphine in the presence of 5% HCl in diethyl ether gave the amine precursor **3.10** in 51% yield. Condensation of **3.10** with methyl-squarate ester in methanol at RT for 18 hours thereafter afforded the axle precursor **3.11** in 94% yield.



Scheme 3.2. *Synthesis of synthon* ***3.11***

3.3.3 Synthesis of the target [2]rotaxanes

In a typical reaction, macrocycles **3.5**, **3.6** and **3.7** and bis-azide **3.11** were first pre-complexed with one equivalent of $NaBAr^F_4$ in dichloromethane for 30 minutes to form the pseudo[2]rotaxane assembly (Scheme 3.3). A dichloromethane solution of 2.5 equivalents of terphenyl stopper alkyne **2.13,** catalytic amounts of $Cu[(CH_3CN)_4]PF_6$ and the rate accelerating agent TBTA were then added, following which the reaction mixture was left stirring for 96 hours at room temperature under an inert atmosphere. After an aqueous work-up with basic EDTA/NH_4OH and purification using preparative TLC, the target [2]rotaxanes **3.12**, **3.13** and **3.14** were isolated in 14, 13 and 19% yields respectively. All three novel rotaxanes were characterised by ^1H NMR, ^{13}C NMR and ESI-HRMS.



Scheme 3.3. *Synthesis of heteroditopic [2]rotaxanes* ***3.12-3.14****.*

Evidence of the successful formation of the target [2]rotaxanes was observed by comparison of their ^{1}H NMR spectra with the spectra of their respective macrocycle and axle components (Figures 3.9, 3.10 and 3.11). For all rotaxane systems, diagnostic upfield shifts of the macrocycle aromatic protons were indicative of mechanical bond formation. These shifts were attributed to donor-acceptor interactions between the electron-rich aromatic units in the macrocycle and electron-deficient squaramide axle component. Furthermore, downfield perturbations in the macrocycle component chemical shifts corresponding to the internal cavity protons namely H_b and H_c in [2]rotaxanes **3.13** and **3.14** were seen, alluding to possible intercomponent HB interactions between macrocycle amide HB donors and the Lewis basic squaramide carbonyls as a result of interlocked structure synthesis.

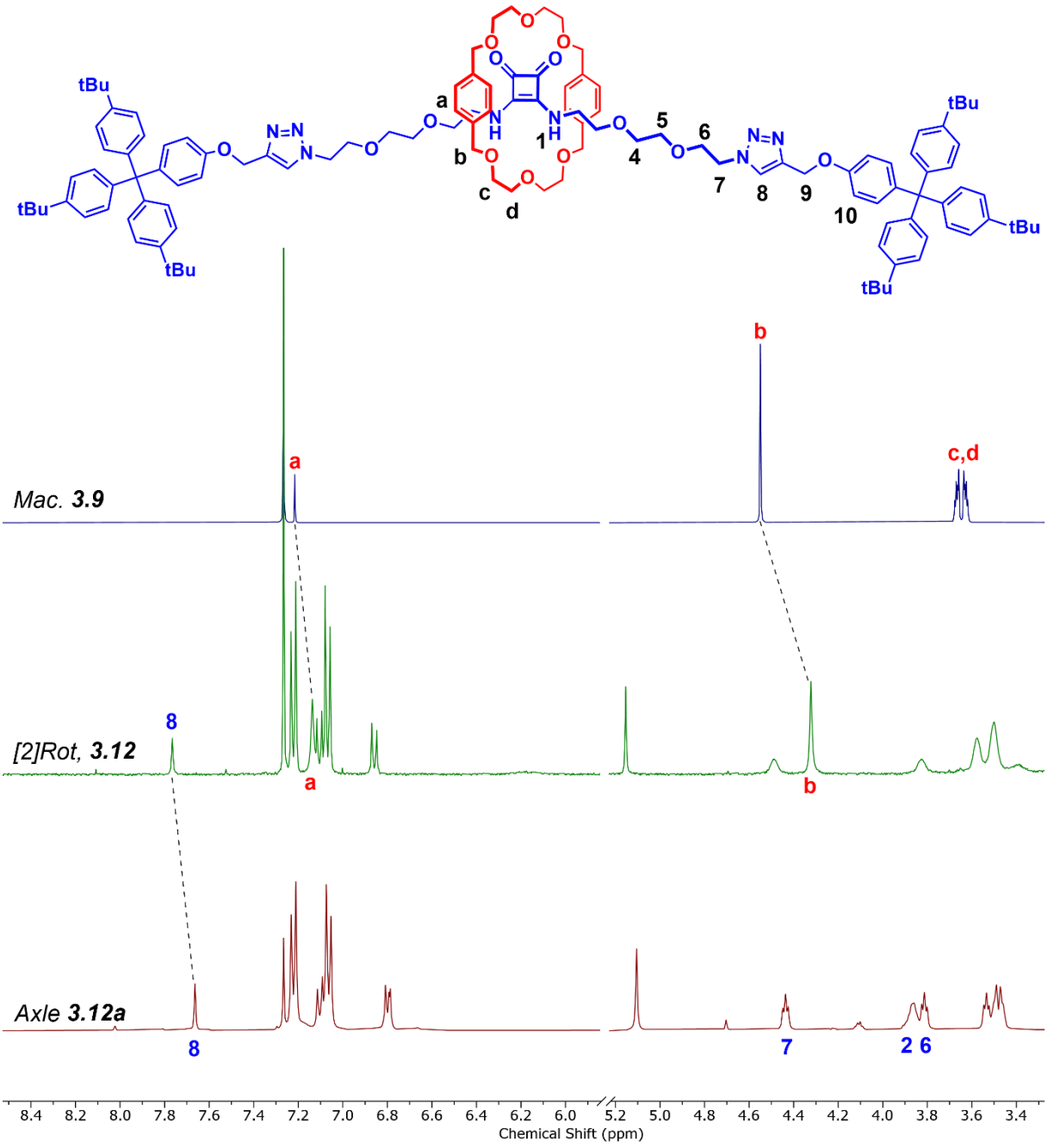


Figure 3.9. *Truncated stacked ^{1}H NMR spectra of i) macrocycle **3.5** ii) [2]rotaxane **3.12** and iii) axle component **3.12a** ($CDCl_3$, 500 MHz, 298K).*

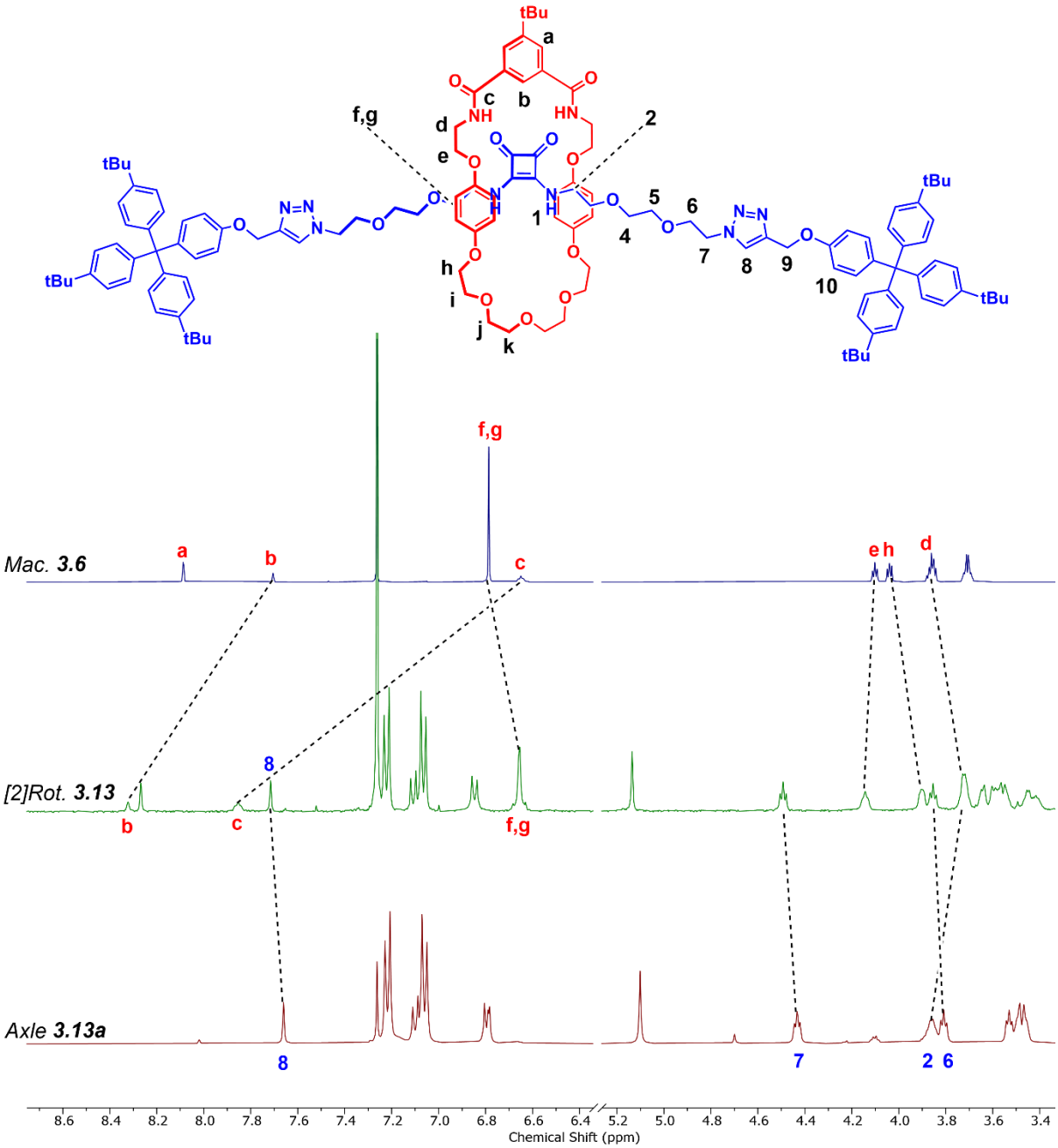


Figure 3.10. *Truncated stacked ^{1}H NMR spectra of i) macrocycle **3.6** ii) [2]rotaxane **3.13** and iii) axle component **3.13a** ($CDCl_3$, 500 MHz, 298K).*

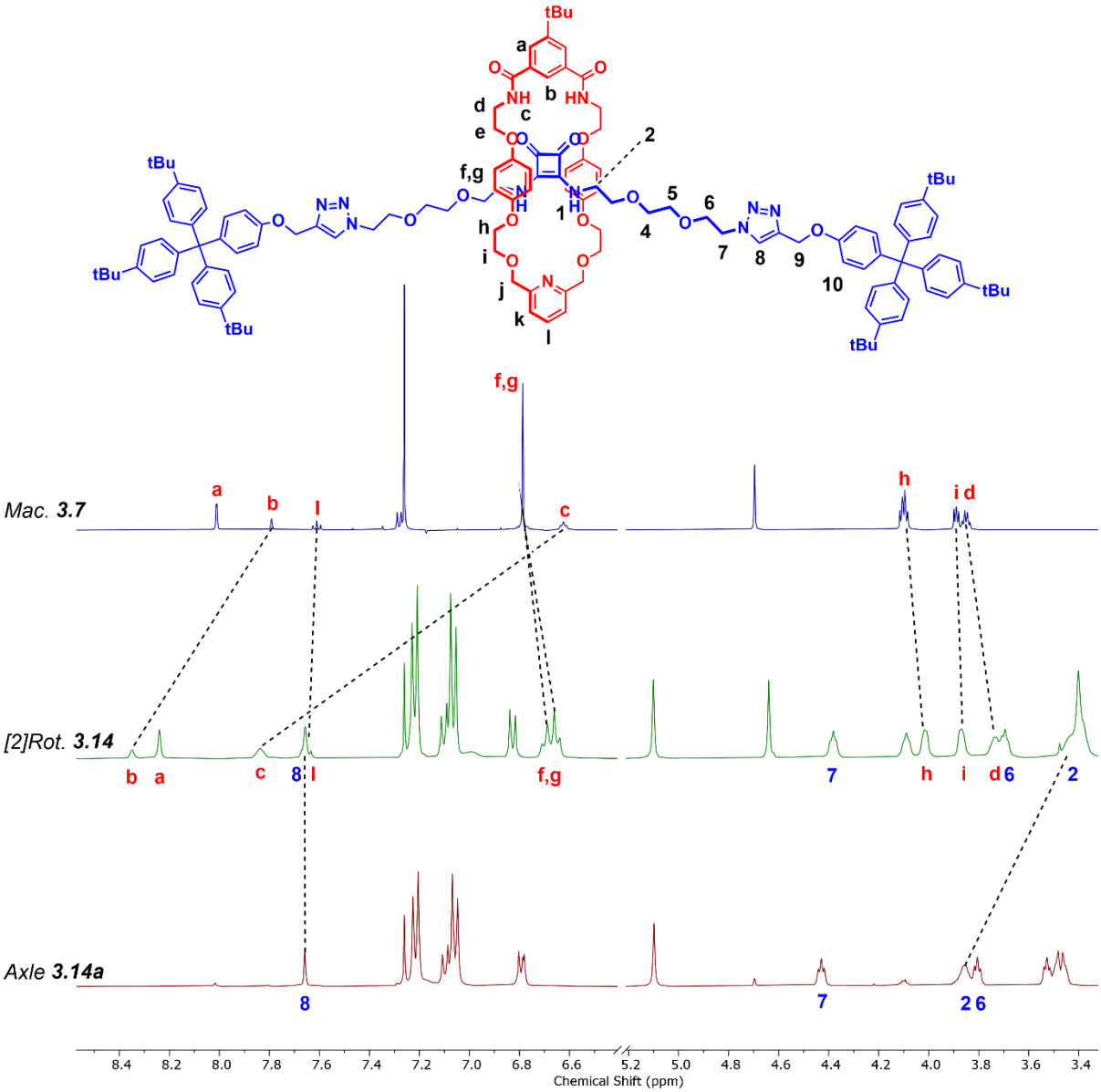


Figure 3.11. *Truncated stacked ^{1}H NMR spectra of i) macrocycle **3.7** ii) [2]rotaxane **3.14** and iii) axle component **3.14a** ($CDCl_3$, 500 MHz, 298K).*

In order to further elucidate these inter-component HB interactions, and any impact this may have on the rotaxane's co-conformational dynamism, ^{1}H-^{1}H ROESY NMR studies in $CDCl_3$ were carried out on [2]rotaxanes **3.13** and **3.14**. A representative example is shown for rotaxane **3.14** which revealed through space coupling interactions between the axle squaramide NH protons and the macrocycle protons namely H_b, H_h, H_i and H_j (Figure 3.12). Meanwhile, no interactions were observed between the axle triazole protons and the protons of the macrocycle, suggesting that the macrocycle resides at the squaramide centre of the

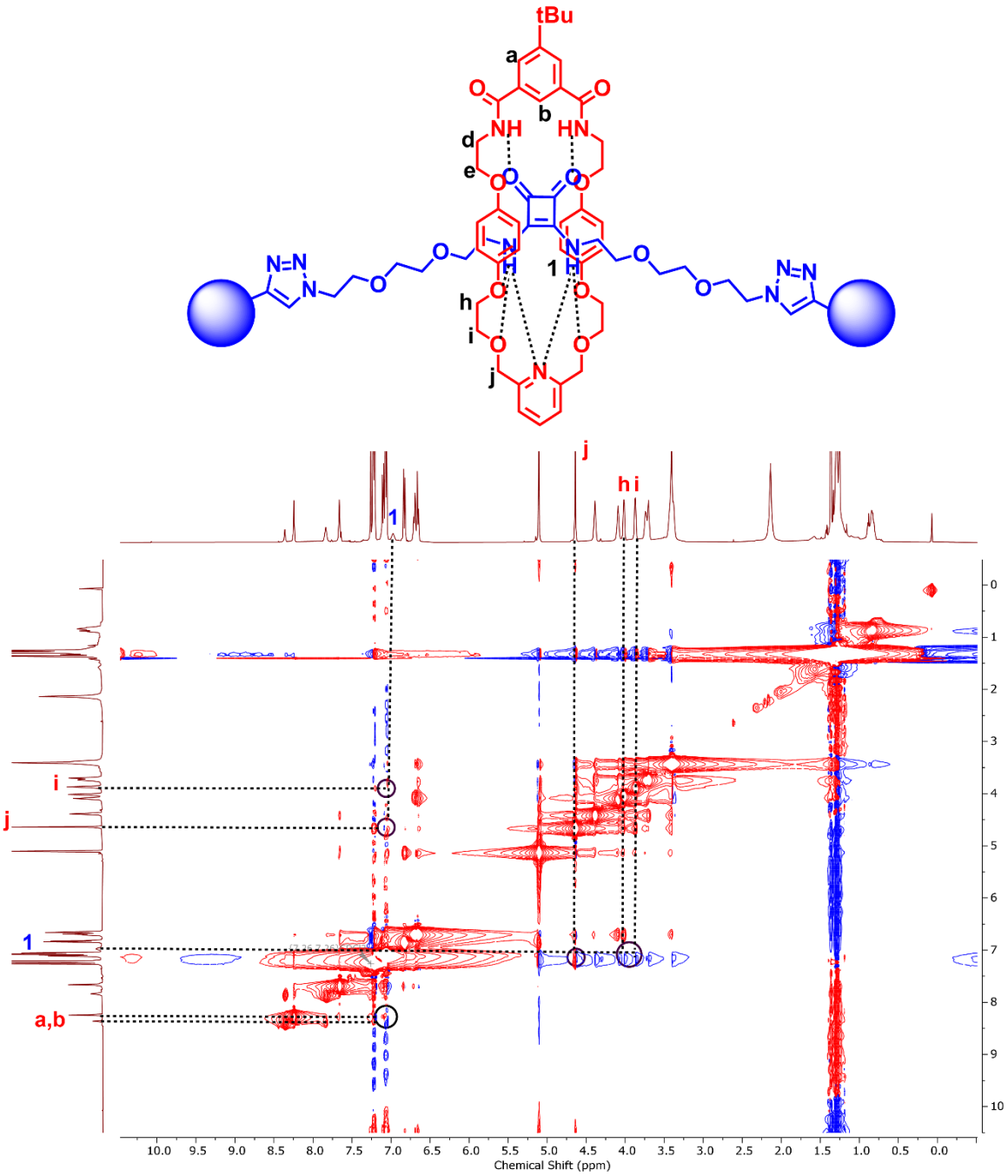


Figure 3.12. *Possible co-conformation of [2]rotaxane* ***3.14*** *as conferred by the attached truncated* ^{1}H-^{1}H *ROESY NMR spectrum in* $CDCl_3$.

axle, presumably due to favourable intercomponent HB interactions between the axle-squaramide HB NH donors and polyether or pyridyl linking groups of the macrocycles.

Furthermore, to confirm the of crucial templating role played by the sodium cation in achieving MIM formation, the synthesis of [2]rotaxane **3.13** was repeated in the absence of a sodium template, wherein no evidence of the interlocked product was observed. This was

attributed to the noted weak intercomponent association affinities observed in the absence of a sodium template (Table 3.1), consistent with the pseudo-rotaxane experimental results observed in section 3.3.1.

3.4 Host-guest recognition studies

3.4.1 Quantitative ^{1}H NMR halide binding titration studies

Following the synthesis of the [2]rotaxanes, investigation of their halide anion binding properties was undertaken *via* quantitative ^{1}H NMR titration studies in 3:7 $CD_3CN/CDCl_3$ solvent media.

In the case of [2]rotaxane **3.12**, the addition of TBA chloride and bromide led to significant downfield shifts of the axle squaramide protons H_1 and upfield shifts of the macrocycle xylene protons H_a, indicating anion binding within the interlocked cavity of the [2]rotaxane (Figure 3.13). By contrast, upon titration with TBAI no evidence of iodide binding was seen. On the other hand, the addition of halides to [2]rotaxanes **3.13** and **3.14** induced downfield shifts in the macrocycle amide protons H_c and internal benzene proton H_b, suggesting anion recognition within the amide binding cleft of the [2]rotaxanes (Figures 3.14 and 3.15). Interestingly, in the case of all rotaxanes, negligible perturbations in the axle triazole protons H_8 suggested it did not partake in anion binding. Bindfit[237] analysis of the generated titration isotherms using a 1:1 host-guest stochiometric binding model gave anion binding constants shown in Table 3.2.

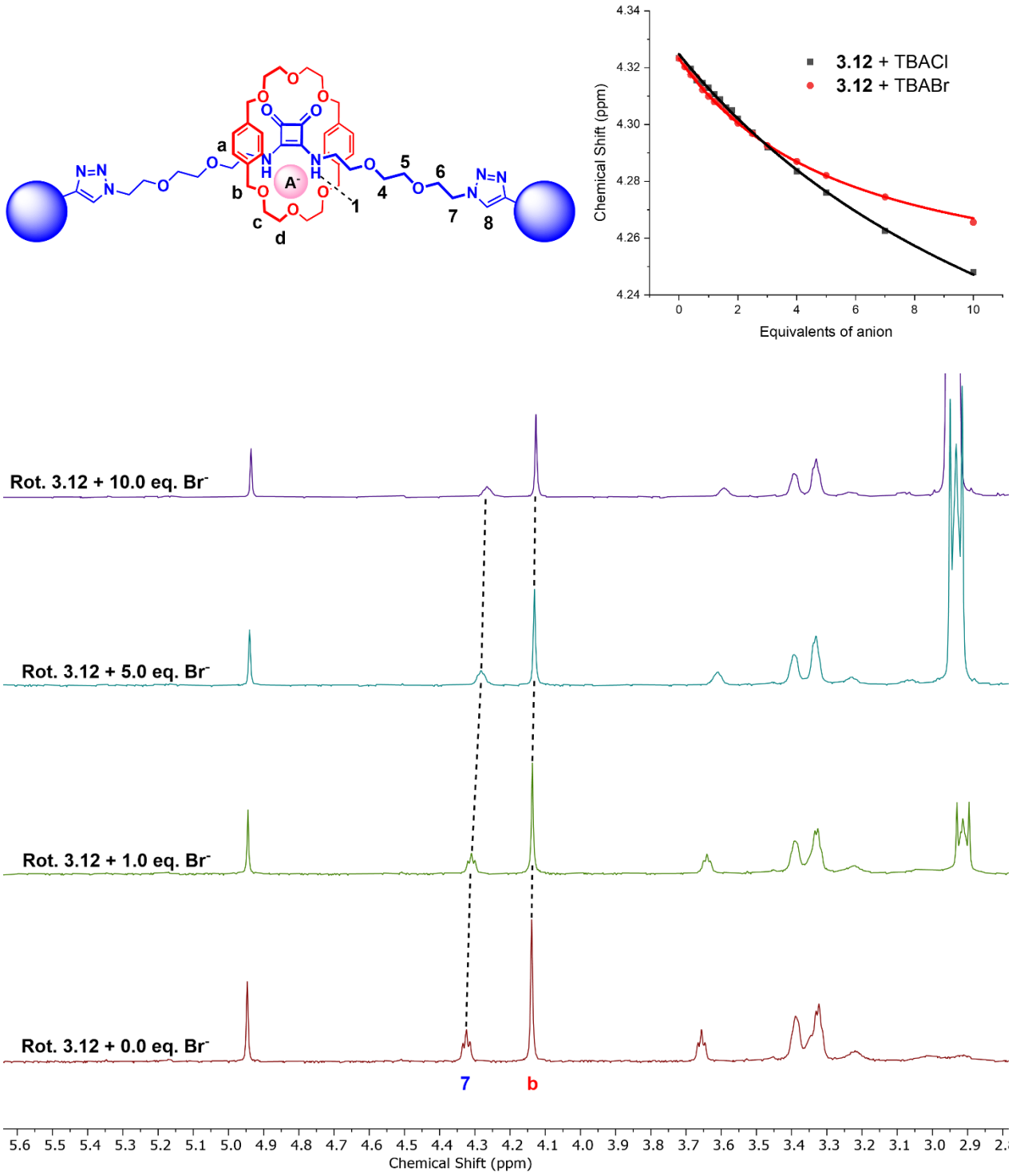


Figure 3.13. *^{1}H NMR spectra of [2]rotaxane **3.12** upon addition of 1, 5 and 10 equivalents of TBABr (500 MHz, 298 K, 7:3 $CDCl_3/CD_3CN$). Inset: Binding isotherms showing changes in chemical shift of squaramide proton b upon increasing equivalents of halide anions.*

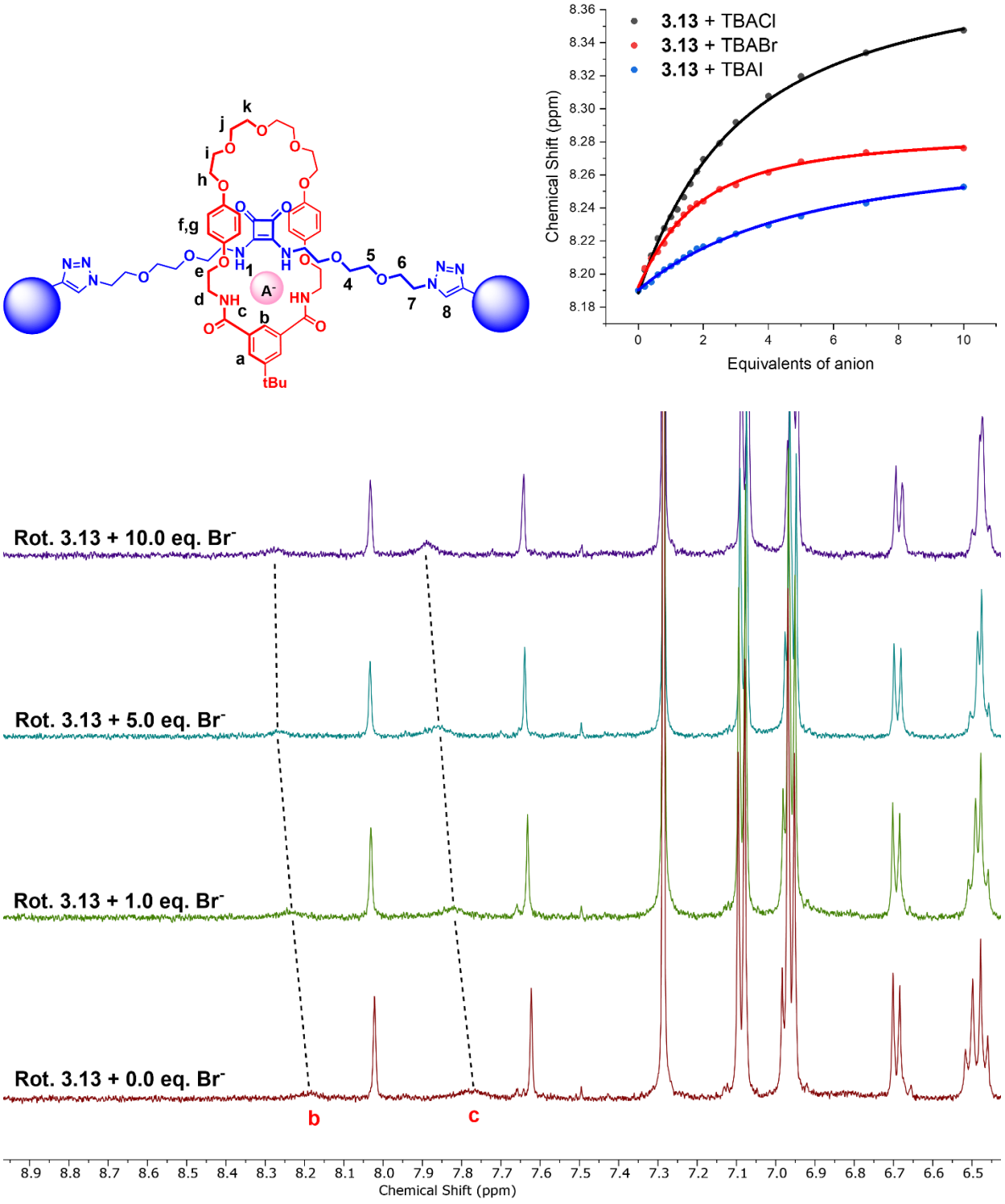


Figure 3.14. *^{1}H NMR spectra of [2]rotaxane **3.13** upon addition of 1, 5 and 10 equivalents of TBABr (500 MHz, 298 K, 7:3 $CDCl_3/CD_3CN$). Inset: Binding isotherms showing changes in chemical shift of internal benzene proton b upon increasing equivalents of halide anions.*

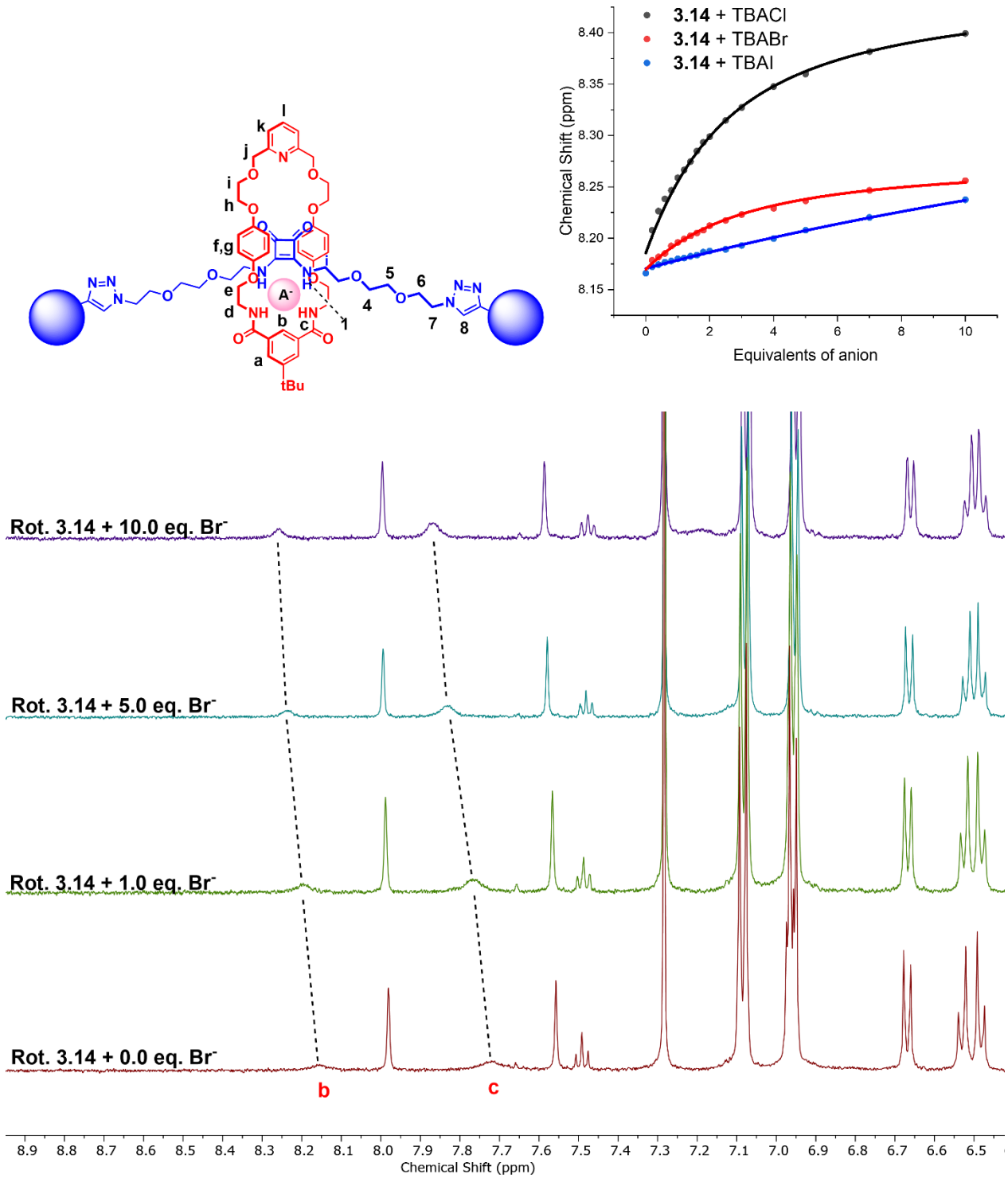


Figure 3.15. *^{1}H NMR spectra of [2]rotaxane **3.14** upon addition of 1, 5 and 10 equivalents of TBABr (500 MHz, 298 K, 7:3 $CDCl_3/CD_3CN$). Inset: Binding isotherms showing changes in chemical shift of internal benzene proton b upon increasing equivalents of halide anions.*

Table 3.2: *Halide anion association constants K_a (M^{-1}) for [2]rotaxanes **3.12**, **3.13** and **3.14** [1.0 mM] in 3:7 $CD_3CN/CDCl_3$ at 298 K.*[a]

Anion	[2]Rot. **3.12**	[2]Rot. **3.13**	[2]Rot. **3.14**
Cl^-	163	476	543
Br^-	204	580	494
I^-	-[b]	154	67

[a] K_a values calculated using Bindfit[237] software using a 1:1 host-guest binding model. All anions added as their TBA salts. Error percentages less than 10% unless specified. Global fit performed for all systems. [b] No binding.

Notably, while [2]rotaxanes **3.12** and **3.13** displayed a preference for bromide, [2]rotaxane **3.14** showcased a preference for chloride, attributable to MIM host-halide guest size-complementarity. As expected, the anion binding affinities of [2]rotaxane **3.12** were lower in comparison to rotaxanes **3.13** and **3.14**, accredited to the lack of additional HB NH donors in the macrocycle component of rotaxane **3.12**.

3.4.2 Quantitative ^{1}H NMR sodium cation binding titration studies

The sodium cation binding affinities of the [2]rotaxanes were next investigated by conducting ^{1}H NMR titration experiments involving the gradual addition of $NaBAr^F{}_4$ to a 1mM solution of each rotaxane in 3:7 $CD_3CN/CDCl_3$ solvent mixture. For all receptors, increasing sodium cation concentration induced perturbations in the resonances corresponding to the ethylene glycol protons in the axle and the macrocycle indicating the concerted participation of both axle and macrocycle polyether oxygens in cation binding (Figures 3.16, 3.17 and 3.18). Additionally, in the case of rotaxane **3.14**, the proton resonances of the macrocycle pyridyl group experienced significant perturbations. Also of note were the upfield shifts of the internal benzene proton H_b and amide protons H_c of the respective rotaxane macrocycle components of rotaxanes **3.13** and **3.14**. This behaviour was ascribed to the possible disruption of the intercomponent

HB interactions between the macrocycle HB donors and the axle squaramide carbonyls upon cation association.

Further evidence of the hypothesised cation binding mode was achieved through qualitative ^{13}C NMR titration studies in $CDCl_3$ which revealed that the addition of an equivalent of $NaBAr^F_4$ to [2]rotaxane **3.14** caused characteristic axle squaramide carbonyl peaks at 183 ppm and 168 ppm to shift upfield, indicative of their assistance in cation binding (Figure 3.19). Importantly, this suggested that the addition of a sodium cation elicited the preorganisation of the anion binding cavity such that all amide donors are arranged to concomitantly bind guest anions. Monitoring the perturbations of the chemical resonances proximal to the cation binding site by Bindfit[237] analysis determined 1:1 stoichiometric rotaxane host-sodium cation guest binding constants summarised in Table 3.3.

Table 3.3: *Cation association constants K_a (M^{-1}) for [2]rotaxanes **3.12**, **3.13** and **3.14** [1.0 mM] in 3:7 $CD_3CN/CDCl_3$ at 298 K.[a]*

Cation	[2]Rot. **3.12**	[2]Rot. **3.13**	[2]Rot. **3.14**
Na^+	$>10^4$	1193	1506

[a] K_a values calculated using Bindfit[237] software using a 1:1 host-guest binding model. Sodium cation added as $NaBAr^F_4$. Error percentages less than 10% unless specified. Global fit performed for all systems.

Inspection of the binding data revealed that sodium binding to [2]rotaxane **3.12** was too strong to be quantified, likely due to a more complementary size-fit between the smaller interlocked binding cavity in the rotaxane and sodium cation, a trend previously witnessed with the rotaxane's macrocycle.[262] Notably, the incorporation of a pyridyl dimethoxy motif in the macrocycle component of [2]rotaxane **3.14** resulted in an increase in its sodium binding affinity in comparison to the polyether containing macrocycle analogue in rotaxane **3.13**.

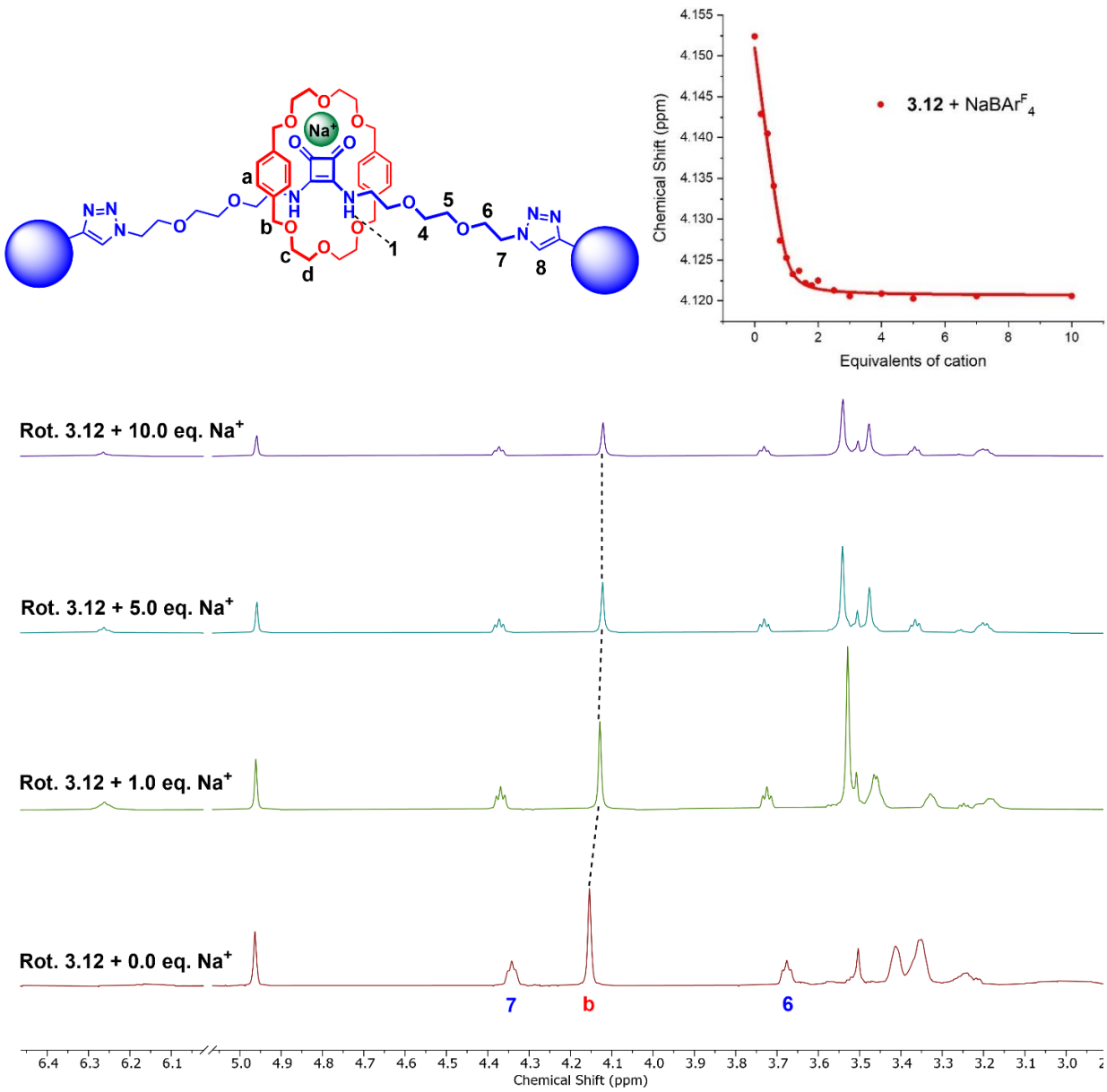


Figure 3.16. *^{1}H NMR spectra of [2]rotaxane **3.12** upon addition of 1, 5 and 10 equivalents of $NaBAr^F_4$ (500 MHz, 298 K, 7:3 $CDCl_3/CD_3CN$). Inset: Binding isotherms showing changes in chemical shift of macrocycle proton b upon increasing equivalents of halide anions.*

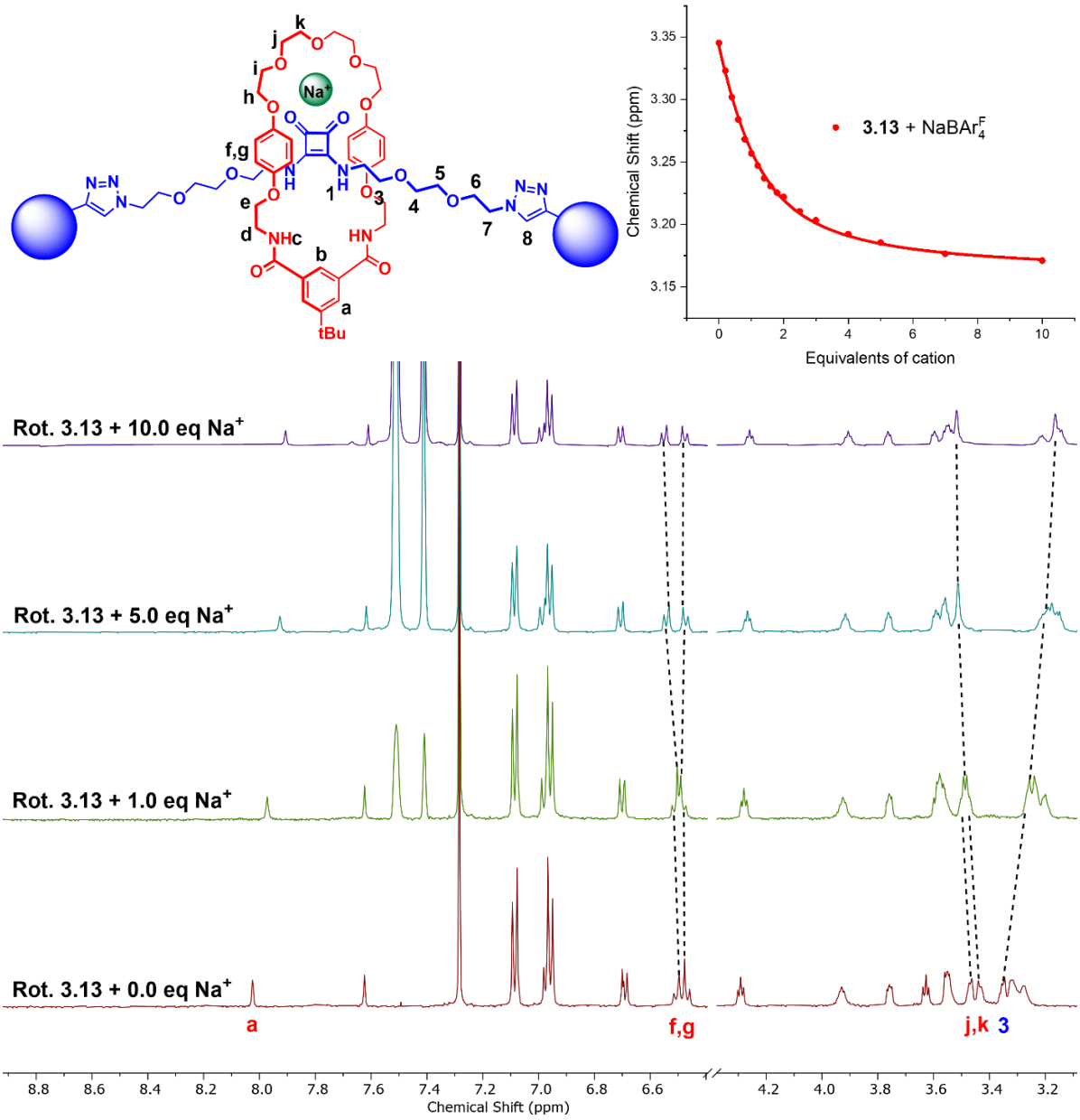


Figure 3.17. *^{1}H NMR spectra of [2]rotaxane **3.13** upon addition of 1, 5 and 10 equivalents of NaBAr$^F_4$ (500 MHz, 298 K, 7:3 $CDCl_3$/CD_3CN). Inset: Binding isotherms showing changes in chemical shift of axle proton 3 upon increasing equivalents of halide anions.*

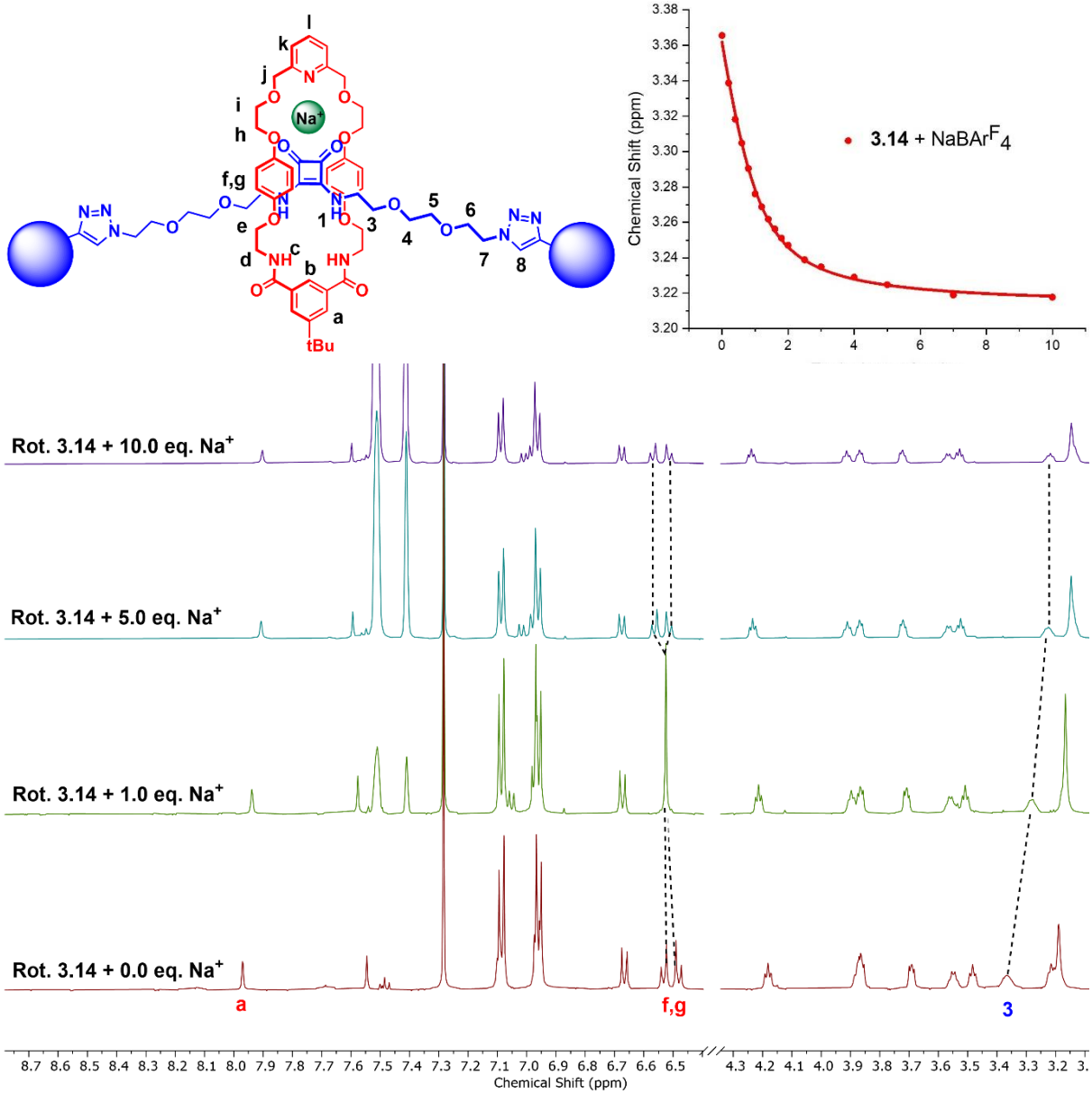


Figure 3.18. *^{1}H NMR spectra of [2]rotaxane **3.14** upon addition of 1, 5 and 10 equivalents of $NaBAr^{F}_{4}$ (500 MHz, 298 K, 7:3 $CDCl_3/CD_3CN$). Inset: Binding isotherms showing changes in chemical shift of axle proton 3 upon increasing equivalents of halide anions.*

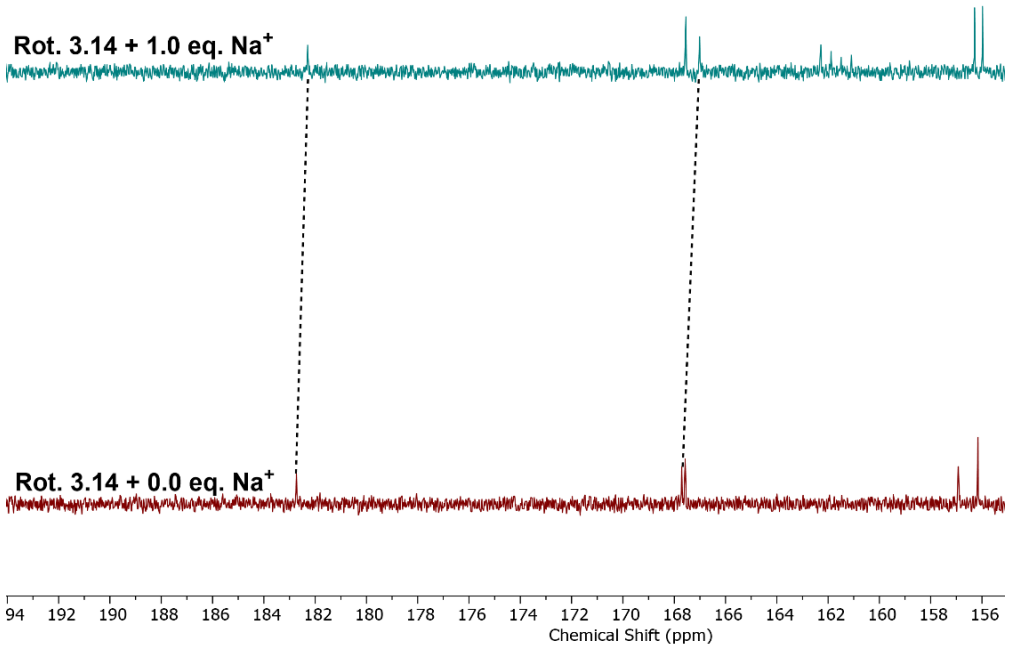


Figure 3.19. *^{13}C NMR spectra of [2]rotaxane **3.14** upon addition of 1 equivalent of $NaBAr^F_4$ (500 MHz, 298 K, 7:3 $CDCl_3/CD_3CN$).*

3.4.3 Quantitative ^{1}H NMR ion-pair binding titration studies

Having established the capabilities of the rotaxane receptors to bind individual halide anions and sodium cation, efforts were directed towards investigating their ion-pair binding properties. In a typical ^{1}H NMR titration experiment, aliquots of TBA halides were sequentially added to a 1mM solution of each rotaxane pre-complexed with an equivalent of $NaBAr^F_4$.

Addition of bromide and iodide salts to the pre-complexed [2]rotaxane hosts **3.13** and **3.14** evoked significant downfield perturbations of the proton resonances in the anion binding cavity, namely the internal benzene proton H_b and amide protons H_c, (Figures 3.21 and 3.22). Alternatively for [2]rotaxane **3.13,** chemical shift perturbations of the squaramide proton H_1 were followed to generate the titration binding isotherms (Figure 3.20), which became non-visible in the case of the other rotaxanes presumably due to hydrogen bonding mediated broadening. For all three systems, perturbations were also noted in the protons

proximal to the cation binding regions of the rotaxanes indicative of cooperative enhancement of cation binding upon anion association. Bindfit[237] analysis of the titration isotherm data confirmed a 1:1 host-guest anion binding stoichiometry and enabled calculation of apparent association constants (Table 3.4).

Table 3.4: *Apparent association constants K_a (M^{-1}) for [2]rotaxanes* ***3.12-3.14*** *[1.0 mM] in the presence of 1 equiv. $NaBAr^F_4$ in 3:7 $CD_3CN/CDCl_3$ at 298 K.[a]*

Host	Cation	% cation bound	Anion	K_a (M^{-1})
[2]Rot. **3.12**	Na^+ (1 eq.)	>75%	Cl^-	-[b]
			Br^-	1307
			I^-	367
[2]Rot. **3.13**	Na^+ (1 eq.)	41%	Cl^-	-[b]
			Br^-	$>10^4$
			I^-	1476
[2]Rot. **3.14**	Na^+ (1 eq.)	45%	Cl^-	646
			Br^-	$>10^4$
			I^-	1298

[a] K_a values calculated using Bindfit[237] software using a 1:1 host-guest binding model. Sodium cation added as $NaBAr^F_4$. All anions added as their TBA salts. Global fit performed for all systems. Error percentages less than 10% unless specified. [b] Salt recombination.

Analysis of the binding data revealed that the introduction of an equivalent of $NaBAr^F_4$ to all interlocked hosts led to a remarkable amplification of the bromide and iodide binding strength, *ca.* 20-fold for [2]rotaxanes **3.13** and **3.14**. This ion-pair binding cooperativity effect can be credited to favourable axle separated cation-anion electrostatic effects and macrocyclic preorganisation instigated in the presence of a co-bound sodium cation.

Interestingly, addition of chloride to the sodium-complexed [2]rotaxane receptors, **3.12** and **3.13** results in salt recombination and eventual precipitation of NaCl owing to the receptors not being able to overcome the high lattice enthalpy of the NaCl ion-pair. In contrast [2]rotaxane **3.14** successfully binds the NaCl ion-pair. This difference in behaviour could be rationalised by considering the % bound sodium to these interlocked hosts under these

titration conditions (Table 3.4), which can be generated using previously obtained cation association constant values. Since [2]rotaxane **3.12** exhibits the highest sodium cation association constant, it consequently has the highest % Na cation bound (>75%) amongst the three rotaxane receptors. Conversely, rotaxanes **3.13** and **3.14** possess similar cation association constants and hence comparable sodium cation bound percentages of 41% and 45% respectively.

Despite displaying a strong affinity for sodium, the inability of rotaxane **3.12** to bind the NaCl ion-pair is attributed to the lack of NH donors in its macrocycle. On the other hand [2]rotaxane **3.13**, although furnished with additional macrocyclic isophthalamide NH donors still fails to bind the ion-pair due to insufficient Na^+ binding. In comparison, [2]rotaxane **3.14** which possesses only a *ca.* 4% increase in % Na^+ bound, effectively overcomes the competing lattice enthalpy of the NaCl salt. It is also interesting to note that the cooperative effect of sodium complexation on [2]rotaxane **3.14** is more pronounced in the case of the heavier halides, bromide and iodide which demonstrate a striking 20-fold enhancement in the presence of sodium, as opposed to the modest amplification witnessed in the case of chloride from 543 M^{-1} to 646 M^{-1}. This could be ascribed to the higher competing lattice enthalpy of NaCl which serves to diminish the cooperative enhancement behaviour. Importantly, these results emphasise the crucial interplay between a ditopic receptor's cation and anion binding properties, as well as the lattice enthalpy of the cation-anion salt, which collectively determine the ion-pair binding capabilities of heteroditopic host systems.

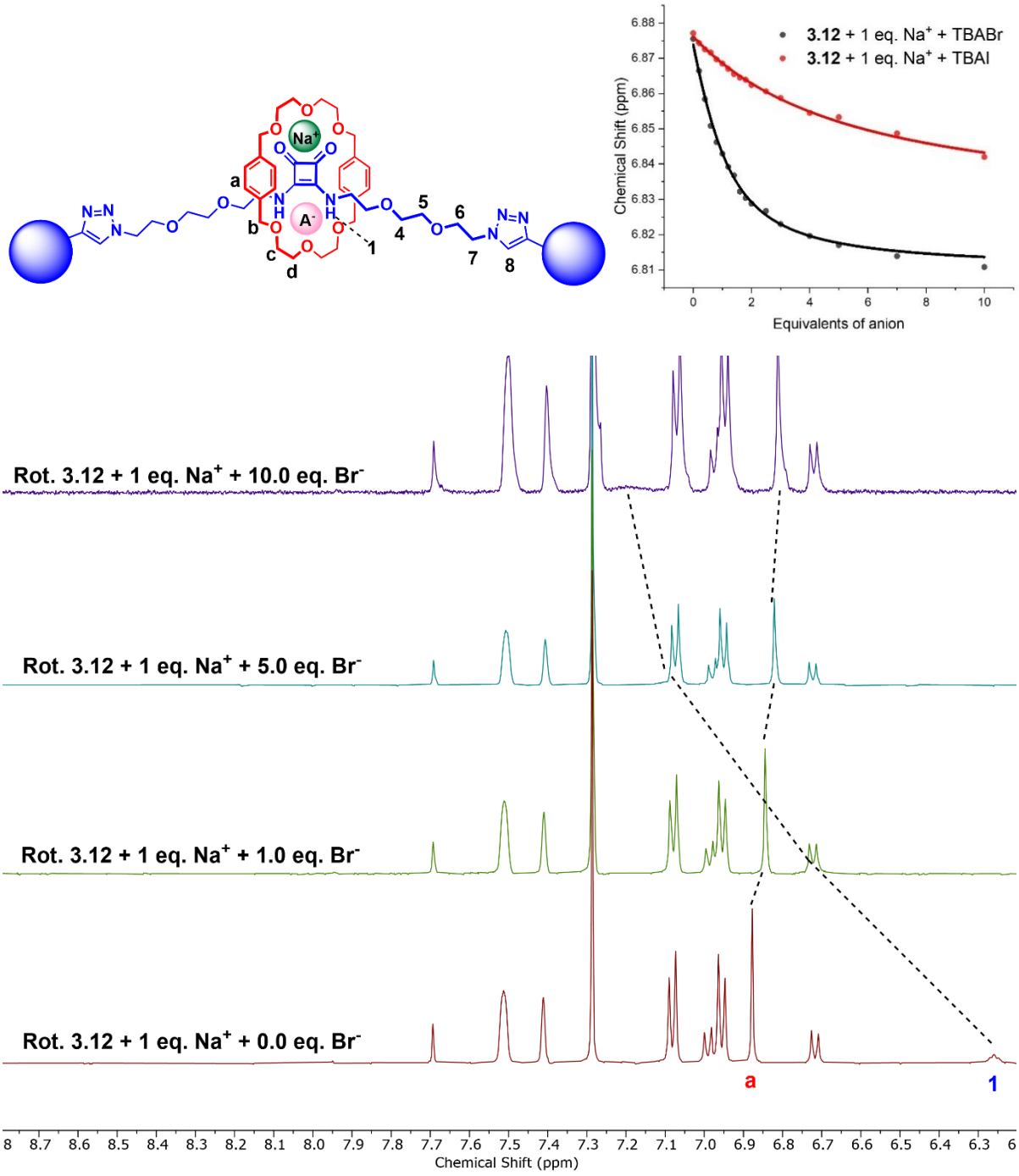


Figure 3.20. *^{1}H NMR spectra of [2]rotaxane **3.12** upon addition of 1, 5 and 10 equivalents of TBABr in the presence of 1 equivalent of $NaBAr^{F}{}_{4}$ (500 MHz, 298 K, 7:3 $CDCl_3/CD_3CN$). Inset: Binding isotherms showing changes in chemical shift of macrocyclic xylene proton a upon increasing equivalents of halide anions.*

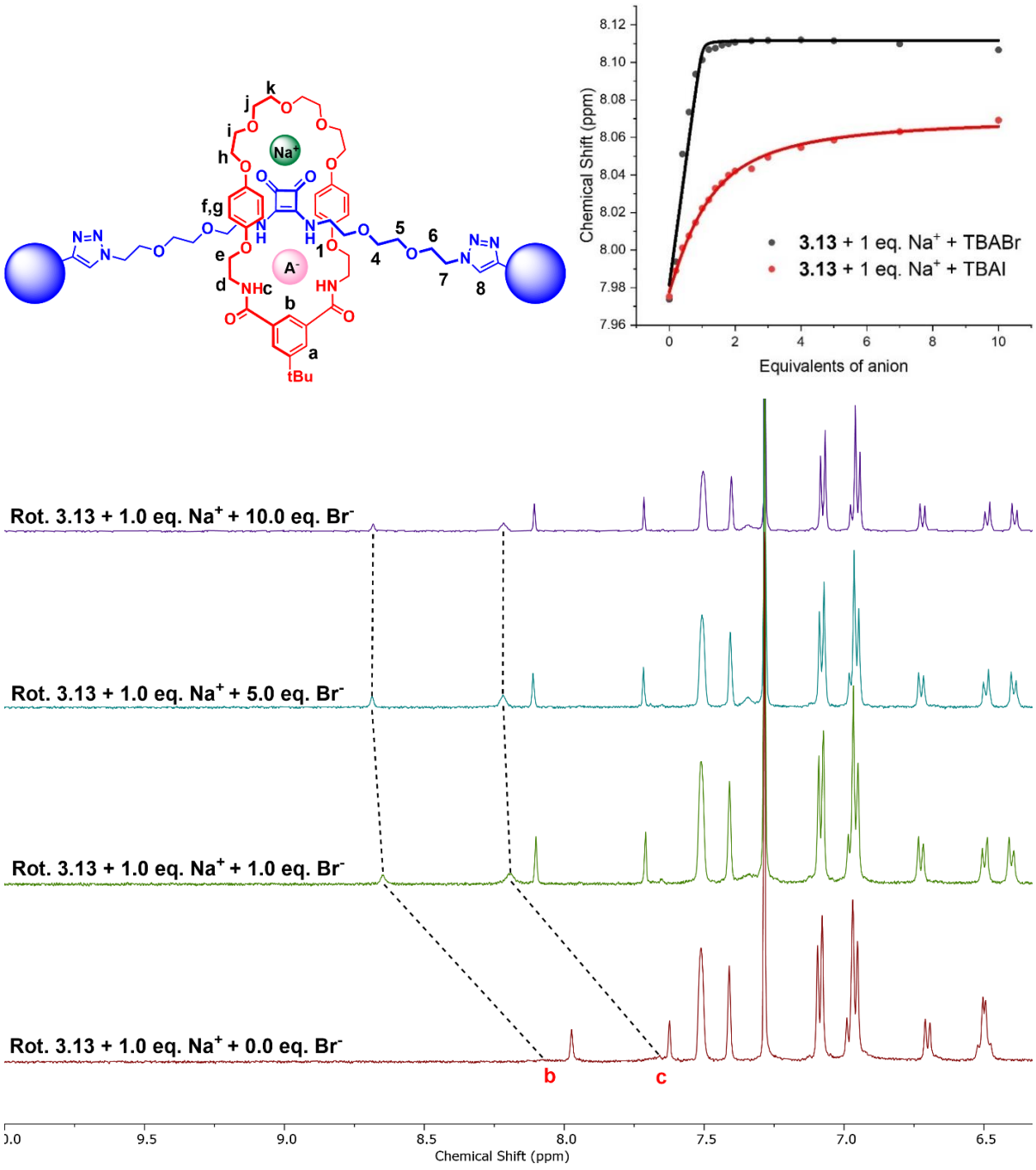


Figure 3.21. *^{1}H NMR spectra of [2]rotaxane **3.13** upon addition of 1, 5 and 10 equivalents of TBABr in the presence of 1 equivalent of $NaBAr^{F}{}_{4}$ (500 MHz, 298 K, 7:3 $CDCl_3/CD_3CN$). Inset: Binding isotherms showing changes in chemical shift of internal benzene proton b upon increasing equivalents of halide anions.*

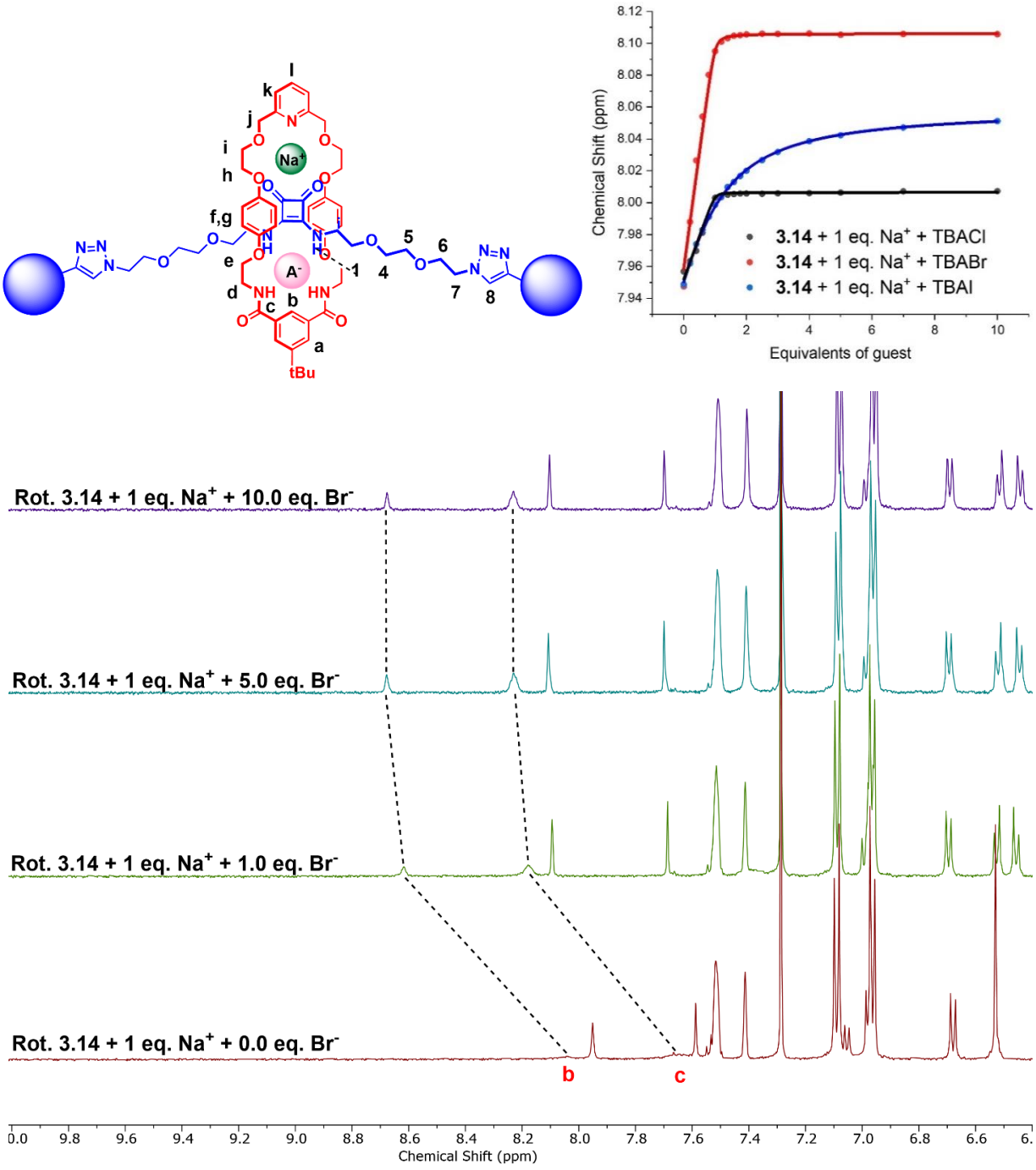


Figure 3.22. *^{1}H NMR spectra of [2]rotaxane **3.14** upon addition of 1, 5 and 10 equivalents of TBABr in the presence of 1 equivalent of $NaBAr^{F}{}_{4}$ (500 MHz, 298 K, 7:3 $CDCl_3/CD_3CN$). Inset: Binding isotherms showing changes in chemical shift of internal benzene proton b upon increasing equivalents of halide anions.*

3.4.4 Preliminary solid-liquid extraction studies

In light of the promising ion-pair binding results, the ability of the [2]rotaxanes to extract sodium halide salts into organic solvent media was studied with the aim of exploring the extent of real-world utility and effectiveness of these receptors. In a typical solid-liquid extraction experiment, a 1 mM solution of each interlocked host in $CDCl_3$ was subjected to an excess (*ca.* 5-fold) microcrystalline sample of solid NaX (X = Cl, Br, I) salt, following which the solution was sonicated for 20 minutes, filtered and its ^{1}H NMR spectrum recorded.

Analysis of the pre- and post-extraction ^{1}H NMR spectra revealed all three [2]rotaxanes effectively extracted NaBr and NaI. Predictably, [2]rotaxanes **3.13** and **3.14** showed noticeably larger perturbations relative to [2]rotaxane **3.12** upon complexation (Figures 3.23, 3.24 and 3.25). Although it was not possible to calculate the % extraction efficiencies from this qualitative study, complexation induced shifts (CIS) of the macrocycle amide signal H_c and internal benzene proton H_b of [2]rotaxanes **3.13** and **3.14** were consistent with the enhanced NaBr over NaI affinity witnessed during solution-phase ion-pair binding studies.

In line with the ion-pair binding results, [2]rotaxanes **3.12** and **3.13** were unable to extract NaCl into $CDCl_3$. Interestingly, despite ^{1}H NMR evidence of solution-phase NaCl ion-pair binding by [2]rotaxane **3.14**, the interlocked host was also incapable at extracting solid NaCl. This deviation could be attributed to the relatively modest cooperative enhancement in chloride binding strength displayed by the rotaxane upon sodium complexation and serves to emphasize the complex ion-pair equilibria and solvent effects operating in solution,

precluding direct translation of solution-phase ion-pair binding results into solid-liquid extraction capability.

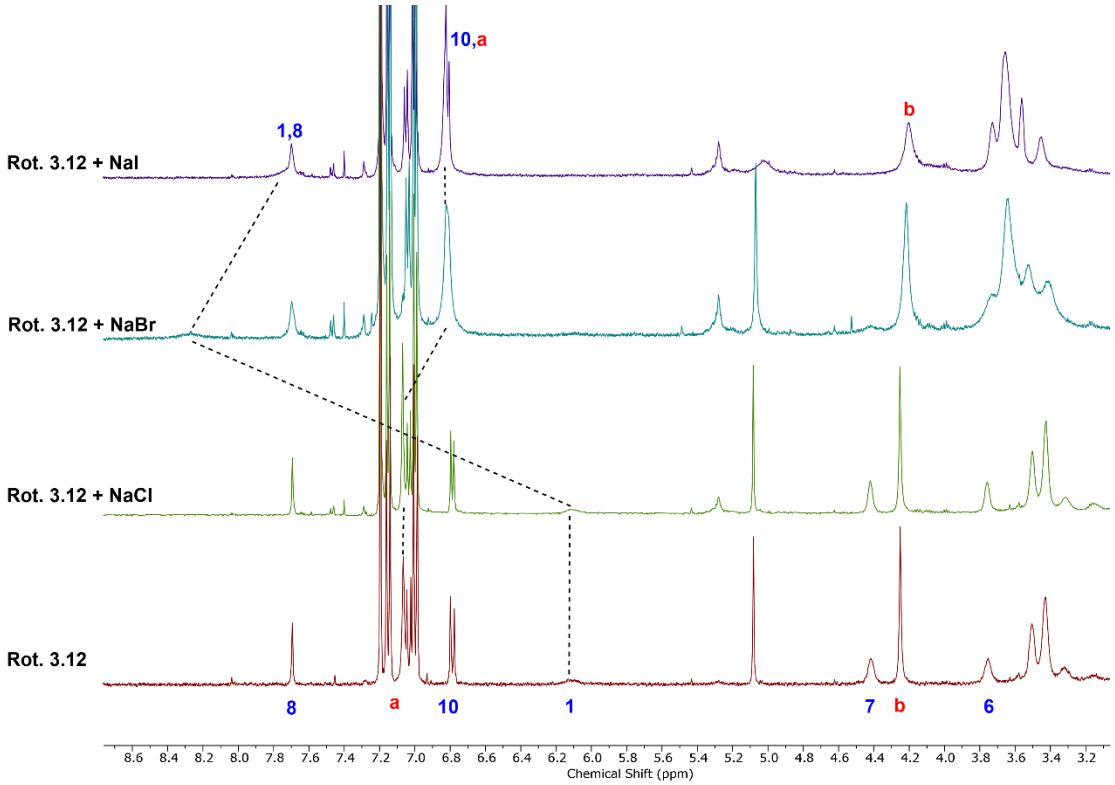


Figure 3.23. *Pre- and post-extraction ^{1}H NMR spectra of [2]rotaxane **3.13** with excess NaCl, NaBr and NaI ($CDCl_3$, 500MHz, 298K).*

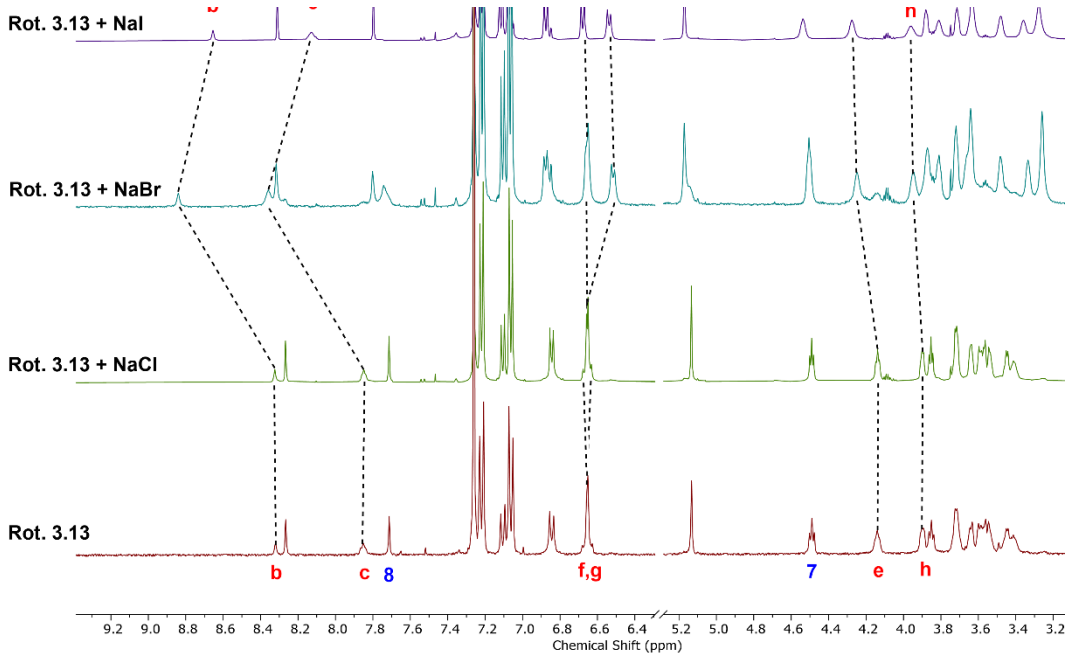


Figure 3.24. *Pre- and post-extraction ^{1}H NMR spectra of [2]rotaxane **3.13** with excess NaCl, NaBr and NaI ($CDCl_3$, 500MHz, 298K).*

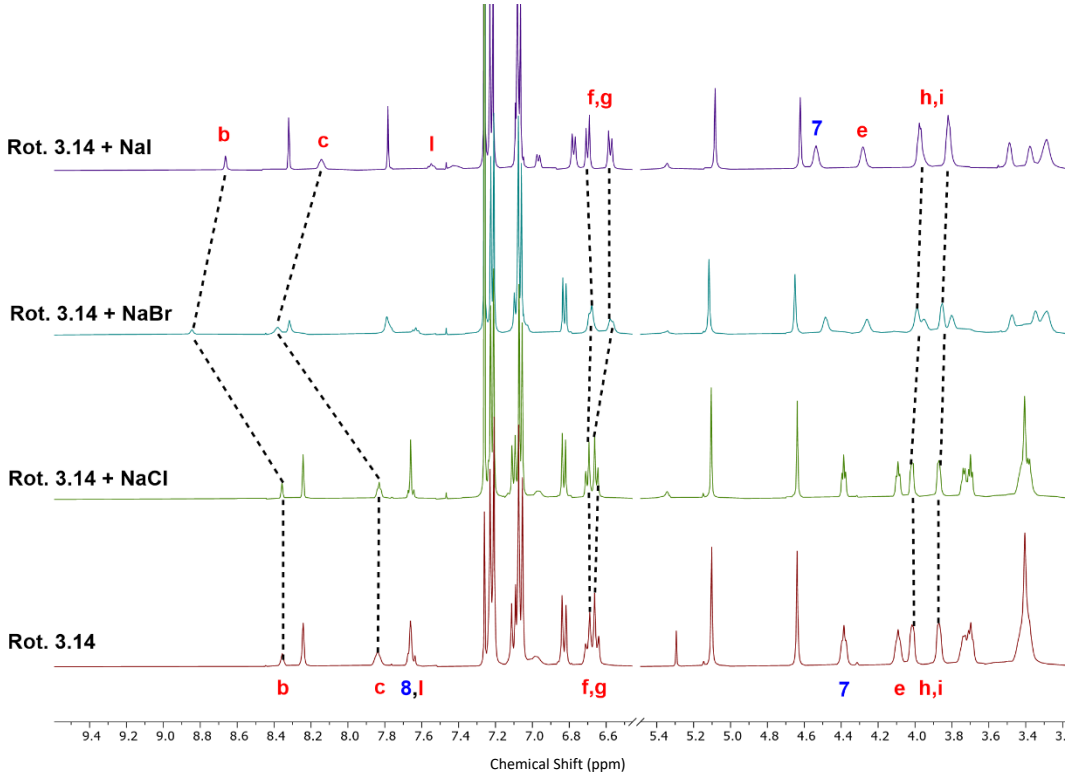


Figure 3.25. *Pre- and post-extraction ^{1}H NMR spectra of [2]rotaxane* ***3.14*** *with excess NaCl, NaBr and NaI ($CDCl_3$, 500MHz, 298K).*

3.5 Conclusions and Future work

To summarise, the first examples of squaramide containing heteroditopic [2]rotaxanes synthesised using an unprecedented sodium cation template-directed MIM synthesis exploiting coordination of the Lewis basic squaramide carbonyls was reported. Extensive cation, anion and ion-pair ^{1}H NMR titration studies demonstrated that the presence of a co-bound sodium cation significantly augmented the bromide and iodide binding affinities of these heteroditopic MIM receptors, *ca.* 20-fold with [2]rotaxanes **3.13** and **3.14**, underscoring the advantages of mechanical bond-induced positive cooperativity in ion-pair recognition. Conversely, [2]rotaxane **3.12** displayed a relatively smaller enhancement in halide binding strength owing to the lack of amide NH donors in the macrocyclic component

of the MIM. Notably, in the presence of sodium, all receptors exhibited impressive bromide selectivity.

Amongst the three rotaxane receptors, only [2]rotaxane **3.14** demonstrated successful binding of the NaCl ion-pair, underpinning the importance of strong concomitant cation and anion association in overcoming competing lattice enthalpies to achieve ion-pair recognition. Furthermore, preliminary solid sodium halide salt-liquid extraction studies demonstrated the ability of all three MIM receptor systems to extract NaBr and NaI into organic media, consistent with their solution phase ion-pair recognition properties.

In light of these impressive ion-pair binding results, future work for this project could entail incorporating sigma-hole donors including halogen bonding motifs into analogous rotaxane systems (Figure 3.26), especially given the encouraging binding affinities and selectivity trends witnessed with the XB rotaxanes in the previous chapter. Furthermore, the sodium cation-template methodology employed in this chapter could also be further utilised to synthesise squaramide-appended [2]catenane structures (Figure 3.27).

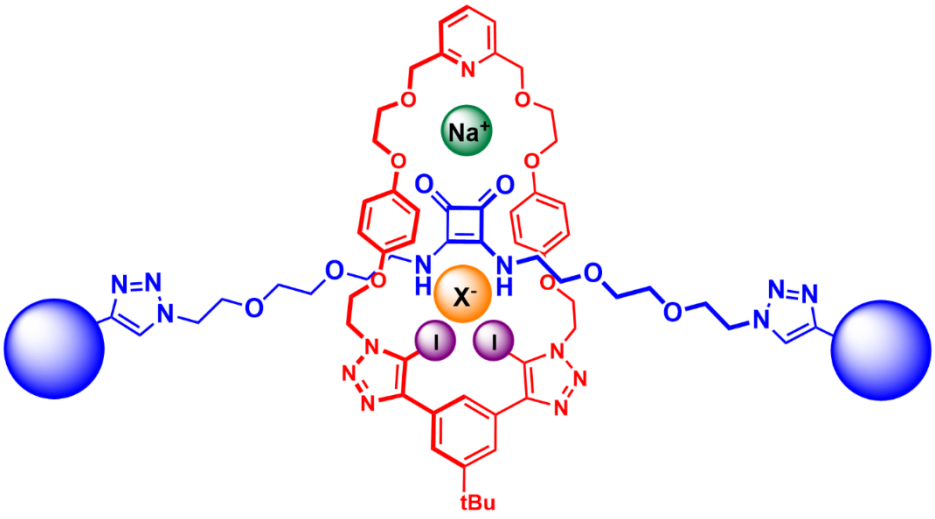


Figure 3.26. *A squaramide functionalised XB [2]rotaxane.*

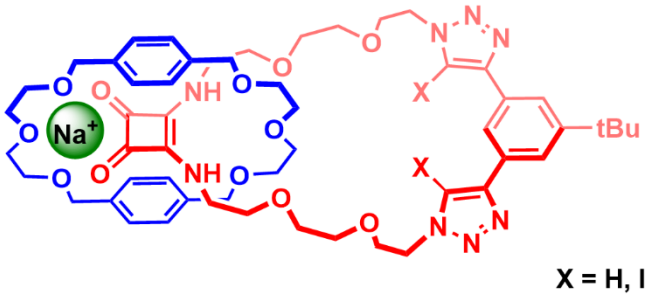


Figure 3.27. *A squaramide functionalised [2]catenane.*

Chapter 4: Bis-squaramide-based [2]Rotaxanes for Anion Recognition in Aqueous-organic Solvent Mixtures

4.1 Introduction

As mentioned in Chapter 1 section 1.3, anions are ubiquitous in nature and are involved across a myriad of chemical and biological processes, making their recognition a crucial and relevant area of research. However, this can be challenging owing to their inherent properties that include size/geometry variation and pH dependence.[79-86] Building complementary host cavities to achieve selective recognition of target anion guest species has therefore garnered significant interest and continues to be a subject of ongoing research.

In protic polar and aqueous containing solvent systems, achieving strong binding of anionic guests becomes an even more daunting task due to their intrinsically high free energies of solvation (See Chapter 1, section 1.3.2).[87] Whilst the introduction of positive charge is frequently regarded as a potential strategy to increase the anion affinity of a receptor by overcoming the effects of solvation in highly competitive protic aqueous solvent media, this is often to the detriment of selectivity between negatively charged species.[263] The three dimensional encapsulating binding cavities afforded by the mechanical bond offer an

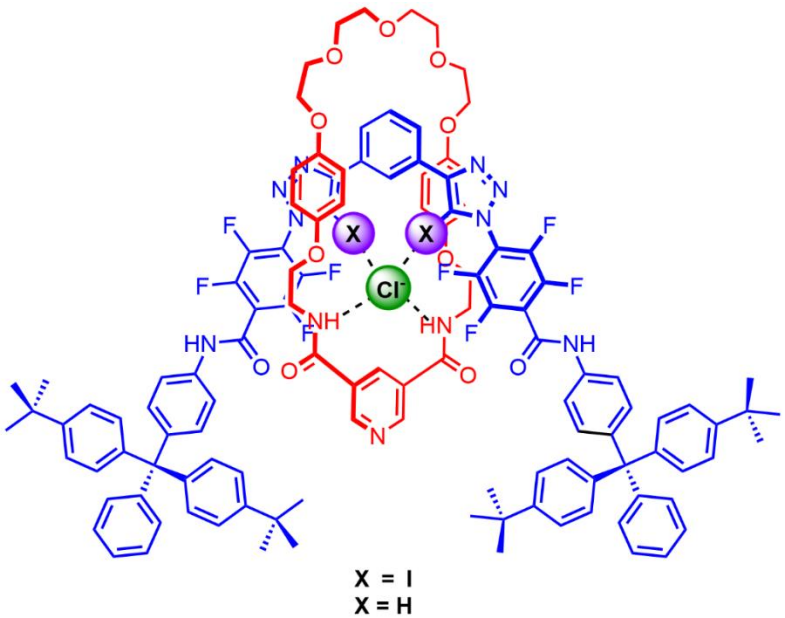


Figure 4.1. *Beer's neutral XB [2]rotaxane preferentially binding chloride in 5:95 D_2O/d_6-acetone mixtures.*[200]

attractive avenue towards topologically preorganised recognition environments, which can mitigate some of the challenges associated with anion recognition in aqueous containing media.[264] This is demonstrated in a recently reported series of neutral XB [2]rotaxanes by Beer and co-workers which are capable of halide recognition in 5:95 water/acetone solvent mixtures.[200] Extensive ^{1}H NMR binding studies in aqueous-organic solvent mixtures reveal a remarkable anti-Hofmeister bias, with chloride and bromide bound more strongly than iodide. This is in sharp contrast to the typical Hofmeister preference ($Cl^- < Br^- < I^-$) exhibited by the non-interlocked acyclic axle components, highlighting the crucial role of the size-constrained solvent shielded rotaxane MIM binding cavity (Figure 4.1).

4.2 Chapter objectives

Biotic protein-based host systems typically achieve strong and selective recognition of anionic species through the concerted action of multiple hydrogen bonding (HB) donor motifs, which effectively sequesters the negatively charged guest (see Chapter 1, section 1.2.2). Taking inspiration from this approach, the key objective of the project discussed in this chapter was to integrate two potent squaramide HB donor motifs into the axle component of a [2]rotaxane host structure to achieve anion recognition in aqueous-containing media. To the best of our knowledge, there have been no reports of incorporating multiple squaramide units into a MIM-based host architecture for concerted anion guest binding.

A series of neutral, potent [2]rotaxanes containing bis-squaramide functionalised axle components and an isophthalamide macrocycle are prepared using active metal template methodology. Wherein the two squaramide units in the axle component are connected *via* an aryl or aliphatic spacer and are envisaged to bind a diverse series of anions through a

combination of complementary HB interactions supplemented by the isophthalamide containing macrocycle component (Figure 4.2).

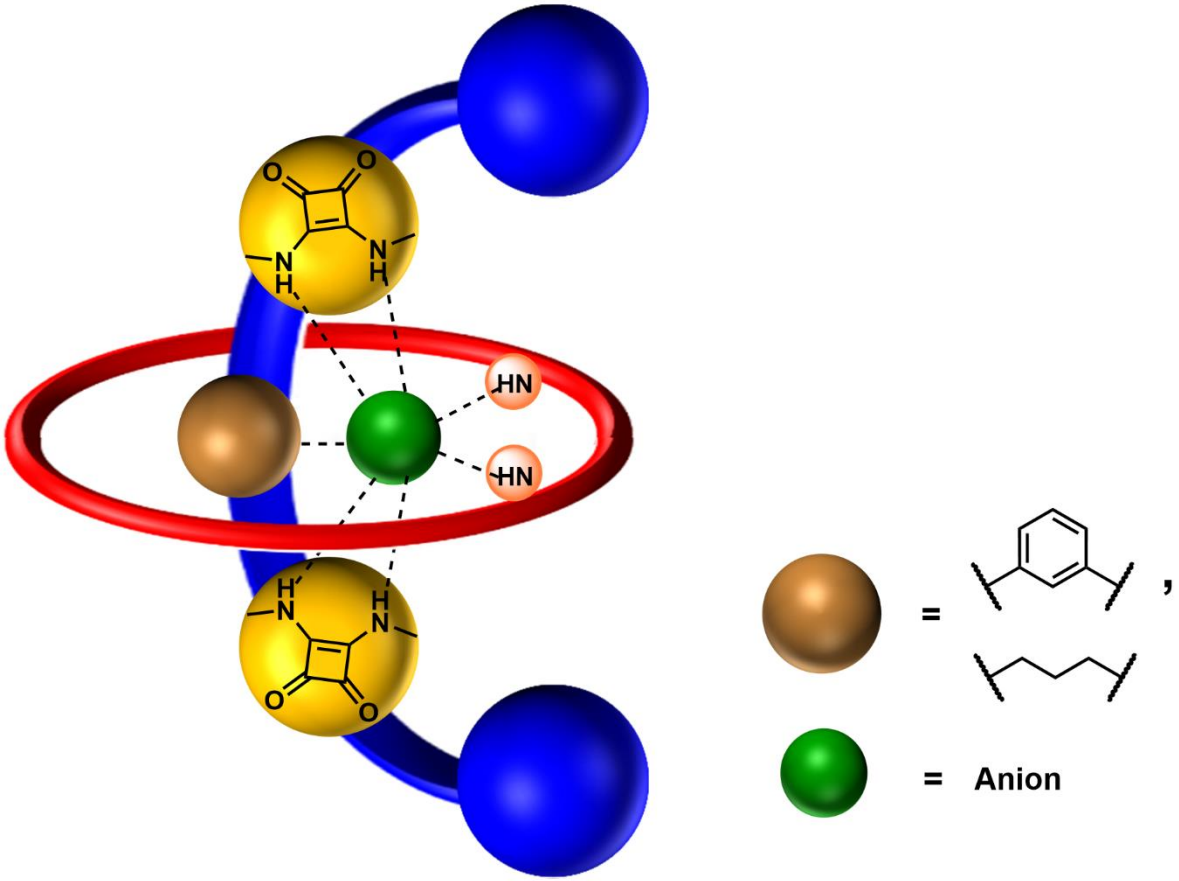


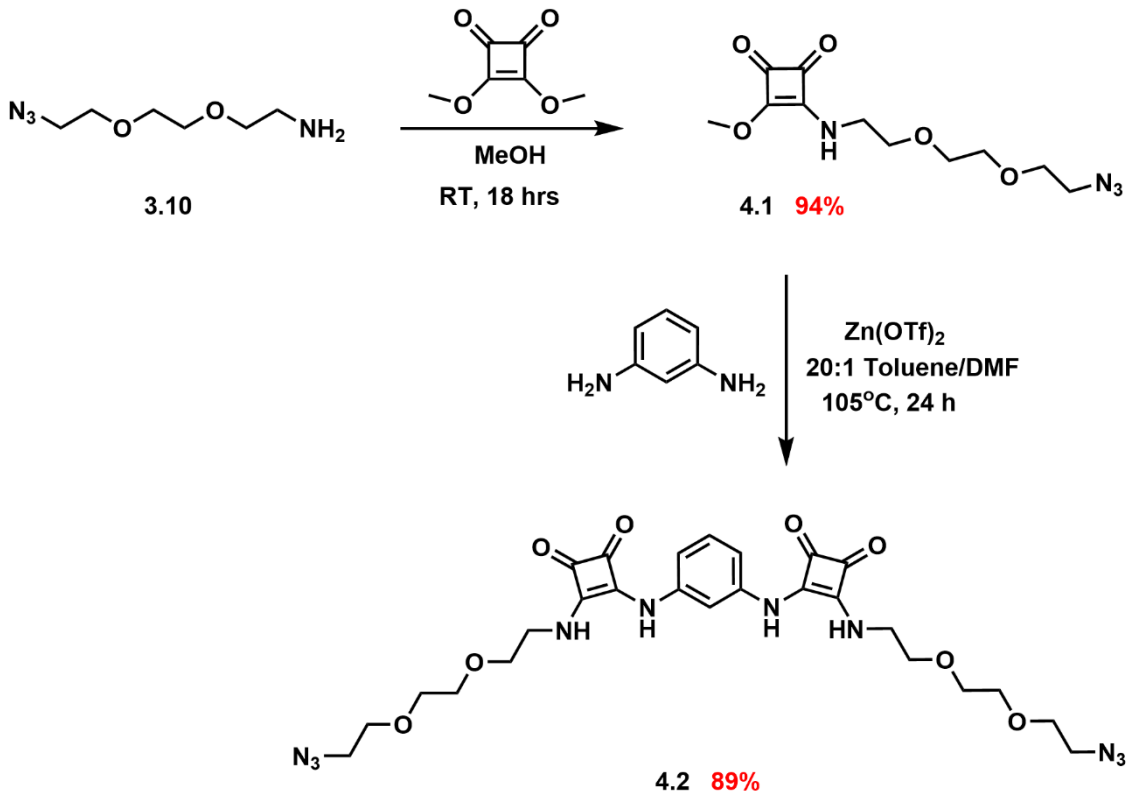
Figure 4.2. *Cartoon representation of the target bis-squaramide based [2]rotaxane host systems.*

4.3 Synthesis and characterisation

4.3.1 Synthesis of bis-azide functionalised bis-squaramide axle precursors

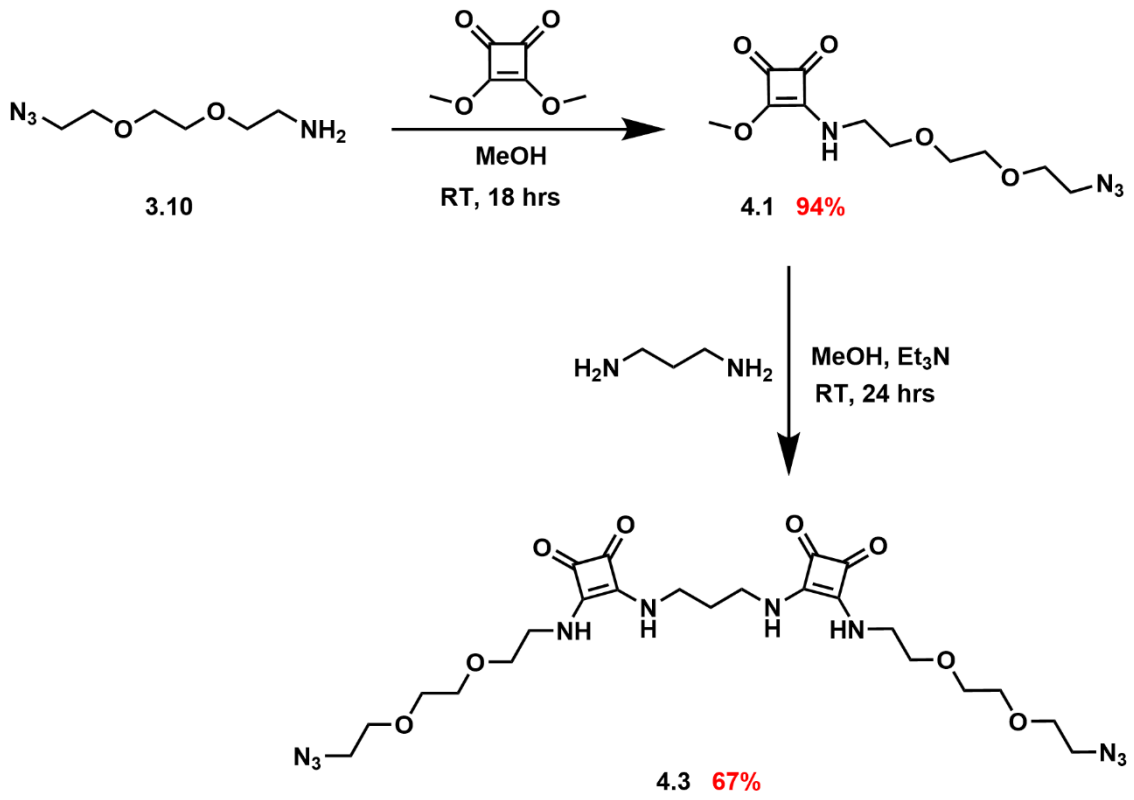
The synthesis of the target [2]rotaxanes began with the preparation of the bis-azide functionalised bis-squaramide axle precursors, **4.2** and **4.3**. To this end, an equimolar amount of previously synthesised azide-amine ether derivative **3.10** was first reacted with squarate ester in methanol *via* a condensation reaction to afford the mono-azide precursor, **4.1** in 94% yield. Two equivalents of compound **4.1** was subsequently coupled with 1,3-diaminobenzene

in the presence of zinc triflate in a 20:1 toluene/DMF solvent mixture at 105^{0}C overnight. Purification by column chromatography gave the desired bis-azide functionalised bis-squaramide axle precursor **4.2** in 89% yield (Scheme 4.1).



Scheme 4.1. *Synthesis of bis-azide functionalised bis-squaramide axle precursor* ***4.2****.*

Alternatively, the preparation of alkyl linked bis-azide functionalised bis-squaramide analogue **4.3** was achieved by subjecting mono-azide precursor **4.1** to a condensation reaction with 1,3-diaminopropane in methanol in the presence of a base at room temperature. Having stirred the reaction overnight, chromatographic purification afforded the propyl-based bis-squaramide azide precursor, **4.3** in 67% yield (Scheme 4.2). Both bis-azide precursors, **4.4** and **4.5**, were characterised using ^{1}H NMR, ^{13}C NMR and ESI-HRMS in d_6-DMSO owing to poor solubility of the synthons in common organic solvents.

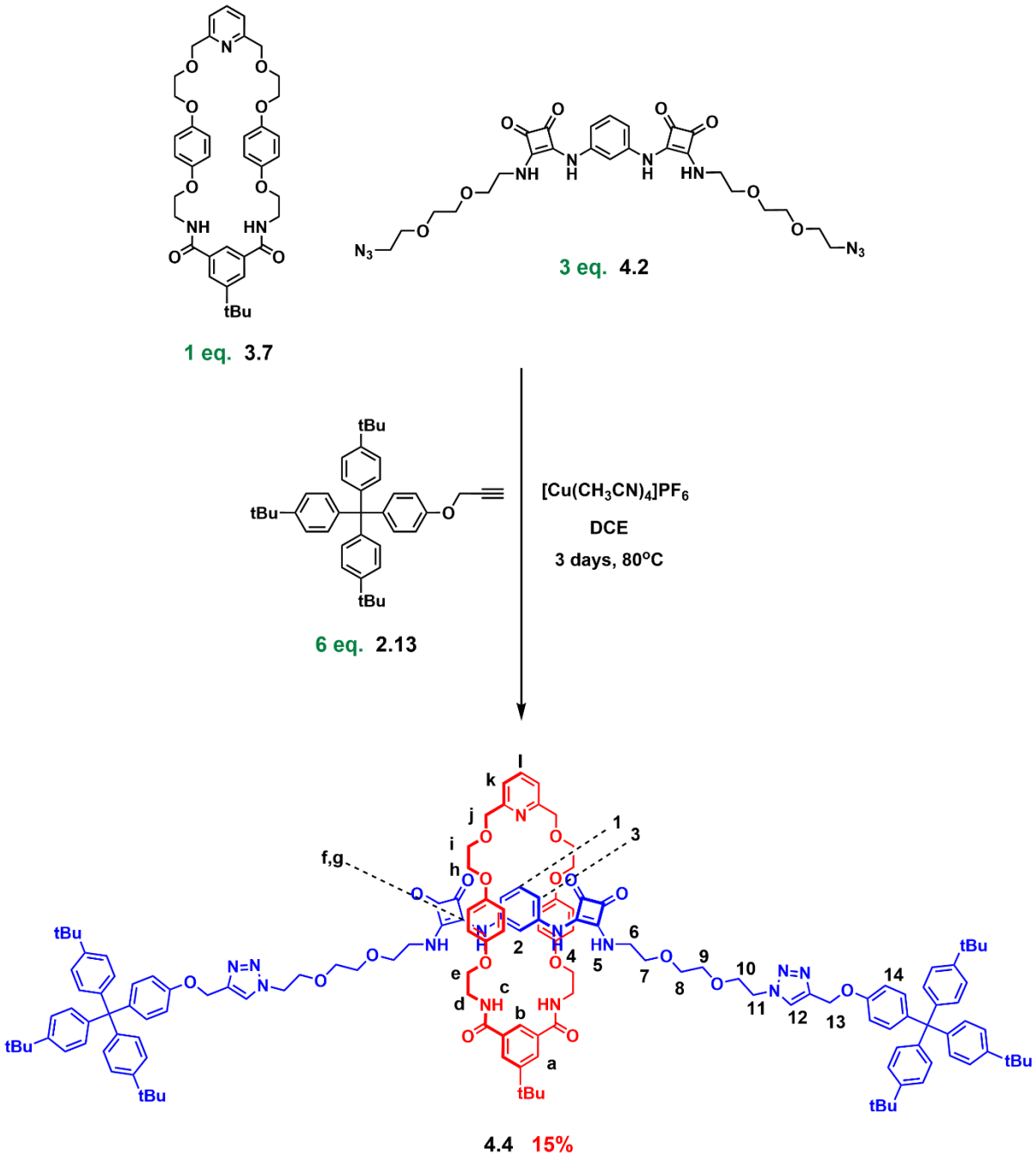


Scheme 4.2. *Synthesis of bis-azide functionalised bis-squaramide axle precursor* ***4.3****.*

4.3.2 Synthesis of bis-squaramide [2]rotaxanes

The novel bis-azide-squaramide axle precursors were thereafter employed in a conventional active metal template methodology previously discussed in Chapter 2 to synthesise the target [2]rotaxanes.[182] Macrocycle **3.7** was chosen due to its pyridyl motif which is known to assist in AMT--CuAAC rotaxane synthesis.

Accordingly, an equimolar mixture of macrocycle **3.7** and $Cu(CH_3CN)_4PF_6$ in dichloroethane was combined with six and three equivalents of stopper alkyne **2.13** and bis-azide **4.2** respectively (Scheme 4.3). The reaction was left to stir at 80^0C for three days following which the crude mixture was subjected to an aqueous workup with EDTA/NH_4OH. Purification by preparative TLC afforded [2]rotaxane **4.4** in 15% yield which was characterised in $CDCl_3$ by ^{1}H NMR, ^{13}C NMR, ^{1}H-^{1}H ROESY NMR and ESI-HRMS.



Scheme 4.3. *Synthesis of [2]rotaxane* ***4.4***

Evidence of [2]rotaxane formation was obtained *via* comparison of the ^{1}H NMR spectrum of the interlocked product with those of its macrocycle and axle components in $CDCl_3$ (Figure 4.3). Diagnostic upfield shifts and splitting of the hydroquinone protons $H_{f,g}$ as a result of donor-acceptor interactions between the electron deficient squaramide unit and electron-rich macrocycle hydroquinone units were indicative of successful mechanical bond

formation. Furthermore, the downfield shifts of the macrocycle protons H_b and H_c and upfield shifts of the axle protons H_2 and H_4 were attributed to shielding effects arising from the macrocycle residing in the vicinity of the two squaramide components, a co-conformation *x*presumably stabilised by extensive intercomponent HB interactions.

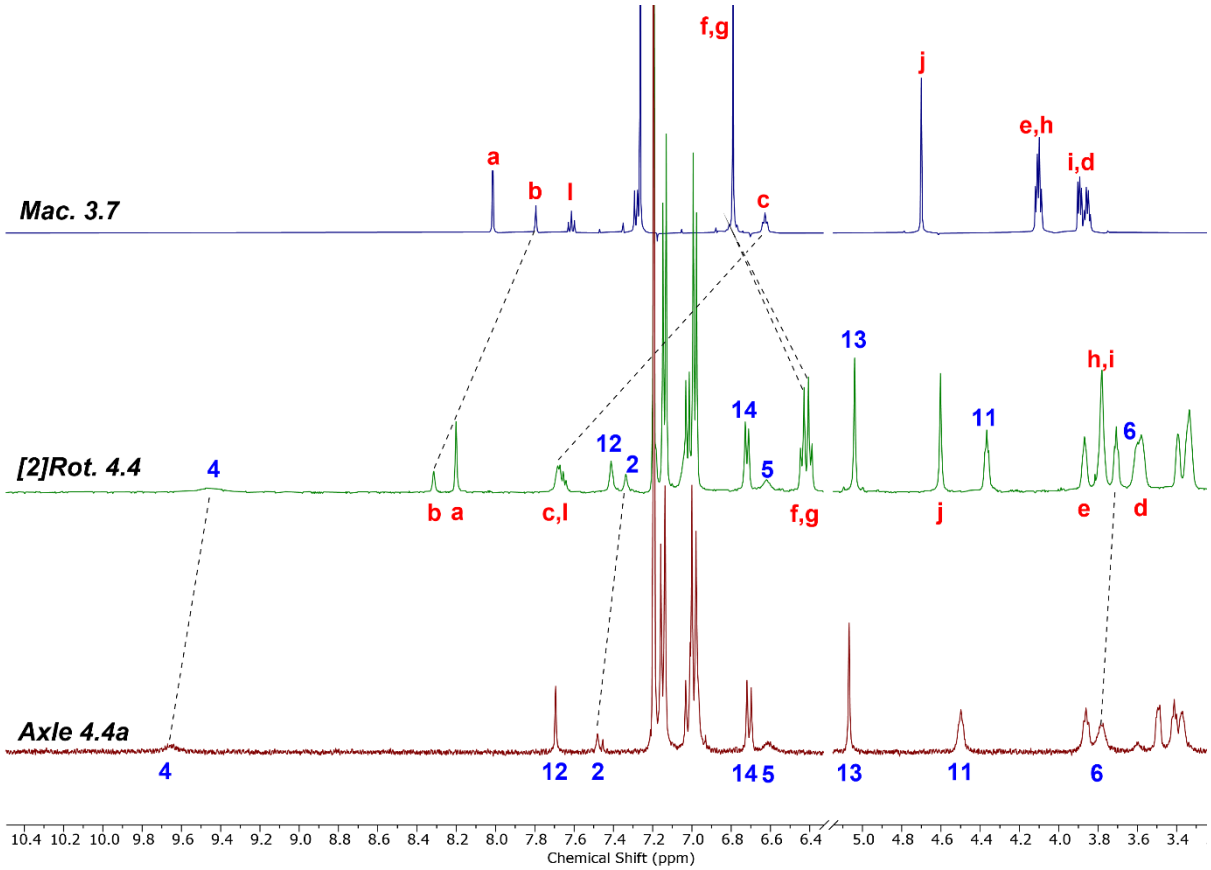


Figure 4.3. *Truncated stacked ^{1}H NMR spectra of i) macrocycle **3.7** ii) [2]rotaxane **4.4** and iii) axle component **4.4a** ($CDCl_3$, 500 MHz, 298K).*

Further proof of such intercomponent interactions were obtained from a ^{1}H-^{1}H ROESY NMR study in $CDCl_3$ (Figure 4.4) which revealed through-space interactions between the axle squaramide protons and the protons of the macrocycle, but not between the axle triazole protons and the macrocycle protons, consistent with the macrocycle preferentially residing at the squaramide station of the axle.

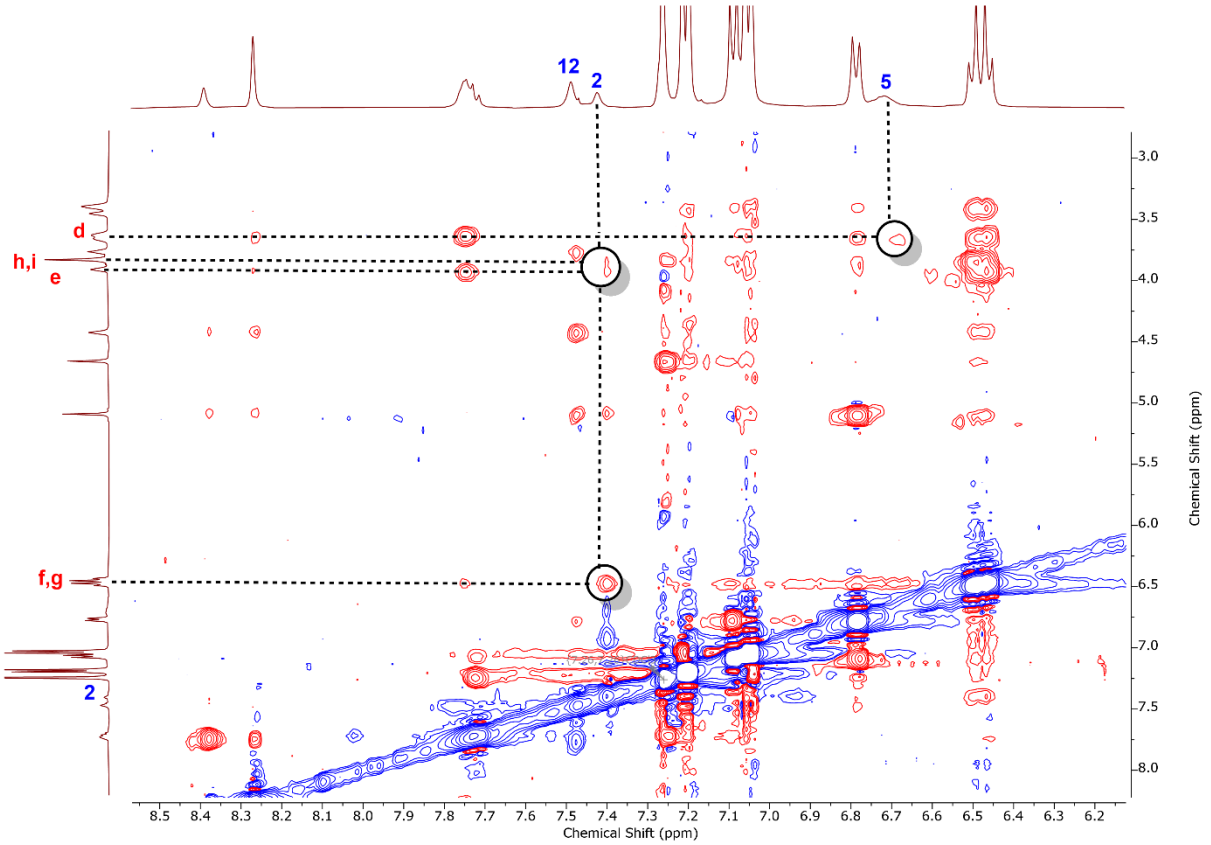
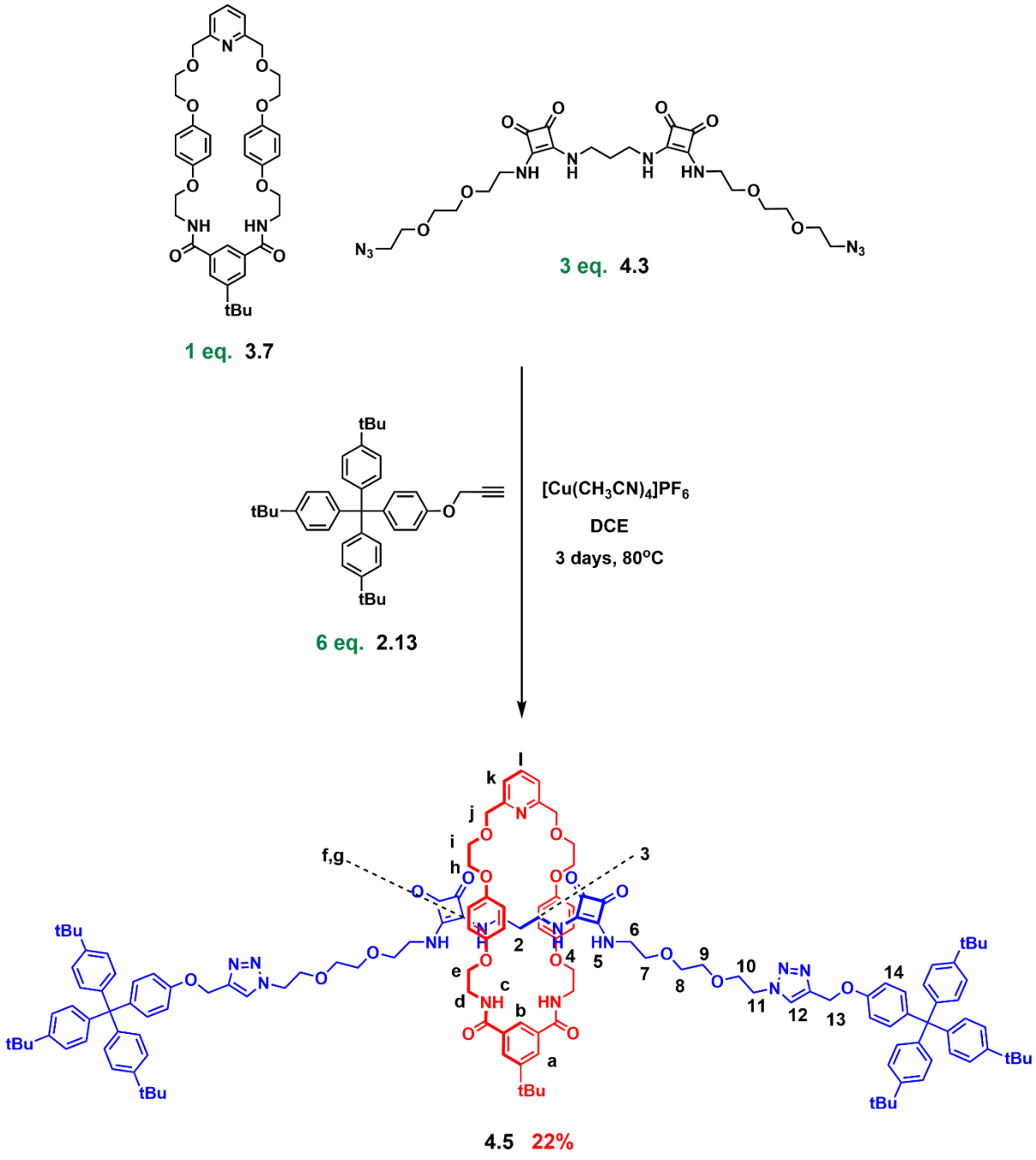


Figure 4.4. *Truncated ^{1}H-^{1}H ROESY NMR spectrum of [2]rotaxane* ***4.4*** *in $CDCl_3$.*

An analogous rotaxane synthesis was undertaken with bis-azide axle precursor **4.3**, macrocycle **3.7** and stopper alkyne **2.13** in the presence of $Cu(CH_3CN)_4PF_6$ in dichloroethane at 80^0C (Scheme 4.4). Using previously stated AMT conditions, the reaction mixture was monitored for 3 days by TLC following which an aqueous workup with EDTA/NH_4OH and



Scheme 4.4. *Synthesis of [2]rotaxane* ***4.5****.*

purification *via* preparative TLC gave [2]rotaxane **4.5** in a 22% yield. Novel [2]rotaxane **4.5** was characterised in $CDCl_3$ using ^1H NMR, ^{13}C NMR, ^1H-^1H ROESY NMR and ESI-HRMS.

The formation of [2]rotaxane **4.5** was established *via* comparison of the ^1H NMR spectra of macrocycle **3.7**, the interlocked product **4.5** and its axle component, **4.5a** in $CDCl_3$ (Figure 4.5). In general, upfield shifts and splitting of the hydroquinone protons $H_{f,g}$ were consistent with the existence of donor-acceptor interactions between the macrocycle electron-rich hydroquinone units and the electron deficient squaramide units in the axle. Of further note were the significant downfield shifts of the macrocycle protons, H_b and H_c and upfield shifts of the axle protons, H_2 and H_4 which alluded to the macrocycle again residing in

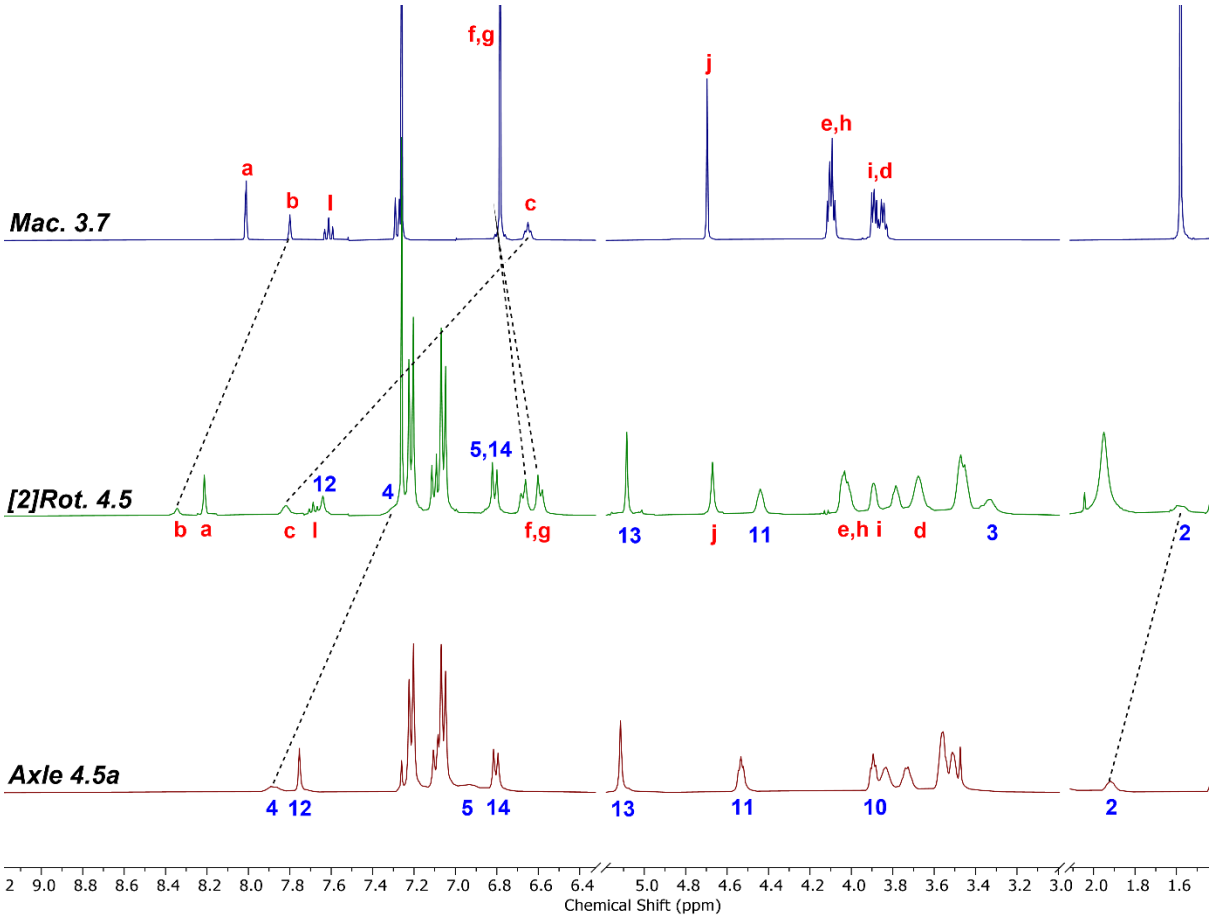


Figure 4.5. *Truncated stacked ^1H NMR spectra of i) macrocycle **3.7** ii) [2]rotaxane **4.5** and iii) axle component **4.5a** ($CDCl_3$, 500 MHz, 298K).*

the neighbourhood of the two squaramide components as a consequence of intercomponent HB interactions and resultant shielding effects arising because of mechanical bond formation.

Evidence of such intercomponent behaviour was provided by a ^{1}H-^{1}H ROESY NMR study of rotaxane **4.5** in $CDCl_3$ which revealed through-space interactions between the axle squaramide protons and the protons of the macrocycle indicative of the macrocycle residing near the squaramide station of the axle (Figure 4.6). Notably, through-space interactions were also observed between the axle spacer protons, $H_{2,3}$ and protons in close proximity to the axle's triazole units, $H_{11,13}$, which hints at possible co-conformational convergence of the flexible axle TEG groups around the interlocked cavity. Furthermore, the presence of through-space interactions between the triazole protons, H_{12} and the macrocyclic protons provided additional evidence supporting the behaviour of the flexible axle component.

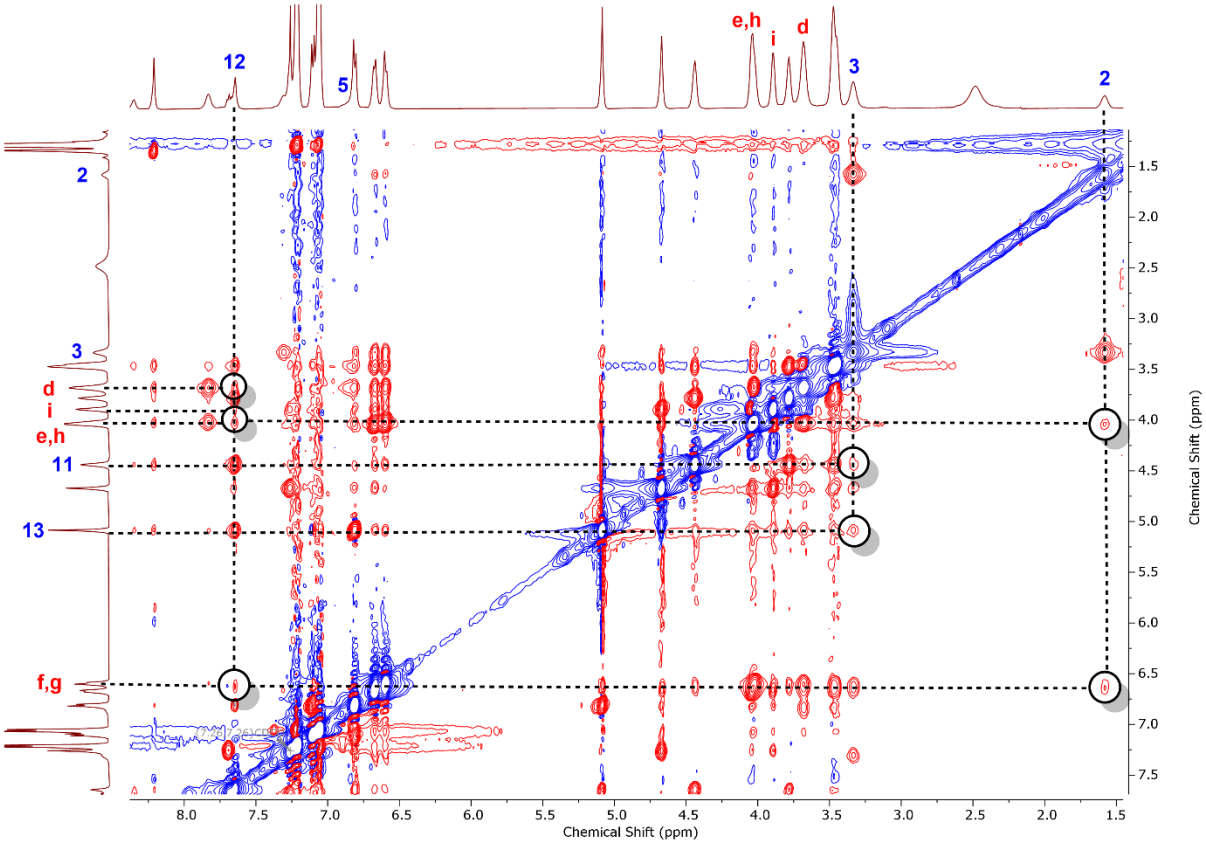


Figure 4.6. *Truncated ^{1}H-^{1}H ROESY NMR spectrum of [2]rotaxane **4.5** in $CDCl_3$.*

Following the synthesis of the target bis-squaramide containing [2]rotaxanes, mono-squaramide [2]rotaxane **3.14** was also prepared again using AMT methodology (Figure 4.7) as a control to study the effects of cooperativity between the squaramide units on the anion recognition properties of rotaxanes **4.4** and **4.5**.

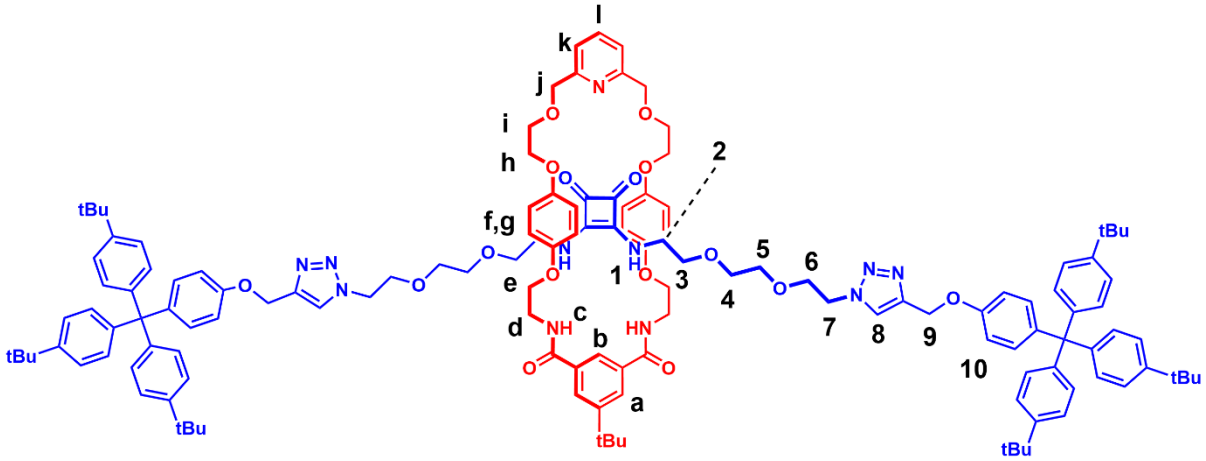


Figure 4.7. *Control [2]rotaxane* ***3.14****.*

4.4 Host-guest recognition studies

An extensive series of anion binding studies were conducted on the [2]rotaxanes in aqueous-acetone solvent mixtures to investigate the role of anion identity, hydration and geometry on binding affinity and selectivity. A variety of anions spanning the Hofmeister series were selected including halides and a range of oxoanions.[88] To this end, aliquots of TBA salts were sequentially added to a 1 mM solution of each rotaxane in 5:95 D_2O/d_6-acetone solvent media.

4.4.1 Quantitative ^{1}H NMR anion binding titration studies with [2]rotaxane **3.14**

^{1}H NMR anion binding studies were first undertaken with mono-squaramide-functionalised [2]rotaxane **3.14**. Typically, the successive addition of anion salt aliquots to [2]rotaxane **3.14** induced downfield perturbations in the proton signals corresponding to the chemical environments adjacent to the NH HB donors of the macrocycle and the axle squaramide units, H_b and H_2, suggesting that all anions were binding within the amide binding cleft and interlocked cavity of the [2]rotaxane (Figure 4.8 and 4.9). Notably, for all three [2]rotaxane systems, the amide resonances of the macrocycle and axle components were not observed in this protic solvent medium due to hydrogen-deuterium exchange. Hence, Bindfit[237] analysis of the titration isotherms obtained by monitoring proton H_b determined 1:1 host:guest stoichiometric halide association constants summarised in Table 4.1.

Table 4.1: *Anion association constants K_a (M^{-1}) for [2]rotaxane* ***3.14*** *[1.0 mM] in 95:5-d_6-acetone-D_2O at 298 K.*[a]

Anion	[2]Rot. **3.14**	
TBA^+ salts	**Binding model (Host: Guest)**	***K_1 (M^{-1})***
Cl^-	1:1	90
Br^-	1:1	34
I^-	-	-[b]
NO_3^-	-	-[b]
NO_2^-	-	-[b]
OBz^-	1:1	46
OAc^-	**1:1**	**317**
HSO_4^-	1:1	223
$H_2PO_4^-$	1:1	38

[a] K_a values calculated using Bindfit[237] software using a 1:1 host-guest binding model by monitoring internal benzene proton H_b. All anions added as their TBA salts. Error percentages less than 10% unless specified. [b] = No binding. Anion with the highest association constant is highlighted in red.

Analysis of the binding data revealed that acetate was most strongly bound by the rotaxane host whereas the anion affinities of I^-, NO_3^-, NO_2^- were too weak to be quantified. This observed order of binding strength broadly correlates to the relative basicities of the anions. Moreover, the preference for acetate could be attributed to optimal geometric and size complementarity achieved with the trigonal planar acetate anion and the spatial arrangement of the multiple NH donor groups present in the [2]rotaxane. Additionally, this trend was also indicative of an emerging anti-Hofmeister bias in the system, made possible by the effective hydrophobic cavity created upon mechanical bond formation.

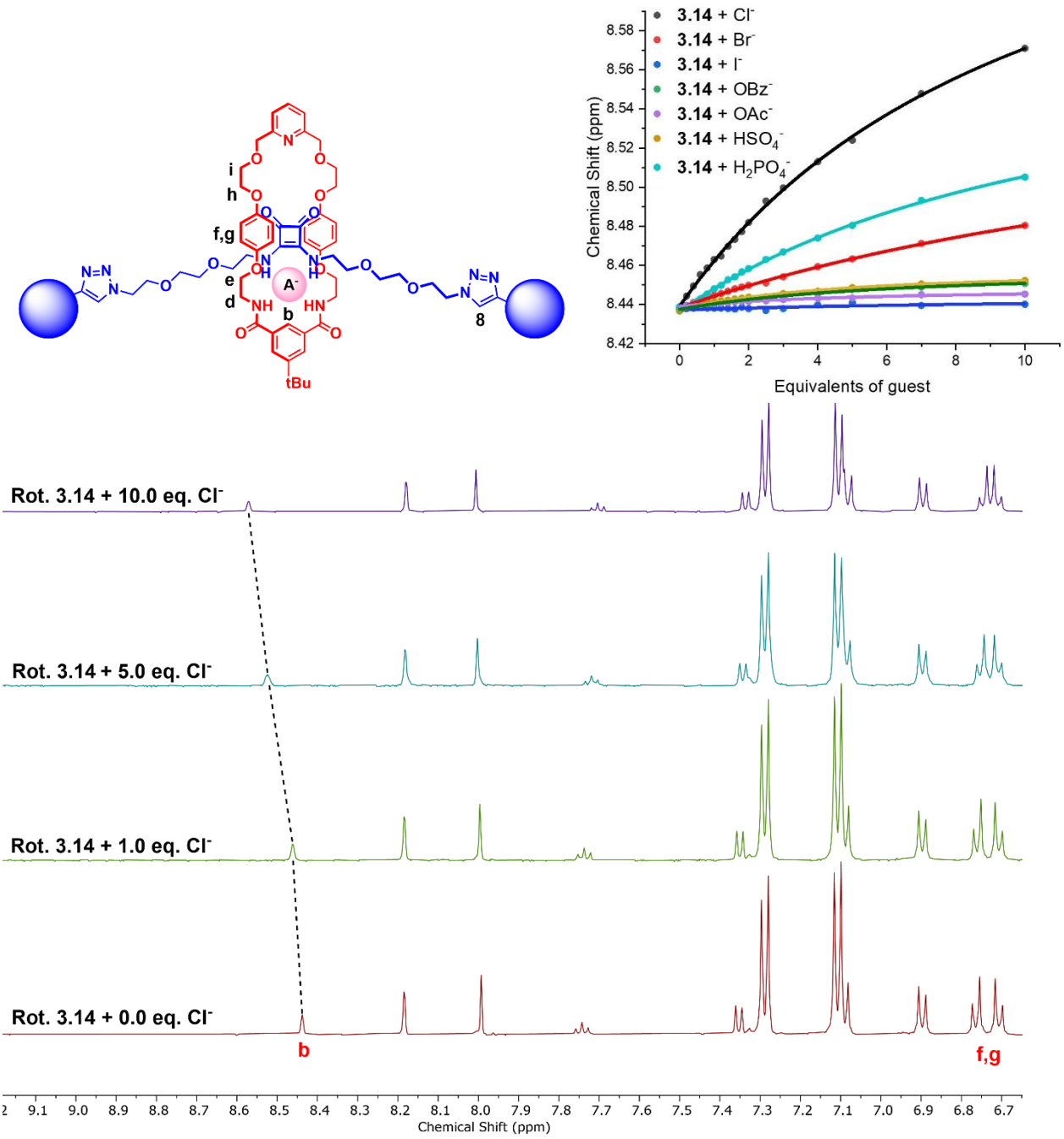


Figure 4.8. *^{1}H NMR spectra of [2]rotaxane **3.14** upon addition of 1, 5 and 10 equivalents of TBACl (500 MHz, 298 K, 95:5-d_6-acetone-D_2O). Inset: Binding isotherms showing changes in chemical shift of internal benzene proton b upon increasing equivalents of various anions.*

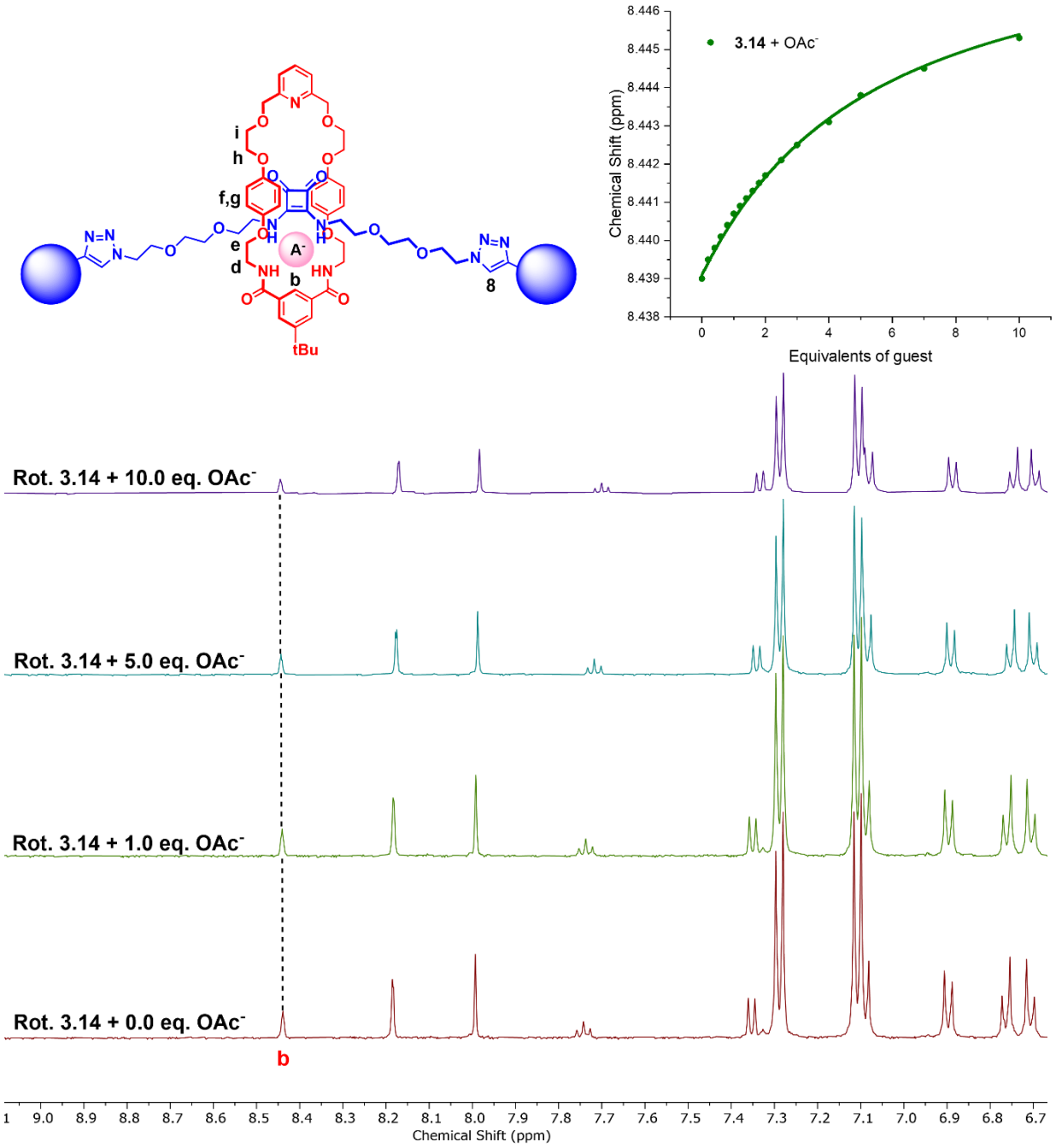


Figure 4.9. *^{1}H NMR spectra of [2]rotaxane **3.14** upon addition of 1, 5 and 10 equivalents of TBAOAc (500 MHz, 298 K, 95:5-d_6-acetone-D_2O). Inset: Binding isotherms showing changes in chemical shift of internal benzene proton b upon increasing equivalents of acetate anion.*

4.4.2 Quantitative ^{1}H NMR anion binding titration studies with bis-squaramide [2]rotaxane **4.4**

Analogous ^{1}H NMR titration experiments were undertaken with the bis-squaramide functionalised [2]rotaxanes **4.4** and **4.5**. In the case of the aryl-linked [2]rotaxane **4.4**, in general the addition of anions led to downfield shifts in the macrocycle proton H_b and axle

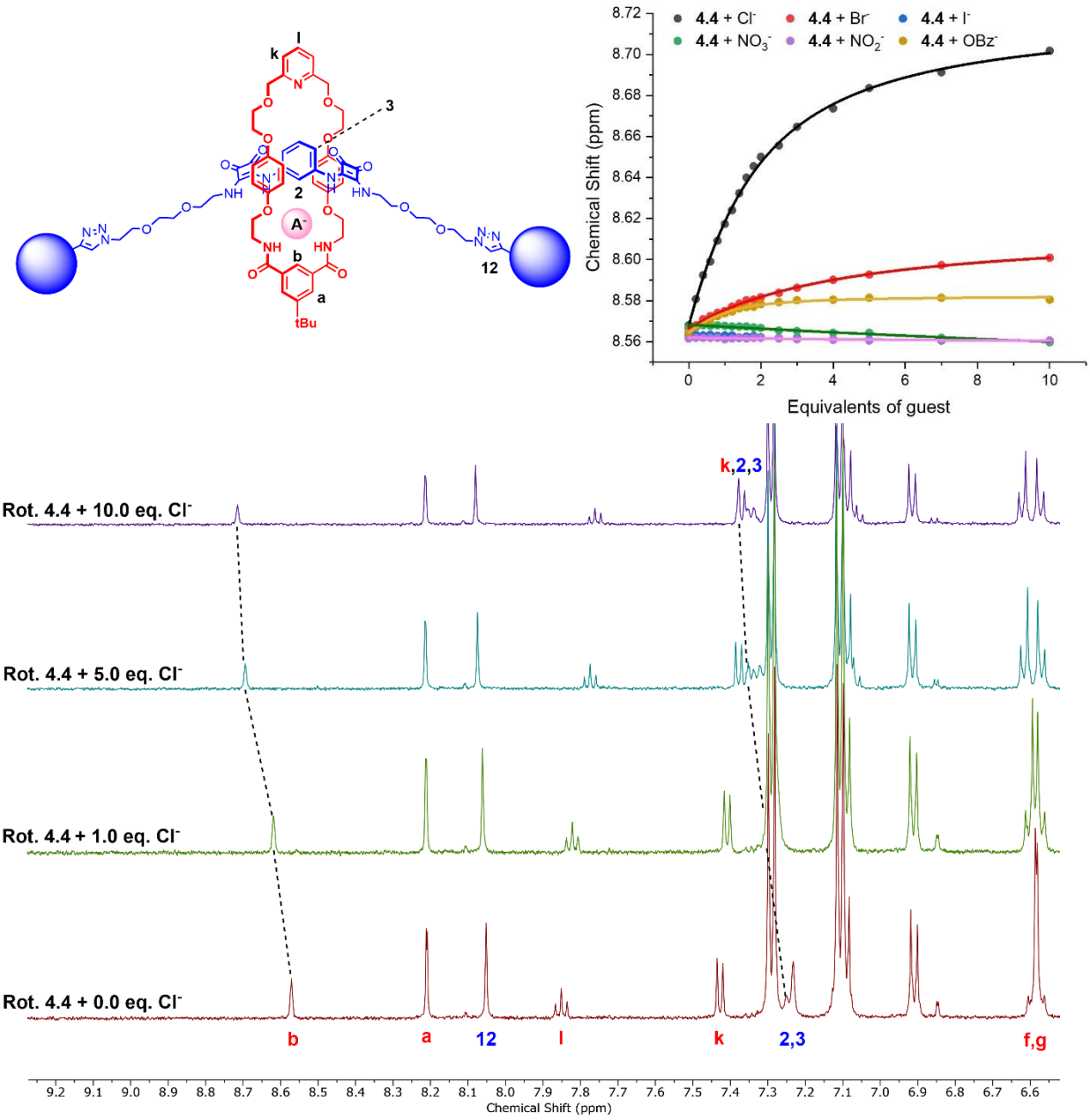


Figure 4.10. *^{1}H NMR spectra of [2]rotaxane **4.4** upon addition of 1, 5 and 10 equivalents of TBACl (500 MHz, 298 K, 95:5-d_6-acetone-D_2O). Inset: Binding isotherms showing changes in chemical shift of internal benzene proton b upon increasing equivalents of various anions.*

spacer proton H_2 indicative of binding occurring within the interlocked cavity of the [2]rotaxane *via* the macrocycle and squaramide NH donors (Figure 4.10). Notably, upon addition of oxoanions such as OAc^-, HSO_4^- and $H_2PO_4^-$ the proton peaks proximal to the anion binding site initially moved downfield until 0.8-1 equivalents before shifting upfield upon subsequent anion addition up to 10 equivalents, alluding to the existence of complex equilibria in the system (Figure 4.11, 4.12 and 4.13). This complex behaviour necessitated a more detailed study into the binding stoichiometries adopted by the interlocked host upon anion association.

To this end, five possible stoichiometric binding models including 1:1 and four variants of 1:2 host-guest binding models were considered for every anion titration, wherein the suitability of each binding model was determined through statistical analysis as detailed by Thordarson and co-workers.[265] Table 4.2 outlines the four complex 1:2 binding models based on the correlations between the step-wise binding constants, K_1 and K_2 and the induced chemical shifts upon formation of 1:1 and 1:2 complexes, δ_1 and δ_2 respectively.

Table 4.2: *Possible stoichiometric anion binding models for [2]rotaxanes* ***4.4*** *and* ***4.5*** *and the difference in their respective relationships between K_1, K_2, δ_1 and δ_2.[a]*

Binding models (Host: Guest)	**Relationship between K_1 and K_2**	**Relationship between δ_1 and δ_2**
1:1	Not applicable[b]	Not applicable[b]
1:2 (Full)	$K_1 \neq 4K_2$	$\delta_2 \neq 2\delta_1$
1:2 (Non-cooperative)	$K_1 = 4K_2$	$\delta_2 \neq 2\delta_1$
1:2 (Additive)	$K_1 \neq 4K_2$	$\delta_2 = 2\delta_1$
1:2 (Statistical)	$K_1 = 4K_2$	$\delta_2 = 2\delta_1$

[a] K_1 and K_2 represent the step-wise binding constants and δ_1 and δ_2 represent the chemical shifts induced by the formation of 1:1 and 1:2 stoichiometric host-guest complexes respectively. [b] Only K_1 and δ_1 are involved in 1:1 binding.

Monitoring the perturbations of the proton resonances near the anion binding site resulted in titration isotherms which were fitted to each of the five binding models using Bindfit.[237] Accordingly, the covariance fit values of each model to the measured isotherms (Cov_{fit}) were obtained and the corresponding covariance fit factors (Cov_{fit} factor) were determined. Wherein Cov_{fit} factor was defined as the ratio of the Cov_{fit} value generated for a simple 1:1 binding model to the Cov_{fit} value generated for the various 1:2 binding models. As per Thordarson, the lower the value of Cov_{fit}, the higher the corresponding Cov_{fit} factor value, and better the quality of the fit. This analysis however requires certain considerations to be taken in order to judge the suitability of each model including the number of fitted parameters employed, practical feasibility of the obtained binding constants and their associated errors etc. Therefore, it was concluded that, for a complex binding model to be applicable, its Cov_{fit} factor value would have to be significantly higher than that of the simple 1:1 binding model (i.e., Cov_{fit} factor > 10).

Table 4.3 shows the apparent anion association constants, the number of involved fitted parameters and the calculated Cov_{fit} and Cov_{fit} factor values acquired by fitting the binding data of [2]rotaxane **4.4** to the different binding models. In accordance with the trends witnessed during spectral analysis, the majority of the anions were determined to bind to [2]rotaxane **4.4** in a 1:1 stoichiometry, whereas the OAc^-, HSO_4^- and $H_2PO_4^-$oxoanion binding isotherms fit best to a 1:2 binding model. Interestingly, in the case of acetate anion the Cov_{fit} values of the 1:2 (Full) and 1:2 (Non-cooperative) binding models were 17- and 12-times lower than the Cov_{fit} value of the 1:1 model, indicating that both models could be considered appropriate descriptors of the binding data. It is important to note here however, that between the two likely models, although the 1:2 Full model with its higher Cov_{fit} factor value suggests that it fits the data better, the possibility that the elevated value might just be an

artifact of the model incorporating a higher number of fitted parameters makes it difficult to conclusively ascertain the exact binding mode adopted by the receptor. Therefore, both 1:2 (Full) and 1:2 (Non-cooperative) models were considered while describing the binding of acetate. Alternatively, for HSO_4^- and $H_2PO_4^-$, both anions showed a preference for the 1:2 (Non-cooperative) binding model, rationalised by the unsuitable association constants attained with the other models. Intriguingly, the binding data also suggests that while the smaller carboxylate anion acetate binds to the receptor *via* a 1:2 binding mode, the larger benzoate anion prefers a 1:1 binding mode.

Table 4.3: *Anion association constants (K_a/M^{-1}) for [2]rotaxane **4.4** [1.0 mM] in 95:5-d_6-acetone-D_2O at 298 K.*[a]

Anion	Binding Model (Host: Guest)	No. of fitted parameters	K_1 (M^{-1})	K_2 (M^{-1})	Cov_{fit} (x 10^{-3})	Cov_{fit} factor [b]
Cl^-	**1:1**	**3**	**556**	**-**	**0.204**	**1**
	1:2 (Full)	5	2653	345	0.141	1.4
	1:2 (Non-cooperative)	4	1078	270	0.161	1.3
	1:2 (Additive)	4	2278	333	0.150	1.3
	1:2 (Statistical)	3	2193	-	0.384	0.5
Br^-	**1:1**	**3**	**226**	**-**	**0.315**	**1**
	1:2 (Full)	5	4718(11)	190	0.184	1.7
	1:2 (Non-cooperative)	4	615	154	0.204	1.5
	1:2 (Additive)	4	621	147	0.288	1.0
	1:2 (Statistical)	3	629	-	0.291	1.0
I^-	**1:1**	**3**	**35**	**-**	**6.327**	**1**
	1:2 (Full)	5	7225(120)	71	5.226	1.2
	1:2 (Non-cooperative)	4	480	120	5.363	1.2
	1:2 (Additive)	4	170(14)	172(20)	5.5	1.1
	1:2 (Statistical)	3	76	-	6.309	1.0
NO_3^-	**1:1**	**3**	**42**	**-**	**4.929**	**1**
	1:2 (Full)	5	-	-	-	-
	1:2 (Non-cooperative)	4	186	47	4.901	1.0
	1:2 (Additive)	4	121	43(21)	4.909	1.0
	1:2 (Statistical)	3	92	-	4.926	1.0
	1:1	**3**	**124**	**-**	**0.957**	**1**
	1:2 (Full)	5	740	54	0.877	1.0

NO_2^-	1:2 (Non-cooperative)	4	213	53	0.992	0.9
	1:2 (Additive)	4	206	25	0.914	1.0
	1:2 (Statistical)	3	303		1.024	0.9
OBz^-	**1:1**	**3**	**701**	**-**	**0.886**	**1**
	1:2 (Full)	5	2202	210	0.111	7.9
	1:2 (Non-cooperative)	4	1051	263	0.376	2.3
	1:2 (Additive)	4	845	10(31)	0.835	1.0
	1:2 (Statistical)	3	2997	-	2.185	0.4
OAc^-	1:1	3	365	-	9.25	1
	1:2 (Full)	**5**	**3279(10)**	**232**	**0.557**	**17**
	1:2 (Non-cooperative)	**4**	**996**	**249**	**0.760**	**12**
	1:2 (Additive)	4	1094(24)	175(27)	9	0.9
	1:2 (Statistical)	3	1172	-	10	0.9
HSO_4^-	1:1	3	-	-	-	-
	1:2 (Full)	5	5(24)	$> 10^6$ (22)	29.017	-
	1:2 (Non-cooperative)	**4**	**5533(23)**	**1383**	**34.436**	**-**
	1:2 (Additive)	4	2912(49)	<0	164.5	-
	1:2 (Statistical)	3	2(>10^7)	-	504.4	
$H_2PO_4^-$	1:1	3	183	-	14	1
	1:2 (Full)	5	-	54	0.877	15
	1:2 (Non-cooperative)	**4**	**3627**	**53**	**0.971**	**14**
	1:2 (Additive)	4	5(>10^3)	>10^5	1.4	9.6
	1:2 (Statistical)	3	516	-	12	1.1

[a] Step-wise K_1 and K_2 values calculated using Bindfit[237] with different binding models by monitoring squaramide proton H_b. All anions added as their TBA salts; Error percentages less than 10% unless specified. [b] Cov_{fit} factor = Cov_{fit} of 1:1 binding model divided by the Cov_{fit} of the respective model. Binding models best fitted for the titration isotherms are highlighted in red.

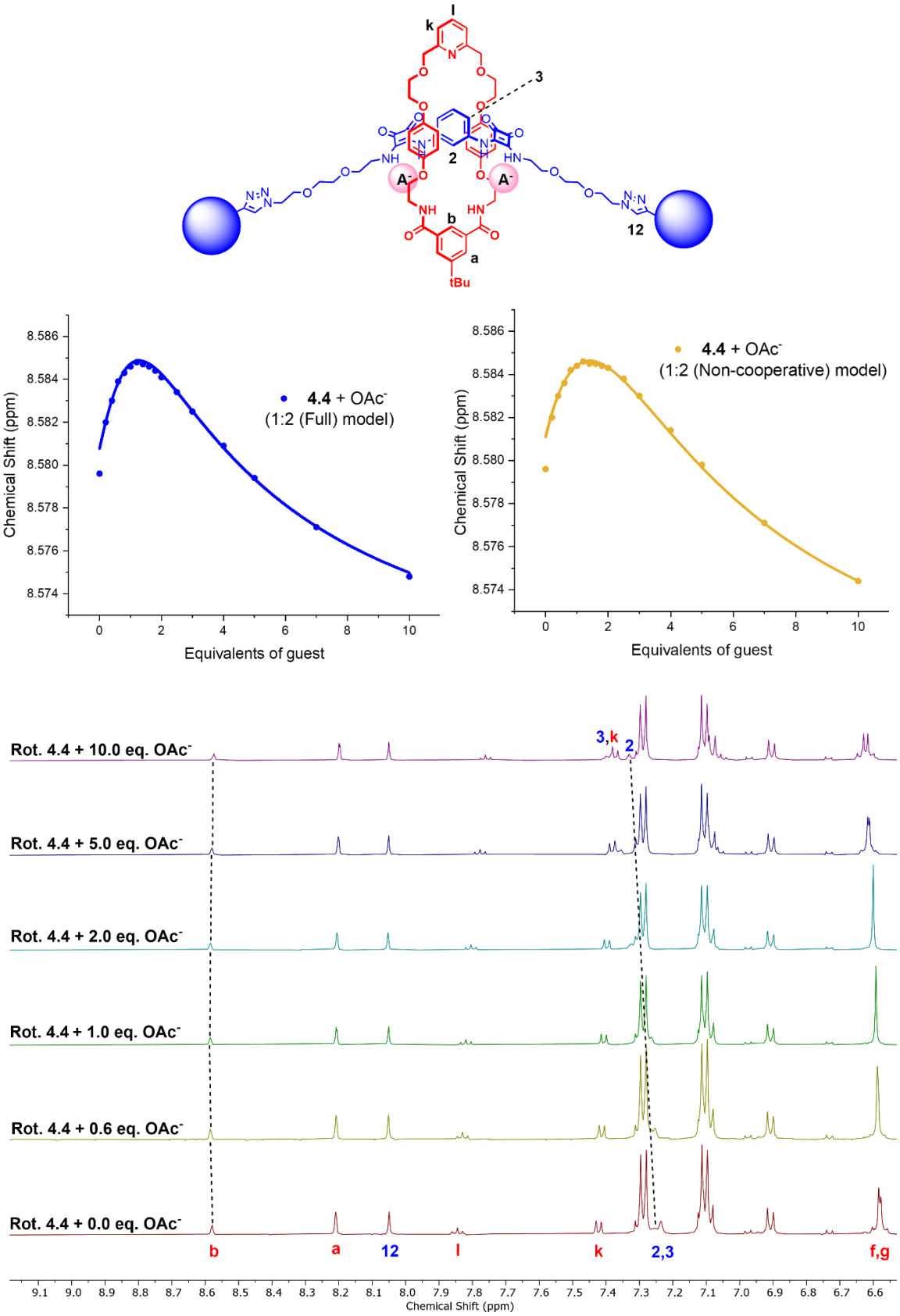


Figure 4.11. *^{1}H NMR spectra of [2]rotaxane **4.4** upon addition of 1, 5 and 10 equivalents of TBAOAc (500 MHz, 298 K, 95:5-d_6-acetone-D_2O). Inset: Binding isotherms fitted to a 1:2 (Full) model and 1:2 (Non-cooperative) model, showing changes in chemical shift of internal benzene proton b upon increasing equivalents of acetate anions.*

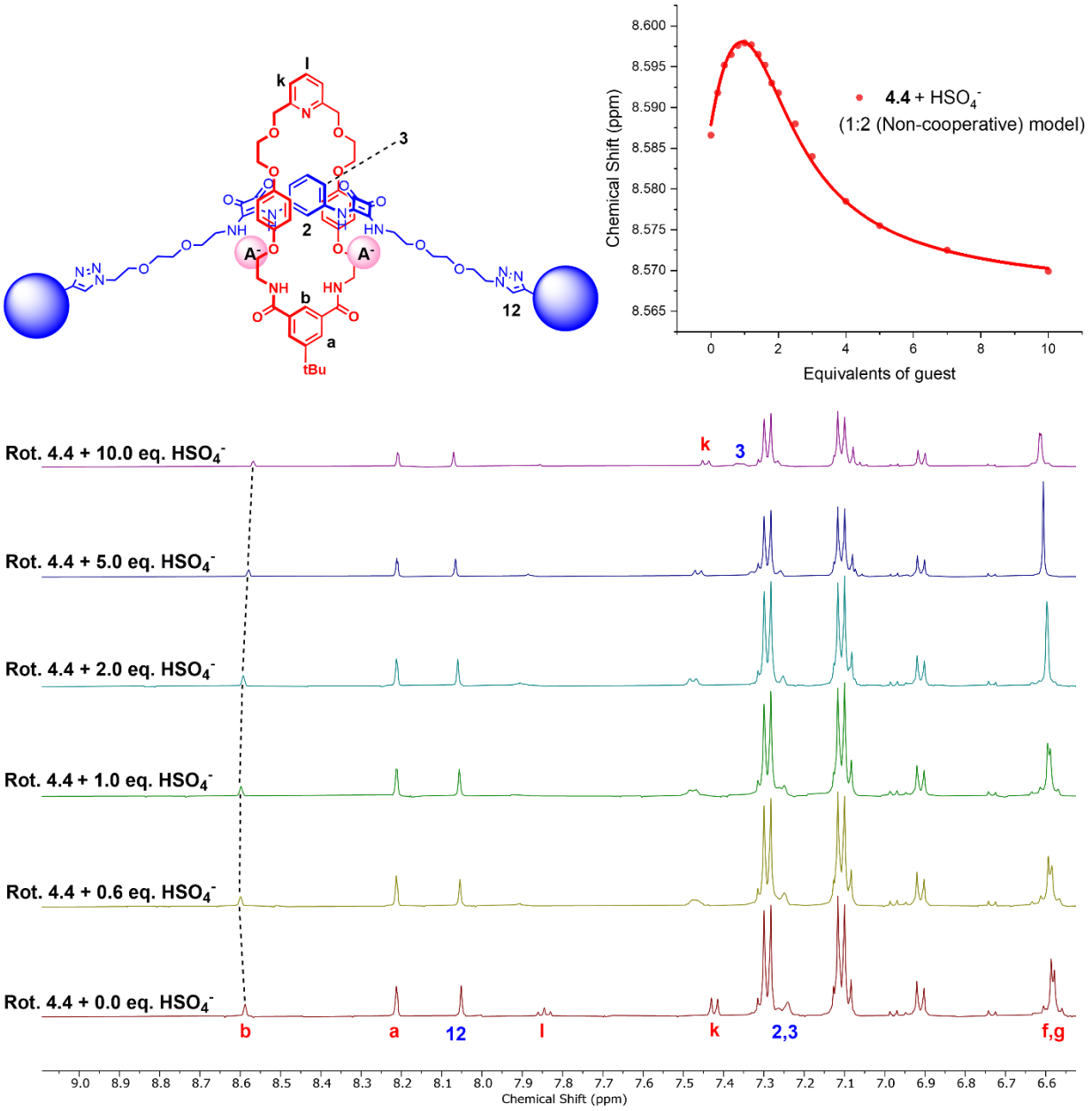


Figure 4.12. *^{1}H NMR spectra of [2]rotaxane **4.4** upon addition of 1, 5 and 10 equivalents of $TBAHSO_4$ (500 MHz, 298 K, 95:5-d_6-acetone-D_2O). Inset: Binding isotherm fit to a 1:2 (Non-cooperative) model, showing changes in chemical shift of internal benzene proton b upon increasing equivalents of hydrogen sulfate anions.*

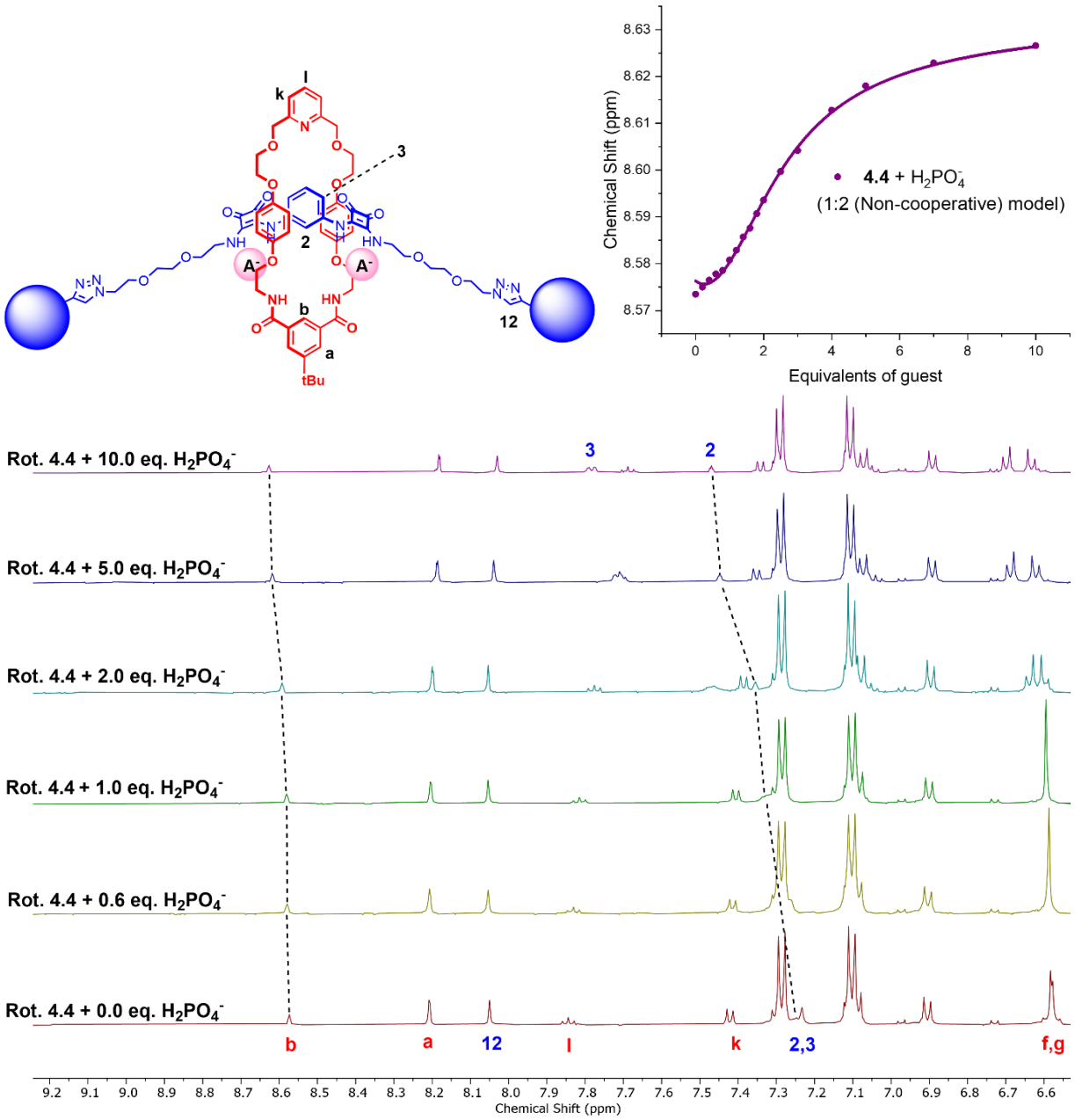


Figure 4.13. *^{1}H NMR spectra of [2]rotaxane **4.4** upon addition of 1, 5 and 10 equivalents of $TBAH_2PO_4$ (500 MHz, 298 K, 95:5-d_6-acetone-D_2O). Inset: Binding isotherm fit to a 1:2 (Non-cooperative) model, showing changes in chemical shift of internal benzene proton b upon increasing equivalents of dihydrogen phosphate anions.*

Having established the binding models and stoichiometries of each anion for [2]rotaxane **4.4**, the affinities of the various anions for mono-squaramide functionalised rotaxane **3.14** and bis-squaramide functionalised rotaxane **4.4** were compared (Table 4.4). Inspection of the binding data for bis-squaramide [2]rotaxane **4.4** reveals a considerable

amplification in anion binding affinities across the board relative to the control mono-squaramide [2]rotaxane **3.14**, highlighting the advantages of incorporating potent multi-squaramide HB donor binding sites into MIM host design. In general, the binding trends observed for [2]rotaxane **4.4** suggest that amongst the halides the receptor exhibits a selectivity for the charge dense chloride with a *ca.* 6-fold enhancement observed in the case of both chloride and bromide association constants relative to the control rotaxane **3.14**. Meanwhile in the case of the oxoanions, by adopting a more complex binding mode, the receptor is able to achieve a dramatic increase in K_1 for anions $H_2PO_4^-$ (*ca.* 95-fold), HSO_4^- (*ca.* 25-fold) and OBz^- (*ca.* 15-fold), while displaying a modest preference for HSO_4^-. Furthermore, as witnessed in the case of [2]rotaxane **3.14**, an anti-Hofmeister bias towards anion binding is observed with [2]rotaxane **4.4** as well. In order to confirm that this trend was indeed a mechanical bond effect, preliminary anion binding studies were also attempted with the axle component of [2]rotaxane **4.4** under analogous conditions. However, poor solubility of the axle in the chosen solvent media precluded such investigations.

Table 4.4: *Anion association constants K_a (M^{-1}) for [2]rotaxane **3.14** and **4.4** [1.0 mM] in 95:5-d_6-acetone-D_2O at 298 K.*[a]

Anion	[2]Rot. **3.14**		[2]Rot. **4.4**		
	Binding model (Host: Guest)	***K_1* (M^{-1})**	**Binding model (Host: Guest)**	***K_1* (M^{-1})**	***K_2* (M^{-1})**
Cl^-	1:1	90	1:1	574	-
Br^-	1:1	34	1:1	225	-
I^-	-	-[b]	1:1	35	-
NO_3^-	-	-[b]	1:1	42	-
NO_2^-	-	-[b]	1:1	124	-

OBz^-	1:1	46	1:1	701	-
OAc^-	**1:1**	**317**	1:2 (Full)	3279 (10)	232
			1:2 (Non-cooperative)	996	249
HSO_4^-	1:1	223	**1:2 (Non-cooperative)**	**5533 (23)**	**1383**
$H_2PO_4^-$	1:1	38	1:2 (Non-cooperative)	3627	906

[a] K_a values calculated using Bindfit[237] software using a 1:1 host-guest binding model by monitoring internal benzene proton H_b. All anions added as their TBA salts. Error percentages less than 10% unless specified. [b] = No binding. Anion with the highest association constant is highlighted in red.

4.4.3 Quantitative ^{1}H NMR anion binding titration studies with [2]rotaxane **4.5**

Analogous ^{1}H NMR anion binding studies were conducted with [2]rotaxane **4.5** under identical titration conditions. Upon increasing anion concentration, the downfield shifts in the internal benzene proton of the macrocycle H_b and the axle spacer proton H_2 indicated that *all* anions bind within the interlocked cavity of the [2]rotaxane (Figure 4.14). Additionally notable perturbations in the proton resonances of the triazole units and neighbouring methylene protons were observed, suggesting their proximity to the binding cavity and potential assistance in anion recognition. Such behaviour was consistent with the previously discussed ^{1}H-^{1}H ROESY NMR results which had revealed through-space interactions between the protons in the vicinity of the triazoles and the protons neighbouring the squaramide units in the axle. The determined binding constants were calculated with Bindfit[237] using a 1:1 stoichiometric host-guest binding model and are summarised in Table 4.5.

Analysis of the acquired binding data revealed that contrary to what was observed with [2]rotaxane **4.4**, oxoanions $H_2PO_4^-$, OAc^- and HSO_4^- also bound to [2]rotaxane **4.5** *via* a

1:1 binding mode. Furthermore, owing to the complex anion binding behaviour displayed by the bis-squaramide rotaxane **4.4**, all obtained anion isotherms with rotaxane **4.5** were also attempted to be fitted to the various 1:2 models, none of which fit the data as well as the simple 1:1 model.

Table 4.5: *Anion association constants K_a (M^{-1}) for [2]rotaxane **3.14**, **4.4** and **4.5** [1.0 mM] in 95:5-d_6-acetone-D_2O at 298 K.*[a]

Anion	[2]Rot. **3.14**		[2]Rot. **4.4**			[2]Rot. **4.5**	
	Binding model (Host: Guest)	***K_1 (M^{-1})***	**Binding model (Host: Guest)**	***K_1 (M^{-1})***	***K_2 (M^{-1})***	**Binding model (Host: Guest)**	***K_1 (M^{-1})***
Cl^-	1:1	90	1:1	574	-	1:1	621
Br^-	1:1	34	1:1	225	-	1:1	226
I^-	-	-[b]	1:1	35	-	1:1	58
NO_3^-	-	-[b]	1:1	42	-	1:1	130
NO_2^-	-	-[b]	1:1	124	-	1:1	160
OBz^-	1:1	46	1:1	701	-	**1:1**	**916**
OAc^-	**1:1**	**317**	1:2 (Full)	3279 (10)	232	1:1	668
			1:2 (Non-cooperative)	996	249		
HSO_4^-	1:1	223	**1:2 (Non-cooperative)**	**5533 (23)**	**1383**	1:1	224
$H_2PO_4^-$	1:1	38	1:2 (Non-cooperative)	3627	906	1:1	451

[a] K_a values calculated using Bindfit[237] software using a 1:1 host-guest binding model by monitoring internal benzene proton H_b. All anions added as their TBA salts. Error percentages less than 10% unless specified. [b] = No binding. Anion with the highest association constant is highlighted in red.

This difference in the stoichiometric oxoanion binding mode may be attributed to the greater flexibility of the axle propyl alkyl spacer motif between the squaramide motifs in [2]rotaxane **4.5**, allowing the MIM host system to accommodate these anions within the cavity of the rotaxane. As expected, the anion binding affinities of [2]rotaxane **4.5** were strikingly higher than those obtained with the control rotaxane **3.14** (*ca.* 20- and 12-fold higher in the case of OBz^- and $H_2PO_4^-$ respectively) owing to the presence of additional squaramide NH donors within the axle component Interestingly, the magnitudes of 1:1 K_1 anion binding constants for [2]rotaxane **4.5** were also higher than those obtained with [2]rotaxane **4.4**. In general, analogous to the binding trends obtained with [2]rotaxane **4.4**, receptor **4.5** also demonstrates a preference for chloride over the heavier halides, displaying a 7-fold enhancement in the chloride binding affinity compared to the control rotaxane **3.14**. Notably, amongst the oxoanions, benzoate is bound the strongest exhibiting a striking 20-fold enhancement in anion association relative to [2]rotaxane **3.14**, suggesting size complementarity (Figure 4.15). Furthermore, the obtained binding data also suggested an anti-Hofmeister bias being brought about by [2]rotaxane **4.5** similar to what was seen with the other rotaxanes. As observed with the axle component of rotaxane **4.4**, poor solubility of the corresponding axle component of [2]rotaxane **4.5** precluded the calculation of anion binding affinities under analogous conditions.

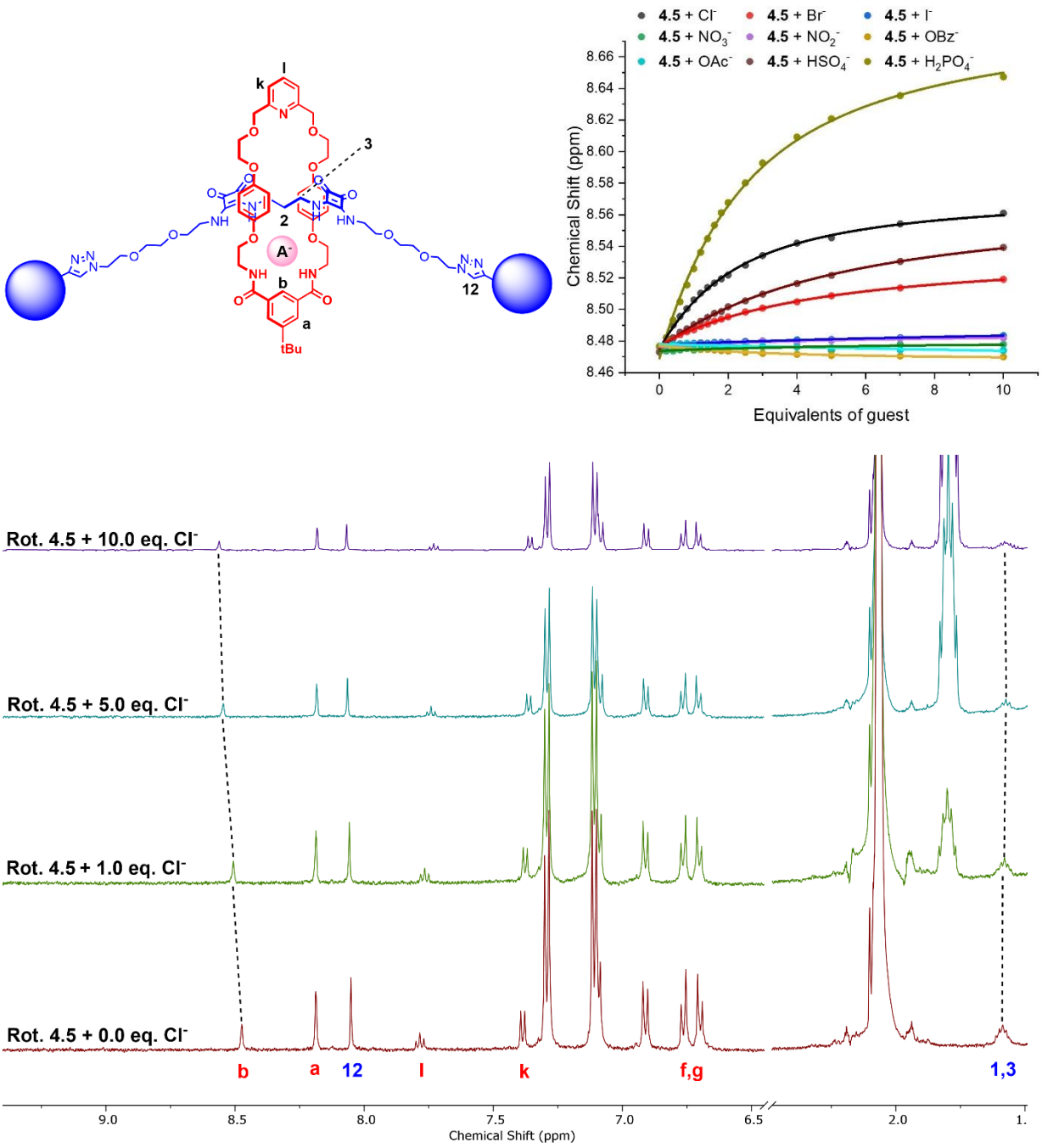


Figure 4.14. *^{1}H NMR spectra of [2]rotaxane **4.5** upon addition of 1, 5 and 10 equivalents of TBACl (500 MHz, 298 K, 95:5-d_6-acetone-D_2O). Inset: Binding isotherms showing changes in chemical shift of internal benzene proton b upon increasing equivalents of various anions.*

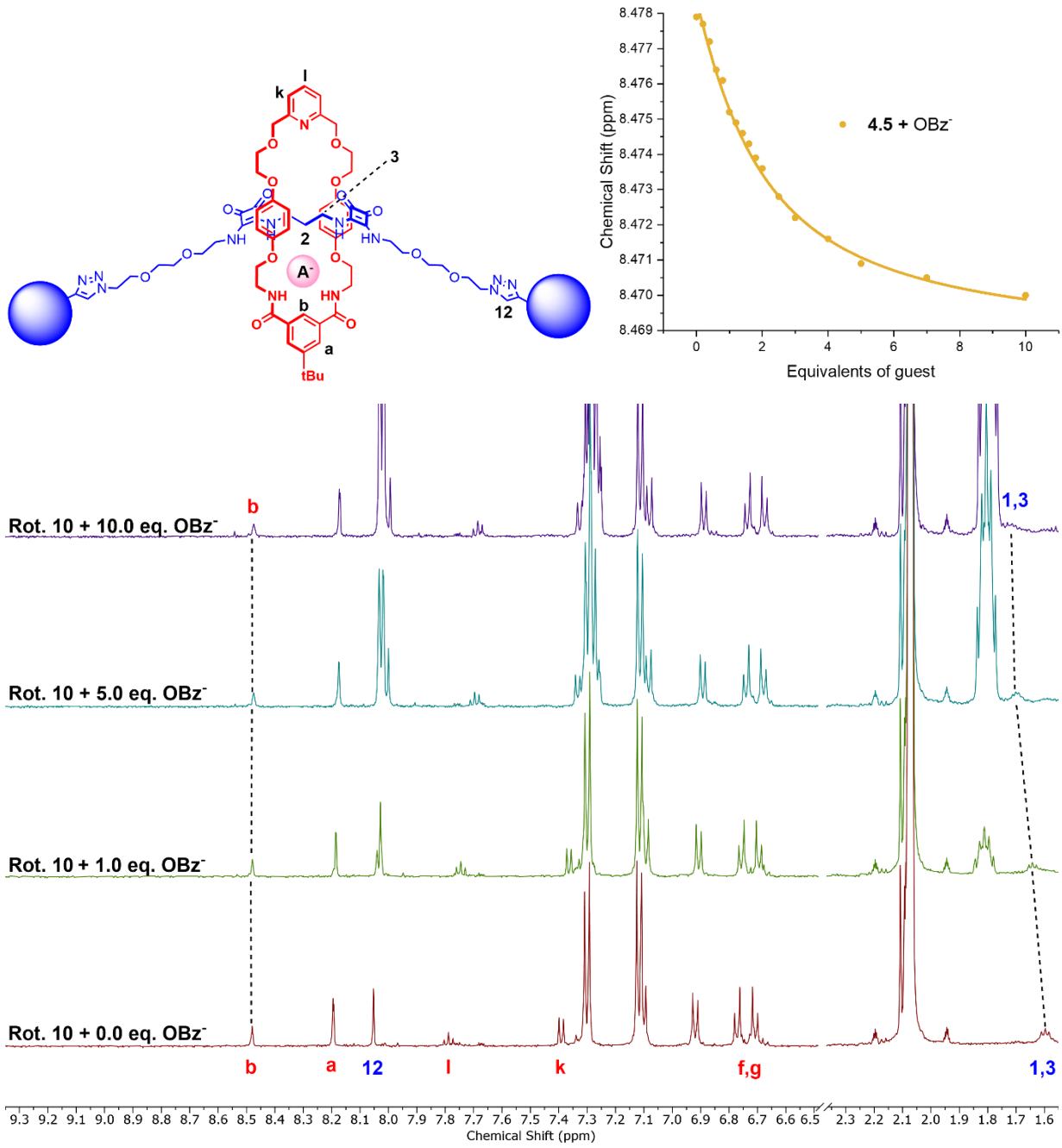


Figure 4.15. *^{1}H NMR spectra of [2]rotaxane **4.5** upon addition of 1, 5 and 10 equivalents of TBAOBz (500 MHz, 298 K, 95:5-d_6-acetone-D_2O). Inset: Binding isotherms showing changes in chemical shift of internal benzene proton b upon increasing equivalents of benzoate anions.*

4.5 Conclusions and Future work

In conclusion, two novel neutral bis-squaramide functionalised [2]rotaxanes were synthesised using active metal template methodology. Extensive ^{1}H NMR anion titration studies in

aqueous-organic mixtures demonstrated that introduction of a second squaramide unit into the respective rotaxane's axle component resulted in significant amplification in anion binding affinity, with the largest enhancement witnessed in the case of the benzoate anion, *ca.* 15- and 20-fold with rotaxanes **4.4** and **4.5** respectively.

Notably, propyl spacer containing [2]rotaxane **4.5** bound all anions *via* a 1:1 host-guest binding stoichiometry as opposed to the aryl spacer containing rotaxane **4.4** which displayed a 1:2 binding mode for oxoanion recognition, emphasising the advantages of designing flexible receptor binding cavities enabling effective sequestration of a diverse range of anions. Moreover, the effects of this flexibility-driven preorganization in [2]rotaxane **4.5** was further evident through its higher 1:1 anion binding affinities compared to [2]rotaxane **4.4** with the aryl spacer functionalization. Importantly, an anti-Hofmeister bias towards anion recognition was observed for both rotaxane systems in aqueous-organic media, a rare phenomenon brought into effect by a combination of the MIM hydrophobic cavity and strong HB donor binding capabilities of the bis-squaramide axle components.

Future work for this project would involve carrying out molecular modelling studies with the bis-squaramide [2]rotaxanes to help elucidate the various MIM host-anion guest binding modes observed during ^{1}H NMR based host-guest recognition studies. Furthermore, the results of this chapter indicate that exploiting cooperative binding effects instigated by incorporating multiple HB donor units can produce potent and effective neutral anion receptors capable of functioning in aqueous containing media. Future efforts can be directed towards the incorporation of XB sigma-hole donor units into the rotaxane's macrocycle component which are known to demonstrate enhanced anion affinities and selectivity trends over their HB analogues in polar protic and aqueous solvent media (Figure 4.16).

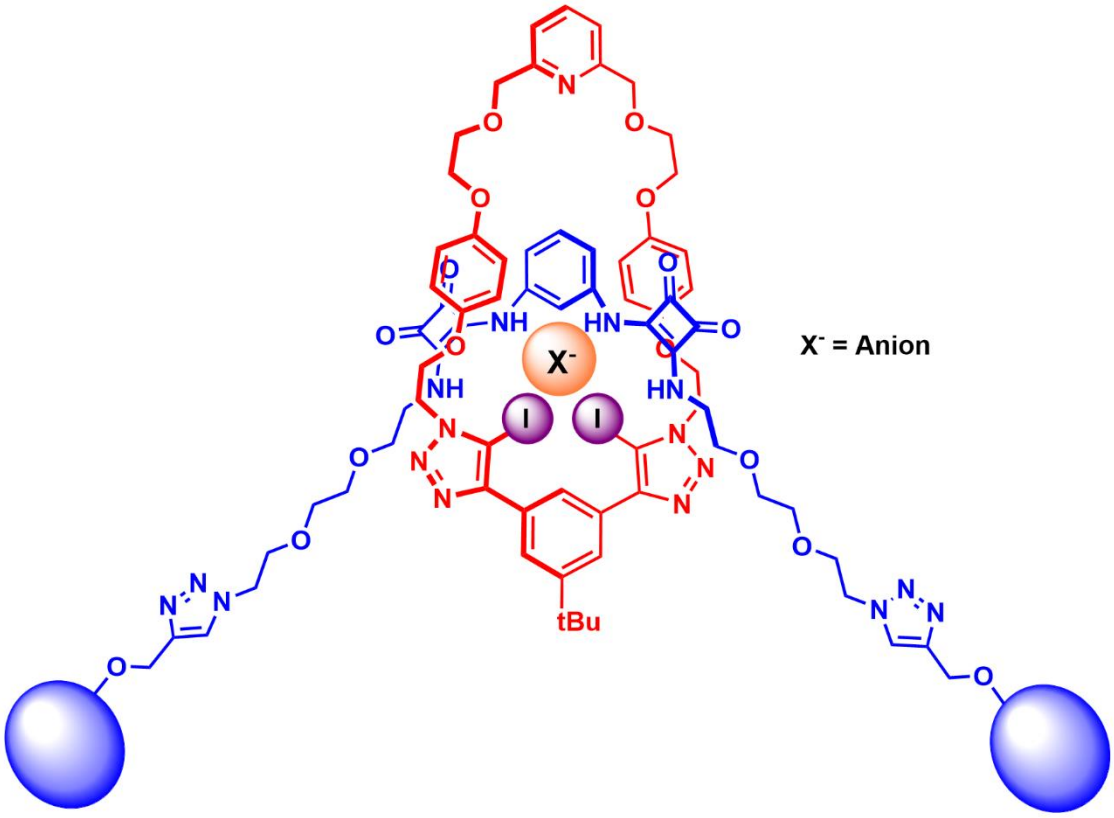


Figure 4.16. *A bis-squaramide functionalised XB [2]rotaxane.*

Chapters 2 and 3 have demonstrated that squaramide based interlocked receptors can facilitate potent ambidentate ion-pair binding. In light of the promising anion binding affinities witnessed with the bis-squaramide receptors in this chapter, future work could also involve investigating the ion-pair binding capabilities of rotaxanes **4.4** and **4.5** in polar solvent systems (Figure 4.17).

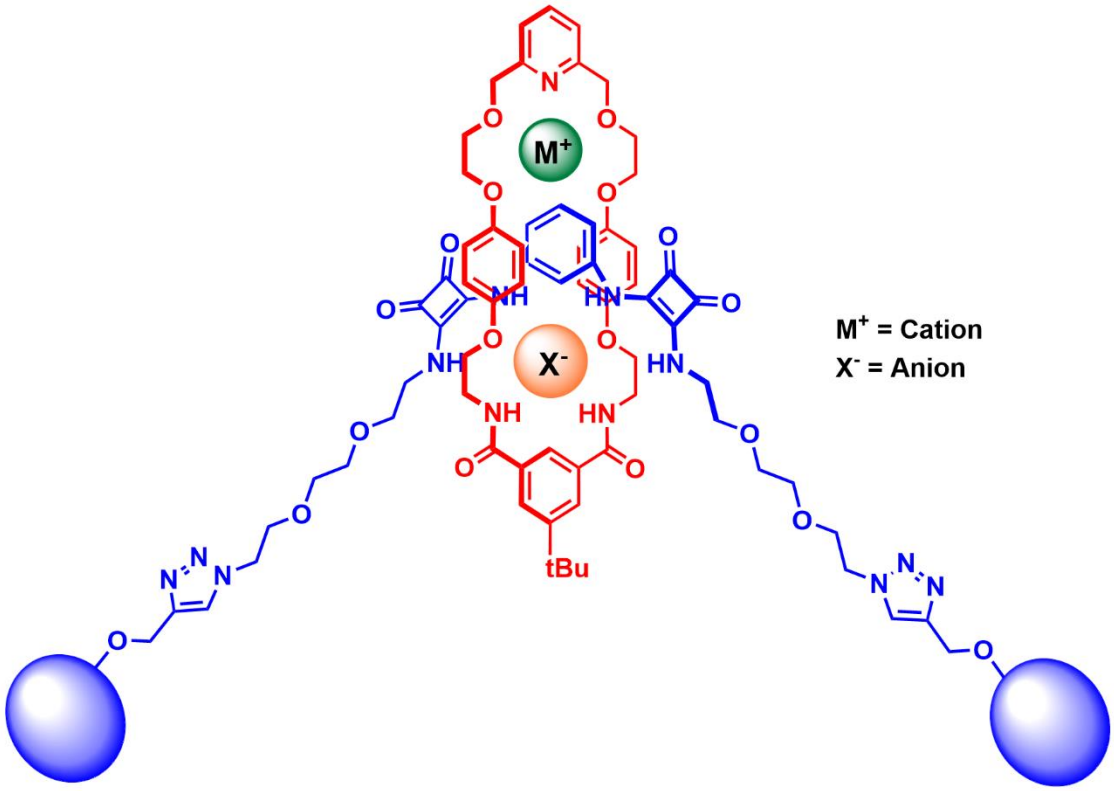


Figure 4.17. *Ion-pair recognition using bis-squaramide functionalised [2]rotaxane.*

Chapter 5: Conclusions and Future Work

The work detailed in this thesis sought to exploit the potency of squaramide HB donor motifs when incorporated into mechanically interlocked rotaxane structural frameworks for applications in host-guest anion and ion-pair recognition in polar organic and aqueous/organic solvent mixtures.

Chapter 2 investigated the active metal template synthesis of a series of novel squaramide-based axle containing heteroditopic [2]rotaxanes containing XB and HB anion binding donors for lithium halide ion-pair recognition (Figure 5.1). Extensive cation, anion and ion-pair ^{1}H NMR titration studies in 3:7 $CD_3CN/CDCl_3$ solvent media demonstrated that a co-bound lithium metal cation evoked notable enhancements of halide binding strengths of the [2]rotaxane receptors, highlighting the advantages of positive cooperative electrostatic effects instigated by heteroditopic MIM host design. Importantly, XB functionalised receptors exhibited superior anion and ion-pair binding affinities in comparison to their HB rotaxane analogues, impressively even binding the LiCl ion-pair and underpinning the improved selectivity and binding profiles offered by sigma-hole XB systems. Introduction of a coumarin motif in the axle component unfortunately led to a diminution in halide binding affinity, possibly due to competing coumarin-based intercomponent MIM HB interactions and steric inaccessibility of the anion binding site, consistent with the larger halide anions preferring an exotopic coordination mode. Qualitative optical sensing studies conducted with the coumarin-based [2]rotaxanes under analogous solvent conditions showed significant ion-pair binding mediated perturbations in the absorbance and fluorescence properties of the coumarin receptors, suggesting promising prospects in the development of future MIM-based heteroditopic optical sensors. Preliminary solid-liquid extraction studies revealed all four rotaxanes extracted LiBr into organic media in addition to XB rotaxanes also successfully extracting the LiCl ion-pair.

Future work for this project could entail integrating other sigma-hole donors such as chalcogen and pnictogen bonding motifs in addition to incorporating fluorophores like BODIPY units into these heteroditopic MIM structures to evaluate their ion-pair binding and sensing properties *via* solution-based NMR and fluorescence studies.

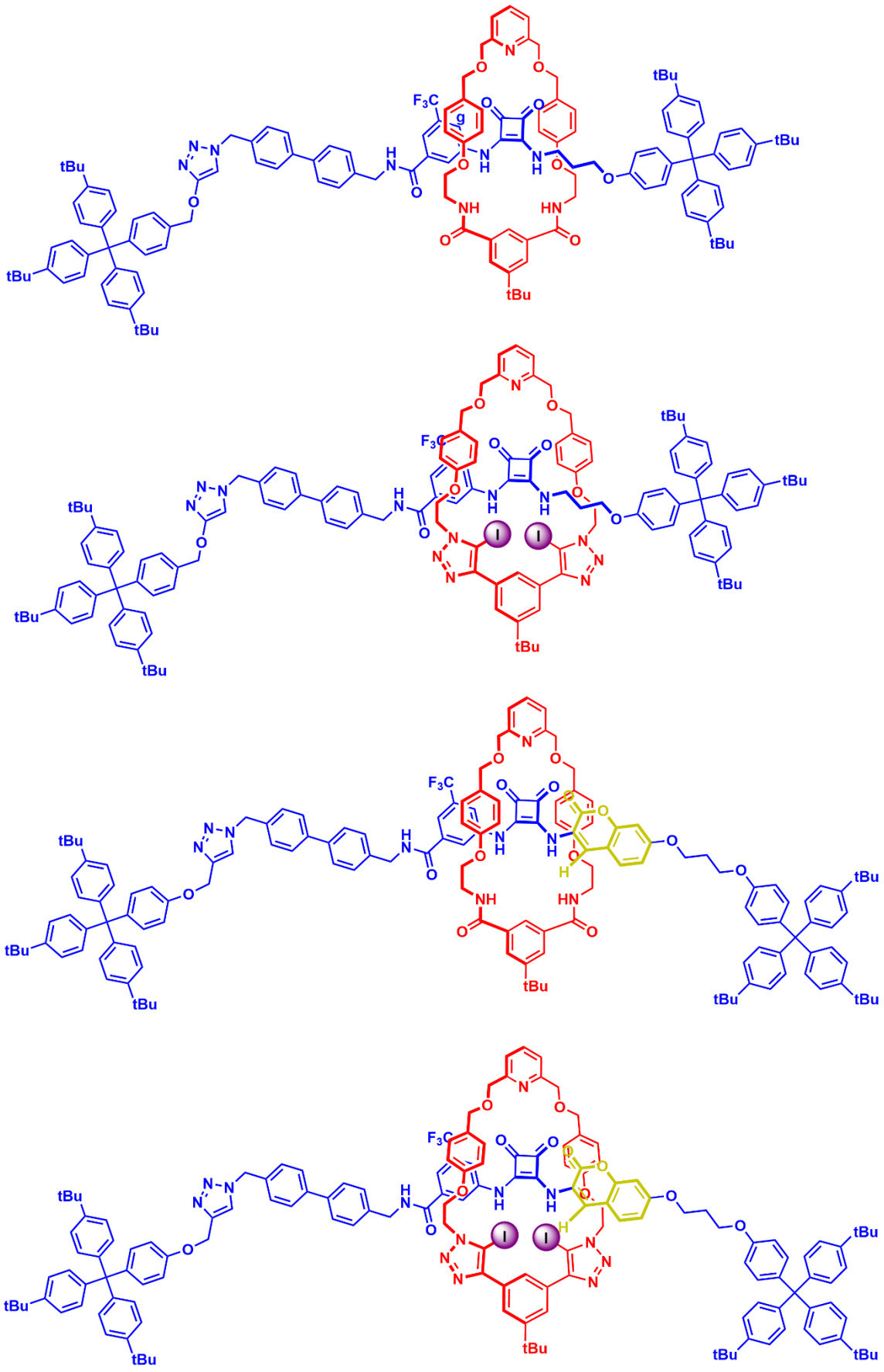


Figure 5.1. *HB and XB functionalised squaramide-based [2]rotaxanes synthesised in Chapter 2.*

Chapter 3 described the preparation of a series of squaramide containing heteroditopic [2]rotaxanes using an unprecedented sodium cation template-directed MIM synthesis exploiting Lewis basic squaramide carbonyl alkali metal cation coordination (Figure 5.2). Quantitative ^{1}H NMR host-guest titration studies in 3:7 $CD_3CN/CDCl_3$ solvent media revealed that the presence of a co-bound sodium cation resulted in a *ca.* 20-fold enhancement in bromide and iodide binding affinities of these heteroditopic MIM receptors, highlighting the advantages of mechanical bond-induced cooperativity in ion-pair recognition. Notably, in the presence of sodium, all receptors exhibited impressive bromide selectivity.

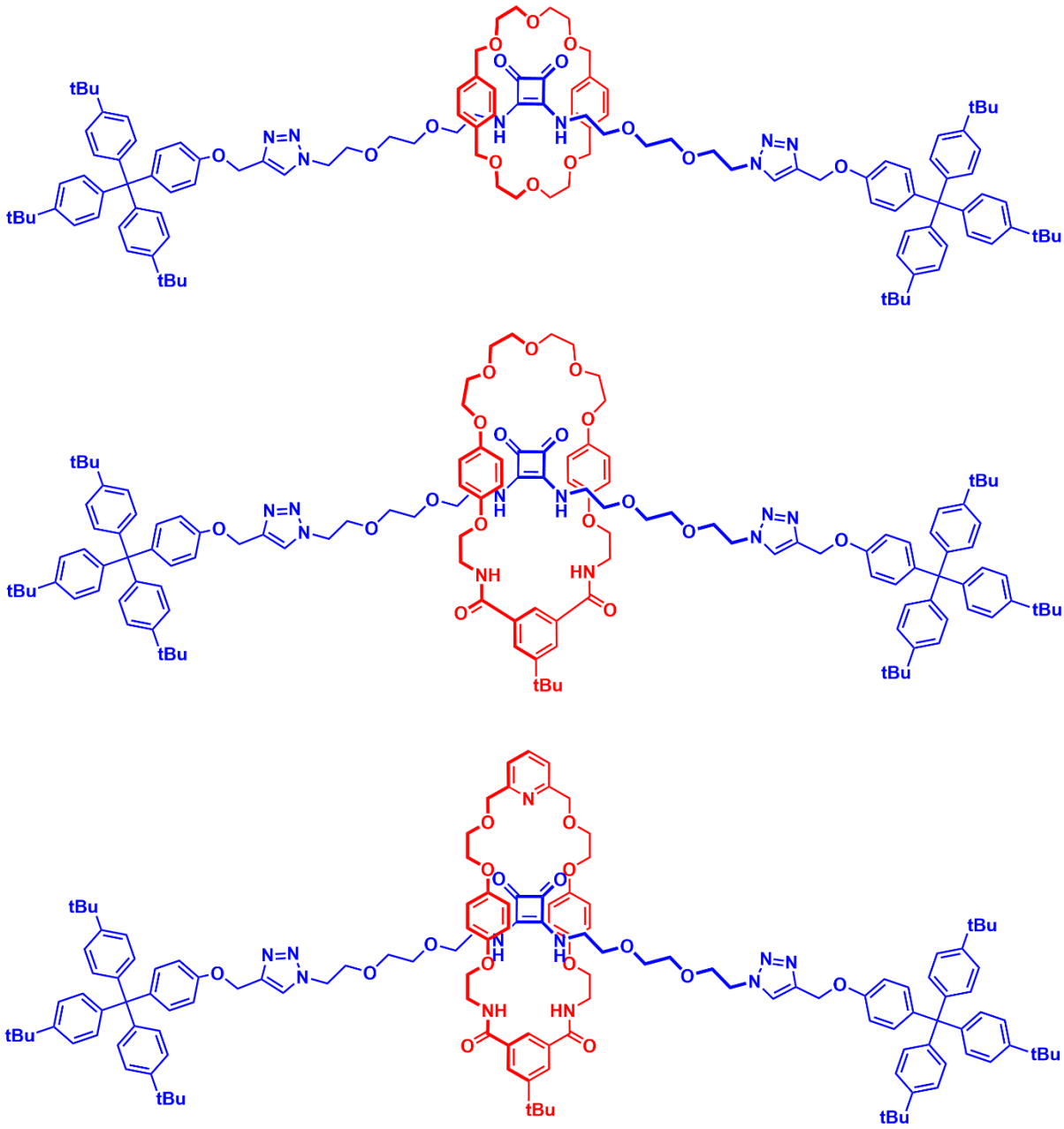


Figure 5.2. *Squaramide-based [2]rotaxanes synthesised in Chapter 3.*

Amongst the rotaxane systems studied in this chapter, only the receptor furnished with a pyridyl-isophthalamide macrocyclic component was successful in binding the NaCl ion-pair, underpinning the importance of strong concomitant cation and anion association in overcoming competing lattice enthalpies to achieve ion-pair recognition. Furthermore, preliminary solid sodium halide salt-liquid extraction studies evinced the ability of all MIM receptor systems to extract NaBr and NaI into organic media, in line with their solution phase ion-pair recognition properties.

Future work for this chapter could again involve introducing sigma hole donor groups into these receptors. Additionally, the novel sodium templated methodology may be extended to synthesise [2]catenane heteroditopic host structures.

Chapter 4 presented two novel bis-squaramide functionalised axle component containing [2]rotaxanes, synthesised using active metal template methodology (Figure 5.3). Anion ^{1}H NMR titration studies conducted in aqueous-organic mixtures (95:5 d_6-acetone/D_2O) showed the introduction of a second squaramide unit into the respective rotaxane's axle component significantly augmented their anion binding affinity, with the largest enhancement witnessed

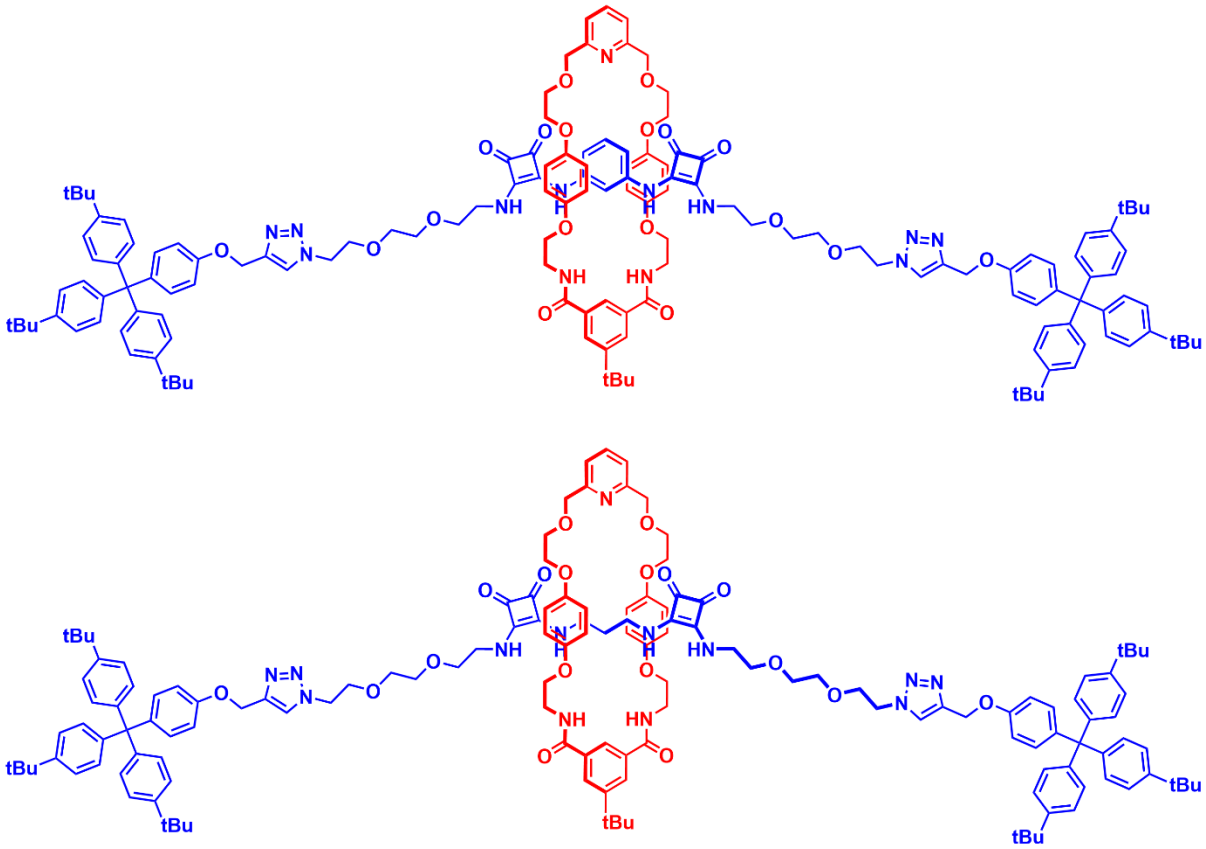


Figure 5.3. *Bis-squaramide based [2]rotaxanes synthesised in Chapter 4.*

in the case of the benzoate anion, attributed to size complementarity with the multi-donor amide-based MIM donor cavity. Interestingly, the flexible propyl spaced bis-squaramide axle containing [2]rotaxane bound all anions *via* a 1:1 host-guest binding stoichiometry. By contrast, the more rigid aryl phenyl linked bis-squaramide containing rotaxane displayed a 1:2 host-guest binding mode for oxoanion recognition, emphasising the advantages of designing flexible receptor binding cavities for the effective sequestration of a diverse range of anions. Notably the propyl spaced bis-squaramide axle containing [2]rotaxane proved to be the more potent anion host system. An anti-Hofmeister series bias towards anion recognition was observed for both rotaxane systems in aqueous-organic media, a rare phenomenon brought into effect by a combination of the MIM hydrophobic cavity and strong HB donor binding capabilities of the bis-squaramide axle components.

Further amplification of the cooperative anion binding effect brought about by incorporating multiple squaramide HB donor motifs could be achieved by furnishing the MIM receptors with sigma hole donors which are known to exhibit enhanced binding affinities in polar protic and aqueous media. Moreover, the presence of cation binding cavities in these bis-squaramide [2]rotaxane receptors offer potential avenues for future ion-pair binding investigations.

In summary, the results of this thesis underscore the exciting potential offered by the squaramide motif in mechanical bond host design, exploiting its unique ambidentate nature containing both preorganised Lewis acidic HB donors for anion binding and Lewis basic carbonyl moieties for alkali metal cation template directed MIM synthesis and cation recognition. Furthermore, incorporation of sigma-hole donor motifs is seen to significantly improve the anion guest-binding capabilities of the receptor systems paving the way for future mechanical bond heteroditopic receptor design. Integration of multiple squaramide donors into MIMs is also seen to enable remarkably high anion binding affinities in polar aqueous-organic mixtures, even bringing about a rare anti-Hofmeister anion binding trend.

Chapter 6: Experimental

6.1 General procedures

6.1.1 Materials and methods foy synthesis and characterisation

All commercial-grade chemicals and solvents were used without further purification unless otherwise mentioned. Where dry solvents were used, they were purged with N_2, dried by passing through an MBraun MPSP-800 column and then used immediately. The H_2O used was de-ionized and micro filtered using a Milli-Q® Millipore machine. Triethylamine was distilled over and stored over potassium hydroxide. TBTA (tris(benzyltriazolemethyl)amine) was synthesised[1] and stored at room temperature. TBA salts, catalyst $[Cu(CH_3CN)_4]PF_6$ were stored prior to use under vacuum in a desiccator containing phosphorus pentoxide and self-indicating silica gel. Cation salts used in titration experiments were dried on a high vacuum line prior to use. Aqueous ammonia ($NH_4OH_{(aq)}$) refers to an approximately 10% solution of NH_3 in water, brine refers to a saturated aqueous solution of NaCl, EDTA solution refers to a 0.02 M EDTA, 1% NH_3, aqueous. Thin layer chromatography (TLC) analysis was performed using Merck silica Kieselgel 60 F_{254} 0.25 mm, and Merck Alumina 60 $F_{254,}$ neutral with spots visualised under UV light (254 nm) and/ or staining with $KMnO_4$ solution (only for silica TLC). Column chromatography was performed using silica gel 60 (particle size 40-63 uM) and alumina gel (activated, neutral, Brockmann activity) under a positive N_2 head pressure. Preparatory TLC was carried out on 20 x 20 cm glass plates with 1 mm silica thickness.

6.1.2 Instrumentation

NMR spectra were recorded on Bruker AVIII HD Nanobay 400 MHz, Bruker AVIIIHD 500 MHz and Bruker NEO 600 with broadband helium cryoprobes. Chemical shifts are quoted in parts per million (ppm) relative to the residual solvent peak with signal splittings denoted as singlet

(s), doublet (d), triplet (t), quartet (quart.), quintet (quint.), septet (sep.) and multiplet (m); with broad peaks being denoted with (br).

Low resolution electrospray ionisation mass spectrometry (ESI-MS) was performed using the Waters Micromass LCT for characterisation of compounds previously reported in the literature, and high resolution ESI-MS (HRMS) was recorded using Bruker microTOF spectrometer for novel compounds. Absorption spectra were recorded on a Horiba Duetta™ spectrofluorometer whilst fluorescence spectra were recorded on a Horiba Duetta™ spectrofluorometer using a quartz cuvette with path length of 1 cm.

6.1.3 Solution-based studies

6.1.3.1 ^{1}H NMR titration studies

All deuterated solvents and tetrabutylammonium (TBA) salts used were purchased from chemical suppliers. All ^{1}H NMR titration experiments were performed on a Bruker AVIIIHD 500 MHz spectrometer. In a typical anion recognition experiment, a solution of the appropriate tetrabutylammonium (TBA) salt was added to 0.5 mL of a 1.0 mM solution of the receptor molecule at 298 K. Both TBA salt and receptor were dissolved in the same solvent mixture. TBA was chosen as the counter-cation due to its non-coordinating nature. 17 data points (0.00, 0.20, 0.40, 0.60, 0.80, 1.00, 1.20, 1.40, 1.60, 1.80, 2.00, 2.50, 3.00, 4.00, 5.00, 7.00, 10.00 equivalents) are obtained for each titration to ensure a good fit to the appropriate host-guest binding models.

For cation recognition titration experiments, aliquots of the appropriate cation salt ($LiClO_4$ or $NaBAr^F{}_4$) were added to a 0.5 mL of a 1.0 mM solution of the receptor. Both the receptor and cation salt were dissolved in the same solvent mixture. In the case of $LiClO_4$, 21 data points

(0.00, 0.10, 0.20, 0.30, 0.40, 0.50, 0.60, 0.70, 0.80, 0.90, 1.00, 1.10, 1.20, 1.30, 1.40, 1.50, 1.60, 1.70, 1.80, 1.90, 2.00) were collected. Poor solubility of $LiClO_4$ prevented addition of higher equivalents. As for $NaBAr^F{}_4$, 17 data points (0.00, 0.20, 0.40, 0.60, 0.80, 1.00, 1.20, 1.40, 1.60, 1.80, 2.00, 2.50, 3.00, 4.00, 5.00, 7.00, 10.00) were obtained.

For ion-pair recognition titration experiments, aliquots of the appropriate TBA salt were added to a solution of the receptor molecule pre-complexed with an equivalent of a suitable cation salt ($LiClO_4$ or $NaBAr^F{}_4$) at 298 K. Both TBA salts and pre-complexed receptors were dissolved in the same solvent media. 17 data points (0.00, 0.20, 0.40, 0.60, 0.80, 1.00, 1.20, 1.40, 1.60, 1.80, 2.00, 2.50, 3.00, 4.00, 5.00, 7.00, 10.00) are obtained for each titration to ensure a good fit to the appropriate host-guest binding models.

Before each titration and after each aliquot addition, the temperature of the solution in the NMR tube was allowed to equilibrate to room temperature before their ^1H NMR spectra was recorded. The values of the observed chemical shift and concentration of anion were entered into BindFit[240] or OriginLab for every titration point. Following initial estimates made of the limiting chemical shifts and binding constants, these parameters were refined using non-linear least-squares analyses to obtain the best fit between empirical and calculated chemical shifts based on a host-guest 1:1 or 1:2 binding stoichiometry (or otherwise stated). In all cases, convergence of the best fit values of the binding constants and their errors were obtained. In graphical binding isotherms, empirical data points are represented by the filled or hollow points, while continuous lines represent the calculated binding curves.

6.1.3.2 Optical studies

Optical studies were performed on a Horiba Duetta^{TM} spectrofluorometer. In a typical experiment, an excess of tetrabutylammonium bromide (TBABr) or lithium perchlorate ($LiClO_4$) was added to 1.0 mL stock solution of a known concentration of the receptor molecule. In a typical experiment, an excess of the anion/cation salt was first added to the receptor solution in the cuvette and thoroughly mixed by upturning the cuvette several times before any spectra were recorded. An absorption and fluorescence spectra were thereafter generated. This was followed by the addition of excess cation/anion salt to the pre-complexed system which was again thoroughly mixed. An absorption and fluorescence spectra of the complexed receptor was again recorded. Temperatures were maintained at 298 K to within a margin of ± 0.5 K.

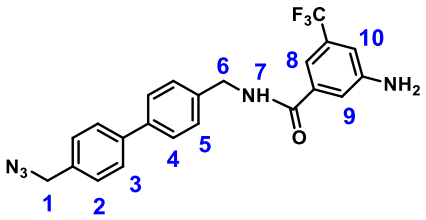
6.1.3.3 Solid-liquid extraction studies

The potential of the [2]rotaxanes synthesised in chapter 2 and chapter 3 to function as alkali metal halide salt extractants was evaluated by carrying out preliminary ^{1}H-NMR solid-liquid extraction studies. All ^{1}H NMR spectra were recorded on a Bruker AVIIIHD 500 MHz spectrometer. All deuterated solvents and lithium halide salts used were purchased from chemical suppliers. In a typical experiment, an excess of a solid alkali metal halide salt (MCl, MBr, MI where $M^+ = Li^+$, Na^+) was added to 1.0 mM a solution of each receptor in $CDCl_3$ (700 µL) and the mixture was sonicated for 20 min. The excess salt was subsequently removed by filtration and the ^{1}H NMR spectrum of the solution was recorded.

6.2 Synthesis from Chapter 2

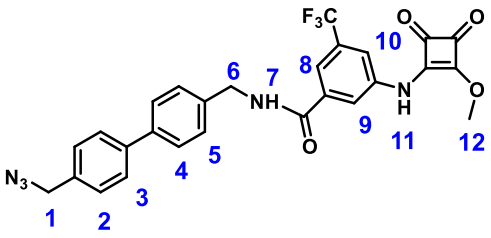
Compounds 2.1,[234] 2.2,[266] 2.6,[267] 2.7,[268] 2.9,[235] 2.10,[269] 2.12,[223] 2.13,[270] 2.16,[223] and 2.18[271] were prepared according to literature procedures and spectroscopic data were consistent with those reported.

Bi-phenyl mono-azide precursor (2.3)



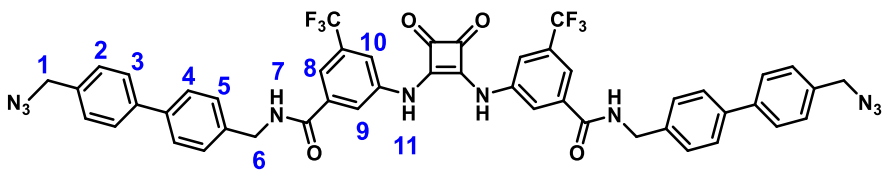
To a solution of azide **2.2** (992.10 mg, 4.163 mmol) and amine (853.99 mg, 4.163 mmol) in THF/$CHCl_3$ 3:1 (20 mL), coupling reagents EDC (710.99 mg, 4.58 mmol) and HOBt (618.75 mg, 4.58 mmol) were added at room temperature. The resulting mixture was left to stir at room temperature for two days. After removing the solvent under vacuum, purification by column chromatography (eluent: EtOAc/CH_2Cl_2 5:95 *v/v*) afforded the target squaramide as a white solid (1.354 g, 79%). **^{1}H NMR** (600 MHz, $CDCl_3$) δ = 7.58 (dd, *J* = 8.4, 6.8 Hz, 4H, $H_{4,5}$), 7.40 (dd, *J* = 13.5, 8.0 Hz, 4H, $H_{2,3}$), 7.32 – 7.27 (m, 2H, $H_{8,10}$), 6.99 (s, 1H, H_9), 6.56 (s, 1H, H_7), 4.66 (d, *J* = 5.7 Hz, 2H, H_6), 4.38 (s, 2H, H_1). **^{13}C NMR** (151 MHz, $CDCl_3$) δ = 166.60, 166.58, 147.53, 140.76, 140.14, 137.29, 136.42, 134.68, 132.16, 128.86, 128.58, 127.64, 127.61, 123.82, 114.10, 112.72, 77.41, 77.16, 76.91, 54.63, 44.03. **HRMS** (ESI +ve) m/z: 426.1534 ($[M+H]^+$, $C_{22}H_{18}F_3N_5O$ requires 426.1536).

Squaramide appended bi-phenyl mono-azide precursor (2.4)



Mono-azide precursor **2.3** (390.9 mg, 0.864 mmol), squarate ester (245.6 mg, 1.728 mmol) and zinc triflate (125.65, 10 mol%) were dissolved in a solution of $CHCl_3$/MeOH 1:1 (8 mL) at room temperature under a N_2 atmosphere. The resulting mixture was left to stir at room temperature for 2 days. After removing the solvent under vacuum, purification by column chromatography (eluent: EtOAc/CH_2Cl_2 1:1 *v/v*) afforded the target squaramide as a yellow solid (336.30 mgs, 73%). **^{1}H NMR** (600 MHz, DMSO) δ = 11.10 (s, 1H, H_{11}), 9.30 (t, J = 5.9 Hz, 1H, H_7), 8.12 (s, 1H, H_{10}), 7.97 (s, 1H, H_8), 7.94 (s, 1H, H_9), 7.72 – 7.63 (m, 4H, $H_{4,5}$), 7.51 – 7.40 (m, 4H, $H_{2,3}$), 4.54 (d, J = 5.8 Hz, 2H, H_6), 4.49 (s, 2H, H_1), 4.39 (s, 3H, H_{12}).**^{13}C NMR** (151 MHz, $CDCl_3$) δ = 184.46, 164.33, 139.71, 138.60, 138.28, 136.43, 134.70, 129.05, 128.01, 126.86, 126.67, 122.43, 118.41, 60.76, 53.26, 42.58, 40.06, 39.94, 39.80, 39.66, 39.52, 39.38, 39.24, 39.10. **HRMS** (ESI -ve) m/z: 534.1391 ([M-H]$^-$, $C_{27}H_{20}F_3N_5O_4$ requires 534.1395).

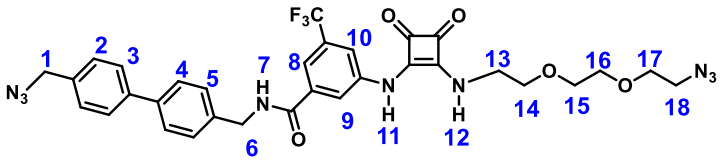
Symmetrical squaramide-based bis-azide (2.5)



Azide **2.4** (337.10 mg, 0.629 mmol), amine **2.3** (401.60 mg, 0.944 mmol) and zinc triflate (68.66, 10 mol%) were dissolved in a solution of toluene/DMF 19:1 (25 mL) at room temperature under a N_2 atmosphere. The resulting mixture was left to stir at 105°C overnight.

After removing the solvent under vacuum, purification by column chromatography (eluent: CH_3OH/CH_2Cl_2 2:98 *v/v*) afforded the target squaramide as a yellow solid (128.64 mgs, 22%). **^{1}H NMR** (600 MHz, DMSO) δ = 10.43 (s, 1H, H_{11}), 9.32 (t, *J* = 5.9 Hz, 1H, H_7), 8.09 (s, 1H, H_{10}), 8.02 (s, 1H, H_8), 7.95 (s, 1H, H_9), 7.70 – 7.65 (m, 2H, H_5), 7.67 – 7.62 (m, 2H, H_4), 7.47 – 7.40 (m, 4H, $H_{2,3}$), 4.54 (d, *J* = 5.8 Hz, 2H, H_6), 4.49 (s, 2H, H_1). **^{13}C NMR** (151 MHz, DMSO) δ = 165.76, 164.21, 139.72, 138.58, 138.27, 136.35, 134.71, 129.05, 128.00, 126.85, 126.66, 124.60, 122.79, 121.65, 117.81, 53.27, 42.59, 40.06, 39.93, 39.80, 39.66, 39.52, 39.38, 39.24, 39.10. **HRMS** (ESI -ve) m/z: 927.2585 ($[M-H]^-$, $C_{48}H_{34}F_6N_{10}O_4$ requires 927.2596).

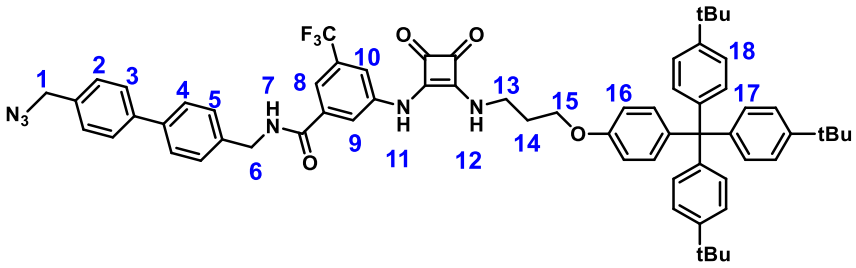
Asymmetrical TEG-based squaramide axle precursor synthon (2.8)



Azide **2.4** (100.00 mg, 0.187 mmol), amine **2.7** (48.80 mg, 0.280 mmol) and zinc triflate (20.36, 10 mol%) were dissolved in a solution of toluene/DMF 19:1 (8 mL) at room temperature under a N_2 atmosphere. The resulting mixture was left to stir at 105°C overnight. After removing the solvent under vacuum, purification by column chromatography (eluent: EtOAc/CH_2Cl_2 1:1 *v/v*) afforded the target squaramide as a yellow solid (112.63 mgs, 89%). **^{1}H NMR** (600 MHz, DMSO) δ = 9.89 (s, 1H, H_{11}), 8.91 (t, *J* = 6.5 Hz, 1H, H_7), 8.68 (s, 1H, H_{10}), 8.59 (s, 1H, H_8), 8.30 (s, 1H, H_9), 8.20 – 8.06 (m, 4H, $H_{4,5}$), 8.02 – 7.89 (m, 4H, $H_{2,3}$), 7.78 (s, 1H, H_{12}), 5.13 (d, *J* = 5.9 Hz, 2H, H_6), 4.94 (s, 2H, H_1), 4.36 (d, *J* = 4.7 Hz, 2H, H_{13}), 4.23 – 4.05 (m, 8H, $H_{14\text{-}17}$), 3.81 (s, 2H, H_{18}). **^{13}C NMR** (151 MHz, DMSO) δ = 215.93, 175.44, 173.68, 151.40, 151.15, 149.74, 149.31, 145.55, 139.54, 138.84, 137.69, 137.48, 131.21, 127.80, 80.89, 80.31, 64.44, 61.01, 54.73,

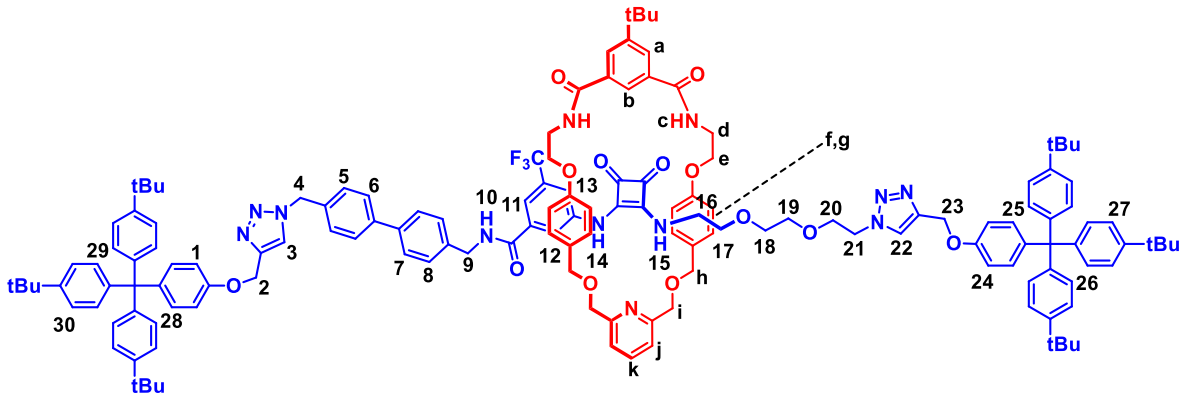
53.60, 40.08, 39.98, 39.92, 39.83, 39.77, 39.67, 39.61, 39.52, 39.36, 39.21, 39.06. **HRMS** (ESI +ve) m/z: 678.2394 ($[M+H]^+$, $C_{32}H_{30}F_3N_9O_5$ requires 678.2395).

Asymmetrical stopper-appended squaramide axle precursor synthon (2.11)



Azide **2.4** (378.93 mg, 0.707 mmol), amine **2.10** (596.4 mg, 1.06 mmol) and zinc triflate (77.17, 10 mol%) were dissolved in a solution of toluene/DMF 19:1 (28 mL) at room temperature under a N_2 atmosphere. The resulting mixture was left to stir at 105°C overnight. After removing the solvent under vacuum, purification by column chromatography (eluent: EtOAc/CH_2Cl_2 15:85 *v/v*) afforded the target squaramide as a yellow solid (557.70 mgs, 74%). **^{1}H NMR** (600 MHz, DMSO) δ = 9.89 (s, 1H, H_{11}), 8.91 (t, *J* = 6.5 Hz, 1H, H_7), 8.68 (s, 1H, H_{10}), 8.59 (s, 1H, H_8), 8.30 (s, 1H, H_9), 8.20 – 8.06 (m, 4H, $H_{4,5}$), 8.02 – 7.89 (m, 4H, $H_{2,3}$), 7.78 (s, 1H, H_{12}), 5.13 (d, *J* = 5.9 Hz, 2H, H_6), 4.94 (s, 2H, H_1), 4.36 (d, *J* = 4.7 Hz, 2H, H_{13}), 4.23 – 4.05 (m, 8H, $H_{14\text{-}17}$), 3.81 (s, 2H, H_{18}). **^{13}C NMR** (151 MHz, DMSO) δ = 215.93, 175.44, 173.68, 151.40, 151.15, 149.74, 149.31, 145.55, 139.54, 138.84, 137.69, 137.48, 131.21, 127.80, 80.89, 80.31, 64.44, 61.01, 54.73, 53.60, 40.08, 39.98, 39.92, 39.83, 39.77, 39.67, 39.61, 39.52, 39.36, 39.21, 39.06. **HRMS** (ESI +ve) m/z: 1087.5058 ($[M+Na]^+$, $C_{66}H_{67}F_3N_6O_4Na$ requires 1087.5068).

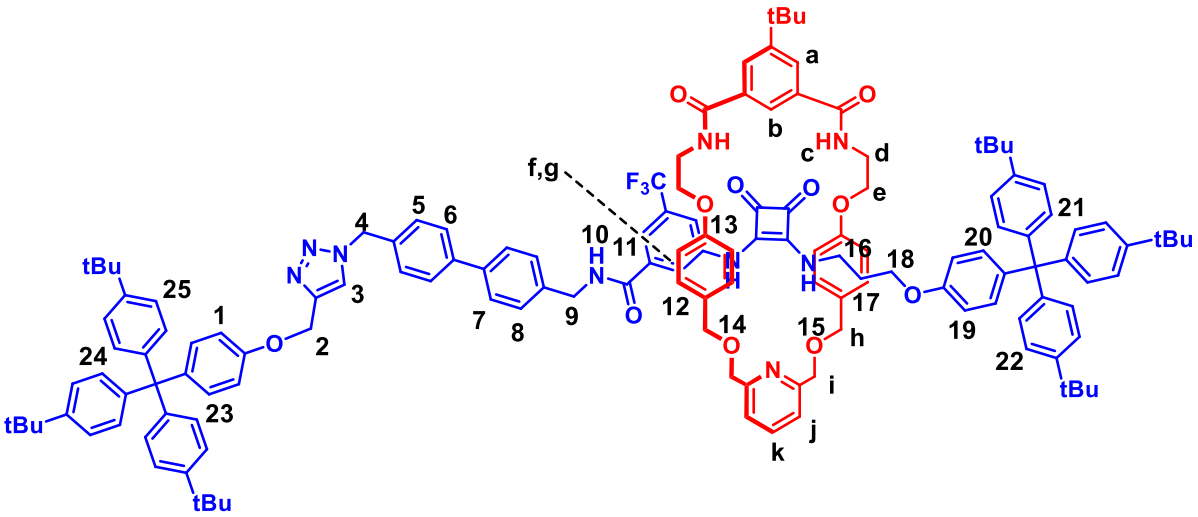
[2]rotaxane (2.14)



Macrocycle **2.12** (8.0 mg, 0.013 mmol) and $[Cu(CH_3CN)_4]PF_6$ (4.78 mg, 0.013 mmol) were dissolved in dry, degassed CH_2Cl_2 (0.8 mL) and stirred for 30 minutes at room temperature. A solution of bis-azide **2.8** (43.46 mg, 0.064 mmol) and terphenyl stopper alkyne **2.13** (69.62 mg, 0.13 mmol) in CH_2Cl_2 (0.8 mL) was added dropwise to the mixture. The reaction was left to stir at room temperature for seven days, during which monitoring the reaction using TLC revealed no evidence of the desired product. However, heating to 40°C for the next five days led to reaction products as indicated by TLC analysis. Following dilution of the reaction mixture with CH_2Cl_2, the organic layer was washed with EDTA/NH_4OH (2 × 25 mL) and H_2O (2 × 25 mL), dried over $MgSO_4$, filtered and concentrated under vacuum. The crude was purified by preparative TLC in MeOH/ CH_2Cl_2 3:97 *v/v* to afford [2]rotaxane **2.14** as a white solid (1.8 mg, 6%). **^{1}H NMR** (500 MHz, $CDCl_3$) δ = 9.27 (s, 1H, H_{14}), 8.43 (s, 1H, H_b), 8.35 (s, 1H, H_{10}), 8.21 (d, J = 1.5 Hz, 2H, H_a), 8.09 (s, 1H, H_3), 7.61 (d, J = 8.1 Hz, 4H, $H_{22,11,c}$), 7.52 (d, J = 8.2 Hz, 1H, H_k), 7.80 (s, 1H, H_{13}), 7.45 (d, J = 7.8 Hz, 2H, H_5), 7.42 (d, J = 8.1 Hz, 2H, H_8), 7.33 (d, J = 8.4 Hz, 4H, $H_{6,j}$), 7.29 (dd, J = 8.6, 2.1 Hz, 14H, $H_{27,30,7}$), 7.16 – 7.05 (m, 16H, $H_{25,26,28,29}$), 7.02 (d, J = 8.5 Hz, 4H, H_g), 6.92 (dd, J = 8.8, 6.4 Hz, 4H, $H_{24,1}$), 6.64 (d, J = 8.2 Hz, 4H, H_f), 5.66 (s, 2H, H_4), 5.14 (s, 2H, H_2), 5.11 (s, 2H, H_{23}) 4.58 – 4.42 (m, 14H, $H_{h,l,9,e}$), 4.14 (t, J = 5.2 Hz, 2H, H_{17}), 3.79 (t, J = 5.1 Hz, 2H, H_d), 3.62 (m, 8H, $H_{d,18,19,21}$), 3.47 (m, 4H, $H_{16,20}$) 1.36 (s, 9H, H_{mactBu}), 1.28 (d, J = 2.0

Hz, 54H, H_{axtBu}). **HRMS** (ESI +ve) m/z: 2388.0134 ($[M+H]^+$, $C_{149}H_{163}F_3N_{12}O_{13}$ requires 2388.0498).

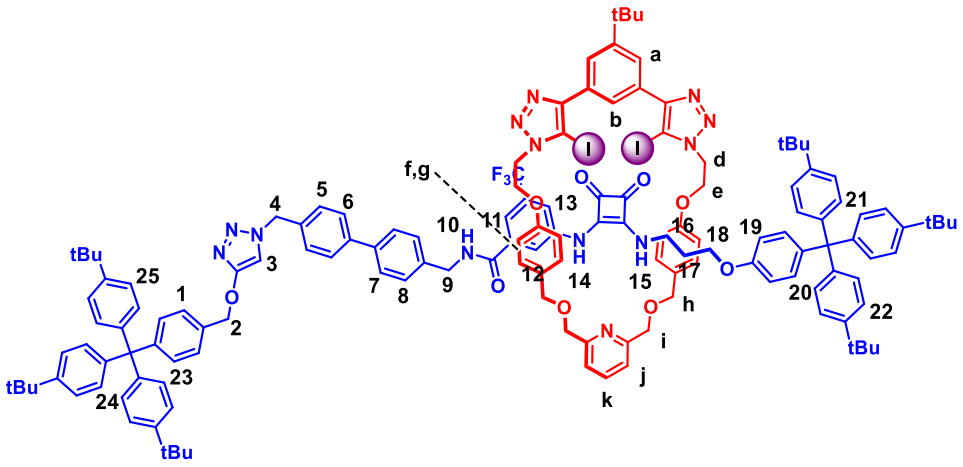
[2]rotaxane (2.15)



Macrocycle **2.12** (20.0 mg, 0.032 mmol) and $[Cu(CH_3CN)_4]PF_6$ (12.05 mg, 0.032 mmol) were dissolved in dry, degassed CH_2Cl_2 (1.0 mL) and stirred for 30 minutes at room temperature. A solution of bis-azide **2.11** (170.78 mg, 0.16 mmol) in CH_2Cl_2 (1.2 mL) was added followed by a dropwise addition of a solution of terphenyl stopper alkyne **2.15** (87.02 mg, 0.16 mmol) in CH_2Cl_2 (1.0 mL). The reaction mixture was stirred at room temperature for 5 days, following which it was diluted with CH_2Cl_2 (40 mL). The organic layer was washed with EDTA/NH_4OH (2 × 25 mL) and H_2O (2 × 25 mL), dried over $MgSO_4$, filtered and concentrated under vacuum. The crude was purified by preparative TLC in 80:20 CH_2Cl_2/EtOAc to afford [2]rotaxane **2.15** as a white solid (14 mg, 30%). **^{1}H NMR** (600 MHz, Acetone) δ = 9.23 (s, 1H, H_{14}), 8.41 (s, 1H, H_b), 8.34 (s, 1H, H_{10}), 8.22 (d, J = 1.5 Hz, 2H, H_a), 8.09 (s, 1H, H_3), 8.01 (s, 1H, H_{13}), 7.96 (s, 2H, H_c), 7.83 (s, 1H, H_{11}), 7.74 (s, 1H, H_k), 7.66 (s, 1H, H_{12}), 7.67 – 7.60 (m, 2H, H_5), 7.57 – 7.51 (m, 2H, H_8), 7.45 – 7.41 (m, 2H, H_6), 7.38 (d, J = 8.0 Hz, 2H, H_7), 7.33 – 7.28 (m, 14H, $H_{24,21,j}$), 7.18 – 7.14 (m, 6H, H_{22}), 7.12 – 7.10 (m, 8H, $H_{19,\ 25}$), 7.09 – 7.07 (m, 2H, H_1), 6.99 (d, J = 8.1 Hz, 4H,

H_g), 6.95 – 6.89 (m, 2H, H_{23}), 6.72 (d, J = 8.6 Hz, 2H, H_{20}), 6.65 (d, J = 8.1 Hz, 4H, H_f), 5.68 (s, 2H, H_2), 5.15 (s, 2H, H_4), 4.53 (d, J = 11.6 Hz, 2H, H_9), 4.48 (q, J = 13.4 Hz, 6H, $H_{h,i}$), 4.40 (d, J = 10.9 Hz, 2H, H_h), 4.15 (dq, J = 10.6, 5.3 Hz, 4H, H_e), 3.81 (s, 2H, H_{18}), 3.76 – 3.68 (m, 2H, H_d), 3.64 – 3.58 (m, 2H, H_{16}), 3.53 (d, J = 9.6 Hz, 2H, H_d), 1.87 (s, 2H, H_{17}), 1.37 (s, 9H, H_{mactBu}), 1.29 (s, 54H, H_{axtBu}). **^{13}C NMR** (151 MHz, Acetone) δ = 182.8, 167.8, 167.6, 156.3, 152.5, 152.5, 152.4, 148.5, 144.3, 144.2, 140.5, 133.9, 132.5, 130.9, 128.9, 124.4, 124.2, 124.0, 123.9, 121.3, 115.4, 115.2, 113.3, 77.4, 77.2, 76.9, 70.8, 70.7, 70.6, 70.3, 70.3, 70.2, 69.5, 67.5, 66.3, 63.2, 62.1, 50.4, 43.8, 39.5, 35.2, 34.4, 31.5, 31.4. **HRMS** (ESI +ve) m/z: 2232.1785 ($[M+H]^+$, $C_{143}H_{154}F_3N_9O_{11}$ requires 2232.1825).

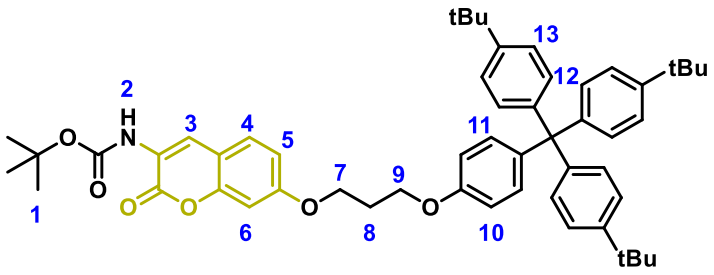
[2]rotaxane (2.17)



Macrocycle **2.16** (20.0 mg, 0.022 mmol) and $[Cu(CH_3CN)_4]PF_6$ (8.07 mg, 0.022 mmol) were dissolved in dry, degassed $C_2H_5Cl_2$ (0.7 mL) and stirred for 30 minutes at room temperature, followed by the dropwise addition of solution containing bis-azide **2.11** (115.34 mg, 0.1082 mmol) and terphenyl stopper alkyne **2.13** (58.77 mg, 0.1082 mmol) in CH_2Cl_2 (1.4 mL). The reaction was left to stir at 80°C for 3 days, then diluted with CH_2Cl_2 (40 mL) upon cooling to room temperature. The organic layer was washed with EDTA/NH_4OH (2 × 25 mL) and H_2O (2 × 25 mL), dried over $MgSO_4$, filtered and concentrated under vacuum. The crude was purified by preparative TLC in 70:30 EtOAc/CH_2Cl_2 to afford [2]rotaxane **2.17** as a pale white solid (13.16 mg, 24%). **^{1}H NMR** (600 MHz, Acetone) δ = 9.83 (s, 1H, H_{14}), 8.24 – 8.15 (m, 3H, $H_{10,13,b}$), 8.04 – 7.97 (m, 3H, $H_{11,a}$), 7.96 (s, 1H, H_3), 7.79 (s, 1H, H_{12}), 7.60 (t, J = 7.7 Hz, 1H, H_k), 7.30 (dd, J = 8.5, 4.1 Hz, 12H, $H_{24,21}$), 7.22 (d, J = 7.7 Hz, 3H, $H_{j,15}$), 7.16 (s, 4H, $H_{5,8}$), 7.14 – 7.09 (m, 16H, $H_{22,25,6,7}$), 7.10 – 7.05 (m, 2H, H_{23}), 6.98 (dd, J = 15.2, 8.3 Hz, 6H, $H_{g,\ 20}$), 6.92 – 6.86 (m, 2H, H_1), 6.68 – 6.61 (m, 4H, H_f), 6.48 (s, 2H, H_{19}), 5.47 (s, 2H, H_2), 5.09 (s, 2H, H_4), 4.92 (t, J = 5.0 Hz, 4H, H_e), 4.47 – 4.36 (m, 10H, $H_{h,d,9}$), 4.24 (s, 4H, H_i), 3.68 (s, 2H, H_{18}), 3.60 (s, 2H, H_{16}), 1.79 (s, 2H, H_{17}) 1.40 (s, 9H, H_{mactBu}), 1.30 (s, 54H, H_{axtBu}). **^{13}C NMR** (151 MHz, Acetone) δ = 182.8, 167.8, 167.6, 156.3, 152.5, 152.5, 152.4, 148.5, 144.3, 144.2, 140.5, 133.9, 132.5, 130.9, 128.9,

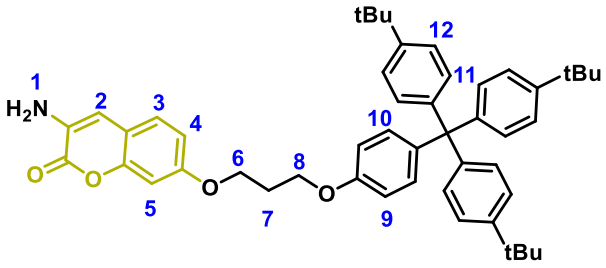
124.4, 124.2, 124.0, 123.9, 121.3, 115.4, 115.2, 113.3, 77.4, 77.2, 76.9, 70.8, 70.7, 70.6, 70.3, 70.3, 70.2, 69.5, 67.5, 66.3, 63.2, 62.1, 50.4, 43.8, 39.5, 35.2, 34.4, 31.5, 31.4. **HRMS** (ESI +ve) m/z: 1266.5026($[M+2H]^{2+}$, $C_{145}H_{152}F_3I_2N_{13}O_9$ requires 1266.5028).

Boc-protected coumarin stopper (2.18a)



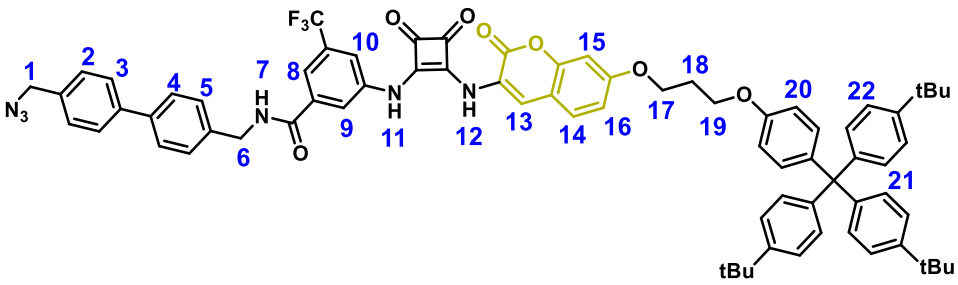
To a mixture of Boc-protected coumarin amine (474 mg, 1.71 mmol) and K_2CO_3 (429 mg, 3.11 mmol) in dry MeCN (20 mL) bromine-stopper **2.18** (971 mg, 1.55 mmol) was added at room temperature under a N_2 atmosphere. The solution was heated at reflux for 16 h. Upon cooling, the solution was filtered and washed with $CHCl_3$ and the resulting filtrate was reduced under vacuum. Upon drying, the residue was re-dissolved in $CHCl_3$ (20 mL) and washed with water (3 x 20 mL), brine (20 mL), dried over $MgSO_4$, filtered and concentrated under vacuum. The crude was then purified by silica column chromatography (eluent: CH_2Cl_2) to yield a yellow powder (845 mg, 67 %). **^{1}H NMR** (500 MHz, $CDCl_3$); δ 8.23 (s, 1H, H_2), 7.34 (d, J = 8.6 Hz, 1H, H_4), 7.29 (s, 1H, H_3), 7.25 – 7.20 (m, 6H, H_{12}), 7.10 – 7.05 (m 8H, $H_{11,13}$), 6.86 (dd, J = 8.6, 2.4 Hz, 1H, H_5), 6.83 (d, J = 2.4 Hz, 1H, H_6), 6.80 – 6.75 (m, 2H, H_{10}), 4.20 (m, 2H, H_7), 4.14 (m, 2H, H_9), 2.27 (m, 2H, H_8), 1.53 (s, 9H, H_{BocTBu}), 1.30 (s, 27H, H_{StTBu}); **^{13}C NMR** (126 MHz, $CDCl_3$); δ 160.03, 156.52, 152.62, 150.93, 148.31, 144.11, 139.81, 132.29, 130.71, 128.09, 124.04, 122.14, 121.26, 113.34, 112.94, 101.33, 65.04, 63.88, 63.05, 53.43, 34.30, 31.39, 29.17, 28.24; **HRMS** (ESI +ve) m/z: 822.4731 ([M + H]+, $C_{54}H_{64}O_6N$, requires 822.4728).

Coumarin-based stopper amine (2.19)



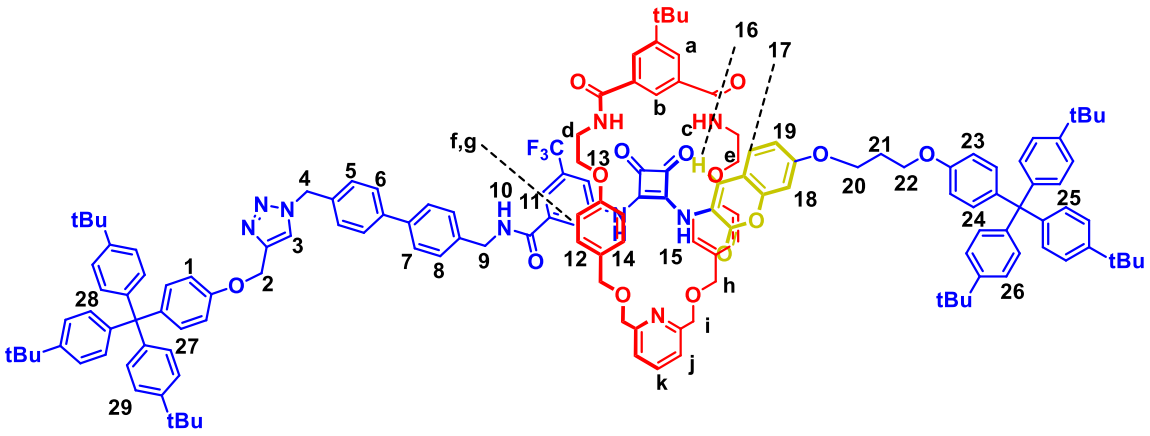
BOC-protected coumarin stopper **2.18a** (147 mg, 0.179 mmol) was dissolved in CH2Cl2 (1.0 mL) and cooled to 0 °C using an ice bath before TFA (1.0 mL) was slowly added. The mixture was left to heat to room temperature over 3 hours. CHCl3 (20 mL) was then added and the solution and washed with a saturated solution of NaHCO3 (3 x 20 mL), water (20 mL) and brine (20 mL). The organic phase was dried over MgSO4, filtered and had the solvent removed under vacuum to yield an off white solid (128 mg, 99 %). **^{1}H NMR** (500 MHz, $CDCl_3$); δ 7.24 – 7.19 (m, 6H, H_{11}), 7.18 (d, *J* = 8.4 Hz, 1H, H_3), 7.10 – 7.05 (m, 8H, $H_{10,12}$), 6.84 – 6.76 (m, 4H, $H_{9,2,4}$), 6.68 (s, 1H, H_5), 4.17 (m, 2H, H_6), 4.13 (m, 2H, H_8), 4.04 (s, 2H, H_1), 2.26 (m, 2H, H_7), 1.30 (s, 29H, H_{tBu}); **^{13}C NMR** (126 MHz, $CDCl_3$); δ 159.73, 158.32, 156.56, 150.32, 148.30, 144.12, 139.76, 132.28, 130.71, 129.71, 125.81, 124.04, 114.41, 112.95, 112.85, 112.23, 101.47, 64.95, 63.98, 63.05, 34.30, 31.39, 29.22; **HRMS** (ESI +ve) m/z: 722.4203 ([M + H]+, $C_{49}H_{56}O_4N$, requires 722.4204)

Coumarin-based axle precursor azide (2.20)



Azide **2.4** (37.63 mg, 0.070 mmol), amine **2.19** (76.1 mg, 0.105 mmol) and zinc triflate (7.66, 10 mol%) were dissolved in a solution of toluene/DMF 19:1 (3 mL) at room temperature under a N_2 atmosphere. The resulting mixture was left to stir at 105°C overnight. After removing the solvent under vacuum, purification by column chromatography (eluent: EtOAc/CH_2Cl_2 20:80 *v/v*) afforded the target coumarin based azide precursor as a yellow solid (65.2 mgs, 76%). **^{1}H NMR** (700 MHz, Acetone) δ = 8.52 (s, 1H, H_7), 8.34 (s, 1H, H_{10}), 8.30 (s, 1H, H_{13}), 8.25 (s, 1H, H_8), 7.95 (s, 1H, H_9), 7.68 (d, J = 7.9 Hz, 2H, H_5), 7.63 (d, J = 7.9 Hz, 2H, H_4), 7.54 (d, J = 8.6 Hz, 2H, H_{14}), 7.48 (dd, J = 10.7, 8.0 Hz, 4H, $H_{2,3}$), 7.34 – 7.29 (m, 6H, H_{22}), 7.15 – 7.10 (m, 8H, H_{21}), 7.11 – 7.08 (m, 2H, H_{21}), 7.00 (d, J = 8.6 Hz, 1H, H_{16}), 6.96 (s, 1H, H_{15}), 6.89 – 6.84 (m, 2H, H_{20}), 4.68 (d, J = 5.7 Hz, 2H, H_6), 4.48 (s, 2H, H_1), 4.30 (t, J = 6.2 Hz, 2H, H_{17}), 4.20 (t, J = 6.1 Hz, 2H, H_{19}), 2.28 (t, J = 6.1 Hz, 2H, H_{18}), 1.30 (s, 27H, H_{tBu}). **^{13}C NMR** (176 MHz, Acetone) δ = 206.26, 165.60, 157.96, 153.02, 149.30, 145.39, 141.58, 140.48, 140.17, 139.71, 135.98, 132.96, 131.56, 129.96, 129.69, 129.27, 128.13, 127.91, 125.19, 114.44, 114.22, 102.21, 66.22, 65.02, 64.03, 54.89, 44.08, 29.85. **HRMS** (ESI -ve) m/z: 1224.5303 ([M-H]$^-$, $C_{75}H_{71}F_3N_6O_7$ requires 1224.5296).

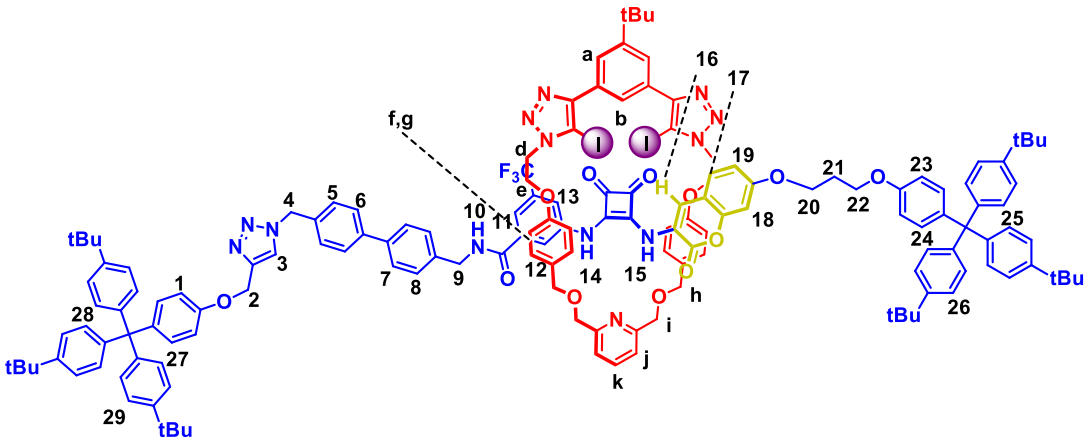
[2]rotaxane (2.21)



Macrocycle **2.12** (20.0 mg, 0.032 mmol) and $[Cu(CH_3CN)_4]PF_6$ (11.95 mg, 0.032 mmol) were dissolved in dry, degassed CH_2Cl_2 (1.0 mL) and stirred for 30 minutes at room temperature. A solution of bis-azide **2.20** (196.46 mg, 0.16 mmol) in CH_2Cl_2 (1.2 mL) was added followed by a dropwise addition of a solution of terphenyl stopper alkyne **2.13** (87.02 mg, 0.16 mmol) in CH_2Cl_2 (1.0 mL). The reaction mixture was stirred at room temperature for 5 days, then was diluted with CH_2Cl_2 (40 mL). The organic layer was washed with EDTA/NH_4OH (2 × 25 mL) and H_2O (2 × 25 mL), dried over $MgSO_4$, filtered and concentrated under vacuum. The crude was purified by preparative TLC in 80:20 CH_2Cl_2/EtOAc to afford [2]rotaxane **2.21** as a yellow solid (25.31 mg, 33%). **^{1}H NMR** (600 MHz, Acetone) δ = 10.67 (s, 1H, H_{14}), 8.79 (s, 1H, H_{15}), 8.47 (t, J = 6.0 Hz, 1H, H_{10}), 8.39 (d, J = 2.1 Hz, 1H, H_b), 8.22 (d, J = 1.5 Hz, 2H, H_a), 8.14 (s, 1H, H_{11}), 8.12 (s, 2H, $H_{3,16}$), 7.99 – 7.91 (m, 4H, $H_{c,k,12}$), 7.77 (s, 1H, H_{13f}), 7.66 – 7.62 (m, 2H, H_5), 7.56 (d, J = 8.2 Hz, 2H, H_8), 7.49 (t, J = 7.6 Hz, 3H, $H_{17,j}$), 7.44 (d, J = 8.1 Hz, 2H, H_6), 7.39 (d, J = 8.0 Hz, 2H, H_8), 7.30 (dd, J = 8.5, 6.2 Hz, 12H, $H_{26,29}$), 7.14 – 7.06 (m, 16H, $H_{24,25,27,28}$), 7.00 – 6.90 (m, 8H, $H_{18,19,g}$), 6.88 – 6.84 (m, 2H, H_{23}), 6.63 – 6.58 (m, 4H, H_f) 5.69 (s, 2H, H_4), 5.15 (s, 2H, H_2), 4.69 (q, J = 12.9 Hz, 4H, H_h), 4.56 (d, J = 5.3 Hz, 2H, H_9), 4.48 – 4.42 (m, 4H, H_i), 4.30 (t, J = 6.2 Hz, 2H, H_{20}), 4.19 (t, J = 6.0 Hz, 2H, H_{22}), 4.13 (dt, J = 6.0, 4.2 Hz, 4H, H_e), 3.83 – 3.54 (m, 4H,

H_d), 2.28 (p, J = 6.2 Hz, 2H, H_{21}), 1.38 (s, 9H, H_{mactBu}), 1.28 (d, J = 5.4 Hz, 54H, H_{axtBu}). **^{13}C NMR** (151 MHz, Acetone) δ = 182.8, 167.8, 167.6, 156.3, 152.5, 152.5, 152.4, 148.5, 144.3, 144.2, 140.5, 133.9, 132.5, 130.9, 128.9, 124.4, 124.2, 124.0, 123.9, 121.3, 115.4, 115.2, 113.3, 77.4, 77.2, 76.9, 70.8, 70.7, 70.6, 70.3, 70.3, 70.2, 69.5, 67.5, 66.3, 63.2, 62.1, 50.4, 43.8, 39.5, 35.2, 34.4, 31.5, 31.4. **HRMS** (ESI +ve) m/z: 1196.6024 ($[M+2H]^{2+}$, $C_{152}H_{158}F_3N_9O_{14}$requires 1196.6030).

[2]rotaxane (2.22)



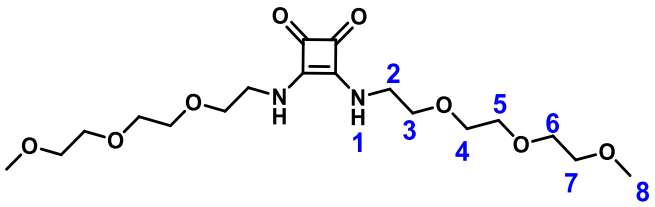
Macrocycle **2.16** (20.0 mg, 0.022 mmol) and $[Cu(CH_3CN)_4]PF_6$ (8.07 mg, 0.022 mmol) were dissolved in dry, degassed $C_2H_5Cl_2$ (1.0 mL) and stirred for 30 minutes at room temperature, followed by the dropwise addition of solution containing bis-azide **2.20** (132.68 mg, 0.11 mmol) and terphenyl stopper alkyne **2.13** (58.77 mg, 0.11 mmol) in CH_2Cl_2 (1.5 mL). The reaction was left to stir at 80°C for 3 days, then diluted with CH_2Cl_2 (40 mL). The organic layer was washed with EDTA/NH_4OH (2 × 25 mL) and H_2O (2 × 25 mL), dried over $MgSO_4$, filtered and concentrated under vacuum. The crude was purified by preparative TLC in 90:10 CH_2Cl_2/EtOAc to afford [2]rotaxane **2.22** as a yellow solid (19.68 mg, 38%). **^{1}H NMR** (500 MHz, Acetone) δ = 8.32 (m, 2H, $H_{b,10}$), 8.21 (s, 1H, H_{13}), 8.14 (s, 1H, H_{11}), 8.03 (s, 1H, H_3), 8.01 (d, J = 1.6 Hz, 2H, H_a), 7.89 (s, 1H, H_{12}), 7.85 (s, 1H, H_{16}), 7.79 (t, J = 7.8 Hz, 1H, H_k), 7.43 (d, J = 7.8 Hz, 2H, H_5), 7.38 (t, J = 6.5 Hz, 4H, $H_{8,j}$), 7.35 – 7.25 (m, 16H, $H_{29,26,6,7}$), 7.16 – 7.05 (m, 16H, $H_{24,25,27,28}$), 7.01 (d, J = 8.5 Hz, 1H, H_{17}), 6.92 (dd, J = 13.2, 8.6 Hz, 6H, $H_{g,1}$), 6.80 (d, J = 8.7 Hz, 2H, H_{23}), 6.64 (d, J = 9.5 Hz, 2H, $H_{18,19}$), 6.58 (d, J = 8.5 Hz, 4H, H_f), 5.58 (s, 2H, H_4), 5.12 (s, 2H, H_2), 4.91 (d, J = 5.4 Hz, 4H, H_e), 4.55 (s, 2H, H_9), 4.48 (s, 4H, H_h), 4.41 (s, 4H, H_i), 4.40 – 4.26 (m, 4H, H_d), 4.08 (d, J = 5.9 Hz, 4H, $H_{20,22}$), 2.15 – 2.09 (m, 2H, H_{21}), 1.43 (s, 9H, H_{mactBu}), 1.29 (d, J = 3.5 Hz, 54H, H_{axtBu}). **^{13}C NMR** (176 MHz, Acetone) δ = 206.1, 161.1, 158.8, 158.6, 157.8,

157.5, 152.4, 150.8, 149.2, 149.2, 145.3, 145.2, 144.7, 141.5, 140.6, 140.3, 139.9, 139.3, 135.7, 132.8, 132.0, 131.5, 131.4, 131.0, 130.3, 129.4, 129.3, 129.1, 128.0, 127.7, 125.5, 125.1, 124.7, 121.8, 115.0, 114.3, 114.1, 113.9, 113.7, 101.9, 80.4, 73.0, 72.6, 67.7, 65.9, 64.8, 63.9, 62.4, 53.9, 50.9, 43.9, 29.4. **HRMS** (ESI +ve) m/z: 2692.0095 ($[M+H]^+$, $C_{154}H_{156}F_3I_2N_{13}O_{12}$ requires 2692.0144).

6.3 Experimental from Chapter 3

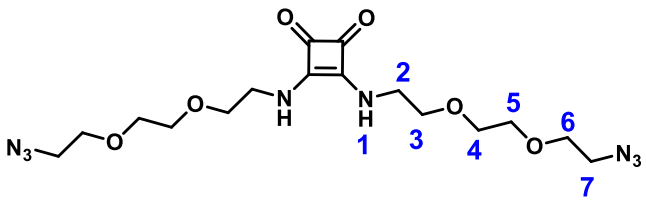
Compounds 3.1,[272] 3.2,[273] 3.3,[274] 3.5,[259] 3.6,[260] 3.7[261] 3.8,[275] 3.9,[2] 3.10,[276] and Tris[(1-benzyl-1H-1,2,3- triazol-4-yl)methyl]amine (TBTA),[277] were prepared according to literature procedures and spectroscopic data were consistent with those reported.

Squaramide tetraethylene glycol-based axle precursor (3.4)



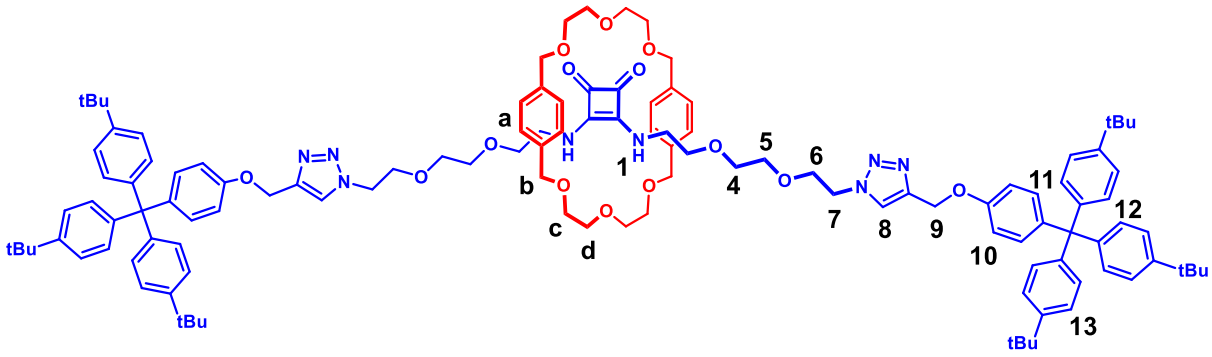
To a solution of squarate ester (30 mg, 0.211 mmol) in methanol (1 mL), a solution of tri(ethyleneglycol) functionalised amine **3.3** (72.36 mg, 0.443 mmol)) dissolved in methanol (0.5 mL) was added dropwise under a N_2 atmosphere. The resulting mixture was left to stir at room temperature overnight. After removing the solvent under vacuum, purification by column chromatography (eluent: EtOAc/CH_2Cl_2 5:95 *v/v*) afforded the target squaramide as a yellow oil (49 mgs,57%) yield. **^{1}H NMR** (500 MHz, $CDCl_3$) δ = 6.72 (s, 2H, H_1), 3.85 (q, J = 5.3 Hz, 4H, H_2), 3.68 – 3.61 (m, 16H, $H_{3\text{-}6}$), 3.63 – 3.57 (m, 4H, H_7), 3.39 (s, 6H, H_8). **^{13}C NMR** (151 MHz, CDCl3) δ = 206.9, 183.6, 168.1, 77.2, 77.0, 76.8, 71.8, 70.7, 70.4, 70.0, 69.9, 58.9, 43.9. **HRMS** (ESI +ve) m/z: 427.2044 ($[M+Na]^+$, $C_{16}H_{26}N_8O_6Na$ requires 427.2051).

Squaramide diethylene glycol-based bis-azide (3.11)



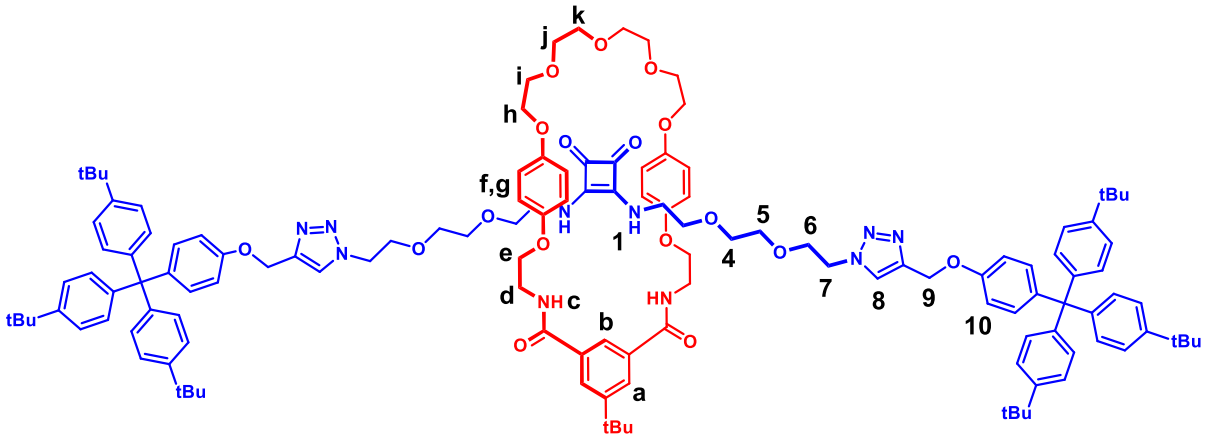
To a solution of squarate ester (75 mg, 0.53 mmol) in methanol (1 mL), a solution of tri(ethyleneglycol) functionalised amine **3.7** (193.07 mg, 1.1083 mmol)) dissolved in methanol (1 mL) was added dropwise under a N_2 atmosphere. The resulting mixture was left to stir at room temperature overnight. After removing the solvent under vacuum, purification by column chromatography (eluent: CH_3OH/CH_2Cl_2 3:97 *v/v*) afforded the target squaramide as a yellow oil (211 mgs,94%). **^{1}H NMR** (600 MHz, $CDCl_3$) δ = 6.42 (t, J = 6.1 Hz, 2H, H_1), 3.83 (q, J = 5.3 Hz, 4H, H_2), 3.67 (q, J = 5.5 Hz, 16H, $H_{3\text{-}6}$), 3.40 (t, J = 4.9 Hz, 4H, H_7). **^{13}C NMR** (151 MHz, CDCl3) δ = 207.0, 183.4, 168.1, 77.2, 77.0, 76.8, 70.6, 70.5, 70.5, 70.2, 70.1, 70.0, 69.9, 50.7, 44.0, 40.9, 39.3. **HRMS** (ESI +ve) m/z: 427.2041 ($[M+H]^+$, $C_{16}H_{26}N_8O_6$ requires 427.2048).

[2]rotaxane (3.12)



Macrocycle **3.5** (20.0 mg, 0.048 mmol) and $NaBAr_4^F$ (42.56 mg, 0.048 mmol) were dissolved in dry, degassed CH_2Cl_2 (0.5 mL) and stirred for 30 minutes at room temperature. A solution of bis-azide **3.11** (46.54 mg, 0.048 mmol) in CH_2Cl_2 (0.5 mL) was next added and the mixture stirred for a further 30 minutes. A solution of terphenyl stopper alkyne **2.13** (65.16 mg, 0.060 mmol) in CH_2Cl_2 (0.7 mL) was subsequently added, followed by a dropwise addition of a premixed solution of $[Cu(CH_3CN)_4]PF_6$ (4.47 mg, 0.012 mmol) and TBTA (6.37 mg, 0.012 mmol) in CH_2Cl_2 (0.7 mL). The reaction mixture was stirred at room temperature for 48 hours, then diluted with CH_2Cl_2 (40 mL). The organic layer was washed with EDTA/NH_4OH (2 × 25 mL) and H_2O (2 × 25 mL), dried over $MgSO_4$, filtered and concentrated under vacuum. The crude was purified by preparative TLC in 70:25:5 CH_2Cl_2/EtOAc/MeOH to afford [2]rotaxane **3.12** as a white solid (13 mg, 14%). **^{1}H NMR** (500 MHz, $CDCl_3$) δ = 7.76 (s, 2H, H_8), 7.24 – 7.19 (m, 12H, H_{13}), 7.13 (s, 8H, H_a), 7.12 – 7.09 (m, 4H, H_{11}), 7.08 – 7.04 (m, 12H, H_{12}), 6.85 (d, J = 8.7 Hz, 4H, H_{10}), 6.18 (s, 2H, H_1), 5.15 (s, 4H, H_9), 4.49 (s, 4H, H_7), 4.31 (s, 8H, H_b), 3.82 (s, 4H, H_6), 3.57 (s, 8H, H_d), 3.49 (s, 12H, $H_{c,3}$), 3.41 – 3.04 (m, 12H, $H_{2,4,5}$), 1.29 (s, 54H, H_{axtBu}), 1.25 (s, 9H, H_{mactBu}). **HRMS** (ESI +ve) m/z: 1951.1102 ($[M+Na]^+$, $C_{120}H_{150}N_8O_{14}$ requires 1951.1197).

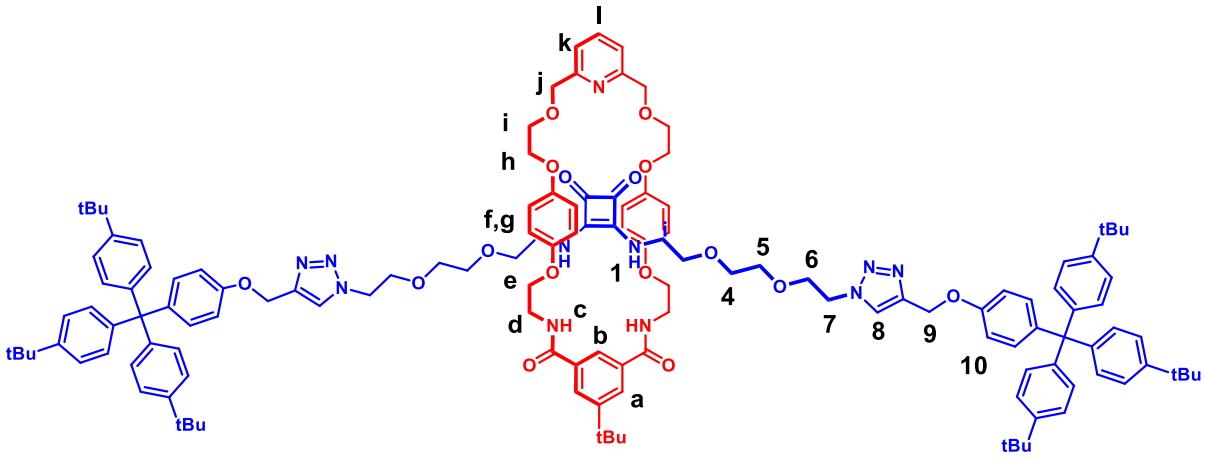
[2]rotaxane (3.13)



Macrocycle **3.6** (13.0 mg, 0.019 mmol) and $NaBAr_4^F$ (17.70 mg, 0.019 mmol) were dissolved in dry, degassed CH_2Cl_2 (0.5 mL) and stirred for 30 minutes at room temperature. A solution of bis-azide **3.11** (8.52 mg, 0.019 mmol) in CH_2Cl_2 (0.5 mL) was next added and the mixture stirred for a further 30 minutes. A solution of terphenyl stopper alkyne **2.13** (13.554 mg, 0.0497 mmol) in CH_2Cl_2 (0.5 mL) was subsequently added, followed by a dropwise addition of a premixed solution of $[Cu(CH_3CN)_4]PF_6$ (3.72 mg, 0.01 mmol) and TBTA (5.30 mg, 0.01 mmol) in CH_2Cl_2 (0.5 mL). The reaction mixture was stirred at room temperature for 48 hours, then diluted with CH_2Cl_2 (40 mL). The organic layer was washed with EDTA/NH_4OH (2 × 25 mL) and H_2O (2 × 25 mL), dried over $MgSO_4$, filtered and concentrated under vacuum. The crude was purified by preparative TLC in 70:25:5 CH_2Cl_2/EtOAc/MeOH to afford [2]rotaxane **3.13** as a white solid (5.6 mg, 13%). **^{1}H NMR** (500 MHz, $CDCl_3$) δ = 8.31 (s, 1H, H_b), 8.26 (s, 2H, H_a), 7.83 (s, 2H, H_c), 7.70 (s, 2H, H_8), 7.22 (d, J = 8.3 Hz, 12H, H_{13}), 7.11 (d, J = 8.6 Hz, 4H, H_{11}), 7.06 (d, J = 8.3 Hz, 12H, H_{12}), 6.84 (d, J = 8.6 Hz, 4H, H_{10}), 6.64 (t, J = 6.6 Hz, 8H, $H_{f,g}$), 5.13 (s, 4H, H_9), 4.48 (t, J = 5.1 Hz, 4H, H_7), 4.16 – 4.10 (m, 4H, H_e), 3.90 (s, 4H, H_h), 3.84 (t, J = 5.2 Hz, 4H, H_6), 3.72 (d, J = 5.4 Hz, 8H, $H_{i,d}$), 3.64 (d, J = 5.1 Hz, 4H, H_j), 3.59 (d, J = 5.0 Hz, 4H, H_k), 3.54 (d, J = 5.8 Hz, 4H, $H_{3,4}$), 3.44 (s, 8H, $H_{5,2}$) 1.37 (s, 9H, H_{mactBu}), 1.31 – 1.27 (m, 54H, H_{axtBu}). **^{13}C NMR**

(151 MHz, CDCl3) δ = 182.8, 167.8, 167.6, 156.3, 152.5, 152.5, 152.4, 148.5, 144.3, 144.2, 140.5, 133.9, 132.5, 130.9, 128.9, 124.4, 124.2, 124.0, 123.9, 121.3, 115.4, 115.2, 113.3, 77.4, 77.2, 76.9, 70.8, 70.7, 70.6, 70.3, 70.3, 70.2, 69.5, 67.5, 66.3, 63.2, 62.1, 50.4, 43.8, 39.5, 35.2, 34.4, 31.5, 31.4. **HRMS** (ESI +ve) m/z: 2163.2295 ($[M+H]^+$, $C_{132}H1_{64}N_{10}O_{17}$ requires 2163.2382).

[2]rotaxane (3.14)

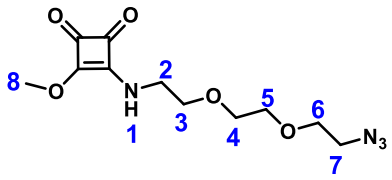


Macrocycle **3.7** (13.5 mg, 0.019 mmol) and $NaBAr_4^F$ (17.50mg, 0.019 mmol) were dissolved in dry, degassed CH_2Cl_2 (0.5 mL) and stirred for 30 minutes at room temperature. A solution of bis-azide **3.11** (8.42 mg, 0.019 mmol) in CH_2Cl_2 (0.5 mL) was next added and the mixture stirred for a further 30 minutes. A solution of terphenyl stopper alkyne **2.13** (26.79 mg, 0.019 mmol) in CH_2Cl_2 (0.5 mL) was subsequently added, followed by a dropwise addition of a premixed solution of $[Cu(CH_3CN)_4]PF_6$ (3.68 mg, 0.010 mmol) and TBTA (5.24 mg, 0.010 mmol) in CH_2Cl_2 (0.5 mL). The reaction mixture was stirred at room temperature for 48 hours, then diluted with CH_2Cl_2 (40 mL). The organic layer was washed with EDTA/NH_4OH (2 × 25 mL) and H_2O (2 × 25 mL), dried over $MgSO_4$, filtered and concentrated under vacuum. The crude was purified by preparative TLC in 70:25:5 CH_2Cl_2/EtOAc/MeOH to afford [2]rotaxane **3.14** as a white solid (8.2 mg, 19%). **^{1}H NMR** (600 MHz, $CDCl_3$) δ = 8.28 (s, 1H, H_b), 8.17 (s, 2H, H_a), 7.77 (s, 2H, H_c), 7.57 (d, J = 9.1 Hz, 3H, $H_{l,8}$), 7.18 – 7.10 (m, 12H, H_{13}), 7.03 (d, J = 8.8 Hz, 4H, H_{11}), 7.01 – 6.97 (m, 12H, H_{12}), 6.92 (s, 2H, H_1), 6.78 – 6.71 (m, 4H, H_{10}), 6.60 (q, J = 8.8 Hz, 8H, $H_{f,g}$), 5.03 (s, 4H, H_9), 4.57 (s, 4H, H_j), 4.31 (t, J = 5.3 Hz, 4H, H_7), 4.02 (s, 4H, H_e), 3.94 (d, J = 4.5 Hz, 4H, H_h), 3.80 (t, J = 4.3 Hz, 4H, H_i), 3.66 (d, J = 5.7 Hz, 4H, H_d), 3.62 (t, J = 5.1 Hz, 4H, H_6), 3.35 (q, J = 11.9 Hz, 16H, $H_{2,3,4,5}$), 1.29 (s, 9H, H_{mactBu}), 1.22 (s, 54H, H_{axtBu}). **^{13}C NMR** (151 MHz,

CDCl3) δ = 182.9, 167.8, 167.7, 157.1, 156.3, 152.9, 152.3, 152.3, 148.5, 144.2, 144.2, 140.4, 138.1, 133.9, 132.5, 131.0, 130.8, 130.6, 128.9, 124.4, 124.2, 124.0, 123.9, 121.8, 121.4, 115.5, 115.5, 113.3, 77.4, 77.2, 76.9, 73.9, 70.7, 70.4, 70.3, 70.0, 69.4, 68.3, 66.6, 63.2, 62.0, 50.3, 43.8, 39.6, 35.2, 34.4, 31.5, 31.4, 29.8, 23.3, 22.8, 14.3, 14.3, 1.2. **HRMS** (ESI +ve) m/z: 2218.2129 ($[M+Na]^+$, $C_{135}H_{163}N_{11}O_{16}$ requires 2218.2205).

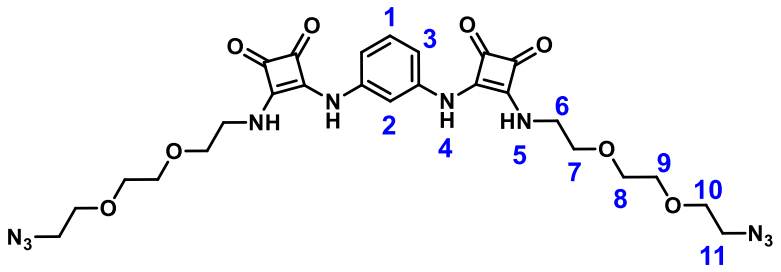
6.4 Experimental from Chapter 4

Squaramide trithylene glycol-based azide (4.1)



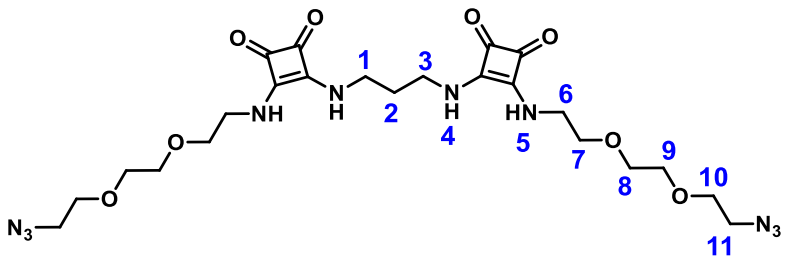
To a solution of squarate ester (100 mg, 0.704 mmol) in methanol (1 mL), a solution of tri(ethyleneglycol) functionalised amine **3.3** (147.10 mg, 0.084 mmol) and triethylamine (1 mL) dissolved in methanol (1.5 mL) was then added dropwise under a N_2 atmosphere. The resulting mixture was left to stir at room temperature overnight. After removing the solvent under vacuum, purification by column chromatography (eluent: Ch_3OH/CH_2Cl_2 2:98 *v/v*) afforded the target squaramide as a yellow oil (211 mgs,94%). **^{1}H NMR** (600 MHz, $CDCl_3$) δ = 6.33 (s, 1H, H_1), 4.39 (s, 3H, H_8), 3.72 – 3.63 (m, 8H, $H_{2\text{-}5}$) 3.64 – 3.57 (m, 2H, H_6), 3.42 (t, J = 4.9 Hz, 2H, H_7). **^{13}C NMR** (151 MHz, $CDCl_3$) δ = 183.73, 172.56, 77.37, 77.16, 76.95, 70.86, 70.71, 70.32, 70.27, 69.93, 60.59, 50.86, 50.81. **HRMS** (ESI +ve) m/z: 307.1013 ($[M+Na]^+$, $C_{11}H_{16}N_4O_5Na$ requires 307.1004).

Squaramide aryl spacer-based bis-azide (4.2)



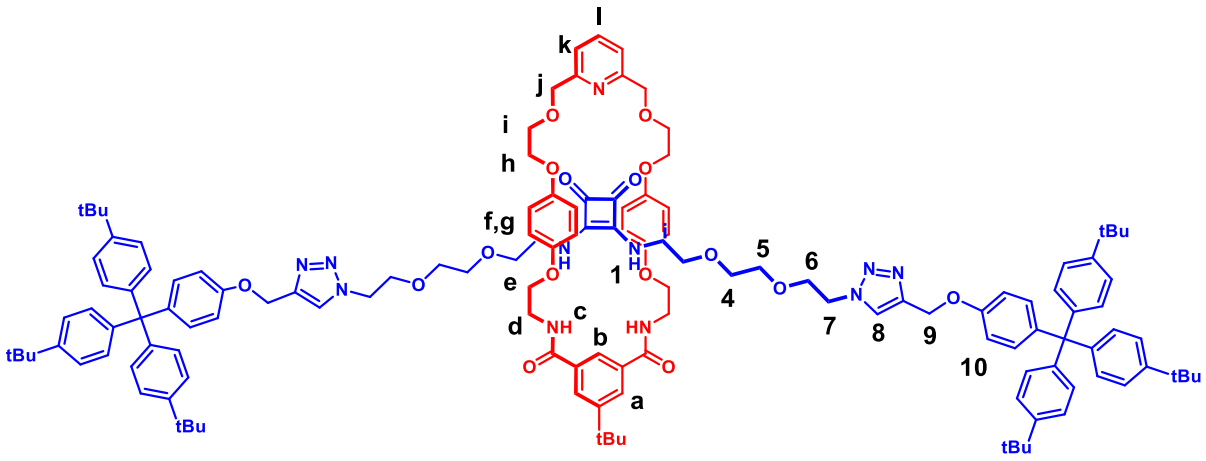
Azide **4.1** (660 mg, 2.32 mmol), diaminobenzene (119.56 mg, 1.11 mmol) and zinc triflate (40.19, 10 mol%) were dissolved in a solution of toluene/DMF 19:1 (11 mL) under a N_2 atmosphere at room temperature. The resulting mixture was left to stir at 105°C overnight. After removing the solvent under vacuum, purification by column chromatography (eluent: CH_3OH/CH_2Cl_2 4:96 *v/v*) afforded the target squaramide as a yellow solid (600 mgs, 89%). **^{1}H NMR** (600 MHz, DMSO) δ = 9.74 (s, 2H, H_4), 7.88 (s, 2H, H_5), 7.48 (s, 1H, H_2), 7.28 (t, *J* = 8.1 Hz, 1H, H_1), 7.15 (d, *J* = 8.0 Hz, 2H, H_3), 3.78 (q, *J* = 5.1 Hz, 4H, H_6), 3.64 – 3.58 (m, 16H, $H_{7\text{-}10}$), 3.38 (t, *J* = 4.9 Hz, 4H, H_{11}). **^{13}C NMR** (151 MHz, $CDCl_3$) δ = 184.14, 180.19, 169.27, 163.44, 139.98, 130.26, 112.35, 107.41, 69.98, 69.69, 69.59, 69.23, 49.96, 43.57. **HRMS** (ESI +ve) m/z: 635.2277 ($[M+Na]^+$, $C_{26}H_{32}N_{10}O_8Na$ requires 635.2297).

Squaramide alkyl spacer-based bis-azide (4.3)



To a solution of azide **4.1** (200 mg, 0.704 mmol) in methanol (2 mL), a solution of 1,3 diaminopropane (25 mg, 0.084 mmol) and triethylamine (0.188 mL) dissolved in methanol (2.3 mL) was added dropwise under a N_2 atmosphere . The resulting mixture was left to stir at room temperature overnight. After removing the solvent under vacuum, purification by column chromatography (eluent: CH_3OH/CH_2Cl_2 7:93 *v/v*) afforded the target squaramide as a white solid (130 mgs, 67%). **^{1}H NMR** (600 MHz, DMSO) δ = 7.45 (s, 4H, $H_{4,5}$), 3.66 (s, 4H, H_6), 3.62 – 3.52 (m, 20H, $H_{1,3,7\text{-}10}$), 3.41 – 3.36 (m, 4H, H_{11}), 1.80 (p, J = 6.9 Hz, 2H, H_2). **^{13}C NMR** (151 MHz, DMSO) δ = 182.47, 167.70, 70.17, 69.66, 69.58, 69.22, 49.96, 43.14, 40.62, 40.05, 32.39. **HRMS** (ESI +ve) m/z: 601.2435 ($[M+Na]^+$, $C_{23}H_{24}N_{10}O_8Na$ requires 601.2453).

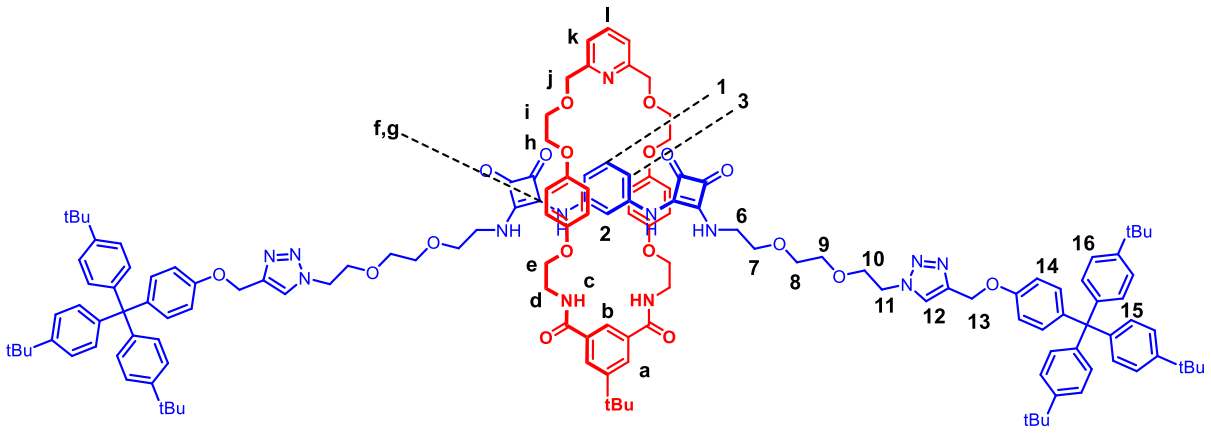
[2]rotaxane (3.14)



Macrocycle **3.10** (17.00 mg, 0.025 mmol) and $[Cu(CH_3CN)_4]PF_6$ (9.27mg, 0.025 mmol) were dissolved in dry, degassed dichloromethane (1.2 mL) and stirred for 30 minutes at room temperature. A solution of bis-azide **3.3** (31.81 mg, 0.075 mmol) and terphenyl stopper alkyne **2.13** (80.97 mg, 0.15 mmol) in dichloromethane (1.2 mL) was subsequently added dropwise to the Cu-complexed macrocycle solution. The reaction mixture was stirred at room temperature for 72 hours, following which it was diluted with CH_2Cl_2 (40 mL). The organic layer was washed with EDTA/NH_4OH (2 × 25 mL) and H_2O (2 × 25 mL), dried over $MgSO_4$, filtered and concentrated under vacuum. The crude was purified by preparative TLC in 70:25:5 CH_2Cl_2/EtOAc/MeOH to afford [2]rotaxane **3.11** as a white solid (16.37 mg, 30%). **^{1}H NMR** (600 MHz, $CDCl_3$) δ = 8.28 (s, 1H, H_b), 8.17 (s, 2H, H_a), 7.77 (s, 2H, H_c), 7.57 (d, J = 9.1 Hz, 3H, $H_{l,8}$), 7.18 – 7.10 (m, 12H, H_{13}), 7.03 (d, J = 8.8 Hz, 4H, H_{11}), 7.01 – 6.97 (m, 12H, H_{12}), 6.92 (s, 2H, H_1), 6.78 – 6.71 (m, 4H, H_{10}), 6.60 (q, J = 8.8 Hz, 8H, $H_{f,g}$), 5.03 (s, 4H, H_9), 4.57 (s, 4H, H_j), 4.31 (t, J = 5.3 Hz, 4H, H_7), 4.02 (s, 4H, H_e), 3.94 (d, J = 4.5 Hz, 4H, H_h), 3.80 (t, J = 4.3 Hz, 4H, H_i), 3.66 (d, J = 5.7 Hz, 4H, H_d), 3.62 (t, J = 5.1 Hz, 4H, H_6), 3.35 (q, J = 11.9 Hz, 16H, $H_{2,3,4,5}$), 1.29 (s, 9H, H_{mactBu}), 1.22 (s, 54H, H_{axtBu}). **^{13}C NMR** (151 MHz, CDCl3) δ = 182.9, 167.8, 167.7, 157.1, 156.3, 152.9, 152.3, 152.3, 148.5, 144.2, 144.2, 140.4, 138.1, 133.9, 132.5, 131.0,

130.8, 130.6, 128.9, 124.4, 124.2, 124.0, 123.9, 121.8, 121.4, 115.5, 115.5, 113.3, 77.4, 77.2, 76.9, 73.9, 70.7, 70.4, 70.3, 70.0, 69.4, 68.3, 66.6, 63.2, 62.0, 50.3, 43.8, 39.6, 35.2, 34.4, 31.5, 31.4, 29.8, 23.3, 22.8, 14.3, 14.3, 1.2. **HRMS** (ESI +ve) m/z: 2218.2129 ([M+Na]+, $C_{135}H_{163}N_{11}O_{16}$ requires 2218.2205).

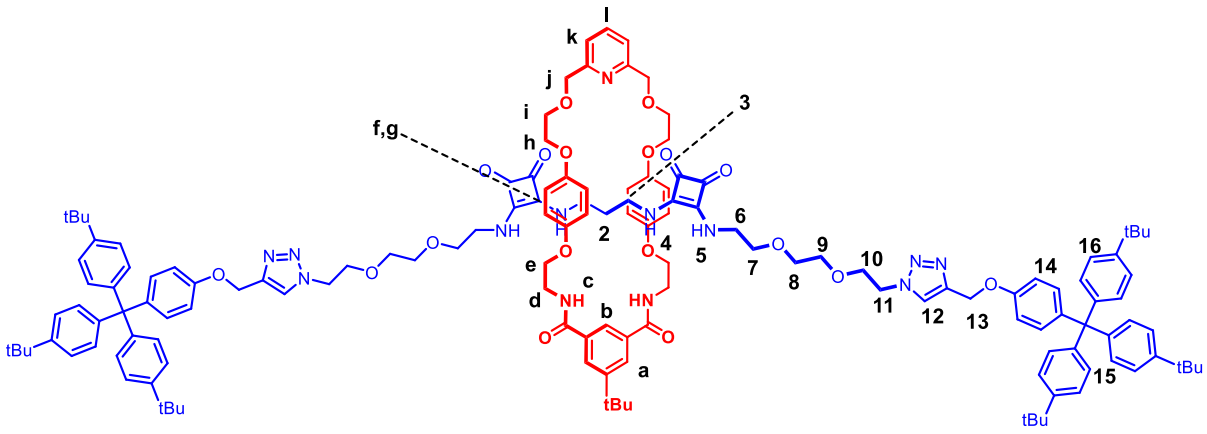
[2]rotaxane (4.4)



Macrocycle **3.10** (13.68 mg, 0.02 mmol) and $[Cu(CH_3CN)_4]PF_6$ (7.46mg, 0.02 mmol) were dissolved in dry, degassed dichloroethane (1.0 mL) and stirred for 30 minutes at room temperature. A solution of bis-azide **4.2** (36.76 mg, 0.06 mmol) and terphenyl stopper alkyne **2.13** (65.16 mg, 0.12 mmol) in dichloroethane (1.0 mL) was subsequently added dropwise to the Cu-complexed macrocycle solution. The reaction mixture was stirred at 80°C for 72 hours, following which it was cooled to room temperature and diluted with CH_2Cl_2 (40 mL). The organic layer was washed with EDTA/NH_4OH (2 × 25 mL) and H_2O (2 × 25 mL), dried over $MgSO_4$, filtered and concentrated under vacuum. The crude was purified by preparative TLC in 60:35:5 CH_2Cl_2/EtOAc/MeOH to afford [2]rotaxane **4.4** as a white solid (5.3 mg, 15%). **^{1}H NMR** (400 MHz, $CDCl_3$) δ = 9.52 (s, 2H, H_5), 8.38 (s, 1H, H_b), 8.27 (s, 2H, H_a), 7.73 (dd, J = 14.7, 7.1 Hz, 3H, $H_{c,l}$), 7.48 (s, 2H, H_{12}), 7.40 (s, 1H, H_1), 7.26 (s, 2H, H_3), 7.20 (d, J = 8.4 Hz, 12H, H_{16}), 7.07 (dd, J = 18.7, 8.7 Hz, 19H, $H_{k,15,2}$), 6.79 (d, J = 8.4 Hz, 4H, H_{14}), 6.69 (s, 2H, H_4), 6.52 – 6.43 (m, 8H, $H_{f,g}$), 5.11 (s, 4H, H_{13}), 4.67 (s, 4H, H_j), 4.43 (d, J = 5.4 Hz, 4H, H_{11}), 3.93 (s, 4H, H_e), 3.85 (s, 8H, $H_{h,7}$), 3.77 (t, J = 5.1 Hz, 4H, H_{10}), 3.65 (d, J = 14.2 Hz, 8H, $H_{d,9}$), 3.46 (s, 4H, H_i), 3.40 (s, 8H, $H_{8,6}$), 1.38 (s, 9H, H_{mactBu}), 1.28 (s, 54H, H_{axtBu}). **^{13}C NMR** (151 MHz, Acetone) δ 206.26, 181.55, 167.61, 158.62, 157.65, 153.76, 152.68, 149.35, 145.40, 144.36, 141.21, 140.76,

139.53, 135.51, 133.64, 133.02, 132.18, 131.61, 131.04, 129.80, 128.94, 125.55, 125.24, 123.30, 122.95, 116.04, 115.85, 114.50, 113.80, 74.31, 71.30, 71.03, 70.97, 70.57, 70.13, 68.49, 68.17, 67.51, 64.09, 62.46, 55.65, 50.95, 45.05, 44.92, 40.86, 40.73, 39.85, 35.74, 35.03, 31.83, 30.49, 30.37, 30.24, 30.11, 29.98, 29.85, 29.73, 29.60. **HRMS** (ESI +ve) m/z: 2381.2749 ($[M+H]^+$, $C_{145}H_{169}N_{13}O_{18}$ requires 2381.2781).

[2]rotaxane (4.5)



Macrocycle **3.10** (13.50 mg, 0.019 mmol) and $[Cu(CH_3CN)_4]PF_6$ (7.86mg, 0.019 mmol) were dissolved in dry, degassed dichloroethane (1.0 mL) and stirred for 30 minutes at room temperature. A solution of bis-azide **4.3** (34.27 mg, 0.06 mmol) and terphenyl stopper alkyne **2.13** (64.30 mg, 0.118 mmol) in dichloroethane (1.0 mL) was subsequently added dropwise to the Cu-complexed macrocycle solution. The reaction mixture was stirred at 80°C for 72 hours, following which it was cooled to room temperature and diluted with CH_2Cl_2 (40 mL). The organic layer was washed with EDTA/NH_4OH (2 × 25 mL) and H_2O (2 × 25 mL), dried over $MgSO_4$, filtered and concentrated under vacuum. The crude was purified by preparative TLC in 70:30:6 CH_2Cl_2/EtOAc/MeOH to afford [2]rotaxane **4.5** as a white solid (5.6 mg, 12%). **^{1}H NMR** (500 MHz, $CDCl_3$) δ = 8.36 (s, 1H, H_b), 8.21 (d, J = 1.4 Hz, 2H, H_a), 7.85 (s, 2H, H_c), 7.69 (t, J = 7.9 Hz, 1H, H_l), 7.65 (s, 2H, H_{12}), 7.26 (s, 2H, H_k), 7.21 (d, J = 8.6 Hz, 12H, H_{16}), 7.14 – 7.02 (m, 16H, H_{15}), 6.88 (s, 2H, H_4), 6.85 – 6.78 (m, 4H, H_{14}), 6.71 – 6.55 (m, 8H, $H_{f,g}$), 5.08 (s, 4H H_{13}), 4.67 (s, 4H, H_j), 4.44 (t, J = 5.0 Hz, 4H, H_{11}), 4.03 (p, J = 4.1 Hz, 8H, $H_{e,h}$), 3.90 (d, J = 4.4 Hz, 4H, H_i), 3.78 (t, J = 5.0 Hz, 4H, H_{10}), 3.68 (s, 8H, $H_{d,7}$), 3.50 – 3.43 (m, 12H, $H_{6,8,9}$), 3.32 (s, 4H, $H_{1,3}$), 1.57 (s, 2H, H_2), 1.34 (s, 9H, H_{mactBu}), 1.29 (s, 54H, H_{axtBu}). **^{13}C NMR** (151 MHz, Acetone) δ 206.26, 184.28, 168.16, 167.73, 158.70, 157.67, 154.01, 153.88, 152.71, 149.34,

145.42, 144.35, 140.72, 138.60, 135.65, 133.65, 133.00, 132.18, 131.61, 129.80, 128.73, 125.55, 125.25, 123.59, 121.91, 116.41, 116.39, 114.50, 74.54, 71.48, 71.07, 71.03, 70.53, 70.17, 68.74, 68.50, 67.68, 64.09, 62.46, 50.93, 44.76, 44.64, 41.74, 40.64, 40.51, 39.85, 30.52, 30.49, 30.37, 30.24, 30.12, 29.99, 29.86, 29.73, 29.60. **HRMS** (ESI +ve) m/z: 2349.2976 ($[M+H]^+$, $C_{142}H_{171}N_{13}O_{18}$ requires 2349.3005).

References

1. F. Emil, *Berichte der Deutschen Chemischen Gesellschaft*, 1894, **27**, 2985-2993.
2. F. Emil, *Berichte der Deutschen Chemischen Gesellschaft*, 1890, **23**, 2611-2624.
3. C. J. Pedersen, *Journal of the American Chemical Society*, 1967, **89**, 7017-7036.
4. J.-M. Lehn, *Science*, 1985, **227**, 849-856.
5. D. J. Cram, *Angewandte Chemie International Edition in English*, 1986, **25**, 1039-1057.
6. J. P. Sauvage, *Angewandte Chemie International Edition*, 2017, **56**, 11080-11093.
7. J. F. Stoddart, *Angewandte Chemie International Edition*, 2017, **56**, 11094-11125.
8. B. L. Feringa, *Angewandte Chemie International Edition*, 2017, **56**, 11060-11078.
9. J. M. Lehn, *Angewandte Chemie International Edition in English*, 1988, **27**, 89-112.
10. P. Kumar, S. Banerjee, A. Radha, T. Firdoos, S. C. Sahoo and S. K. Pandey, *New Journal of Chemistry*, 2021, **45**, 2249-2263.
11. K. Ariga, J. P. Hill, M. V. Lee, A. Vinu, R. Charvet and S. Acharya, *Science and Technology of Advanced Materials*, 2008, **9**, 014109.
12. P. Beer, P. D. Beer, T. A. Barendt and J. Y. C. Lim, *Supramolecular Chemistry: Fundamentals and Applications*, Oxford university press, 2022.
13. J. F. Stoddart, *Annual Reports Section "B" (Organic Chemistry)*, 1988, **85**, 353-386.
14. D. N. Reindhoudt and P. J. Dijkstra, *Pure and Applied Chemistry*, 1988, **60**, 477-482.
15. M. J. Webber and R. Langer, *Chemical Society Reviews*, 2017, **46**, 6600-6620.
16. S. Bernhard and M. W. Tibbitt, *Advanced Drug Delivery Reviews*, 2021, **171**, 240-256.
17. W. Feng, M. Jin, K. Yang, Y. Pei and Z. Pei, *Chemical Communications*, 2018, **54**, 13626-13640.
18. M. Teresa Albelda, J. C. Frías, E. García-España and H.-J. Schneider, *Chemical Society Reviews*, 2012, **41**, 3859.
19. B. O. Okesola and D. K. Smith, *Chemical Society Reviews*, 2016, **45**, 4226-4251.
20. E. R. Kay, D. A. Leigh and F. Zerbetto, *Angewandte Chemie International Edition*, 2007, **46**, 72-191.
21. P. Hobza, R. Zahradník and K. Müller-Dethlefs, *Collection of Czechoslovak Chemical Communications*, 2006, **71**, 443-531.
22. M. K. Gilson, *Current opinion in structural biology*, 1995, **5**, 216-223.
23. J. W. Steed and J. L. Atwood, *Supramolecular chemistry*, John Wiley & Sons, 2022.
24. Y. Yang, W. Feng, J. Hu, S. Zou, R. Gao, K. Yamato, M. Kline, Z. Cai, Y. Gao, Y. Wang, Y. Li, Y. Yang, L. Yuan, X. C. Zeng and B. Gong, *Journal of the American Chemical Society*, 2011, **133**, 18590-18593.
25. Ł. Tabisz, Z. Rozwadowski, A. Katrusiak and B. Łęska, *Scientific Reports*, 2020, **10**.
26. K. A. Sharp and B. Honig, *Annual review of biophysics and biophysical chemistry*, 1990, **19**, 301-332.
27. C. Wang, L. Guan, D. Danovich, S. Shaik and Y. Mo, *Journal of Computational Chemistry*, 2016, **37**, 34-45.
28. H. Umeyama and K. Morokuma, *Journal of the American Chemical Society*, 1977, **99**, 1316-1332.
29. S. J. Grabowski, *Journal of Physical Organic Chemistry*, 2004, **17**, 18-31.
30. I. K. McDonald and J. M. Thornton, *Journal of molecular biology*, 1994, **238**, 777-793.
31. R. Kumar, J. R. Schmidt and J. L. Skinner, *The Journal of chemical physics*, 2007, **126**.

32. H. R. Drew, R. M. Wing, T. Takano, C. Broka, S. Tanaka, K. Itakura and R. E. Dickerson, *Proceedings of the National Academy of Sciences*, 1981, **78**, 2179-2183.
33. H. Luecke and F. A. Quiocho, *Nature*, 1990, **347**, 402.
34. J. W. Pflugrath and F. A. Quiocho, *Nature*, 1985, **314**, 257.
35. T. Clark, M. Hennemann, J. S. Murray and P. Politzer, *Journal of molecular modeling*, 2007, **13**, 291-296.
36. M. J. Langton, S. W. Robinson, I. Marques, V. Félix and P. D. Beer, *Nature chemistry*, 2014, **6**, 1039-1043
37. J. Y. C. Lim and P. D. Beer, *Chem*, 2018, **4**, 731-783.
38. P. Politzer and J. Murray, *Crystals*, 2017, **7**, 212.
39. P. Metrangolo, F. Meyer, T. Pilati, G. Resnati and G. Terraneo, *Angewandte Chemie International Edition*, 2008, **47**, 6114-6127.
40. J. S. Murray, P. Lane, T. Clark, K. E. Riley and P. Politzer, *Journal of Molecular Modeling*, 2012, **18**, 541-548.
41. J. S. Murray, P. Lane and P. Politzer, *Journal of Molecular Modeling*, 2009, **15**, 723-729.
42. A. Bauzá and A. Frontera, *Angewandte Chemie International Edition*, 2015, **54**, 7340-7343.
43. P. W. Snyder, J. Mecinović, D. T. Moustakas, S. W. Thomas Iii, M. Harder, E. T. Mack, M. R. Lockett, A. Héroux, W. Sherman and G. M. Whitesides, *Proceedings of the National Academy of Sciences*, 2011, **108**, 17889-17894.
44. M. B. Hillyer and B. C. Gibb, *Annual review of physical chemistry*, 2016, **67**, 307-329.
45. M. S. Cubberley and B. L. Iverson, *Journal of the American Chemical Society*, 2001, **123**, 7560-7563.
46. M. Fernández-Vidal, S. H. White and A. S. Ladokhin, *The Journal of membrane biology*, 2011, **239**, 5-14.
47. A. S. Mahadevi and G. N. Sastry, *Chemical reviews*, 2013, **113**, 2100-2138.
48. J. Sunner, K. Nishizawa and P. Kebarle, *The Journal of Physical Chemistry*, 1981, **85**, 1814-1820.
49. D. P. Weimann and C. A. Schalley, *Supramolecular Chemistry*, 2008, **20**, 117-128.
50. M. E. Weber, E. K. Elliott and G. W. Gokel, *Organic & biomolecular chemistry*, 2006, **4**, 83-89.
51. D. Quiñonero, C. Garau, A. Frontera, P. Ballester, A. Costa and P. M. Deyà, *Chemical physics letters*, 2002, **359**, 486-492.
52. O. B. Berryman, V. S. Bryantsev, D. P. Stay, D. W. Johnson and B. P. Hay, *Journal of the American Chemical Society*, 2007, **129**, 48-58.
53. S. Li, S.-X. Fa, Q.-Q. Wang, D.-X. Wang and M.-X. Wang, *The Journal of Organic Chemistry*, 2012, **77**, 1860-1867
54. S. Guha and S. Saha, *Journal of the American Chemical Society*, 2010, **132**, 17674-17677.
55. O. B. Berryman, F. Hof, M. J. Hynes and D. W. Johnson, *Chemical communications*, 2006, 506-508.
56. Y. Fraenkel, J. M. Gershoni and G. Navon, *FEBS letters*, 1991, **291**, 225-228.
57. Y. Beldjoudi, A. Narayanan, I. Roy, T. J. Pearson, M. M. Cetin, M. T. Nguyen, M. D. Krzyaniak, F. M. Alsubaie, M. R. Wasielewski and S. I. Stupp, *Journal of the American Chemical Society*, 2019, **141**, 17783-17795.

58. J. L. Sessler, P. A. Gale and W.-S. Cho, *Anion receptor chemistry*, Royal Society of Chemistry, Cambridge, 2006.
59. N. Busschaert, C. Caltagirone, W. Van Rossom and P. A. Gale, *Chemical Reviews*, 2015, **115**, 8038-8155.
60. X. Wu, A. M. Gilchrist and P. A. Gale, *Chem*, 2020, **6**, 1296-1309.
61. S. J. Butler and K. A. Jolliffe, *ChemPlusChem*, 2021, **86**, 59-70.
62. T. R. Bell-Horwath, A. K. Vadukoot, F. S. Thowfeik, G. Li, M. Wunderlich, J. C. Mulloy and E. J. Merino, *Bioorganic & Medicinal Chemistry Letters*, 2013, **23**, 2951-2954.
63. W. S. Brotherton, R. J. Clark and L. Zhu, *The Journal of Organic Chemistry*, 2012, **77**, 6443-6455.
64. M. P. Anderson, R. J. Gregory, S. Thompson, D. W. Souza, S. Paul, R. C. Mulligan, A. E. Smith and M. J. Welsh, *Science.*, 1991, **253**, 202–205.
65. E. Parravicini, C. Fontana, G. L. Paterlini, P. Tagliabue, F. Rovelli, K. Leung and R. I. Stark, *Pediatrics*, 1996, **98**, 730-734.
66. M. A. Horwitz and V. Gouverneur, in *Anion-Binding Catalysis*, 2022, 111-140.
67. S. Mitra and S. Mukherjee, in *Anion-Binding Catalysis*, 2022, 161-199.
68. R. Papagna, L. Vogel and S. M. Huber, in *Anion-Binding Catalysis*, 2022, 307-343.
69. J.-c. Lee, K. Kurniawan, S. Kim, V. T. Nguyen and B. D. Pandey, *Separation & Purification Reviews*, 2023, **52**, 242-261.
70. V. T. Nguyen, S. Riaño and K. Binnemans, *Green Chemistry*, 2020, **22**, 8375-8388.
71. M. Sadeq, C. L. Moe, B. Attarassi, I. Cherkaoui, R. ElAouad and L. Idrissi, *International Journal of Hygiene and Environmental Health*, 2008, **211**, 546-554.
72. M. R. Alyce, H. D. James and K. Alan David, *Ochsner Journal*, 2014, **14**, 392.
73. G. F. McIsaac, M. B. David, G. Z. Gertner and D. A. Goolsby, *Nature*, 2001, **414**, 166-167.
74. J. L. Hatfield and R. F. Follett, *Nitrogen in the Environment*, Elsevier Inc., 2nd edn., 2008.
75. S. Chang and S. H. Lamm, *International Journal of Toxicology*, 2003, **22**, 175-186.
76. P. K. Dasgupta, J. V. Dyke, A. B. Kirk and W. A. Jackson, *Environmental Science & Technology*, 2006, **40**, 6608-6614.
77. J.L. Way, *Annual Review of Pharmacology and Toxicology*, 1984, **24**, 451-481.
78. A. J. McConnell and P. D. Beer, *Angewandte Chemie International Edition*, 2012, **51**, 5052-5061.
79. R. D. Shannon, *Acta Crystallographica*, 1976, **32**, 751–767.
80. K. H. Stern, *Chemical Reviews*, 1959, **59**, 1–64.
81. J. W. Steed and J. L. Atwood, in *Supramolecular Chemistry*, John Wiley & Sons, Ltd, 2009, 1–31.
82. A. E. Hargrove, S. Nieto, T. Zhang, J. L. Sessler and E. V. Anslyn, *Chemical Reviews*, 2011, **111**, 6603-6782.
83. P. D. Beer and P. A. Gale, *Angewandte Chemie International Edition*, 2001, **40**, 486-516.
84. Philip A. Gale, Ethan N. W. Howe and X. Wu, *Chem*, 2016, **1**, 351-422.
85. M. Teresa Albelda, M. Alexandra Bernardo, E. Garcia-España, M. Luz Godino-Salido, S. V. Luis, M. João Melo, F. Pina and C. Soriano, *Journal of the Chemical Society, Perkin Transactions 2*, 1999.
86. H. B. Leavesley, L. Li, K. Prabhakaran, J. L. Borowitz and G. E. Isom, *Society of Toxicology*, 2007, **101**, 101–11

87. M. G. Cacace, E. M. Landau and J. J. Ramsden, *Quarterly Reviews of Biophysics*, 1997, **30**, 241-277.
88. M. J. Langton, C. J. Serpell and P. D. Beer, *Angewandte Chemie International Edition*, 2016, **55**, 1974-1987.
89. A. B. Pardee, *Journal of Biological Chemistry*, 1966, **241**, 5886-5892.
90. D. Gonzalez, M. Richez, C. Bergonzi, E. Chabriere and M. Elias, *Scientific Reports*, 2014, **4**, 6636.
91. J. B. Wittenberg and L. Isaacs, in *Supramolecular Chemistry*, John Wiley & Sons, Ltd, 2012.
92. D. J. Cram, *Science*, 1988, **240**, 760-767.
93. G. Cooke and V. M. Rotello, *Chemical Society Reviews*, 2002, **31**, 275-286.
94. C. H. Park and H. E. Simmons, *Journal of the American Chemical Society*, 1968, **90**, 2431-2432.
95. J. M. Lehn, E. Sonveaux and A. K. Willard, *Journal of the American Chemical Society*, 1978, **100**, 4914–4916.
96. F. P. Schmidtchen and G. Müller, *Journal of the Chemical Society, Chemical Communications*, 1984.
97. P. Blondeau, J. Benet-Buchholz and J. de Mendoza, *New Journal of Chemistry*, 2007, **31**, 736-740.
98. C. Schmuck and M. Schwegmann, *Journal of the American Chemical Society*, 2005, **127**, 3373-3379.
99. K. Sato, S. Arai and T. Yamagishi, *Tetrahedron Letters*, 1999, **40**, 5219-5222.
100. K. Chellappan, N. J. Singh, I.-C. Hwang, J. W. Lee and K. S. Kim, *Angewandte Chemie International Edition*, 2005, **44**, 2899-2903.
101. J. Cai, B. P. Hay, N. J. Young, X. Yang and J. L. Sessler, *Chemical Science*, 2013, **4**, 1560-1567.
102. R. A. Pascal, J. Spergel and D. Van Engen, *Tetrahedron Letters*, 1986, **27**, 4099-4102.
103. S. Kubik, R. Kirchner, D. Nolting and J. Seidel, *Journal of the American Chemical Society*, 2002, **124**, 12752-12760.
104. S. J. Brooks, P. A. Gale and M. E. Light, *Chemical Communications*, 2006, 4344-4346.
105. G. V. Oshovsky, W. Verboom, R. H. Fokkens and D. N. Reinhoudt, *Chemistry – A European Journal*, 2004, **10**, 2739-2748.
106. C. Xiong-Jie, L. Zhi, and C. Wen-Hua, *Mini Reviews in Organic Chemistry*, 2018, **15**, 148–156.
107. R. M. Owen, C. B. Carlson, J. Xu, P. Mowery, E. Fasella and L. L. Kiessling, *ChemBioChem*, 2007, **8**, 68-82.
108. A. P. Davis, S. M. Draper, G. Dunne and P. Ashton, *Chemical Communications*, 1999, 2265-2266.
109. A. M. Gilbert, M. M. Antane, T. M. Argentieri, J. A. Butera, G. D. Francisco, C. Freeden, E. G. Gundersen, R. F. Graceffa, D. Herbst, B. H. Hirth, J. R. Lennox, G. McFarlane, N. W. Norton, D. Quagliato, J. H. Sheldon, D. Warga, A. Wojdan and M. Woods, *Journal of Medicinal Chemistry*, 2000, **43**, 1203-1214.
110. F. R. Wurm and H.-A. Klok, *Chemical Society Reviews*, 2013, **42**, 8220-8236.
111. H. Y. Bae and C. E. Song, *ACS Catalysis*, 2015, **5**, 3613-3619.

112. V. Amendola, G. Bergamaschi, M. Boiocchi, L. Fabbrizzi and M. Milani, *Chemistry – A European Journal*, 2010, **16**, 4368-4380.
113. L. Qin, A. Hartley, P. Turner, R. B. P. Elmes and K. A. Jolliffe, *Chemical Science*, 2016, **7**, 4563-4572.
114. R. Prohens, S. Tomàs, J. Morey, P. M. Deyà, P. Ballester and A. Costa, *Tetrahedron Letters*, 1998, **39**, 1063-1066.
115. L. Qin, J. R. Wright, J. D. E. Lane, S. N. Berry, R. B. P. Elmes and K. A. Jolliffe, *Chemical Communications*, 2019, **55**, 12312-12315.
116. A. Frontera, J. Morey, A. Oliver, M. N. Piña, D. Quiñonero, A. Costa, P. Ballester, P. M. Deyà and E. V. Anslyn, *The Journal of Organic Chemistry*, 2006, **71**, 7185-7195.
117. S. Peng, Q. He, G. I. Vargas-Zúñiga, L. Qin, I. Hwang, S. K. Kim, N. J. Heo, C.-H. Lee, R. Dutta and J. L. Sessler, *Chemical Society Reviews*, 2020, **49**, 865-907.
118. S. H. Kim, J. Lee, G. I. Vargas-Zúñiga, V. M. Lynch, B. P. Hay, J. L. Sessler and S. K. Kim, *The Journal of Organic Chemistry*, 2018, **83**, 2686-2693.
119. Y. Li and A. H. Flood, *Angewandte Chemie International Edition*, 2008, **47**, 2649-2652.
120. Y. Liu, W. Zhao, C. H. Chen and A. H. Flood, *Science.*, 2019, **365**, 159–161.
121. A. Brown and P. D. Beer, *Chemical Communications*, 2016, **52**, 8645-8658.
122. M. G. Sarwar, B. Dragisic, S. Sagoo and M. S. Taylor, *Angewandte Chemie International Edition*, 2010, **49**, 1674–1677.
123. A. Borissov, J. Y. C. Lim, A. Brown, K. E. Christensen, A. L. Thompson, M. D. Smith and P. D. Beer, *Chemical Communications*, 2017, **53**, 2483-2486.
124. R. Tepper, B. Schulze, H. Görls, P. Bellstedt, M. Jäger and U. S. Schubert, *Organic Letters*, 2015, **17**, 5740-5743.
125. C. J. Massena, A. M. S. Riel, G. F. Neuhaus, D. A. Decato and O. B. Berryman, *Chemical Communications*, 2015, **51**, 1417-1420.
126. S. W. Robinson, C. L. Mustoe, N. G. White, A. Brown, A. L. Thompson, P. Kennepohl and P. D. Beer, *Journal of the American Chemical Society*, 2015, **137**, 499-507.
127. L. González, F. Zapata, A. Caballero, P. Molina, C. Ramírez de Arellano, I. Alkorta and J. Elguero, *Chemistry – A European Journal*, 2016, **22**, 7533-7544.
128. T. Gunnlaugsson, H. D. P. Ali, M. Glynn, P. E. Kruger, G. M. Hussey, F. M. Pfeffer, C. M. G. dos Santos and J. Tierney, *Journal of Fluorescence*, 2005, **15**, 287-299.
129. P. Ashokkumar, H. Weißhoff, W. Kraus and K. Rurack, *Angewandte Chemie International Edition*, 2014, **53**, 2225-2229.
130. C. Alexander, J. A. Thom, A. M. Kenwright, K. E. Christensen, T. J. Sørensen and S. Faulkner, *Chemical Science*, 2023, **14**, 1194-1204.
131. H. Miyaji, P. Anzenbacher Jr, J. L. Sessler, E. R. Bleasdale and P. A. Gale, *Chemical Communications*, 1999, 1723-1724.
132. L. C. Murfin, K. Chiang, G. T. Williams, C. L. Lyall, A. T. A. Jenkins, J. Wenk, T. D. James and S. E. Lewis, *Frontiers in Chemistry*, 2020, **8**.
133. K. A. Nielsen, J. O. Jeppesen, E. Levillain and J. Becher, *Angewandte Chemie International Edition*, 2003, **42**, 187-191.
134. J. Y. C. Lim, M. J. Cunningham, J. J. Davis and P. D. Beer, *Chemical Communications*, 2015, **51**, 14640-14643.

135. R. Hein, A. Docker, J. J. Davis and P. D. Beer, *Journal of the American Chemical Society*, 2022, **144**, 8827-8836.
136. P. D. Beer, P. K. Hopkins and J. D. McKinney, *Chemical Communications*, 1999, **13**, 1253-1254.
137. Q. He, G. M. Peters, V. M. Lynch and J. L. Sessler, *Angewandte Chemie International Edition*, 2017, **56**, 13396-13400.
138. J. H. Lee, J. H. Lee, Y. R. Choi, P. Kang, M.-G. Choi and K.-S. Jeong, *The Journal of Organic Chemistry*, 2014, **79**, 6403-6409.
139. G. Grauwels, H. Valkenier, A. P. Davis, I. Jabin, K. Bartik, *Angewandte Chemie International Edition,* 2019, **131**, 6995.
140. D. Jagleniec, Ł. Dobrzycki, M. Karbarz and J. Romański, *Chemical Science*, 2019, **10**, 9542-9547.
141. S. Pang, X. Sun, Z. Yan, C. Wang, K. Ye, S. Ma, L. Zhu and C. Bao, *Chemical Communications*, 2023, **59**, 3866-3869.
142. M. Karbarz and J. Romański, *Inorganic Chemistry*, 2016, **55**, 3616-3623.
143. A. J. McConnell and P. D. Beer, *Angewandte Chemie International Edition*, 2012, **51**, 5052-5061.
144. L. A. J. Chrisstoffels, F. de Jong, D. N. Reinhoudt, S. Sivelli, L. Gazzola, A. Casnati, R. Ungaro, J. Am. Chem. Soc. 1999, 121, 10142–10151.
145. K. D. Patryk Niedbała, J. Narodowiec, M. Ceborska, J. M. Granda, *ChemRxiv*, 2022, 1.
146. S. K. Kim, J. L. Sessler, D. E. Gross, C.-H. Lee, J. S. Kim, V. M. Lynch, L. H. Delmau and B. P. Hay, *Journal of the American Chemical Society*, 2010, **132**, 5827-5836.
147. J. M. Mahoney, A. M. Beatty and B. D. Smith, *Journal of the American Chemical Society*, 2001, **123**, 5847-5848.
148. C. Suksai, P. Leeladee, D. Jainuknan, T. Tuntulani, N. Muangsin, O. Chailapakul, P. Kongsaeree and C. Pakavatchai, *Tetrahedron Letters*, 2005, **46**, 2765-2769.
149. M. Ciardi, F. Tancini, G. Gil-Ramírez, E. C. Escudero Adán, C. Massera, E. Dalcanale and P. Ballester, *Journal of the American Chemical Society*, 2012, **134**, 13121-13132.
150. M. D. Lankshear, A. R. Cowley and P. D. Beer, *Chemical Communications*, 2006, **6**, 612-614.
151. K., Nobumasa, K. Fujisawa, C. Fujimoto, Y. Morooka, S. Hashimoto, T. Kitagawa, K. Toriumi, K. Tatsumi, and A. Nakamura, *Journal of the American Chemical Society*, 1992, **4**, 1277-1291.
152. Y. Agnus, R. Louis, J. P. Gisselbrecht and R. Weiss, *Journal of the American Chemical Society*, 1984, **106**, 93-102.
153. D. J. White, N. Laing, H. Miller, S. Parsons, P. A. Tasker and S. Coles, *Chemical Communications*, 1999, **2000**, 3773-3782.
154. D. Jagleniec, Ł. Dobrzycki, M. Karbarz and J. Romański, *Chemical Science*, 2019, **10**, 9542-9547.
155. P. D. Beer, P. K. Hopkins and J. D. McKinney, *Chemical Communications*, 1999.
156. J. H. Lee, J. H. Lee, Y. R. Choi, P. Kang, M.-G. Choi and K.-S. Jeong, *The Journal of Organic Chemistry*, 2014, **79**, 6403-6409.
157. G. Grauwels, H. Valkenier, A. P. Davis, I. Jabin and K. Bartik, *Angewandte Chemie International Edition,* 2019, **131**, 6995

158. F. Otón, M. d. C. González, A. Espinosa, C. Ramírez de Arellano, A. Tárraga and P. Molina, *The Journal of Organic Chemistry*, 2012, **77**, 10083-10092.
159. D. B. Amabilino and J. F. Stoddart, Chemical Reviews, 1995, **95**, 2725-2828.
160. J. S. Siegel, Science, 2004, **304**, 1256.
161. J. F. Nierengarten, C. O. Dietrich-Buchecker and J. P. Sauvage, *Journal of the American Chemical Society*, 1994, **116**, 375-376.
162. V. Marcos, A. J. Stephens, J. Jaramillo-Garcia, A. L. Nussbaumer, S. L. Woltering, A. Valero, J. F. Lemonnier, I. J. Vitorica-Yrezabal and D. A. Leigh, Science, 2016, **352**, 1555–1559
163. J. J. Danon, A. Krüger, D. A. Leigh, J. Lemonnier, A. J. Stephens, I. J. Vitorica-Yrezabal and S. L. Woltering, Science, 2017, **355**, 159–162
164. K. S. Chichak, S. J. Cantrill, A. R. Pease, S.-H. Chiu, G. W. V. Cave, J. L. Atwood and J. F. Stoddart, Science, 2004, **304**, 1308.
165. C. D. Pentecost, K. S. Chichak, A. J. Peters, G. W. V. Cave, S. J. Cantrill and J. F. Stoddart, *Angewandte Chemie International Edition*, 2007, **46**, 218-222.
166. D. A. Leigh, R. G. Pritchard and A. J. Stephens, *Nature Chemistry*, 2014, **6**, 978-982.
167. N. Hoyas Pérez and J. E. M. Lewis, *Organic & Biomolecular Chemistry*, 2020, **18**, 6757-6780.
168. P. Ruggli, *Justus Liebigs Annalen der Chemie*, 1912, **392**, 92-100.
169. H. L. Frisch and E. Wasserman, *Journal of the American Chemical Society*, 1961, **83**, 3789—3795.
170. G. Schill and A. Lüttringhaus, *Angewandte Chemie International Edition*, 1964, **3**, 546-547. 168.
171. G. Schill and C. Zürcher, *Angewandte Chemie International Edition*, 1969, **8**, 988-988.
172. C. O. Dietrich-Buchecker, J. P. Sauvage and J. M. Kern, *Journal of the American Chemical Society*, 1984, **106**, 3043 —3045.
173. S. M. Goldup, D. A. Leigh, P. J. Lusby, R. T. McBurney and A. M. Z. Slawin, *Angewandte Chemie International Edition*, 2008, **47**, 6999-7003.
174. A.-M. L. Fuller, D. A. Leigh, P. J. Lusby, A. M. Z. Slawin and D. B. Walker, *Journal of the American Chemical Society*, 2005, **127**, 12612-12619.
175. J.-C. Chang, S.-H. Tseng, C.-C. Lai, Y.-H. Liu, S.-M. Peng and S.-H. Chiu, *Nature Chemistry*, 2017, **9**, 128-134.
176. D. A. Leigh, P. J. Lusby, R. T. McBurney, A. Morelli, A. M. Z. Slawin, A. R. Thomson and D. B. Walker, *Journal of the American Chemical Society*, 2009, **131**, 3762-3771.
177. J. D. Crowley, S. M. Goldup, N. D. Gowans, D. A. Leigh, V. E. Ronaldson and A. M. Z. Slawin, *Journal of the American Chemical Society*, 2010, **132**, 6243-6248.
178. D. A. Leigh, R. G. Pritchard and A. J. Stephens, *Nature Chemistry*, 2014, **6**, 978–982.
179. F. Zapata, O. A. Blackburn, M. J. Langton, S. Faulkner and P. D. Beer, *Chemical Communications*, 2013, **49**, 8157-8159.
180. D. G. Hamilton, J. K. M. Sanders, J. E. Davies, W. Clegg and S. J. Teat, *Chemical Communications*, 1997.
181. S.-T. Tung, C.-C. Lai, Y.-H. Liu, S.-M. Peng and S.-H. Chiu, *Angewandte Chemie International Edition*, 2013, **52**, 13269-13272.

182. J. Berná, J. D. Crowley, S. M. Goldup, K. D. Hänni, A.-L. Lee and D. A. Leigh, *Angewandte Chemie International Edition*, 2007, **46**, 5709-5713.
183. J. Winn, A. Pinczewska and S. M. Goldup, *Journal of the American Chemical Society*, 2013, **135**, 13318-13321.
184. M. Franz, J. A. Januszewski, D. Wendinger, C. Neiss, L. D. Movsisyan, F. Hampel, H. L. Anderson, A. Görling and R. R. Tykwinski, *Angewandte Chemie International Edition*, 2015, **54**, 6645-6649.
185. S. Hoekman, M. O. Kitching, D. A. Leigh, M. Papmeyer and D. Roke, *Journal of the American Chemical Society*, 2015, **137**, 7656-7659.
186. S. Saito, E. Takahashi and K. Nakazono, *Organic Letters*, 2006, **8**, 5133-5136.
187. Y. Sato, R. Yamasaki and S. Saito, *Angewandte Chemie International Edition*, 2009, **48**, 504-507.
188. M. Franz, J. A. Januszewski, D. Wendinger, C. Neiss, L. D. Movsisyan, F. Hampel, H. L. Anderson, A. Görling and R. R. Tykwinski, *Angewandte Chemie International Edition*, 2015, **54**, 6645-6649.
189. J. D. Crowley, K. D. Hänni, A.-L. Lee and D. A. Leigh, *Journal of the American Chemical Society*, 2007, **129**, 12092-12093.
190. J. Berná, J. D. Crowley, S. M. Goldup, K. D. Hänni, A.-L. Lee and D. A. Leigh, *Angewandte Chemie International Edition*, 2007, **46**, 5709-5713.
191. J. D. Crowley, S. M. Goldup, N. D. Gowans, D. A. Leigh, V. E. Ronaldson and A. M. Z. Slawin, *Journal of the American Chemical Society*, 2010, **132**, 6243-6248.
192. J. J. Danon, D. A. Leigh, P. R. McGonigal, J. W. Ward and J. Wu, *Journal of the American Chemical Society*, 2016, **138**, 12643-12647.
193. S. M. Goldup, D. A. Leigh, R. T. McBurney, P. R. McGonigal and A. Plant, *Chemical Science*, 2010, **1**, 383-386.
194. J. D. Crowley, K. D. Hänni, A.-L. Lee and D. A. Leigh, *Journal of the American Chemical Society*, 2007, **129**, 12092-12093.
195. M. Denis and S. M. Goldup, *Nature Reviews Chemistry*, 2017, **1**, 0061.
196. J. E. M. Lewis, R. J. Bordoli, M. Denis, C. J. Fletcher, M. Galli, E. A. Neal, E. M. Rochette and S. M. Goldup, *Chemical Science*, 2016, **7**, 3154-3161.
197. G. M. Hübner, J. Gläser, C. Seel and F. Vögtle, *Angewandte Chemie International Edition*, 1999, **38**, 383-386.
198. J. A. Wisner, P. D. Beer and M. G. B. Drew, *Angewandte Chemie International Edition*, 2001, **40**, 3606-3609.
199. J. A. Wisner, P. D. Beer, N. G. Berry and B. Tomapatanaget, *Proceedings of the National Academy of Sciences*, 2002, **99**, 4983-4986.
200. A. Docker, Y. C. Tse, H. M. Tay, A. J. Taylor, Z. Zhang and P. D. Beer, *Angewandte Chemie International Edition*, 2022, **61**, e202214523.
201. M. J. Langton and P. D. Beer, *Chemical Communications*, 2014, **50**, 8124-8127.
202. K. M. Bąk, B. Trzaskowski and M. J. Chmielewski, ChemRxiv, 2023.
203. N. H. Evans, H. Rahman, A. V. Leontiev, N. D. Greenham, G. A. Orlowski, Q. Zeng, R. M. J. Jacobs, C. J. Serpell, N. L. Kilah, J. J. Davis and P. D. Beer, *Chemical Science*, 2012, **3**, 1080-1089.
204. M. J. Langton and P. D. Beer, *Accounts of Chemical Research*, 2014, **47**, 1935-1949.

205. K. Hiratani, M. Kaneyama, Y. Nagawa, E. Koyama and M. Kanesato, *Journal of the American Chemical Society*, 2004, **126**, 13568-13569.
206. N. H. Evans, H. Rahman, A. V. Leontiev, N. D. Greenham, G. A. Orlowski, Q. Zeng, R. M. J. Jacobs, C. J. Serpell, N. L. Kilah, J. J. Davis and P. D. Beer, *Chemical Science*, 2012, **3**, 1080-1089.
207. C. Allain, P. D. Beer, S. Faulkner, M. W. Jones, A. M. Kenwright, N. L. Kilah, R. C. Knighton, T. J. Sørensen and M. Tropiano, *Chemical Science*, 2013, **4**, 489-493.
208. S. S. Zhu, P. J. Carroll and T. M. Swager, *Journal of the American Chemical Society*, 1996, **118**, 8713-8714.
209. M. Cirulli, A. Kaur, J. E. M. Lewis, Z. Zhang, J. A. Kitchen, S. M. Goldup and M. M. Roessler, *Journal of the American Chemical Society*, 2019, **141**, 879-889.
210. M. J. Langton, S. W. Robinson, I. Marques, V. Félix and P. D. Beer, *Nature Chemistry*, 2014, **6**, 1039-1043.
211. J. J. Gassensmith, S. Matthys, J.-J. Lee, A. Wojcik, P. V. Kamat and B. D. Smith, *Chemistry – A European Journal*, 2010, **16**, 2916-2921.
212. M. V. R. Raju and H.-C. Lin, *Organic Letters*, 2013, **15**, 1274-1277.
213. X. Bao, I. Isaacsohn, A. F. Drew and D. B. Smithrud, *Journal of the American Chemical Society*, 2006, **128**, 12229-12238.
214. X. Bao, I. Isaacsohn, A. F. Drew and D. B. Smithrud, *The Journal of Organic Chemistry*, 2007, **72**, 3988-4000.
215. S. Pang, X. Sun, Z. Yan, C. Wang, K. Ye, S. Ma, L. Zhu and C. Bao, *Chemical Communications*, 2023, **59**, 3866-3869.
216. C.-S. Kwan, A. S. C. Chan and K. C.-F. Leung, *Organic Letters*, 2016, **18**, 976-979.
217. K. Xu, K. Nakazono and T. Takata, *Chemistry Letters*, 2016, **45**, 1274-1276.
218. J. M. Mahoney, A. M. Beatty and B. D. Smith, *Inorganic Chemistry*, 2004, **43**, 7617-7621.
219. R. C. Knighton and P. D. Beer, *Chemical Communications*, 2014, **50**, 1540-1542.
220. R. C. Knighton and P. D. Beer, *Organic Chemistry Frontiers*, 2021, **8**, 2468-2472.
221. V. Valderrey, E. C. Escudero-Adán and P. Ballester, *Journal of the American Chemical Society*, 2012, **134**, 10733-10736.
222. M. Denis, L. Qin, P. Turner, K. A. Jolliffe and S. M. Goldup, *Angewandte Chemie International Edition*, 2018, **57**, 5315-5319.
223. V. K. Munasinghe, J. Pancholi, D. Manawadu, Z. Zhang and P. D. Beer, *Chemistry – A European Journal*, 2022, **28**, e202201209.
224. H. M. Tay, Y. C. Tse, A. Docker, C. Gateley, A. L. Thompson, H. Kuhn, Z. Zhang and P. D. Beer, *Angewandte Chemie International Edition*, 2023, **62**, e202214785.
225. J. Beswick, V. Blanco, G. De Bo, D. A. Leigh, U. Lewandowska, B. Lewandowski and K. Mishiro, *Chemical Science*, 2015, **6**, 140-143.
226. R. L. Spicer, C. C. Shearman and N. H. Evans, *Chemistry – A European Journal*, 2023, **29**, e202203502.
227. G. Martin, L. Rentsch, M. Höck and M. Bertau, *Energy Storage Materials*, 2017, **6**, 171-179.
228. L. Kavanagh, J. Keohane, G. Garcia Cabellos, A. Lloyd and J. Cleary, *Journal*, 2018, **7**.
229. L. Talens Peiró, G. Villalba Méndez and R. U. Ayres, *JOM*, 2013, **65**, 986-996.
230. A. Ebensperger, P. Maxwell and C. Moscoso, *Resources Policy*, 2005, **30**, 218-231.

231. P. K. Newman and M. Saunders, *Postgraduate Medical Journal*, 1979, **55**, 701-703.
232. M. Niethammer and B. Ford, *Movement Disorders*, 2007, **22**, 570-573.
233. H.-B. Choi, J.-S. Ryu, W.-J. Shin and N. Vigier, *Nature Communications*, 2019, **10**, 5371.
234. J. R. Thomas, X. Liu and P. J. Hergenrother, *Journal of the American Chemical Society*, 2005, **127**, 12434-12435.
235. S. Hoekman, M. O. Kitching, D. A. Leigh, M. Papmeyer and D. Roke, *Journal of the American Chemical Society*, 2015, **137**, 7656-7659.
236. A. Millet, D. Dailler, P. Larini and O. Baudoin, *Angewandte Chemie International Edition*, 2014, **53**, 2678-2682.
237. BindFit v0.5 | Supramolecular, http://app.supramolecular.org/bindfit/, (accessed 3rd October 2023).
238. D. Cao, Z. Liu, P. Verwilst, S. Koo, P. Jangjili, J. S. Kim and W. Lin, *Chemical Reviews*, 2019, **119**, 10403-10519.
239. J. Wu, R. Sheng, W. Liu, P. Wang, J. Ma, H. Zhang and X. Zhuang, *Inorganic Chemistry*, 2011, **50**, 6543-6551.
240. H. Wang, L. O. Jones, T. Zhao, I. Hwang, V. M. Lynch, N. M. Khashab, G. C. Schatz, Z. A. Page and J. L. Sessler, *Chemical Science*, 2023, **14**, 4120-4125.
241. A. A. Kudale, J. Kendall, C. C. Warford, N. D. Wilkins and G. J. Bodwell, *Tetrahedron Letters*, 2007, **48**, 5077-5080.
242. S. Kumar, K. G. Thorat and M. Ravikanth, *The Journal of Organic Chemistry*, 2017, **82**, 6568-6577.
243. Y. Hong, J. W. Y. Lam and B. Z. Tang, *Chemical Society Reviews*, 2011, **40**, 5361-5388.
244. E. Bassan, Y. Dai, D. Fazzi, A. Gualandi, P. G. Cozzi, F. Negri and P. Ceroni, *Photochemical & Photobiological Sciences*, 2022, **21**, 777-786.
245. J. L. Sessler, S. K. Kim, D. E. Gross, C.-H. Lee, J. S. Kim and V. M. Lynch, *Journal of the American Chemical Society*, 2008, **130**, 13162-13166.
246. A. J. McConnell and P. D. Beer, *Angewandte Chemie International Edition*, 2012, **51**, 5052-5061.
247. B. Qiao, A. Sengupta, Y. Liu, K. P. McDonald, M. Pink, J. R. Anderson, K. Raghavachari and A. H. Flood, *Journal of the American Chemical Society*, 2015, **137**, 9746-9757.
248. Q. He, G. I. Vargas-Zúñiga, S. H. Kim, S. K. Kim and J. L. Sessler, *Chemical Reviews*, 2019, **119**, 9753-9835.
249. A. J. McConnell, A. Docker and P. D. Beer, *ChemPlusChem*, 2020, **85**, 1824-1841.
250. O.A. Karim and J.A. McCammon, *Journal of the American Chemical Society,* 1986, **108**, 1762-1766.
251. J. A. DeSimone and V. Lyall, *American Journal of Physiology-Gastrointestinal and Liver Physiology*, 2006, **291**, G1005-G1010.
252. S. Saha, A. Ghosh, P. Mahato, S. Mishra, S. K. Mishra, E. Suresh, S. Das and A. Das, *Organic Letters*, 2010, **12**, 3406-3409.
253. Y.-H. Kim and J.-I. Hong, *Chemical Communications*, 2002.
254. D. Jagleniec, S. Siennicka, Ł. Dobrzycki, M. Karbarz and J. Romański, *Inorganic Chemistry*, 2018, **57**, 12941-12952.
255. A. M. Desai and P. K. Singh, *Sensors and Actuators B: Chemical*, 2018, **277**, 205-209.

256. D. Jagleniec, S. Siennicka, Ł. Dobrzycki, M. Karbarz and J. Romański, *Inorganic Chemistry*, 2018, **57**, 12941-12952.
257. N. H. Evans, C. J. Serpell and P. D. Beer, *Chemistry – A European Journal*, 2011, **17**, 7734-7738.
258. H. Min Tay, A. Docker, Y. Cheong Tse and P. D. Beer, *Chemistry – A European Journal*, 2023, **29**, e202301316.
259. P.-N. Cheng, C.-F. Lin, Y.-H. Liu, C.-C. Lai, S.-M. Peng and S.-H. Chiu, *Organic Letters*, 2006, **8**, 435-438.
260. A. Brown, T. Lang, K. M. Mullen and P. D. Beer, *Organic & Biomolecular Chemistry*, 2017, **15**, 4587-4594.
261. M. R. Sambrook, P. D. Beer, J. A. Wisner, R. L. Paul, A. R. Cowley, F. Szemes and M. G. B. Drew, *Journal of the American Chemical Society*, 2005, **127**, 2292-2302.
262. Y.-H. Lin, C.-C. Lai and S.-H. Chiu, *Organic & Biomolecular Chemistry*, 2014, **12**, 2907-2917.
263. H.-J. Schneider and A. K. Yatsimirsky, *Chemical Society Reviews*, 2008, **37**, 263-277.
264. L. M. Hancock, E. Marchi, P. Ceroni and P. D. Beer, *Chemistry – A European Journal*, 2012, **18**, 11277-11283.
265. D. Brynn Hibbert and P. Thordarson, *Chemical Communications*, 2016, **52**, 12792-12805.
266. L. M. Hancock and P. D. Beer, *Chemical Communications*, 2011, **47**, 6012-6014.
267. J. I. Gavrilyuk, U. Wuellner and C. F. Barbas, *Bioorganic & Medicinal Chemistry Letters*, 2009, **19**, 1421-1424.
268. E. Klein, S. DeBonis, B. Thiede, D. A. Skoufias, F. Kozielski and L. Lebeau, *Bioorganic & Medicinal Chemistry*, 2007, **15**, 6474-6488.
269. A. H. G. David, P. García-Cerezo, A. G. Campaña, F. Santoyo-González and V. Blanco, *Chemistry – A European Journal*, 2019, **25**, 6170-6179.
270. V. Aucagne, K. D. Hänni, D. A. Leigh, P. J. Lusby and D. B. Walker, *Journal of the American Chemical Society*, 2006, **128**, 2186-2187.
271. H. Zheng, W. Zhou, J. Lv, X. Yin, Y. Li, H. Liu and Y. Li, *Chemistry – A European Journal*, 2009, **15**, 13253-13262.
272. S. H. Jung, J.-W. Lee and H.-J. Kim, *Supramolecular Chemistry*, 2016, **28**, 634-639.
273. X. Xu, A. K. Seiffert, R. Lenaerts, K. Ryskulova, S. Jana, K. Van Hecke, V. V. Jerca and R. Hoogenboom, *Dalton Transactions*, 2021, **50**, 8746-8751.
274. A. Mattarei, M. Azzolini, M. Zoratti, L. Biasutto and C. Paradisi, *Journal*, 2015, **20**, 16085-16102.
275. D. L. Mohler and G. Shen, *Organic & Biomolecular Chemistry*, 2006, **4**, 2082-2087.
276. F. Friscourt, C. J. Fahrni and G.-J. Boons, *Journal of the American Chemical Society*, 2012, **134**, 18809-18815.
277. T. R. Chan, R. Hilgraf, K. B. Sharpless and V. V. Fokin, *Organic Letters*, 2004, **6**, 2853-2855.